LATE HOLOCENE RELATIVE SEA LEVEL IN NEW JERSEY: EXAMINING PROXIES, TIMING, AND MECHANISMS

By

JENNIFER S. WALKER

A dissertation submitted to the

School of Graduate Studies

Rutgers, The State University of New Jersey

In partial fulfillment of the requirements

For the degree of

Doctor of Philosophy

Graduate Program in Oceanography

Written under the direction of

Benjamin Horton

And approved by

_____

_____

_____

_____

New Brunswick, New Jersey

October, 2019

ABSTRACT OF THE DISSERTATION

Late Holocene relative sea level in New Jersey: Examining proxies, timing, and mechanisms

By JENNIFER S. WALKER

Dissertation Director:
Benjamin Horton

Relative sea level (RSL) in New Jersey has exhibited varying rates of change across time and space throughout the late Holocene (last 4000 years), due to factors including glacial isostatic adjustment (GIA), ocean/atmosphere dynamics, and sediment compaction. High resolution sea-level reconstructions from salt-marsh proxies (e.g., foraminifera and geochemistry) have extended the instrumental record beyond the 20th century to link with late Holocene data. In this dissertation, I examined the accuracy of sea-level proxies, timing of the onset of modern rates of sea-level rise, and mechanisms contributing to sea-level change in New Jersey during the late Holocene.

In Chapter 1, I examined temporal and spatial variability of salt-marsh foraminifera and stable carbon isotope geochemistry ($\delta^{13}C$) to include seasonal/interannual and small-scale spatial changes in RSL reconstructions. I conducted a three-year monitoring experiment on four high marsh sampling stations in southern New Jersey, collecting 46 samples through time with 136 spatial replicate samples. Variations in annual standing crop that were observed did not exhibit any interannual or seasonal patterns. Foraminiferal assemblages and dominant species remained consistent on small spatial scales at each

monitoring station over the study period; however, standing crop varied among replicate samples. Temporal and small-scale spatial variability in $\delta^{13}C$ values at each station was very minimal. The foraminifera assemblages were separated into unique site-specific assemblages, and the variation across monitoring stations explained ~87% of the total variation, while ~13% of the variation in foraminiferal assemblages was explained by temporal and/or spatial variability among replicate samples. I developed a method to formally incorporate the temporal and spatial variability of modern foraminiferal distributions into a Bayesian transfer function. I applied this to a Common Era relative sea-level record in New Jersey. Because of the limited variability of foraminifera, RSL reconstructions from high marsh environments remain robust and reproducible.

In Chapter 2, I produced a new high-resolution RSL record in northern New Jersey using a Bayesian transfer function that employs salt-marsh foraminifera and a secondary proxy, stable carbon isotope geochemistry, to examine magnitudes and rates of sea-level change. I found that RSL in northern New Jersey continuously rose over the last 1000 years by 1.5 ± 0.1 m (1σ). RSL rose at a rate of 1.2 ± 0.2 mm/yr (2σ) from 1000 to 1700 CE before accelerating to a rate of rise of 2.1 ± 0.3 mm/yr from 1700 CE to present. I integrated the new northern New Jersey record into an updated global database of instrumental and proxy sea-level records of the Common Era. I used a spatiotemporal empirical hierarchical model with the global database to estimate the timing of the onset of modern elevated rates of sea-level rise. I propose ~1870 CE as the global onset of modern rates of sea-level rise. I examined the spatial variability in timing of modern elevated rates of RSL rise at nineteen sites in the North Atlantic which have the highest resolution of all of the proxy locations in the global RSL database and found asynchronous timing with a distinct spatial pattern.

Elevated rates in RSL appear earliest in the mid-Atlantic region, followed by the northeastern and southeastern U.S., and latest in Canada and Europe. I suggest that the observed spatial pattern in the timing may be due to a combination of steric and ocean dynamic effects from changes in Atlantic Meridional Overturning Circulation and the Gulf Stream.

In Chapter 3, I produced a new late Holocene RSL record in southern New Jersey from basal peat units to examine mechanisms of sea-level change, including GIA, as it is the dominant cause of late Holocene RSL rise in New Jersey. The paleomarsh elevation for each basal sample was estimated through a Bayesian transfer function using salt-marsh foraminifera assemblages and bulk sediment stable carbon isotope geochemistry. Sediment compaction and tidal range change were accounted for in each sample using a geotechnical model and a paleotidal model. I found that RSL rose continuously through the late Holocene by ~6.4 m from 4.6 ka BP to 1.2 ka BP at an average rate of 1.9 ± 0.3 mm/yr. I compared RSL changes from the basal peat record with site-specific GIA models that include two components: an ice history and a viscosity model. I used one 1D model that assumes the lithosphere and mantle viscosity are laterally homogeneous and nine 3D models that allow for mantle viscosity lateral heterogeneity. I found a misfit between model predictions and RSL observations, although the 3D models were an improvement over the 1D model. The remaining misfits suggest the importance of utilizing a wide array of ice model and viscosity model parameters to find a better fit between site-specific GIA predictions and RSL observations.

Acknowledgements

First, I would like to thank my PhD advisor, Ben Horton. Ben has provided continual guidance and support and endless opportunities in the form of research, collaborations, and conferences in order to share my work. He has introduced me to colleagues and connected me to media outlets from a first article in Climate Central to a PBS documentary. I am thankful for the time Ben has dedicated to working with me through the editing process to improve my writing and better articulate my research. I also appreciate him giving me the opportunity to work in Singapore at Nanyang Technological University, where I was welcomed as a student and researcher. I thank Ben for all of his advice and encouragement over the last five years.

I am very thankful for my committee – Bob Kopp, Ken Miller, and Don Barber – for their guidance and encouragement. I thank Bob for always checking in and reminding me to think statistically, Ken for his support from our first engaging conversation at AGU four years ago, and Don for sharing his lab with me at Bryn Mawr, discussing my results, and providing a work environment for me close to home.

I would like to thank Isabel Hong for her friendship and support as we shared our graduate school experience together from the beginning, through conversation in our office and in the field. I especially appreciate Isabel's camaraderie in the last year, bonding during our week in Ireland and through our emotional support animals, Coho and River. In addition, I appreciate the support of our cohort of grad students.

I am very thankful for my lab group – Tim Shaw, Nicole Khan, Ane Garcia-Artola, Tina Dura, Jessica Pilarczyk, Meg Christie, Andra Garner, and Kristen Joyse – for their

friendship, guidance, and assistance in the field. Especially, I would like to thank Jess for introducing me to sea-level research at Penn and Tim for his friendship, for teaching me field and lab methods, and for discussing my early research with me.

I would like to recognize the Rutgers University Marine Field Station, which acted as a backdrop for >30 field visits to sample salt-marsh foraminifera. I would like to thank Ken Able for talking to me about the natural history of New Jersey and introducing me to ghost forests, and Roland Hagan and Ryan Larum for teaching me to drive a boat and assisting me in my fieldwork.

I am forever grateful for the love and support of my family through graduate school.

I am thankful to have received funding from the Community Foundation of New Jersey and David and Arleen McGlade, a Rutgers Graduate School Excellence Fellowship, a Joseph A. Cushman Award for Student Research, three Rutgers University Marine Field Station Graduate Student Awards, a National Science Foundation East Asia and Pacific Summer Institute Fellowship, and a Rutgers University Bevier Fellowship.

Table of Contents

List of Tables

List of Illustrations

Chapter 1

Introduction

Projected sea-level rise over the next century is a serious threat to dense coastal populations, vast infrastructure, and metropolitan areas along the U.S. Atlantic coast. An understanding of past sea-level change and driving mechanisms is necessary to provide context for current change for effective coastal planning and adaptation. Relative sea level (RSL) has exhibited varying rates of change throughout the late Holocene, due to factors including glacial isostatic adjustment, ocean/atmosphere dynamics, and sediment compaction (e.g. Tornqvist et al., 2008; Engelhart et al., 2011; Kemp et al., 2018). High resolution sea-level reconstructions from salt-marsh proxies (e.g., foraminifera) have extended the instrumental record beyond the 20th century to link with late Holocene data (e.g. Gehrels 2000; Kemp et al., 2013, 2017). These reconstructions are necessary to improve understanding of magnitudes and rates of sea-level change at centennial to multi-decadal timescales and driving mechanisms behind sea-level change, and to provide information about sea-level responses to climate change and paleo constraints for model calibration (e.g. Varekamp et al., 1992; Kemp et al., 2011; Horton et al., 2018).

Salt-marsh foraminifera are used as proxies to reconstruct late Holocene sea level, because their modern distributions exhibit vertical zonation, revealing distinct faunal zones which can be further divided into subzones (e.g. Scott and Medioli, 1978; Gehrels, 1994; Horton and Edwards, 2006). A detailed understanding of proxies in the modern environment is a necessary prerequisite for the development of a transfer function to reconstruct sea level; however, temporal and spatial variability of foraminifera has not formally been included into transfer function based sea-level reconstructions. In Chapter 1, I conducted a three-year monitoring study of foraminifera from four high marsh study

sites to assess seasonal and interannual changes and small-scale spatial variability. The foraminifera assemblages were separated into unique site-specific assemblages, and the variation across monitoring stations explains ~87% of the total variation, while only ~13% of the variation in foraminiferal assemblages can be explained by temporal and/or spatial variability among replicate samples. Information about the temporal and spatial variability of modern foraminiferal distributions was formally incorporated into a Bayesian transfer function. Even when accounting for temporal and spatial variability of modern foraminifera, foraminifera-based relative sea-level reconstructions from high marsh environments remain robust and reproducible.

Common Era sea-level reconstructions provide the necessary high-resolution chronology to establish a quantitative estimate of the beginning of modern rates of rise (e.g. Donnelly et al. 2004, Gehrels et al. 2005, Kemp et al. 2011, 2014). Although there is agreement that rates of sea-level rise exceed Common Era background rates by the late 18th to early 20th century (e.g. Shennan and Horton, 2002; Gehrels et al., 2005; Engelhart and Horton, 2012), the timing of increased modern rates of sea-level rise is uncertain. The range of suggested timings may reflect the resolution and types of data used or may intriguingly suggest regional variability due to the gravitational, rotational, and deformational fingerprints of mass loss from ice sheet and glacier melt (e.g. Mitrovica et al., 2009), ocean steric effects (e.g. Cazenave and Llovel, 2010), and/or ocean dynamics (e.g. Ezer, 2015). In Chapter 2, I produced a new high-resolution (decimeter vertical, decadal horizontal) Common Era RSL record in northern New Jersey and integrated it into an updated global database of instrumental and proxy sea-level records of the Common Era (Kopp et al., 2016). I used a spatiotemporal empirical hierarchical model (Kopp et al.., 2016; Ashe et

al., 2019) with the global database to estimate the timing of the onset of modern elevated rates of sea-level rise. I assessed the global timing of the onset of modern rates of sea-level rise and identified spatial variability of elevated rates of sea-level rise among the sites with the highest resolution proxy records. I propose ~1870 CE as the global onset of modern rates of sea-level rise. I examined the timing of modern elevated rates of RSL rise at nineteen sites in the North Atlantic and found asynchronous timing with a distinct spatial pattern. Elevated rates in RSL appear earliest in the mid-Atlantic region, followed by the northeastern and southeastern U.S., and latest in Canada and Europe. I suggest that the observed spatial pattern in the timing may be due to a combination of steric and ocean dynamic effects from changes in Atlantic Meridional Overturning Circulation and the Gulf Stream.

Late Holocene sea-level rise in New Jersey has been dominated by glacial isostatic adjustment (GIA), due to the state's proximity to the margin of the former Laurentide Ice Sheet (e.g. Engelhart and Horton, 2012; Roy and Peltier, 2015; Love et al., 2016). An accurate estimate of the contribution of GIA to late Holocene RSL is important for coastal adaptation, because in many regions subsidence will be a principal reason for regional modification of global sea-level projections (e.g. Kopp et al., 2014; Love et al., 2016). RSL reconstructions at a high resolution are needed to validate GIA models on the U.S. mid-Atlantic coast, but salt-marsh reconstructions are limited by the depth and specific stratigraphy of sediment sequences available (Engelhart and Horton, 2012) as well as local processes involving sediment compaction (e.g. Long et al., 2006; Horton and Shennan, 2009) and tidal range change (e.g. Gehrels et al., 1995; Shennan et al., 2003; Hill et al., 2011). In Chapter 3, I produced a high resolution late Holocene RSL reconstruction from

a salt marsh in southern New Jersey, a region that experienced maximum rates of RSL rise due to the collapsing peripheral forebulge at the former ice margin (e.g. Dyke et al., 2003; Engelhart and Horton, 2012). I used basal peat units, which have minimal sediment compaction (e.g. Shennan and Horton, 2002; Tornqvist et al., 2008). Each data point includes an error for tidal range change and an error for the minimal compaction from a basal peat layer overlying an incompressible substrate. Ages are produced through high precision Accelerator Mass Spectrometry (AMS) radiocarbon dating on plant macrofossils. I found that RSL rose continuously through the late Holocene by an approximate magnitude of 6.4 m from 4.6 ka BP to 1.2 ka BP at an average rate of 1.9 ± 0.3 mm/yr. The resulting high resolution RSL record was compared to site-specific GIA models from Li et al. (2018), but there was a misfit between model predictions and RSL observations, although the 3D models are an improvement over the 1D model. The remaining misfits suggest the importance of utilizing a wide array of ice model and viscosity model parameters to find a better fit between site-specific GIA predictions and RSL observations.

Together these chapters address temporal and spatial variability of sea-level proxies used for RSL reconstructions; timing of the onset of modern elevated rates of sea-level rise in New Jersey, globally, and in the North Atlantic; and mechanisms for sea-level change in the late Holocene in New Jersey, including the dominant influence of GIA.

References

Ashe, Erica L., Niamh Cahill, Carling Hay, Nicole S. Khan, Andrew Kemp, Simon E. Engelhart, Benjamin P. Horton, Andrew C. Parnell, and Robert E. Kopp. 2019. "Statistical Modeling of Rates and Trends in Holocene Relative Sea Level." *Quaternary Science Reviews* 204 (January): 58–77. https://doi.org/10.1016/j.quascirev.2018.10.032.

Cazenave, Anny, and William Llovel. 2010. "Contemporary Sea Level Rise." *Annual Review of Marine Science* 2 (1): 145–73. https://doi.org/10.1146/annurev-marine-120308-081105.

Donnelly, Jeffrey P., Peter Cleary, Paige Newby, and Robert Ettinger. 2004. "Coupling Instrumental and Geological Records of Sea-Level Change: Evidence from Southern New England of an Increase in the Rate of Sea-Level Rise in the Late 19th Century: INCREASE IN THE RATE OF SEA-LEVEL RISE." *Geophysical Research Letters* 31 (5): n/a-n/a. https://doi.org/10.1029/2003GL018933.

Dyke, Arthur S, and David J A Evans. 2003. "Ice-Marginal Terrestrial Landsystems: Northern Laurentide and Innuitian Ice Sheet Margins." *Glacial Landsystems*, 24.

Engelhart, Simon E., and Benjamin P. Horton. 2012. "Holocene Sea Level Database for the Atlantic Coast of the United States." *Quaternary Science Reviews* 54 (October): 12–25. https://doi.org/10.1016/j.quascirev.2011.09.013.

Engelhart, Simon, Benjamin Horton, and Andrew Kemp. 2011. "Holocene Sea-Level Changes Along the United States' Atlantic Coast." *Oceanography* 24 (2): 70–79. https://doi.org/10.5670/oceanog.2011.28.

Ezer, Tal. 2015. "Detecting Changes in the Transport of the Gulf Stream and the Atlantic Overturning Circulation from Coastal Sea Level Data: The Extreme Decline in 2009–2010 and Estimated Variations for 1935–2012." *Global and Planetary Change* 129 (June): 23–36. https://doi.org/10.1016/j.gloplacha.2015.03.002.

Gehrels, W. Roland. 1994. "Determining Relative Sea-Level Change from Salt-Marsh Foraminifera and Plant Zones on the Coast of Maine, U.S.A." *Journal of Coastal Research* 10 (4): 990–1009.

———. 2000. "Using Foraminiferal Transfer Functions to Produce High-Resolution Sea-Level Records from Salt-Marsh Deposits, Maine, USA." *The Holocene* 10 (3): 367–76. https://doi.org/10.1191/095968300670746884.

Gehrels, W. Roland, Jason R. Kirby, Andreas Prokoph, Rewi M. Newnham, Eric P. Achterberg, Hywel Evans, Stuart Black, and David B. Scott. 2005. "Onset of Recent Rapid Sea-Level Rise in the Western Atlantic Ocean." *Quaternary Science Reviews* 24 (18–19): 2083–2100. https://doi.org/10.1016/j.quascirev.2004.11.016.

Gehrels, W. Roland, and Philip L. Woodworth. 2013. "When Did Modern Rates of Sea-Level Rise Start?" *Global and Planetary Change* 100 (January): 263–77. https://doi.org/10.1016/j.gloplacha.2012.10.020.

Gehrels, W.Roland, Daniel F. Belknap, Bryan R. Pearce, and Bin Gong. 1995. "Modeling the Contribution of M2 Tidal Amplification to the Holocene Rise of Mean High Water in the Gulf of Maine and the Bay of Fundy." *Marine Geology* 124 (1–4): 71–85. https://doi.org/10.1016/0025-3227(95)00033-U.

Hill, D. F., S. D. Griffiths, W. R. Peltier, B. P. Horton, and T. E. Törnqvist. 2011. "High-Resolution Numerical Modeling of Tides in the Western Atlantic, Gulf of Mexico, and Caribbean Sea during the Holocene." *Journal of Geophysical Research* 116 (C10). https://doi.org/10.1029/2010JC006896.

Horton, B. P., and I. Shennan. 2009. "Compaction of Holocene Strata and the Implications for Relative Sealevel Change on the East Coast of England." *Geology* 37 (12): 1083–86. https://doi.org/10.1130/G30042A.1.

Horton, Benjamin P, and Robin J Edwards. 2006. "Quantifying Holocene Sea Level Change Using Intertidal Foraminifera: Lessons from the British Isles." *Cushman Foundation for Foraminiferal Research Special Publication* 40: 100.

Horton, Benjamin P, Robert E Kopp, Andra J Garner, Carling C Hay, Nicole S Khan, Keven Roy, and Timothy A Shaw. 2018. "Mapping Sea-Level Change in Time, Space, and Probability," 44.

Kemp, Andrew C., Christopher E. Bernhardt, Benjamin P. Horton, Robert E. Kopp, Christopher H. Vane, W. Richard Peltier, Andrea D. Hawkes, Jeffrey P. Donnelly, Andrew C. Parnell, and Niamh Cahill. 2014. "Late Holocene Sea- and Land-Level Change on the U.S. Southeastern Atlantic Coast." *Marine Geology* 357 (November): 90–100. https://doi.org/10.1016/j.margeo.2014.07.010.

Kemp, Andrew C, Troy D Hill, Christopher H Vane, Niamh Cahill, Philip M Orton, Stefan A Talke, Andrew C Parnell, Kelsey Sanborn, and Ellen K Hartig. 2017. "Relative Sea-Level Trends in New York City during the Past 1500 Years." *The Holocene* 27 (8): 1169–86. https://doi.org/10.1177/0959683616683263.

Kemp, Andrew C, Benjamin P Horton, Jeffrey P Donnelly, Michael E Mann, Martin Vermeer, and Stefan Rahmstorf. 2011. "Climate Related Sea-Level Variations over the Past Two Millennia." *Proceedings of the National Academy of Sciences*, 6.

Kemp, Andrew C., Benjamin P. Horton, Christopher H. Vane, Christopher E. Bernhardt, D. Reide Corbett, Simon E. Engelhart, Shimon C. Anisfeld, Andrew C. Parnell, and Niamh Cahill. 2013. "Sea-Level Change during the Last 2500 Years in New Jersey, USA." *Quaternary Science Reviews* 81 (December): 90–104. https://doi.org/10.1016/j.quascirev.2013.09.024.

Kemp, Andrew C., Alexander J. Wright, Robin J. Edwards, Robert L. Barnett, Matthew J. Brain, Robert E. Kopp, Niamh Cahill, et al. 2018. "Relative Sea-Level Change in Newfoundland, Canada during the Past ~3000 Years." *Quaternary Science Reviews* 201 (December): 89–110. https://doi.org/10.1016/j.quascirev.2018.10.012.

Kopp, Robert E., Andrew C. Kemp, Klaus Bittermann, Benjamin P. Horton, Jeffrey P. Donnelly, W. Roland Gehrels, Carling C. Hay, Jerry X. Mitrovica, Eric D. Morrow, and Stefan Rahmstorf. 2016. "Temperature-Driven Global Sea-Level Variability in the Common Era." *Proceedings of the National Academy of Sciences* 113 (11): E1434–41. https://doi.org/10.1073/pnas.1517056113.

Li, Tanghua, Patrick Wu, Holger Steffen, and Hansheng Wang. 2018. "In Search of Laterally Heterogeneous Viscosity Models of Glacial Isostatic Adjustment with the ICE-6G_C Global Ice History Model." *Geophysical Journal International* 214 (2): 1191–1205. https://doi.org/10.1093/gji/ggy181.

Long, A.J., M.P. Waller, and P. Stupples. 2006. "Driving Mechanisms of Coastal Change: Peat Compaction and the Destruction of Late Holocene Coastal Wetlands." *Marine Geology* 225 (1–4): 63–84. https://doi.org/10.1016/j.margeo.2005.09.004.

Love, Ryan, Glenn A. Milne, Lev Tarasov, Simon E. Engelhart, Marc P. Hijma, Konstantin Latychev, Benjamin P. Horton, and Torbjörn E. Törnqvist. 2016. "The Contribution of Glacial Isostatic Adjustment to Projections of Sea-Level Change along the Atlantic and Gulf Coasts of North America: GIA AND FUTURE SEA-LEVEL CHANGE." *Earth's Future* 4 (10): 440–64. https://doi.org/10.1002/2016EF000363.

Mitrovica, Jerry X., Natalya Gomez, and Peter U. Clark. 2009. "The Sea-Level Fingerprint of West Antarctic Collapse." *Science* 323 (5915): 753–753. https://doi.org/10.1126/science.1166510.

Roy, Keven, and W.R. Peltier. 2015. "Glacial Isostatic Adjustment, Relative Sea Level History and Mantle Viscosity: Reconciling Relative Sea Level Model Predictions for the U.S. East Coast with Geological Constraints." *Geophysical Journal International* 201 (2): 1156–81. https://doi.org/10.1093/gji/ggv066.

Scott, D. S., and F. S. Medioli. 1978. "Vertical Zonations of Marsh Foraminifera as Accurate Indicators of Former Sea-Levels." *Nature* 272 (5653): 528. https://doi.org/10.1038/272528a0.

Shennan, I, T Coulthard, R Flather, B Horton, M Macklin, J Rees, and M Wright. 2003. "Integration of Shelf Evolution and River Basin Models to Simulate Holocene Sediment Dynamics of the Humber Estuary during Periods of Sea-Level Change and Variations in Catchment Sediment Supply." *The Science of The Total Environment* 314–316 (October): 737–54. https://doi.org/10.1016/S0048-9697(03)00081-0.

Shennan, Ian, and Ben Horton. 2002. "Holocene Land- and Sea-Level Changes in Great Britain." *Journal of Quaternary Science* 17 (5–6): 511–26. https://doi.org/10.1002/jqs.710.

Törnqvist, Torbjörn E., Davin J. Wallace, Joep E. A. Storms, Jakob Wallinga, Remke L. van Dam, Martijn Blaauw, Mayke S. Derksen, Cornelis J. W. Klerks, Camiel Meijneken, and Els M. A. Snijders. 2008. "Mississippi Delta Subsidence Primarily Caused by Compaction of Holocene Strata." *Nature Geoscience* 1 (3): 173–76. https://doi.org/10.1038/ngeo129.

Varekamp, J.C., E. Thomas, and O. Plassche. 1992. "Relative Sea-Level Rise and Climate Change over the Last 1500 Years." *Terra Nova* 4 (3): 293–304. https://doi.org/10.1111/j.1365-3121.1992.tb00818.x.

Chapter 1: Incorporating temporal and spatial variability of salt-marsh foraminifera into sea-level reconstructions

Abstract

Foraminifera from high salt-marsh environments have been used extensively to quantitatively reconstruct relative sea level. However, the influence of temporal and spatial variability of salt-marsh foraminifera is poorly known. Here, we conducted a three-year monitoring study of four high salt-marsh monitoring stations in New Jersey. We sampled each station four times per year (September, December, March, June), including four replicate samples at each sampling period, for a total of 46 samples through time with 136 spatial replicate samples. We also sampled each station through time and space for stable carbon isotope geochemistry ($\delta^{13}C$), which can be used as a secondary proxy for sea level.

The foraminiferal assemblages are separated into unique site-specific assemblages dominated by *Trochammina inflata*, *Jadammina macrescens*, and *Tiphotrocha comprimata* (Station 1); *Jadammina macrescens*, *Balticammina pseudomacrescens*, and *Tiphotrocha comprimata* (Station 2); *Tiphotrocha comprimata*, *Balticammina pseudomacrescens*, and *Haplophragmoides* spp. (Station 3); and *Jadammina macrescens*, *Ammoastuta inepta*, *Balticammina pseudomacrescens*, and *Haplophragmoides* spp. (Station 4). The variation across monitoring stations explains ~87% of the total variation in the 182 sample foraminiferal dataset. Only ~13% of the variation in foraminiferal assemblages can be explained by temporal and/or spatial variability among the replicate samples. Variations in annual standing crop that were observed did not exhibit any interannual or seasonal

patterns. Foraminiferal assemblages and dominant species remained consistent on small spatial scales at each monitoring station over the study period; however, standing crop varied among replicate samples. Temporal and small-scale spatial variability in $\delta^{13}C$ values at each station was very minimal.

We applied a Bayesian transfer function to estimate the elevation of the four monitoring stations. Under a 95% uncertainty interval, all samples from each monitoring station predicted a Standardized Water Level Index (SWLI) estimate within the observed elevation range of that station. Combining samples into replicate-aggregate and seasonal-aggregate datasets decreased elevation estimate uncertainty. Additionally, samples from Fall and Winter months had more accurate elevation estimates, as well as lower uncertainties, compared to Spring and Summer.

Information about the temporal and spatial variability of modern foraminiferal distributions was formally incorporated into the Bayesian transfer function through the prior specification of the relevant model parameters. The Bayesian transfer function, with informative-variability priors, was applied to a Common Era relative sea-level record in New Jersey. The average difference in paleomarsh elevation estimates with and without using the informative foraminifera variability prior was <0.01 m and the average difference in estimate uncertainties was 0.01 m. Reconstructed relative sea-level change over the past ~1000 years was also very similar with and without using the informative foraminifera variability prior: ~1.64 m rise with the uninformative prior and a ~1.61 m rise with the informative prior. Furthermore, the average difference in relative sea-level rate predictions

was 0.04 ± 0.12 mm/yr. Therefore, even when accounting for temporal and spatial variability of modern foraminifera, foraminiferal-based relative sea-level reconstructions from high marsh environments remain robust and reproducible.

1. Introduction

Relative sea level (RSL) has exhibited varying rates of change across time and space throughout the late Holocene, due to factors including glacial isostatic adjustment, ocean/atmosphere dynamics, and sediment compaction (e.g. Tornqvist et al., 2008; Engelhart et al., 2011; Kemp et al., 2018). High resolution sea-level reconstructions from salt-marsh proxies (e.g., foraminifera) have extended the instrumental record beyond the 20th century to link with late Holocene data (e.g. Gehrels 2000; Kemp et al., 2013, 2017). The late Holocene salt-marsh sea-level reconstructions illustrate patterns of natural variability at centennial to multi-decadal scales, which improve our understanding of the sea-level response to climate change (e.g. Varekamp et al., 1992; Kemp et al., 2011).

Salt-marsh foraminifera are used as proxies to reconstruct late Holocene sea level, because their modern distributions exhibit vertical zonation, revealing distinct faunal zones which can be further divided into subzones (e.g. Scott and Medioli, 1978; Gehrels, 1994; Horton and Edwards, 2006). Foraminiferal-based transfer functions utilize a modern foraminifera training set to quantify species assemblages' relationship with elevation, which is then applied to fossil assemblages, commonly from high marsh sedimentary sequences, to produce continuous records of sea-level at decimeter vertical resolution (e.g., Horton et al., 1999; Gehrels et al., 2000; Horton and Edwards, 2006; Kemp and Telford, 2015). The

foraminiferal-based transfer function has been recently enhanced using a Bayesian approach that employs foraminifera and a secondary proxy, geochemistry (Cahill et al., 2016; Kemp et al., 2017). Stable carbon isotope geochemistry ($\delta^{13}C$) in bulk sediment represents the dominant vegetation type and can be used as a proxy for sea level, because the transition between C_3 and C_4 dominated salt-marsh plant communities has been shown to act as the boundary for the mean higher high water (MHHW) tidal datum on the U.S. mid-Atlantic coast (e.g. Middleburg et al., 1997; Johnson et al., 2007; Kemp et al., 2012). In southern New Jersey, Kemp et al. (2012) found that $\delta^{13}C$ values of salt-marsh bulk sediment >-22.0‰ were found above MHHW, while values < -18.9‰ were found between mean tide level (MTL) and MHHW.

A detailed understanding of salt-marsh foraminifera (de Rijk, 1995) and geochemistry in the modern environment is a necessary prerequisite for the development of a transfer function to reconstruct sea level. Salt-marsh foraminifera are typically described in the modern environment only on one occasion in time without replicate sampling (e.g. Scott and Medioli, 1978; Horton, 1999; Kemp et al., 2017). However, salt-marsh foraminifera have been found to vary temporally on seasonal and interannual timescales (Buzas et al., 2002; Hippensteel et al., 2002; Martin et al., 2002; Horton and Edwards, 2003; Horton and Murray, 2006; Berkeley et al., 2008), as well as spatially at small (sub-meter) scales (Buzas 1968; Swallow, 2000; Morvan et al., 2006; Kemp et al., 2011). These variations have been shown to affect elevation boundaries of foraminiferal zones by as much as 15% of the tidal range (e.g. Horton and Edwards, 2003). But temporal and spatial variability has not formally been included into transfer function based sea-level reconstructions.

Site-specific differences in the relationship between stable carbon isotope geochemistry and elevation with respect to the local tidal frame are poorly understood. Further, changes in modern bulk salt-marsh sediment stable carbon isotope geochemistry through time (e.g. influence of seasonal variations) and on sub-meter spatial scales (e.g. influence of allochthonous material through tidal activity) is unknown (e.g. Stephenson et al., 1984; Leavitt and Long, 1986, 1991).

Here, we conducted a three-year monitoring study of foraminifera and stable carbon isotope geochemistry from four high marsh study sites of differing salinity regimes to assess seasonal and interannual changes and small-scale spatial variability. This is one of the longest seasonal/interannual monitoring studies of salt-marsh foraminifera (e.g. Hippensteel et al., 2002; Horton and Edwards, 2003; Horton and Murray, 2006) and the longest seasonal/interannual monitoring study of salt-marsh bulk sediment stable carbon isotope geochemistry. The data produced from this study are used to estimate variability in foraminifera and geochemistry over time and space. First, we analyzed the foraminiferal data to estimate: (a) the variation across monitoring stations for each species; and (b) the proportion of variation explained by the monitoring stations and replicate samples. Second, we ran a Bayesian transfer function on all of the data for each monitoring station to obtain a station elevation estimate and to examine variation in elevation estimates over time and across replicates at each station. Third, we formally account for spatial and temporal uncertainties by using the variance estimates from our analysis to inform prior distributions in the Bayesian transfer function related to the foraminifera variability when reconstructing elevations for sea-level studies. These variance estimates are incorporated into a southern

New Jersey relative sea-level record from Kemp et al. (2013) to examine differences in the record with and without the informative foraminifera variability prior.

2. Regional Setting

The field study sites are located in a high marsh environment of southern New Jersey on the U.S. mid-Atlantic coast (Figure 1). The southern New Jersey coast is characterized by a barrier island and lagoon system adjacent to the Atlantic Ocean. Inlets between the barrier islands and lagoons allow water exchange between the ocean and bays (Ferland, 1990).

Modern salt marshes with tidal channels form extensive gently sloping platforms along the coast of southern New Jersey (Ferland, 1990). Low marsh environments are dominated by *Spartina alterniflora* (tall form), while high marsh environments are dominated by *Spartina patens*, *Spartina alterniflora* (short form), and *Distichlis spicata* (Daddario, 1961). The brackish environment between the high marsh and freshwater upland is vegetated by *Phragmites australis* and *Iva fructescens* (Daddario, 1961; Stuckey and Gould, 2000). Our high marsh field sites are located near the Rutgers University Marine Field Station (Tuckerton, New Jersey), in the Mullica River-Great Bay estuary, which is one of the most pristine estuaries on the U.S. mid-Atlantic coast with minimal human disturbance due to lack of agricultural and industrial development and low population density (Kennish, 2004). The 1474 km^2 watershed is part of the Jacques Cousteau National Estuarine Research Reserve and drains the Pinelands National Reserve (Rhodehamel, 1998; Kennish, 2004).

The southern New Jersey coast has a semidiurnal, microtidal (range <2 m) regime, but varies between the ocean and lagoon side of the barriers. The tidal range in the Mullica River-Great Bay estuary that influences our field sites varies from 0.7 m (in Little Egg Harbor) to 1.1 m (near the mouth of Great Bay). Water exchange primarily occurs between the Atlantic Ocean and Little Egg Inlet leading into Great Bay (Chant et al., 2000).

Meteorological data for the region during the sampling timeframe of this study was obtained from the Jacques Cousteau National Estuarine Research Reserve meteorological station at Nacote Creek (~12 km from the monitoring stations) through the National Estuarine Research Reserve System's Centralized Data Management Office (Figure 2). Air temperatures over the three-year study period ranged from -5 to 25 ºC, with lows each year in January and February and highs in July and August. The study period contained the statewide warmest May, November, and December in 2015, statewide warmest August in 2016, and statewide warmest February and April in 2017 on record in New Jersey from 1895-2018 (Office of the New Jersey State Climatologist). Total monthly precipitation ranged from <20 mm to >200 mm. In 2015, the statewide third driest May and the fourth wettest June on record in New Jersey from 1895-2018 were observed (Office of the New Jersey State Climatologist). The Jacques Cousteau National Estuarine Research Reserve water quality station in Great Bay (~2 km from Monitoring Station 1; ~10 km from Monitoring Stations 2, 3, and 4) provided sea surface temperatures and salinity. Sea surface temperatures ranged from 5 to 25 ºC, exhibiting comparable annual fluctuations with lows each year in January and highs in July and August, and salinity ranged from 28 to 32 ppt. Tide gauge data from the Atlantic City tide gauge (~19 km from Monitoring Station 1; ~27

km from Monitoring Stations 2, 3, and 4) was obtained from the Permanent Service for Mean Sea Level. Monthly mean sea levels revealed annual lows in February and March and annual highs in September and October.

In addition, four hurricanes influenced New Jersey over the three-year study period (NOAA), as well as a significant winter storm flooding event. The National Oceanic and Atmospheric Administration (NOAA)-operated tide gauge at Great Bay, Shooting Thorofare (station number 8534319), located <500 m from one of the monitoring stations of this study, recorded flooding from Hurricane Joaquin on October 3, 2015 of 1.4 m MTL, which is in the top ten historic crests observed at this tide gauge (NOAA). The Great Bay tide gauge recorded a 1.6 m MTL crest on January 23, 2016 from the winter storm flooding event, which is second only to the flooding observed during Hurricane Sandy in October 2012 (NOAA).

3. Methods

3.1. Sampling Design

We selected four monitoring stations from high marsh/high marsh-upland transition sites above MHHW along a salinity gradient in the Mullica River-Great Bay estuary (Figure 1). We chose to investigate high marsh sites because high marsh sedimentary sequences are used for sea-level studies since foraminiferal zones are narrower in the high marsh compared to low marsh, providing more accurate elevation estimates (e.g. Gehrels, 2000; Wright et al., 2011).

We sampled a 1x1 m plot four times per year (September, December, March, June) from September 2014 to June 2017 to examine temporal variability of salt-marsh foraminifera and stable carbon isotope geochemistry. Station 4 was established in March 2015. Two samples were taken from each station, one of a standardized volume of 10 cm^3 (10 cm^2 by 1 cm thick), the other of approximately 30 cm^3 (30 cm^2 by 1 cm thick). The smaller sample was employed for foraminiferal analysis. This volume allowed comparison with similar studies (e.g. Scott and Medioli, 1980; Horton and Edwards, 2006; Kemp et al., 2012). The larger sample was for geochemistry and environmental variables. Each modern surface sediment sample was collected with four replicates so that small-scale spatial variability could be analyzed. A different quadrant of each plot was sampled during each sampling period, following methods of Horton et al. (2017), so that each quadrant was only sampled once per year to allow recovery of the marsh surface. In addition, we sampled for foraminifera after one of the hurricanes and after the significant winter storm flooding event during the three-year study period. We sampled Station 1 in the middle of October 2015, two weeks after the approach of Hurricane Joaquin that caused coastal flooding. We sampled all four stations in early February 2016, two weeks after the winter storm.

We surveyed each sampling station to National Oceanic and Atmospheric Administration (NOAA) tidal benchmarks using a total station where elevations were referenced to the North American Vertical Datum (NAVD88). We took multiple elevation measurements within the 1x1 m plot at Stations 3 due to the more hummocky nature of this site. The elevation at Station 1 was converted to tidal datums using VDatum and the NOAA-operated tide gauge at Great Bay, Shooting Thorofare (station number 8534319) located

<500 m from the station. To convert elevations from Stations 2, 3 and 4 to tidal datums, we deployed two automatic water-level loggers (Solinst Levelogger Edge) in tidal channels within 100 m of the stations and leveled them to NOAA tidal benchmarks. We correlated the water-level logger data with those recorded by the NOAA-operated tide gauge at Tuckerton Creek (station number 8534080) located ~1 km north of Stations 2, 3, and 4. Due to differences in tidal range between Station 1 and Stations 2, 3, and 4, we converted the tidal elevations into a standardized water level index (SWLI), following the approach of Horton et al. (1999).

3.2. Foraminiferal Analysis

We counted live and dead foraminifera from four replicate samples (10 cm^3) at each monitoring station from each sampling period for all three years. We stained the modern foraminifera samples with rose Bengal immediately after collection in order to identify live versus dead foraminifera tests (Walton, 1952). Although in some cases rose Bengal may stain dead tests (e.g. Walker et al., 1974; Bernhard, 1988), it still remains a reliable method and is unlikely to affect the interpretation of dead assemblages (Murray and Bowser, 2000). We stored samples in a buffered ethanol solution and refrigerated them (Scott et al., 2001). Samples were wet sieved to isolate the 63-500 µm size fraction and then split into eight equal aliquots using a wet splitter (Scott and Hermelin, 1993). We counted foraminifera under a binocular microscope while immersed in distilled water. Identifications of foraminifera were confirmed with type specimens at the National Museum of Natural History, Smithsonian Institute, Washington, D.C. Plate 1 shows scanning electron microscope (SEM) images of foraminifera from this study. We grouped specimens of the

genera *Haplophragmoides* and *Ammobaculites* into a single group due to difficulties in identifying them to the species level (Kemp et al., 2009). Although live specimens were counted, only the dead assemblages are used in our analyses because the dead assemblages are used in sea-level transfer functions (Horton, 1999). We used Coefficient of Variation (CV) – the ratio of the standard deviation to the mean – to examine the relative variability among replicate samples. All dead foraminifera data are presented in Appendix A and all live foraminifera data are presented in Appendix B. Live foraminifera total counts, dominant foraminifera, and CV among replicates for all samples for each station are displayed in Appendix E.

3.3. Stable Carbon Isotope Geochemical Analysis

We analyzed the $\delta^{13}C$ values from each monitoring station from each sampling period for all three years, as well as from several replicate samples throughout the sampling period. Since the dominant input to salt-marsh sediment is in situ vegetation, $\delta^{13}C$ values were measured in bulk sediment. Bulk sediment stable carbon isotope geochemistry was measured at the Departments of Geology and Environmental Studies at Bryn Mawr College using a cavity ring-down laser spectroscopy (CRDS) following the flash combustion technique described by Balslev-Clausen et al (2013). Prior to isotopic analysis, bulk peat samples were freeze-dried in a Virtis™ benchtop freeze dryer to remove moisture and then ground in a Retsch™ ball mill until finely powdered. Approximately two mg (±0.5 mg) of the dried, powdered sample was weighed on a Mettler Toledo™ XP56 microbalance with 4 µg precision. Weighed samples were sealed in pressed-wall tin capsules and flash combusted at 980°C in a Costech™ ECS 4010 element analyzer using N2 as a carrier gas.

The Costech™ EA has a 50-sample carousel for automated runs. Isotopic composition of the CO_2 produced by combustion is analyzed in a Picarro™ G2201-*i* CRDS instrument. Carbon abundance in each sample was calculated from the peak $^{12}CO_2$ concentration measured by the CRDS system, calibrated by analysis of standard reference material (NIST 1547 Peach leaf). Reproducibility of carbon mass concentration is ±0.8% (1 s.d., n=96). Carbon isotopic composition, reported as $\delta^{13}C$, is standardized to Vienna Pee Dee Belemnite (VPDB) by analysis of standard reference material USGS40 (glutamic acid). The reproducibility of $\delta^{13}C$ values is <0.2‰ based on repeat analyses of NIST 1547 (0.15‰, 1 s.d., n=96) and USGS40 (0.18‰, 1 s.d., n=27). All stable carbon isotope geochemical data are presented in Appendix C.

3.4. Environmental Variables

For each sampling period, we also measured several environmental variables at each of the four monitoring stations (Table 1). We measured porewater salinity in the center of each monitoring station plot during each sampling period using a handheld YSI meter. We analyzed organic matter by loss on ignition (LOI) for samples from each monitoring station from each sampling period. We dried the samples in an oven and ignited the samples in a muffle furnace following the methods of Plater et al. (2015). We analyzed grain size for samples from each monitoring station. We used 30% H_2O_2 to digest the organic fraction of the samples to prepare them for grain-size analysis (Donato et al., 2009). Grain size distributions were measured using a Malvern Mastersizer 3000 laser particle-size analyzer and were described after Folk and Ward (1957). All environmental data are presented in Appendix D.

3.5. Statistical Analysis

We used partitioning around medoids (PAM) to analyze the composition of foraminifera assemblages present at the four monitoring stations (Kaufman and Rousseeuw, 1990). We applied PAM to the entire dataset of raw counts of dead foraminifera, using four groups to correspond to the four monitoring stations, and graphically represented the data with a silhouette plot (Rousseeuw, 1987). Analysis was completed using the 'cluster' package in R. Silhouette widths between -1 and 1 provide an estimate of a sample's classification. Values close to 1 indicate that the sample was assigned to an appropriate group where within group dissimilarity was less than the dissimilarity among the groups. Values close to -1 indicate that the sample was incorrectly classified.

To formally account for spatial and temporal uncertainties and to use variance estimates from our analysis in the Bayesian transfer function, we merged our data with the training set from southern New Jersey (Kemp et al., 2013) and a new unpublished training set from Cheesequake State Park in northern New Jersey (Chapter 2). The taxonomy was harmonized by combining *J. macrescens* and *B. pseudomacrescens*, and *T. inflata* and *S. lobata*. These species are often combined in sea-level transfer functions to avoid inconsistencies in taxonomic identifications (Kemp et al., 2018).

Using the harmonized taxonomy, we performed three different analyses. First, we modeled the raw foraminifera counts from our study sites to estimate the overall species variance as

the combination of variation across monitoring stations and the variation across replicate samples after accounting for any underlying trend that may be present over time.

Second, we ran a Bayesian transfer function (Cahill et al., 2016) using the regional training set on the foraminifera data from each sampling period from each monitoring station to provide an elevation estimate for each monitoring station and to examine variability in these elevation estimates over the three years. Additionally, replicate sample assemblages were combined to produce a replicate-aggregate SWLI estimate for each sampling period for each station to analyze the effect of small-scale spatial foraminiferal variability and increased count size on elevation estimates. All sample assemblages for each season within each station were also combined to produce a seasonal-aggregate SWLI estimate for each season for each station to analyze seasonal variability of elevation estimates.

Here we provide an overview of the Bayesian transfer function. We outline notation for the data as follows:

- y^m are observed modern foraminifera abundances. y_{il}^m is the abundance of species l in surface sample i, with $i = 1, \dots, N$
- T_i^m is the total of the species abundances for surface sample i.
- e^m are the observed standardized modern elevations. e_i^m is the elevation for surface sample i.
- y^f are observed fossil foraminifera abundances. y_{jl}^f is the abundance of species l in fossil sample j, with $j = 1, \dots, M$
- T_j^f is the total of the species abundances for fossil sample j.

A multinomial likelihood is assumed for the modern species abundances y_{il}^{m} as follows:

$$y_{i1}^{m}, y_{i2}^{m} \dots y_{iL}^{m} \sim Multinomial(p_{i1}, p_{ji} \dots . p_{iL}, T_{i}^{m}),$$

where p_{il} is the probability of finding species l at elevation i.

The probability parameters p_{il}^{m} are estimated as a function of a latent response λ_{jl}:

$$p_{il} = f(\lambda_{il}),$$

where f is a softmax transformation used to preserve the sum and boundary constraints of the probabilities for each sample i. The latent response vector λ_{l} contains the response for species l across all samples and is modeled as a function of elevation:

$$\lambda_{l} = g_{l}(e^{m}) + \epsilon_{l},$$

$$\epsilon_{l} \sim N(0, \sigma_{l}^{2}),$$

where g_{l} is a P-spline (e.g. de Boor, 1978; Dierckx, 1993) function that governs the shape of the response curve of species l. The error term ϵ_{l} is added to the P-spline for each species to account for over/under dispersion in the raw data and σ_{l}^{2} is a species-specific variance term.

Third, we incorporated the species variance estimates from the first analysis into the Bayesian transfer function by providing informative priors for parameters related to foraminifera variability which account for spatial and temporal uncertainty in foraminiferal distributions when reconstructing RSL. Specifically, a truncated t-distribution prior is placed on σ_{l}^{2} and the first analysis provided estimates of the hyperparameters that govern the prior distributions of the variance terms. In the absence of this additional information an uninformative prior was used.

We applied the Bayesian transfer function with and without the informative foraminifera variability prior to a southern New Jersey relative sea-level record from Kemp et al. (2013). The Bayesian transfer function produced SWLI estimates of paleomarsh elevation (PME) using fossil foraminifera abundances from a sediment core. The same modeling set up is assumed for fossil abundances, using the f subscript to refer to fossil data and parameters, as follows:

$$y_{j1}^{f}, y_{j2}^{f} \dots y_{jL}^{f} \sim Multinomial(p_{j1}^{f}, p_{j2}^{f} \dots p_{jL}^{f}, T_{j}^{f}),$$

$$p_{j1}^{f} = f(\lambda_{j1}^{f}),$$

$$\lambda_{l}^{f} = g_{l}(e^{f}) + \epsilon_{l},$$

The fossil elevations are contained within the vector e^{f}, which has a prior distribution:

$$e_{j}^{f} \sim N(\mu_{j}, \tau^{2}),$$

$$\mu_{j} \sim U(a_{j}, b_{j})$$

where e_{j}^{f} is the fossil elevation for core sample j. The mean of the prior distribution for e_{j}^{f} has a truncated normal prior. In the absence of secondary proxy information to inform this prior distribution $a_{j} = a$ and $b_{j} = b$, where a and b are fixed at the minimum and maximum observed surface elevations respectively. If secondary proxy information is available (for example, in the form of a geochemical proxy that can provide constraints on the elevational range of the fossil samples) a_{j} and b_{j} are fixed at the minimum and maximum elevations suggested by the secondary proxy for sample j.

We converted SWLI estimates from the Bayesian transfer function to meters relative to Mean Tide Level (MTL). The PME estimates were subtracted from their sample altitude

to obtain RSL. Finally, when combined with sample ages, a RSL reconstruction is produced. We use an Errors-In-Variables Integrated Gaussian Process model (Cahill et al., 2015) that accounts for the vertical and chronological uncertainties of the RSL data to examine a probabilistic assessment of past RSL changes and rates of past RSL change to examine differences in the southern New Jersey record with and without the informative foraminifera variability prior.

4. Results

4.1. Monitoring Stations

All four stations are located in a high marsh or high marsh-upland transition environment above MHHW based on their vegetation and/or local tidal datums (Table 1). Station 1 is a high marsh, high salinity site primarily vegetated by *Spartina alterniflora* (short form) with an average salinity of 39.6 ± 8.8 psu over the three-year sampling period. Station 1 has an elevation of 212-223 SWLI units, which is equivalent to 0.68 ± 0.03 m MTL, or 0.11 m above local MHHW. The substrate of station 1 is a sandy silt and had the lowest organic content of the four monitoring stations of 29.0% ± 7.9% by weight. Stations 2 and 3 are both high marsh, low salinity sites. Station 2 is primarily vegetated by *Spartina patens* and had an average salinity of 13.7 ± 4.9 psu over the three-year sampling period. Station 2 has an elevation of 211-224 SWLI units, which is equivalent to 0.68 m MTL, or 0.27 m above local MHHW. The substrate of station 2 is a sandy silt and had the highest organic content of 81.1% ± 3.5% by weight. Station 3 is primarily vegetated by *Spartina patens* and *Distichlis spicata*, but borders *Phragmites australis*, and had an average salinity slightly lower than Station 2 of 13.1 ± 4.9 psu. Station 3 has a hummocky nature and its elevation

ranges from 192-227 SWLI units, which is equivalent to 0.46 – 0.60 m MTL, or 0.05 – 0.20 m above local MHHW. The substrate of station 3 is a sandy silt with an organic content of 64.3% ± 3.9% by weight. Station 4 is a high marsh-upland transition, brackish site vegetated by *Phragmites australis* and had the lowest salinity of the four monitoring stations with an average of 2.9 ± 2.0 psu over the three-year sampling period. Station 4 has the highest elevation of the four monitoring stations at 248-264 SWLI units, which is equivalent to 0.61 m MTL, or 0.21 m above local MHHW. The substrate of station 4 is a fine silt with an organic content of 53% ± 7.6% by weight. Monitoring Station 4 was established in March 2015; therefore, year one refers to data only from Spring and Summer 2015.

4.2. Foraminiferal Distributions

71,658 modern foraminifera consisting of 14 agglutinated species from 182 samples were counted over the three-year study. Across the stations, 46 samples were taken through time with 136 spatial replicate samples through the sampling period. Sample count sizes ranged from 58 to 1196 tests/10 cm^3 with an average of 389 ± 221 tests/10 cm^3 (Figure 3). The standing crop of foraminifera was greatest in year three when a total of 26194 tests were counted (average 409 ± 200 tests/10 cm^3). Furthermore, the maximum standing crops of foraminifera were found in the last sampling date, Summer 2017, when a total of 7552 dead foraminifera were identified from the four replicates. The average range in count size and coefficient of variation (CV) among replicates was 235 ± 150 tests and 29 ± 14%, respectively.

The dominant foraminifera species across the stations in order of most abundant to least abundant were *Jadammina macrescens* (21408 tests), *Balticammina pseudomacrescens* (14448 tests), *Tiphotrocha comprimata* (13912 tests), *Trochammina inflata* (9688 tests), *Haplophragmoides* spp. (5252 tests), and *Ammoastuta inepta* (1982 tests). None of the foraminifera species exhibited a clear seasonal pattern across all monitoring stations. *J. macrescens* had the lowest average CV among replicates at 48 ± 29% and *A. inepta* had the highest average CV at 97 ± 57%.

We used PAM analysis with four groups to examine the composition of the entire foraminifera dataset. The average silhouette width is 0.56, meaning the samples fit well into four groups, as the value is close to 1 (Figure 4). The samples from Station 1 and Station 4 each fit into a group with an average silhouette width of 0.62, and Station 2 and Station 3 samples each fit into a group with an average silhouette width of 0.51. The higher silhouette widths for Stations 1 and 4 show that the samples in those groups are more similar to each other, and therefore their foraminifera assemblages are more consistent over time and space. All but 11 of 184 samples were assigned to a group corresponding to the monitoring station they were sampled from, indicating that each station has a site-specific assemblage. These 11 samples all had the lowest silhouette widths of all samples and did not as clearly belong to any one group. 10 of the 11 samples were from Stations 2 and 3, which had the lower silhouette widths and therefore less consistent assemblages over time and space.

4.3. Temporal and Spatial Variability of Foraminifera at Monitoring Station 1

Monitoring Station 1's count size ranged from 58 to 616 tests/10 cm^3 with an average of 229 ± 112 tests/10 cm^3 (Figure 5). The standing crop of foraminifera was greatest in year three when a total of 4618 tests were counted (average 289 ± 148 tests/10 cm^3). Furthermore, the maximum standing crops of foraminifera were found in the last sampling date, Summer 2017, when a total of 1596 dead foraminifera were identified from the four replicates. The average range in count size and coefficient of variation (CV) among replicates was 171 ± 129 tests and 33 ± 18%, respectively. Of the four Monitoring Stations, Station 1 had the highest average CV among replicates. Year two had the lowest (96 ± 37 tests; 21 ± 19%) and year three had the highest (284 ± 180 tests; 41 ± 23%) average range in count size and CV. The maximum range of foraminifera and CV among replicates was found in Spring 2017 with 68 to 528 tests/10 cm^3 and 72%, respectively.

We identified 11 foraminifera species from Monitoring Station 1, which were dominated by *Trochammina inflata*, *Jadammina macrescens*, and *Tiphotrocha comprimata* (Figure 5). The remaining 8 species found at Station 1 remained below 10% relative abundance for the majority of all samples (Appendix A).

T. inflata was the dominant species in 47 of the 48 samples from Station 1. *T. inflata* standing crop varied from 22 to 436 tests/10 cm^3 (average 144 ± 80 tests/10 cm^3). Changes in the total standing crop are similar to changes in *T. inflata*. For example, *T. inflata* standing crop also was greatest in year three (3080 total tests; average 193 ± 101 tests/10 cm^3). *T. inflata* exhibited no clear seasonal pattern. Of the three dominant species at

Monitoring Station 1, *T. inflata* had the largest range in standing crop of foraminifera (average of 102 ± 87) but the smallest CV (average of 32 ± 20%) among replicate samples. Similar to the total count, year two had the lowest (54 ± 28 tests; 19 ± 12%) and year three had the highest (191 ± 100 tests; 43 ± 18%) average range in count size and CV.

The second most dominant species, *Jadammina macrescens* had a standing crop that varied from 6 to 166 tests/10 cm^3 (average 53 ± 34 tests/10 cm^3). Similar to the total count and *T. inflata*, *J. macrescens* standing crop also was greatest in year three (1148 total tests; average 72 ± 37 tests/10 cm^3). The maximum standing crops were also found in Summer 2017 when a total of 362 tests were identified from the four replicates. *J. macrescens* exhibited no clear seasonal pattern. *J. macrescens* had an average range in count size and CV among replicates of 52 ± 37 tests and 44 ± 25%, respectively. Similar to *T. inflata*, the replicate range was greatest in the third year of sampling with an average range among samples of 71 ± 57 tests.

The third most dominant species, *T. comprimata*, had a standing crop that varied from 2 to 132 tests/10 cm^3 (average 23 ± 25 tests/10 cm^3). *T. comprimata* standing crop remained stable from 400 total tests in year one (average 25 ± 29 tests/10 cm^3) to 362 total tests in year three (average 23 ± 31 tests/10 cm^3). *T. comprimata* did, however, exhibit a seasonal pattern. For example, the maximum standing crops of each year were found in Spring 2015, Spring 2016, and Spring 2017 when a total of 226 tests, 124 tests, and 192 tests were identified from the four replicates, respectively. Of the three dominant species at Monitoring Station 1, *T. comprimata* had the smallest range in standing crop (average of

35 ± 37) foraminifera but the highest CV (average of 60 ± 25%) among replicate samples. Similar to the total count and *T. inflata*, year two had the lowest (21 ± 3 tests; 45 ± 16%) and year three had the highest (45 ± 53 tests; 70 ± 38%) average range in count size and CV. The replicate sample ranges for *T. comprimata* were greatest in the spring sampling periods for all three years. For example, in year three the range in standing crop among replicates was 122 tests/10cm^3 in spring compared to an average of 19 tests/10cm^3 for the rest of the year.

The live foraminifera assemblage at Monitoring Station 1 had smaller standing crops compared to the dead assemblage, with count sizes ranging from 0 to 214 tests/10 cm^3 with an average of 33 ± 46 tests/10 cm^3 (Appendix E). The standing crop of foraminifera was greatest in year three when a total of 1334 tests were counted (average 70 ± 61 tests/10 cm^3). The average coefficient of variation (CV) among replicates was 80 ± 51%, respectively. Of the four Monitoring Stations, Station 1 had the highest average CV among replicates. We identified 6 live foraminifera species from Monitoring Station 1, which were dominated by *Trochammina inflata*, *Jadammina macrescens*, and *Balticammina pseudomacrescens* (Appendix E); however, *B. pseudomacrescens* was found in very low numbers (<20 tests/10 cm^3). *T. inflata* and *J. macrescens* were also two of the three dominant species in the dead assemblage. None of the species in the live assemblage exhibited a clear seasonal pattern.

4.4. Temporal and Spatial Variability of Foraminifera at Monitoring Station 2

Monitoring Station 2's count size ranged from 186 to 1130 tests/10 cm^3 with an average of 500 ± 225 tests/10 cm^3 (Figure 6). In contrast to Monitoring Station 1, the standing crop of foraminifera was greatest in year one (average 601 ± 269 tests/10 cm^3). Indeed, the maximum standing crops of foraminifera were found in the first sampling date, Fall 2014, when a total of 3262 dead foraminifera were identified from the four replicates. The average range in count size and CV among replicates was 262 ± 149 tests and 26 ± 14%, respectively. Of the four Monitoring Stations, Station 2 had the smallest average CV among replicates. Year one had the highest average range in count size and CV at 393 ± 190 tests and 33 ± 16%, respectively. The greatest range of foraminifera among replicates was found in the first sampling date, Fall 2014, with 478 to 1130 tests/10 cm^3.

We identified 10 foraminifera species from Monitoring Station 2, which were dominated by *Jadammina macrescens*, *Balticammina pseudomacrescens*, and *Tiphotrocha comprimata* (Figure 6). The remaining 7 species found at Station 2 remained below 10% relative abundance for the majority of all samples (Appendix A).

J. macrescens was the dominant species in 35 of the 48 samples. *J. macrescens* standing crop varied from 46 to 656 tests/10 cm^3 (average 239 ± 141 tests/10 cm^3). Changes in the total standing crop are similar to changes in *J. macrescens*. For example, *J. macrescens* standing crop was greater in year one (average 275 ± 161 tests/10 cm^3) and year three (average 299 ± 134 tests/10 cm^3) compared to year two (average 143 ± 60 tests/10 cm^3). *J. macrescens* exhibited no clear seasonal pattern. Of the three dominant species, *J.*

macrescens had the largest average range in standing crop of foraminifera (average of 188 ± 110) but the smallest CV (average of 37 ± 22%) among replicate samples. Similar to the total count, the replicate range was smallest in the second year of sampling with an average range among samples of 93 ± 42 tests.

The second most dominant species, *B. pseudomacrescens*, had a standing crop that varied from 14 to 456 tests/10 cm^3 (average 157 ± 91 tests/10 cm^3). *B. pseudomacrescens* standing crop was relatively stable seasonally and annually except in Spring 2015 when a total of 1296 tests were identified from the four replicates. *B. pseudomacrescens* had an average range in count size and CV among replicates of 124 ± 79 tests and 41 ± 26%, respectively.

The third most dominant species, *T. comprimata*, had a standing crop that varied from 8 to 346 tests/10 cm^3 (average 76 ± 64 tests/10 cm^3). Similar to the total count, *T. comprimata* standing crop was greatest in year one (average 114 ± 81 tests/10 cm^3) with the maximum standing crop found in the first sampling date, Fall 2014, when a total of 748 tests were identified from the four replicates. Unlike at Monitoring Station 1, *T. comprimata* exhibited no clear seasonal pattern. Similar to the total count and *B. pseudomacrescens*, the average replicate range and CV was greatest in year one (154 ± 61 tests; 63 ± 15%).

The live foraminifera assemblage at Monitoring Station 2 had smaller standing crops compared to the dead assemblage, with count sizes ranging from 0 to 282 tests/10 cm^3 with an average of 61 ± 70 tests/10 cm^3 (Appendix E). The standing crop of foraminifera was greatest in year three when a total of 1680 tests were counted (average 88 ± 85 tests/10

cm^3). The average coefficient of variation (CV) among replicates was 64 ± 38%, respectively. We identified 9 live foraminifera species from Monitoring Station 2, which were dominated by *Jadammina macrescens*, *Balticammina pseudomacrescens*, and *Tiphotrocha comprimata* (Appendix E). These are the same three dominant species found in the dead assemblage. None of the species in the live assemblage exhibited a clear seasonal pattern.

4.5. Temporal and Spatial Variability of Foraminifera at Monitoring Station 3

Monitoring Station 3 had count sizes ranging from 212 to 1196 tests/10 cm^3 with an average of 553 ± 198 tests/10 cm^3 (Figure 7). In contrast to Monitoring Stations 1 and 2, the standing crop of foraminifera was greatest in year two (average 622 ± 178 tests/10 cm^3). For example, the maximum standing crops of foraminifera were found in Fall 2015 when a total of 3188 dead foraminifera were identified from the four replicates. Of the four Monitoring Stations, Station 3 had the highest average range in count size among replicates of 339 ± 157 tests. Year one had the highest average range in count size and CV among replicates at 407 ± 235 tests and 35 ± 13%, respectively. In addition, the greatest range of foraminifera among replicates was also found in the first sampling date, Fall 2014, with 504 to 1196 tests/10 cm^3.

We identified 12 foraminifera species from Monitoring Station 3, which were dominated by *Tiphotrocha comprimata*, *Balticammina pseudomacrescens*, and *Haplophragmoides* spp. (Figure 7). The remaining 9 species remained below 10% relative abundance for the majority of all samples (Appendix A).

T. comprimata was the dominant species in 34 of the 48 samples. *T. comprimata* standing crop varied from 60 to 380 tests/10 cm^3 (average 190 ± 74 tests/10 cm^3). Changes in the total standing crop are similar to changes in *T. comprimata*. For example, *T. comprimata* standing crop was also greatest in year two (average 224 ± 75 tests/10 cm^3) and the maximum standing crops were found in Fall 2015 when a total of 1162 tests were identified from the four replicates. Similar to Monitoring Station 1, *T. comprimata* exhibited a seasonal pattern; however, an opposite pattern was observed. Maximum standing crops each year were found in Fall and Winter, and minimum standing crops each year were found in Spring and Summer. For example, in year two, the average standing crop for Fall and Winter was 277 ± 50 tests/10 cm^3 and the average standing crop for Spring and Summer was 170 ± 53 tests/10 cm^3. Of the three dominant species at Monitoring Station 3, *T. comprimata* had the largest range in standing crop (average of 121 ± 48) but the smallest CV (average of 30 ± 13%) among replicate samples. Similar to the total count, the average replicate range and CV was greatest in year one (127 ± 67 tests; 35 ± 16%).

The second most dominant species, *B. pseudomacrescens*, had a standing crop that varied from 38 to 302 tests/10 cm^3 (average 128 ± 60 tests/10 cm^3). *B. pseudomacrescens* standing crop was relatively stable interannually except in Fall 2015 when a total of 910 tests were identified from the four replicates. Seasonally, the standing crop was highest in the fall for all three years. For example, in year two the mean standing crop was 228 ± 52 tests/10cm^3 in fall compared to an average of 113 ± 39 tests/10cm^3 for the rest of the year. *B. pseudomacrescens* had an average range in count size and CV among replicate samples of

106 ± 59 tests and 36 ± 17%, respectively. Similar to the total count and *T. comprimata*, the replicate range and CV was greatest in year one (129 ± 78 tests and 43 ± 20%).

The third most dominant species, *Haplophragmoides* spp., had a standing crop that varied from 12 to 266 tests/10 cm^3 (average 92 ± 60 tests/10 cm^3). *Haplophragmoides* spp. standing crop was greater in year two (average 118 ± 58 tests/10 cm^3) and year three (average 112 ± 63 tests/10 cm^3) compared to year one (average 47 ± 27 tests/10 cm^3). *Haplophragmoides* spp. exhibited no clear seasonal pattern. Similar to the total count, *T. comprimata*, and *B. pseudomacrescens*, the average CV was greatest in year one (56 ± 25%). Average CV among replicates was smallest in the fall for each year at 30%, 20%, and 18% for Fall 2014, Fall 2015, and Fall 2016, respectively.

The live foraminifera assemblage at Monitoring Station 3 had smaller standing crops compared to the dead assemblage, and the smallest live count sizes of the four monitoring stations, ranging from 0 to 78 tests/10 cm^3 with an average of 17 ± 22 tests/10 cm^3 (Appendix E). The standing crop of foraminifera was greatest in year three when a total of 502 tests were counted (average 26 ± 24 tests/10 cm^3). The average coefficient of variation (CV) among replicates was 74 ± 55%, respectively. We identified 9 live foraminifera species from Monitoring Station 3, which were dominated by *Tiphotrocha comprimata*, *Balticammina pseudomacrescens*, and *Trochammina inflata* (Appendix E). *T. comprimata* and *B. pseudomacrescens* were also two of the three dominant species in the dead assemblage. None of the species in the live assemblage exhibited a clear seasonal pattern.

4.6. Temporal and Spatial Variability of Foraminifera at Monitoring Station 4

Monitoring Station 4 had similar count sizes ranging from 88 to 456 tests/10 cm^3 with an average of 252 ± 86 tests/10 cm^3 (Figure 8). Unlike the other three Monitoring Stations, the standing crop of foraminifera remained stable through all three years from an average of 265 ± 100 tests/10 cm^3 in year one to an average of 242 ± 104 tests/10 cm^3 in year two to an average of 256 ± 60 tests/10 cm^3 in year three. Of the four Monitoring Stations, Station 4 had the smallest average range in count size among replicates of 156 ± 68 tests; the average CV was 28% ± 10. Year one had the highest average range and CV in count size among replicates (245 ± 7 tests; 41 ± 2%).

We identified 10 foraminifera species from Monitoring Station 4, which were dominated by *Jadammina macrescens*, *Ammoastuta inepta*, *Balticammina pseudomacrescens*, and *Haplophragmoides* spp. (Figure 8). The remaining 6 species found at station 4 remained below 10% relative abundance for the majority of all samples (Appendix A).

J. macrescens was the dominant species in all 40 samples. *J. macrescens* standing crop varied from 58 to 294 tests/10 cm^3 (average 166 ± 64 tests/10 cm^3). Changes in the total standing crop are similar to changes in *J. macrescens*. For example, *J. macrescens* standing crop remained fairly stable through all three years from an average of 186 ± 83 tests/10 cm^3 in year one to an average of 160 ± 60 tests/10 cm^3 in year three. *J. macrescens* did exhibit a seasonal pattern. The standing crop was lowest in the fall for both years that included samples in September. For example, in year three the average standing crop was 108 ± 17 tests/10cm^3 in fall compared to an average of 178 ± 60 tests/10cm^3 for the rest of

the year. Of the four dominant species, *J. macrescens* had the largest average range in standing crop (average of 96 ± 63) but the smallest CV (average of 25 ± 13%) among replicate samples. Similar to the total count, year one had the highest average range in count size among replicates (181 ± 52 tests) and the greatest CV (44 ± 8%).

The second most dominant species, *A. inepta*, had a standing crop that varied from 2 to 124 tests/10 cm^3 (average 30 ± 30 tests/10 cm^3). *A. inepta* exhibited no clear seasonal pattern. *A. inepta* had an average range in standing crop among replicate samples of 42 ± 31 tests and of the four dominant species at Monitoring Station 4, *A. inepta* had the highest average CV among replicates of 69 ± 26%. The CV was lowest in the fall for both years that included samples in September. For example, in year three the CV was 33% in fall compared to an average of 66 ± 26% for the rest of the year.

The third and fourth most dominant species, *B. pseudomacrescens* and *Haplophragmoides* spp. had standing crops that varied from 0 to 56 tests/10 cm^3 (average of 15 ± 14 tests/10 cm^3). *Haplophragmoides* standing crop showed annual increases from an average of 7 ± 5 tests/10 cm^3 in year one to 22 ± 10 tests/10 cm^3 in year three. In contrast, *B. pseudomacrescens* standing crop showed annual decreases during the study period from an average of 24 ± 14 tests/10 cm^3 in year one to 6 ± 5 tests/10 cm^3 in year three. Neither *B. pseudomacrescens* nor *Haplophragmoides* spp. exhibited a seasonal pattern. Of the four dominant species at Monitoring Station 4, *B. pseudomacrescens* and *Haplophragmoides* spp. had the smallest average range in standing crop among replicate samples of 19 ± 17 and 14 ± 7 tests, respectively.

The live foraminifera assemblage at Monitoring Station 4 had smaller standing crops compared to the dead assemblage, and the largest live count sizes of the four monitoring stations, with count sizes ranging from 0 to 268 tests/10 cm^3 with an average of 74 ± 69 tests/10 cm^3 (Appendix E). The standing crop of foraminifera was greatest in year two when a total of 1858 tests were counted (average 98 ± 74 tests/10 cm^3). The average coefficient of variation (CV) among replicates was 40 ± 30%, respectively. Of the four Monitoring Stations, Station 4 had the lowest average CV among replicates. We identified 8 live foraminifera species from Monitoring Station 4, which were dominated by *Jadammina macrescens*, *Ammoastuta inepta*, *Balticammina pseudomacrescens*, and *Haplophragmoides* spp. (Appendix E). These are the same four dominant species found in the dead assemblage. None of the species in the live assemblage exhibited a clear seasonal pattern.

4.7. Post-Flood Sampling Foraminifera Results

The samples taken after the flooding events in October 2015 and February 2016 had comparable dead foraminifera standing crops, overall species assemblages, and dominant species compared to the rest of the three-year sampling period. The sample from Monitoring Station 1 after flooding associated with Hurricane Joaquin in October 2015 had a standing crop of 134 tests/10 cm^3 (Figure 5). The sample contained 5 species and was dominated by *T. inflata*, *J. macrescens*, and *T. comprimata*, in order of most to least abundant, which is the same as other sampling periods.

The sample from Monitoring Station 1 after flooding in January 2016 had a standing crop of 110 tests/10 cm^3 and was also dominated by *T. inflata*, *J. macrescens*, and *T. comprimata* (Figure 5). At Monitoring Station 2, the sample contained 6 species with a total standing crop of 338 tests/10 cm^3 (Figure 6). The sample was dominated by *J. macrescens*, *B. pseudomacrescens*, and *T. comprimata*, which are the same dominant species found throughout the three years. At Monitoring Station 3, the standing crop was 354 tests/10 cm^3 (Figure 7). We identified 8 species, which were dominated by *T. comprimata*, *Haplophragmoides* spp., and *T. inflata*. *T. comprimata* and *Haplophragmoides* spp. were two of the three dominant species at Station 3 over the three years, in addition to *B. pseudomacrescens*. However, *T. inflata* was the overall fourth dominant species over the sampling period at Station 3 and *B. pseudomacrescens* was present in the post-flooding sample. At Monitoring Station 4, the sample contained 6 species with a total standing crop of 344 tests/10 cm^3 (Figure 8). The dominant species were *J. macrescens*, *A. inepta*, *Haplophragmoides* spp., and *M. petila*. *J. macrescens*, *A. inepta*, and *Haplophragmoides* spp. were three of the four dominant species at Station 4 over the three years, in addition to *B. pseudomacrescens*. However, *M. petila* was the overall fifth dominant species over the sampling period at Station 4 and *B. pseudomacrescens* was present in the post-flooding sample.

4.8. Stable Carbon Isotope Geochemistry

$\delta^{13}C$ values across the stations ranged from -15.7‰ to -28.0‰. Stations 1, 2, and 3 all had average $\delta^{13}C$ values less depleted than -18.9‰, which is associated with a C_4 dominated salt-marsh plant community and corresponds to all three of these sites' *Spartina* vegetation

(Figure 9). Station 1 bulk sediment samples had an average $\delta^{13}C$ value of -16.7‰ ± 0.5 over the three years, Station 2 had an average $\delta^{13}C$ value of -15.7‰ ± 0.5, and Station 3 had an average $\delta^{13}C$ value of -17.5‰ ± 1.8. Stations 1 and 2 exhibited some replicate variability (<1.5‰) and variability through time (<2.4‰), but $\delta^{13}C$ values always remained within the range for C_4 plant communities. Station 3 also exhibited some replicate variability (<0.2‰) and variability through time (<2.0‰) for the first two and half years; however, in the spring and summer of the third year, $\delta^{13}C$ values became more depleted (-19.2‰ to -22.7‰) towards intermediate values between C_3 and C_4 plant communities and closer to C_3 vegetation. Two additional samples from Station 3 taken three months and six months after the anomalous values showed a return to less depleted values (-18.2‰; -17.1‰), which were consistent with the first two and a half years of measurements. Station 4 had an average $\delta^{13}C$ value of -28.0‰ ± 0.2, indicating a C_3 dominated salt-marsh plant community, which corresponds to Station 4's *Phragmites australis* vegetation (Figure 9). Station 4 $\delta^{13}C$ values exhibited the least variability through time (<0.7‰) among the four stations.

4.9. Bayesian Transfer Function Elevation Estimates

We ran a Bayesian transfer function on the foraminiferal data from each sampling period for each monitoring station to obtain an elevation estimate for each monitoring station. We illustrate the analysis for Station 1 in Figure 10 with the remaining stations summarized in Table 2 and Appendix F.

Under a 95% uncertainty interval, all samples from each monitoring station predicted a SWLI estimate within the observed elevation range of that station. For example, at Monitoring Station 1 (observed elevation = 212-223), the smallest 95% uncertainty interval ranges from 178-257 SWLI units, and the largest interval ranges from 120-275 SWLI units. Monitoring Station 1 had the smallest range (197-219) of SWLI estimates among the stations and Monitoring Station 3 had the largest range (133-240). In addition, of the four stations, Monitoring Station 1 had the smallest average SWLI uncertainty in elevation estimates at 26.5 SWLI units, while Monitoring Station 3 had the largest average SWLI uncertainty at 36.5 SWLI units.

SWLI estimates have a relationship with count size and the presence or greater number of rare species. Samples with a smaller count size compared to replicates taken at the same time often have an anomalous SWLI estimate. For example, in Summer 2015 at Monitoring Station 2 (observed elevation = 211-224), the four replicate samples had comparable foraminifera assemblages, but count sizes of 480, 554, 228, and 488 tests and SWLI estimates of 226, 222, 195, and 222, respectively. The presence of rare species, such as *M. fusca* or *Ammobaculites* spp. appears to decrease a sample's SWLI estimate, while *M. petila* appears to increase a sample's SWLI estimate. For example, in Spring 2016 at Monitoring Station 1 (observed elevation = 212-223), the four replicate samples had SWLI estimates of 212, 211, 213, and 201. The replicates had comparable assemblages, except the fourth sample had the presence of *M. fusca* (2 tests).

Replicate sample assemblages were added together to produce a replicate-aggregate SWLI estimate for each sampling period for each station to examine the influence of combining replicate samples taken from a small-scale spatial area on elevation estimates. The range in all SWLI estimates decreased in all four stations when using the replicate-aggregate dataset with the largest decrease at Station 4 (74 SWLI units). The replicate-aggregate dataset decreased the average uncertainty in the SWLI estimates compared to using the full dataset at Monitoring Stations 1, 2, and 4, with the greatest decrease of 11 SWLI units at Station 4; uncertainty did not change at Monitoring Station 3. Of the four seasons, the average uncertainty in the SWLI estimates with the replicate-aggregate dataset compared to using the full dataset decreased for all seasons at Monitoring Stations 1, 2, and 4, with the greatest decrease in Fall for Stations 1 and 2 and in Winter for Station 4. The uncertainty was reduced only in Fall (by 1.5 SWLI units) and Summer (by 1 SWLI unit) at Station 3.

All sample assemblages for each season within each station were also added together to produce a seasonal-aggregate SWLI estimate for each season for each station to examine the influence of seasonal variability of foraminifera on elevation estimates. The average of the Fall, Winter, Spring, and Summer seasonal-aggregate SWLI estimates for each monitoring station did not significantly change from the average SWLI estimate using the full dataset or the replicate-aggregate dataset. The range in all SWLI estimates further decreased from the replicate-aggregate dataset at Stations 1, 3, and 4 when using the seasonal-aggregate dataset with the largest decrease at Station 3 (43 SWLI units). The Fall and Winter seasonal estimates for each monitoring station were within 3 SWLI units of the observed station elevations, while the Spring and Summer seasonal estimates were up to

15 SWLI units different from the observed station elevations. The seasonal-aggregate dataset also lowered the uncertainty in the SWLI estimates compared to using the full dataset or the replicate-aggregate dataset for all seasons except Summer at Monitoring Stations 1 and 4. The uncertainty was reduced only in Winter (by 3.5 SWLI units) and Summer (by 1 SWLI unit) at Station 2 and only in Winter at Station 3 (by 4.5 SWLI units).

4.10. Informing Variability in the Bayesian Transfer Function

The species variance analysis of the entire raw foraminifera dataset illustrates that the variation across monitoring stations made up ~87% of the total variation in the foraminiferal dataset, while the remaining ~13% of the variation can be explained by temporal and/or spatial variability among the replicates. The combination of the variation across monitoring stations and the variation among replicates contributed to an overall variation term that was estimated for the dominant species and subsequently incorporated into the Bayesian transfer function. *J. macrescens*/*B. pseudomacrescens* had the smallest amount of variability overall (across stations and replicates) with a sigma of 2.93. The variation across monitoring stations made up ~77% of the total variation for *J. macrescens*/*B. pseudomacrescens*, while the remaining ~23% of the variation can be explained by the variability among the replicates. *A. inepta* had the largest amount of variability with a sigma of 7.05. The variation across monitoring stations made up ~91% of the total variation for *A. inepta*, while the remaining ~9% of the variation can be explained by the variability among the replicates. For the analysis of each of the remaining dominant species, 79-84% of the variation is attributed to across-station variability and 16-21% is attributed to replicate variability.

We incorporated the species-specific temporal and spatial uncertainty from the species variance analysis into the Bayesian transfer function by providing informative priors for the relevant variation parameters in the model (foraminifera variability prior). This is in addition to a geochemistry prior (Cahill et al., 2016) used to inform elevation estimates. The Bayesian transfer function with/without the informative foraminifera variability prior was applied to the fossil foraminiferal data from a southern New Jersey relative sea-level record of Kemp et al. (2013) (Figure 11). The PME estimates from the transfer function were consistent with and without the informative foraminifera variability prior. The average difference in PME estimates was <0.01 m and all PME estimates overlapped within the 95% uncertainty interval. Furthermore, the average difference in PME estimate uncertainties was 0.01 m. However, it is worth noting that 72% of the PME estimates using the informative foraminifera variability prior were lower than the PME estimates with the uninformative prior, by up to 0.5 m, but there was no clear pattern with the fossil foraminiferal assemblages. 86% of the PME estimate uncertainties were greater when using the informative prior, by up to 0.05 m, but also had no clear pattern with the foraminiferal assemblages.

As one would expect, the Errors-In-Variables Integrated Gaussian Process model found very similar RSL change over the past ~1000 years: ~1.64 m rise with the uninformative foraminifera variability prior and a ~1.61 m rise with the informative prior (Figure 11). Furthermore, the average difference in rate predictions was 0.04 ± 0.12 mm/yr and all rate predictions overlapped within the 95% uncertainty interval. Differences in predicted rates

were largest at the beginning (~0.12 mm/yr) and end (~0.35 mm/yr) of the record where rate predictions from the model have the largest uncertainties.

5. Discussion

5.1. Foraminifera Distributions

The dead foraminiferal distributions from the high marsh and high marsh-upland transition monitoring stations in the Mullica River-Great Bay estuary are similar to other studies in New Jersey and on the U.S. mid-Atlantic coast (e.g. Culver et al., 1996; Hippensteel et al., 2000; Kemp et al., 2011). The four monitoring stations were dominated by *T. inflata*, *J. macrescens*, *T. comprimata*, *B. pseudomacrescens*, *Haplophragmoides* spp., and *A. inepta*. Although Stations 1, 2, and 3 are all located in high marsh above MHHW and Station 4 in high marsh-upland transition above MHHW, the foraminiferal assemblages and dominant foraminifera differ. PAM analysis showed that 173 of the 184 samples were grouped corresponding to the monitoring station they were sampled from, and the species variance estimates illustrated that the variation across monitoring stations made up ~85% of the total variation in the foraminiferal dataset, demonstrating unique site-specific assemblages.

High marsh assemblages of dead foraminifera have been shown to vary both among and within regions (e.g. Ellison and Nichols, 1976; Wright et al., 2011, Kemp et al., 2013). While salt-marsh foraminifera distributions are strongly linked with tidal elevation (e.g. Horton and Edwards, 2006; Kemp et al., 2013), variability in foraminiferal assemblages among high marsh sites may be controlled by secondary environmental factors such as salinity (e.g. Nikitina et al., 2003; Kemp et al., 2009; Wright et al., 2011; Kemp et al., 2012,

2013). Our four monitoring stations exhibit a salinity gradient which varies by up to 35 psu among the stations. Along the Atlantic coast of North America, Wright et al. (2011) demonstrated the spatial differences in high marsh foraminifera assemblages among regions. Similarly, in the Chesapeake Bay region, middle and high-marsh environments consist of assemblages of variable proportions of several dominant species, which were correlated with salinity gradients (Ellison et al., 1965; Ellison and Nichols, 1976). In North Carolina and New Jersey, Kemp et al. (2009, 2013) also found sub-regional groups of foraminifera from high marsh environments where spatial differences in species composition likely reflected the distribution of salinity regimes of the region due to the balance between marine tidal influence and freshwater input from rivers at individual sites. The organic content varies by up to 50% and grain size varies from a fine silt to sandy silt among stations; however, substrate variability has been shown to have minimal influence on marsh foraminiferal assemblages (Alve and Murray, 1999; Horton and Edwards, 2006).

Monitoring Station 1 is found in *Spartina alterniflora* (short form) high marsh, with the highest salinity (39.6 ± 8.8) of the 4 monitoring stations and a foraminifera assemblage dominated by agglutinated species *Trochammina inflata*, *Jadammina macrescens*, and *Tiphotrocha comprimata*. Similar foraminiferal assemblages have been observed in high marsh/high salinity salt marshes. On the U.S. mid-Atlantic coast, *T. inflata* has been recognized as a dominant species in the middle and high marsh (e.g. Hippensteel et al., 2000; Kemp et al., 2009; Kemp et al., 2012). In North Carolina, Kemp et al. (2009) also found *T. inflata*-dominated assemblages associated with higher salinity sites. Kemp et al.

(2012) recognized distinct high marsh groups with varying proportions of *T. inflata*, *J. macrescens*, and *T. comprimata* in New Jersey.

Monitoring Stations 2 and 3 are both found in high marsh/low salinity environments. While both stations are above MHHW and the salinity at these two stations is comparable (Station 2 with an average of 13.7 ± 4.9 and Station 3 with an average of 13.1 ± 4.9), Station 2 has a foraminiferal assemblage dominated by agglutinated *Jadammina macrescens*, *Balticammina pseudomacrescens*, *Tiphotrocha comprimata*, and Station 3 has a foraminiferal assemblage dominated by agglutinated *Balticammina pseudomacrescens*, *Tiphotrocha comprimata*, and *Haplophragmoides* spp. However, Station 3 has a slightly lower elevation than Station 2 and the hummocky nature of the marsh surface at Station 3 results in a larger elevational range (192-228 SWLI units) that was sampled at this monitoring station, which could contribute to the differences in foraminifera assemblages between these two stations. For example, De Rijk and Troelstra (1997) noted variability in assemblages due to local variations in elevation and salinity from the effects of unvegetated marsh surface areas and pond holes with changing salinities from the influence of tides. Further, 10 of the 11 samples that were not assigned to a PAM analysis group corresponding to the monitoring station they were sampled from were from Stations 2 and 3. This incorrect grouping and the lower silhouette widths of these 10 samples suggests a less consistent assemblage over time.

Similar foraminiferal assemblages have been observed in high marsh/low salinity salt marshes that correspond to both Stations 2 and 3. In New Jersey and North Carolina, high

marsh assemblages have been dominated by *J. macrescens*, *T. comprimata*, and *Haplophragmoides* spp. (Kemp et al, 2009, 2012, 2013). Assemblages dominated by *T. comprimata*, which is a dominant species at both Stations 2 and 3, have specifically been associated with lower salinity sites (Kemp et al., 2013). Kemp et al. (2012) found lower abundances of *B. pseudomacrescens* in the high marsh in New Jersey, although it is a dominant species at both Stations 2 and 3. *B. pseudomacrescens* has not been recorded in North Carolina or Virginia (Spencer, 2000; Kemp et al., 2009; Wright et al., 2011), but has been more prevalent in New England and Newfoundland, Canada (de Rijk, 1995; de Rijk and Troelstra, 1997; Gehrels and van de Plassche, 1999; Edwards et al., 2004; Wright et al., 2011). In New Jersey, *Haplophragmoides* spp., which is a dominant species at Station 3, has been found to be a dominant species in high marsh and transitional high marsh-upland environments, often above MHHW (Kemp et al., 2012, 2013), and in Massachusetts, *Haplophragmoides* spp. has been associated with low salinity, high marsh settings (de Rijk, 1995; de Rijk and Troelstra, 1997).

Monitoring Station 4 is found in *Phragmites australis* high marsh-upland transition, with the lowest salinity (2.9 ± 2.0) and highest elevation (248-264 SWLI) of the 4 monitoring stations. The foraminiferal assemblage is dominated by agglutinated species *Jadammina macrescens*, which is consistent with other studies on the U.S. mid-Atlantic coast which found maximum abundances of *J. macrescens* in high marsh-upland transition environments with low salinities (e.g. Spencer, 2000; Nikitina et al., 2003; Robinson and McBride, 2006; Horton and Culver, 2008; Kemp et al., 2009). Beginning with the work of Scott and Medioli (1978, 1980), salt-marsh foraminifera assemblages dominated by *J.*

macrescens have been considered the highest elevational zone at the high marsh-upland transition. *Ammoastuta inepta*, *Balticammina pseudomacrescens*, and *Haplophragmoides* spp. are also found in high abundances at Station 4. In low salinity, brackish high marsh-upland transition environments, *A. inepta* has been found to be a dominant species in New Jersey and North Carolina (Scott et al., 2001; Culver and Horton, 2005; Kemp et al., 2009; Kemp et al, 2013). In New Jersey, Kemp et al. (2012, 2013) found low abundances of *B. pseudomacrescens* in the highest marsh zones and found greater abundances of *Haplophragmoides* spp. in transitional environments above MHHW.

5.2. Temporal Variability

Modern dead assemblages (compared to live or live plus dead assemblages) have been used for sea-level studies, because they most resemble subsurface assemblages and they are thought to minimize temporal variability in modern distributions (e.g. Horton, 1999; Horton and Edwards, 2003; Morvan et al., 2006). Similarly, the dead foraminiferal assemblages and dominant species from the Mullica River-Great Bay estuary remained relatively consistent temporally at each monitoring station during the three-year study period. The species variance analysis suggests that only ~13% of the variation in foraminiferal assemblages can be explained by temporal and/or spatial variability among the replicates.

The variations in annual standing crop that were observed did not have a relationship with time. For example, Station 1's standing crop was greatest in year three whereas Station 2's was greatest in year one, Station 3's was greatest in year two, and Station 4's standing crop

remained stable over the three years. The inconsistency in total and individual standing crops annually among stations suggests changes in regional atmospheric and oceanic climate (air temperature, precipitation, sea surface temperature, salinity, tides) did not drive variability in standing crop (Figure 2). It is likely that the observed changes in standing crop are part of natural interannual fluctuations. Other studies have also found differing foraminiferal densities between years and no clear annual pattern in standing crops (e.g. Murray and Alve, 2000; Buzas et al., 2002; Hippensteel et al., 2002). Seasonal variability of individual foraminiferal species was also inconsistent among the four monitoring stations. For example, although *T. comprimata* exhibited a seasonal pattern at two of the three monitoring stations where it was a dominant species, an opposite seasonal pattern was observed. The absence of a translation from live foraminifera seasonal life cycles into the dead assemblage has been documented (Horton and Murray, 2006, 2007; Morvan et al., 2006).

Additionally, specific storm and flooding events did not affect dead foraminiferal assemblages and dominant species. Since the sampling occurred approximately two weeks after the flooding events, it is evident that the marsh assemblages either experienced no change or rapidly recovered. There was no evidence for the influence of flooding on the marshes, such as the presence of overwash material which can be deposited in marsh environments and identified using changes in foraminifera assemblages (e.g. Hippensteel and Martin, 1999; Culver et al., 2006; Pilarczyk et al., 2014). Therefore, these flooding events were likely not large enough to deposit evidence onto the marshes. Further, after extreme changes in climate, foraminifera assemblages remained unaffected. For example,

May 2015 was the statewide third driest May on record in New Jersey from 1895-2018, which was followed by the fourth wettest June on record the following month, and samples taken at the end of June showed no change in assemblages. Therefore, the dead foraminifera assemblages remained stable despite climate variability and storm and flooding events.

5.3. Spatial Variability

Most studies of small-scale spatial variability of foraminiferal assemblages in salt marshes have focused on living populations (Lynts, 1966; Buzas, 1968; Buzas, 1970; Schafer, 1971; Swallow, 2000; Buzas et al., 2002); few have considered dead assemblages (Morvan et al., 2006; Kemp et al., 2011). However, many studies have stressed the importance of replicate sampling when studying modern foraminifera (Buzas, 1969; Schafer, 1971; Murray and Alve, 2000, Buzas et al., 2002).

Foraminiferal assemblages and dominant species from the Mullica River-Great Bay estuary remained consistent on small spatial scales at each monitoring station over the study period. Kemp et al. (2011) also found that dead foraminifera in high marsh environments exhibited a non-patchy distribution, as well as Buzas (1968) and Morvan et al. (2006) in other subtidal and intertidal environments. The four monitoring stations had comparable average CVs among replicates ranging from 26 to 33%. Further, the most dominant species at each station had the smallest average CV of all of the dominant species at that station, suggesting greater consistency of the most dominant species among replicate samples.

Standing crop, however, varied among replicate samples. For example, the range of total standing crop among replicates at Monitoring Station 3 was 407 ± 235 tests/10 cm^3. Observed small-scale spatial variability in standing crop may be due to a variety of environmental factors affecting the live assemblage, including response to predation (Buzas, 1978, 1982), reproduction (Stouff et al., 1999), availability of food resources (Alve and Murray, 2001; Fontanier et al., 2003) and species interactions (Buzas, 1968; Hayward et al., 1996; Scott et al., 2001), which then may be influencing the distribution of the dead assemblages.

5.4. Stable Carbon Isotope Geochemistry

Bulk sediment $\delta^{13}C$ values are used to represent the dominant vegetation, since the dominant input to salt-marsh sediment is in-situ vegetation (Chmura and Aharon, 1995; Malamud-Roam and Ingram, 2001; Malamud-Roam and Ingram, 2004; Lamb et al., 2006). Monitoring Stations 1, 2, and 3 had average bulk sediment $\delta^{13}C$ values ranging from -15.7‰ to -17.5‰ over the three-year sampling period, which is associated with a C_4 dominated salt-marsh plant community and corresponds to all three of these sites' *Spartina* vegetation. Kemp et al. (2012) found similar bulk sediment $\delta^{13}C$ values for *Spartina*-dominated salt marsh zones in southern New Jersey, ranging from -18.9% to -15.4%. These values are also consistent with other *Spartina* marshes on the U.S. mid-Atlantic coast (e.g. Ember et al., 1987; Middleburg et al., 1997; Kemp et al., 2010). Station 4 had an average $\delta^{13}C$ value of -28.0‰ ± 0.2, indicating a C_3 dominated salt-marsh plant community, which corresponds to Station 4's *Phragmites australis* vegetation. Kemp et al. (2012) found

slightly less depleted bulk sediment $\delta^{13}C$ values for brackish transition marsh zones vegetated by *Phragmites australis*, *Iva fructescens*, and *Typha* spp. in southern New Jersey, ranging from -27.0% to -22.0%. In Massachusetts, Middleburg et al. (1997) recorded a bulk sediment $\delta^{13}C$ value of -24.5% in a salt marsh-upland transition zone vegetated by *Phragmites australis*, *Typha* spp., and *Scirpus* spp.

The temporal and small-scale spatial variability observed at Stations 1, 2 and 4 was very minimal and $\delta^{13}C$ values always remained within the range for C_4 (Stations 1 and 2) or C_3 (Station 4) plant communities. The stability in $\delta^{13}C$ values at these three stations suggests inconsequential influence from seasonal, interannual, or small-scale spatial changes. Milker et al. (2015) also found no significant influence of interannual variations in bulk salt-marsh sediment $\delta^{13}C$ values from three sampling periods over two years. Station 3 also exhibited minimal temporal and spatial variability for the first two and half years; however, in the spring and summer of the third year, $\delta^{13}C$ values became more depleted (-19.2‰ to -22.7‰) towards intermediate values between C_3 and C_4 plant communities and closer to C_3 vegetation. Additional samples from Station 3 taken three months and six months after the anomalous values showed a return to less depleted values (-18.2‰; -17.1‰), which were consistent with the first two and a half years of measurements. The anomalous $\delta^{13}C$ values during two sampling periods most likely suggests a small-scale spatial influence in the marsh environment. For example, bulk sediment $\delta^{13}C$ measurements could be influenced by allochthonous material as dissolved or particulate matter (Lamb et al., 2006; Gebrehiwet et al., 2008). Station 3 is positioned in *Spartina*-vegetated marsh, but is located on the border of *Phragmites australis*. Since *Phragmites australis* has more depleted $\delta^{13}C$

values, it is possible that fragments of *Phragmites australis* were introduced into the two samples with anomalous $\delta^{13}C$ values, perhaps through tidal activity, resulting in more depleted $\delta^{13}C$ values. These results suggest that replicate sampling might be beneficial in those locations on the border of different vegetation communities to account for the potential influence of allochthonous material to the sampling location.

In order to use stable carbon isotope geochemistry as a sea-level indicator, it is necessary to understand the relationship between bulk sediment $\delta^{13}C$ values and tidal elevation (Shennan, 1986; van de Plassche, 1986; Khan et al., 2015). For example, the transition between C_3 and C_4 dominated salt-marsh plant communities has been shown to act as the boundary for the mean higher high water (MHHW) tidal datum on the U.S. mid-Atlantic coast (e.g. Middleburg et al., 1997; Johnson et al., 2007; Kemp et al., 2012). From three sites in southern New Jersey, Kemp et al. (2012) found that $\delta^{13}C$ values of salt-marsh bulk sediment >-22.0‰ were found above MHHW, while values < -18.9‰ were found between mean tide level (MTL) and MHHW. Monitoring Station 4 is consistent with these findings since it has $\delta^{13}C$ values >-22.0‰ and is found above local MHHW. However, Monitoring Stations 1, 2 and 3 in *Spartina* marshes are also found above their local MHHW, but have $\delta^{13}C$ values < -18.9‰. Site-specific ecological conditions could alter the distribution of dominant vegetation as it relates to a tidal datum (e.g. McKee and Patrick, 1988; Kemp et al., 2012; Kemp et al., 2017). For example, McKee and Patrick (1988) observed that elevation limits of *Spartina alterniflora* do not always correspond to a consistent elevation relative to a tidal datum. The variation in *Spartina alterniflora* vertical distribution was

attributed primarily to differences in tidal range; however, local differences in salinity, nutrients, or physical disturbance may also have an influence (McKee and Patrick, 1988).

5.5. Implications for Sea-level Studies

The consistency of the dead foraminiferal assemblages from the Mullica River-Great Bay estuary is reflected by the SWLI estimates for Stations 1-4 from the Bayesian transfer function (Figure 10, Appendix F). The 95% uncertainty interval for each SWLI estimate contained the observed elevation for each sample from its corresponding monitoring station. Station 4 had the largest percentage of estimates within the observed elevation range, which is likely due to the fact that all of the foraminiferal assemblages from this station were overwhelmingly dominated by *J. macrescens*. Using the species variance analysis, *J. macrescens*/*B. pseudomacrescens* had the smallest amount of variability overall (across stations and replicates) with a sigma of 2.93. Additionally, near-monospecific assemblages of *J. macrescens* are consistently associated with the highest elevational zone at the high marsh-upland transition (e.g. Scott and Medioli, 1978, 1980; Spencer, 2000; Horton and Culver, 2008; Kemp et al., 2009). Scott and Medioli (1978, 1980) suggested this assemblage was restricted to a 6 cm vertical range below highest astronomical tide (HAT).

The variability in standing crop and the presence of rare species of the foraminiferal assemblages influenced the elevation estimates and uncertainty from the Bayesian transfer function. Samples with a smaller count size compared to replicates taken at the same time often have a SWLI estimate that is anomalous compared to the other replicates, suggesting

the importance of count size in quantitative studies of foraminifera (e.g. Buzas, 1990; Hayek and Buzas, 1997; Fatela and Taborda, 2002). Other studies recommend microfossil count sizes as low as 50-100 specimens if only the dominant species are being studied, while counts of 300-1000 specimens may be necessary to fully understand the rarer species (Fatela and Taborda, 2002; Patterson and Fishbein, 1989).

The presence or greater number of rare species, *M. fusca* or *Ammobaculites* spp., appears to consistently decrease that sample's SWLI estimate, while the presence or greater number of *M. petila* consistently increases that sample's SWLI estimate. These findings can be understood by the fact that *M. fusca* and *Ammobaculites* spp. are associated with lower elevations (e.g. Hippensteel et al., 2000; Edwards et al., 2004; Horton and Culver, 2008) while *M. petila* is associated with higher elevations (e.g. Scott and Medioli, 1978; Spencer, 2000; Kemp et al., 2009, 2013).

Combining foraminiferal data from replicate samples decreased elevation estimate uncertainty, suggesting the addition of replicate samples provides a greater understanding of a modern site's foraminiferal distributions (e.g. Schafer, 1971; Murray and Alve, 2000, Buzas et al., 2002). Combining foraminiferal data from samples taken in the same seasons generally further lowered elevation estimate uncertainties compared to the replicate-aggregate dataset. Both replicate-aggregate and seasonal-aggregate datasets had more accurate SWLI estimates, as well as lower uncertainties, in Fall and/or Winter compared to Spring or Summer. In a seasonal study of foraminifera, Horton and Edwards (2003) also found that the greatest transfer function precision was obtained using samples collected in

the Winter months and the weakest in the Summer, and suggested a modern foraminifera training set that includes samples spanning all seasons will provide the best-quality data for sea-level studies. Our study supports these findings in that a training set including samples from all seasons, as well as spatial replicate samples, will provide the most informative modern foraminifera data and transfer function estimates with the lowest uncertainties.

For the first time, an informative prior has been developed to account for temporal and spatial variability of modern foraminifera to include in transfer functions to reconstruct relative sea-level change. Incorporating an informative foraminiferal variability prior into the Bayesian transfer function for the Kemp et al. (2013) southern New Jersey record minimally affected paleomarsh elevation (PME) estimates due to the consistency of the Mullica River-Great Bay estuary modern foraminifera assemblages through time and space. All PME estimates with and without the informative foraminifera variability prior overlapped within a 95% uncertainty interval, indicating the minimal influence that temporal/spatial foraminiferal variability in high marsh environments has on RSL reconstructions. High marsh sedimentary environments have been used for sea-level studies partly because of the consistency of high marsh foraminifera assemblages and their narrow elevation zones (e.g. Gehrels, 2000; Kemp et al., 2011; Wright et al., 2011).

In addition, differences in PME estimate uncertainties with and without the informative foraminifera variability prior was minimal; however, most of the uncertainties of the PME estimates were slightly greater when using the informative foraminifera variability prior,

but only at an average of 0.01 m. Similarly, when applied to a RSL reconstruction, total RSL change and predicted rates of change over the past ~1000 years were comparable with and without the informative prior and overlapped within a 95% uncertainty interval. Therefore, although foraminiferal variations have been shown to affect elevation boundaries of foraminiferal zones by as much as 15% of the tidal range (Horton and Edwards, 2003), accounting for modern foraminifera variability still provides consistent high marsh RSL reconstructions.

Salt-marsh foraminifera have been widely used as a proxy for high resolution sea-level reconstructions (e.g. Gehrels 1994; Horton and Edwards, 2006; Kemp et al., 2013). This study demonstrates that foraminiferal-based RSL reconstructions remain robust and reproducible even when accounting for temporal and spatial variability of salt-marsh foraminifera in the modern environment. The informative foraminifera variability prior could be applied to locations with similar high marsh foraminifera assemblages to our study sites in the Mullica River-Great Bay estuary in southern New Jersey, such as elsewhere along the U.S. Atlantic coast (e.g. Culver et al., 1996; Hippensteel et al., 2000; Kemp et al., 2011), where modern foraminifera assemblages have the potential to exhibit temporal and/or small-scale spatial variability.

6. Conclusion

A detailed understanding of salt-marsh foraminifera in the modern environment is necessary to produce relative sea-level reconstructions using foraminiferal-based transfer functions. We sampled four high marsh monitoring stations in the Mullica River-Great Bay

estuary every three months over three years to examine seasonal and interannual changes and small-scale spatial variability in dead modern foraminifera assemblages.

We found four site-specific assemblages where the variation across monitoring stations explained ~87% of the total variation in the foraminiferal dataset, while the remaining ~13% of the variation can be explained by temporal and/or spatial variability among the replicates. We demonstrated that overall foraminiferal assemblages and dominant foraminifera species at each monitoring station over the study period remain consistent both temporally and spatially among replicate samples, including after storm and flooding events. Variations in annual standing crop and among replicate samples did not exhibit any interannual or seasonal patterns. Temporal and small-scale spatial variability in $\delta^{13}C$ values at each station was very minimal.

Using a Bayesian transfer function with a modern foraminifera training set for New Jersey, we found that under a 95% uncertainty interval, all samples from each monitoring station predicted a SWLI estimate within the observed elevation range of that station. Combining replicate samples into a replicate-aggregate dataset lowered the uncertainty of elevation estimates and a seasonal-aggregate dataset further lowered elevation estimate uncertainties. Overall, for the replicate-aggregate and seasonal-aggregate datasets, samples from Fall and Winter months had more accurate elevation estimates, as well as lower uncertainties, compared to Spring and Summer.

Incorporating an informative foraminifera variability prior to account for temporal and spatial changes in modern foraminifera distributions into a relative sea-level record in New Jersey from Kemp et al. (2013), resulted in minimal changes in paleomarsh elevation estimates. Paleomarsh elevation estimate uncertainties only minimally increased when using the informative foraminifera variability prior. Further, reconstructed relative sea-level and rates of change were comparable with and without using the informative prior. Therefore, including an informative foraminifera variability prior in relative sea-level reconstructions to account for temporal and spatial uncertainties in modern foraminifera distributions still results in a robust relative sea-level record.

Acknowledgements

Author Jennifer Walker thanks Steve Culver and Andrew Kemp for their assistance in foraminiferal identification and analysis and thanks Isabel Hong, Ane Garcia-Artola, Andra Garner, and Tina Dura for their assistance in the field. JW was funded by the David and Arleen McGlade Foundation, a Cushman Foundation for Foraminiferal Research Student Research Award, and a Rutgers University Marine Field Station Graduate Student Award.

References

Alve, Elisabeth, and John W. Murray. 1999. "Marginal Marine Environments of the Skagerrak and Kattegat: A Baseline Study of Living (Stained) Benthic Foraminiferal Ecology." *Palaeogeography, Palaeoclimatology, Palaeoecology* 146 (1): 171–93. https://doi.org/10.1016/S0031-0182(98)00131-X.

Alve, Elisabeth, and John W. Murray. 2001. "Temporal Variability in Vertical Distributions of Live (Stained) Intertidal Foraminifera, Southern England." *Journal of Foraminiferal Research* 31 (1): 12–24. https://doi.org/10.2113/0310012.

Balslev-Clausen, David, Tais W. Dahl, Nabil Saad, and Minik T. Rosing. 2013. "Precise and Accurate Δ13C Analysis of Rock Samples Using Flash Combustion–Cavity Ring Down Laser Spectroscopy." *Journal of Analytical Atomic Spectrometry* 28 (4): 516. https://doi.org/10.1039/c2ja30240c.

Berkeley, A., C.T. Perry, S.G. Smithers, and B.P. Horton. 2008. "The Spatial and Vertical Distribution of Living (Stained) Benthic Foraminifera from a Tropical, Intertidal Environment, North Queensland, Australia." *Marine Micropaleontology* 69 (2): 240–61. https://doi.org/10.1016/j.marmicro.2008.08.002.

Bernhard, J. M. 1988. "Postmortem Vital Staining in Benthic Foraminifera; Duration and Importance in Population and Distributional Studies." *Journal of Foraminiferal Research* 18 (2): 143–46. https://doi.org/10.2113/gsjfr.18.2.143.

Buzas, M. A. 1968. "On the Spatial Distribution of Foraminifera." *Contributions from the Cushman Foundation for Foraminiferal Research* 19.

Buzas, M. A. 2002. "Foraminiferal Densities over Five Years in the Indian River Lagoon, Florida: A Model of Pulsating Patches." *The Journal of Foraminiferal Research* 32 (1): 68–92. https://doi.org/10.2113/0320068.

Buzas, M. A. 1965. "The Distribution and Abundance of Foraminifera in Long Island Sound." *Smithsonian Miscellaneous Collections* 149 (1): 1–88.

Buzas, M. A. 1969. "Foraminiferal Species Densities and Environmental Variables in an Estuary." *Limnology and Oceanography* 14 (3): 411–22. https://doi.org/10.4319/lo.1969.14.3.0411.

Buzas, M. A. 1970. "Spatial Homogeneity: Statistical Analyses of Unispecies and Multispecies Populations of Foraminifera." *Ecology* 51 (5): 874–79. https://doi.org/10.2307/1933980.

Buzas, M. A. 1978. "Foraminifera as Prey for Benthic Deposit Feeders: Results of Predator Exclusion Experiments." *Journal of Marine Research* 36 (4): 617–625.

Buzas, M. A. 1982. "Regulation of Foraminiferal Densities by Predation in the Indian River, Florida." *Journal of Foraminiferal Research* 12 (1): 66–71.

Buzas, M. A. 1990. "Another Look at Confidence Limits for Species Proportions." *Journal of Paleontology* 64 (5): 842–43. https://doi.org/10.1017/S002233600001903X.

Cahill, Niamh, Andrew C. Kemp, Benjamin P. Horton, and Andrew C. Parnell. 2015. "Modeling Sea-Level Change Using Errors-in-Variables Integrated Gaussian Processes." *The Annals of Applied Statistics* 9 (2): 547–71. https://doi.org/10.1214/15-AOAS824.

Cahill, Niamh, Andrew C. Kemp, Benjamin P. Horton, and Andrew C. Parnell. 2016. "A Bayesian Hierarchical Model for Reconstructing Relative Sea Level: From Raw Data to Rates of Change." *Climate of the Past* 12 (2): 525–42. https://doi.org/10.5194/cp-12-525-2016.

Chant, R. J., M. C. Curran, K. W. Able, and S. M. Glenn. 2000. "Delivery of Winter Flounder (Pseudopleuronectes Americanus) Larvae to Settlement Habitats in Coves Near Tidal Inlets." *Estuarine, Coastal and Shelf Science* 51 (5): 529–41. https://doi.org/10.1006/ecss.2000.0694.

Chmura, G L, and P Aharon. 1995. "Stable Carbon Isotope Signatures of Sedimentary Carbon in Coastal Wetlands as Indicators of Salinity Regime." *Journal of Coastal Research* 11: 12.

Culver, Stephen J., Dorothea V. Ames, D. Reide Corbett, David J. Mallinson, Stanley R. Riggs, Christopher G. Smith, and David J. Vance. 2006. "Foraminiferal and Sedimentary Record of Late Holocene Barrier Island Evolution, Pea Island, North Carolina: The Role of Storm Overwash, Inlet Processes, and Anthropogenic Modification." Journal of Coastal Research 224 (July): 836–46. https://doi.org/10.2112/03-0103.1.

Culver, Stephen J., and Benjamin P. Horton. 2005. "Infaunal Marsh Foraminifera from the Outer Banks, North Carolina, U.S.A." *Journal of Foraminiferal Research* 35 (2): 148–70. https://doi.org/10.2113/35.2.148.

Culver, Stephen J., Han Jun Woo, George F. Oertel, and Martin A. Buzas. 1996. "Foraminifera of Coastal Depositional Environments, Virginia, U.S.A.: Distribution and Taphonomy." *PALAIOS* 11 (5): 459. https://doi.org/10.2307/3515213.

Daddario, J.J. 1961. *A Lagoon Deposit Profile near Atlantic City, New Jersey*. Vol. 6.

De Boor, C. 1978. "A Practical Guide to Splines." In Applied Mathematical Sciences. Springer. https://doi.org/10.1007/978-1-4612-6333-3.

Dierckx, P. 1993. Curve and Surface Fitting with Splines. Clarendon Press.

Donato, S.V., E.G. Reinhardt, J.I. Boyce, J.E. Pilarczyk, and B.P. Jupp. 2009. "Particle-Size Distribution of Inferred Tsunami Deposits in Sur Lagoon, Sultanate of Oman." *Marine Geology* 257 (1–4): 54–64. https://doi.org/10.1016/j.margeo.2008.10.012.

Edwards, R.J., A.J. Wright, and O. van de Plassche. 2004. "Surface Distributions of Salt-Marsh Foraminifera from Connecticut, USA: Modern Analogues for High-Resolution Sea Level Studies." *Marine Micropaleontology* 51 (1–2): 1–21. https://doi.org/10.1016/j.marmicro.2003.08.002.

Ellison, R.L., and M.M. Nichols. 1976. *Modern and Holocene Foraminifera in the Chesapeake Bay Region*. Vol. 1.

Ellison, Robert L. 1965. "Distribution of Recent Foraminifera in the Rappahannock River Estuary." *College of William & Mary - Virginia Institute of Marine Science*. https://doi.org/10.21220/v53883.

Ember, L M, D F Williams, and T Morris. 1987. "Processes That Influence Carbon Isotope Variations in Salt Marsh Sediments." *Mar. Ecol. Prog. Ser.*, 10.

Engelhart, S E, W R Peltier, and B P Horton. 2011. "Holocene Relative Sea-Level Changes and Glacial Isostatic Adjustment of the U.S. Atlantic Coast," 4.

Fatela, F, and R Taborda. 2002. "Con¢dence Limits of Species Proportions in Microfossil Assemblages." *Marine Micropaleontology*, 6.

Ferland, Mariel A. 1990. "Holocene Depositional History of the Southern New Jersey Barrier and Backbarrier Regions." CERC-TR-90-2. Coastal Engineering Research Center Vicksburg MS. https://apps.dtic.mil/docs/citations/ADA220085.

Folk, R.L. and Ward, W.C. 1957. "Brazos River bar: a study in the significance of grain size parameters." *Journal of Sedimentary Petrology*, 27, 3-26.

Fontanier, C, F. J Jorissen, G Chaillou, C David, P Anschutz, and V Lafon. 2003. "Seasonal and Interannual Variability of Benthic Foraminiferal Faunas at 550m Depth in the Bay of Biscay." *Deep Sea Research Part I: Oceanographic Research Papers* 50 (4): 457–94. https://doi.org/10.1016/S0967-0637(02)00167-X.

Forman, Richard. 2012. *Pine Barrens: Ecosystem and Landscape*. Elsevier.

Gebrehiwet, Tsigabu, Carla M. Koretsky, and R.V. Krishnamurthy. 2008. "Influence of Spartina and Juncus on Saltmarsh Sediments. III. Organic Geochemistry." *Chemical Geology* 255 (1–2): 114–19. https://doi.org/10.1016/j.chemgeo.2008.06.015.

Gehrels, W. Roland. 1994. "Determining Relative Sea-Level Change from Salt-Marsh Foraminifera and Plant Zones on the Coast of Maine, U.S.A." *Journal of Coastal Research* 10 (4): 990–1009.

Gehrels, W. Roland. 2000. "Using Foraminiferal Transfer Functions to Produce High-Resolution Sea-Level Records from Salt-Marsh Deposits, Maine, USA." *The Holocene* 10 (3): 367–76. https://doi.org/10.1191/095968300670746884.

Gehrels, W. Roland, and Orson van de Plassche. 1999. "The Use of Jadammina Macrescens (Brady) and Balticammina Pseudomacrescens Brönnimann, Lutze and

Whittaker (Protozoa: Foraminiferida) as Sea-Level Indicators." *Palaeogeography, Palaeoclimatology, Palaeoecology* 149 (1–4): 89–101. https://doi.org/10.1016/S0031-0182(98)00194-1.

Hayek, Lee-Ann C., and Martin A. Buzas. 2010. *Surveying Natural Populations: Quantitative Tools for Assessing Biodiversity*. Columbia University Press.

Hayward, B. W., H. Grenfell, G. Cairns, and A. Smith. 1996. "Environmental Controls on Benthic Foraminiferal and Thecamoebian Associations in a New Zealand Tidal Inlet." *Journal of Foraminiferal Research* 26 (2): 150–71. https://doi.org/10.2113/gsjfr.26.2.150.

Hippensteel, S. P. 2000. "The Formation of Holocene Marsh Foraminiferal Assemblages, Middle Atlantic Coast, U.S.A.: Implications for Holocene Sea-level Change." *The Journal of Foraminiferal Research* 30 (4): 272–93. https://doi.org/10.2113/0300272.

Hippensteel, Scott P, and Ronald E Martin. 1999. "Foraminifera as an Indicator of Overwash Deposits, Barrier Island Sediment Supply, and Barrier Island Evolution: Folly Island, South Carolina." Palaeogeography, Palaeoclimatology, Palaeoecology 149 (1–4): 115–25. https://doi.org/10.1016/S0031-0182(98)00196-5.

Hippensteel, Scott P., Ronald E. Martin, Daria Nikitina, and James E. Pizzuto. 2002. "Interannual Variation of Marsh Foraminiferal Assemblages (Bombay Hook National Wildlife Refuge, Smyrna, DE): Do Foraminiferal Assemblages Have a Memory?" *The Journal of Foraminiferal Research* 32 (2): 97–109. https://doi.org/10.2113/0320097.

Horton, B. P. 1999. "The Distribution of Contemporary Intertidal Foraminifera at Cowpen Marsh, Tees Estuary, UK: Implications for Studies of Holocene Sea-Level Changes." *Palaeogeography, Palaeoclimatology, Palaeoecology* 149 (1): 127–49. https://doi.org/10.1016/S0031-0182(98)00197-7.

Horton, B. P., R. J. Edwards, and J. M. Lloyd. 1999. "A Foraminiferal-Based Transfer Function: Implications for Sea-level Studies." *Journal of Foraminiferal Research* 29 (2): 117–29. https://doi.org/10.2113/gsjfr.29.2.117.

Horton, B. P., Y. Milker, T. Dura, K. Wang, W. T. Bridgeland, L. Brophy, M. Ewald, et al. 2017. "Microfossil Measures of Rapid Sea-Level Rise: Timing of Response of Two Microfossil Groups to a Sudden Tidal-Flooding Experiment in Cascadia." *Geology* 45 (6): 535–38. https://doi.org/10.1130/G38832.1.

Horton, Benjamin P., and Stephen J. Culver. 2008. "Modern Intertidal Foraminifera of the Outer Banks, North Carolina, U.S.A., and Their Applicability for Sea-Level Studies." *Journal of Coastal Research* 245 (September): 1110–25. https://doi.org/10.2112/08A-0004.1.

Horton, Benjamin P., and Robin J. Edwards. 2003. "Seasonal Distributions of Foraminifera and Their Implications for Sea-Level Studies, Cowpen Marsh, U.K."

http://archives.datapages.com/data/sepm_sp/SP75/Seasonal_Distributions_of_Foraminifera.htm.

Horton, Benjamin P., and John W. Murray. 2006. "Patterns in Cumulative Increase in Live and Dead Species from Foraminiferal Time Series of Cowpen Marsh, Tees Estuary, UK: Implications for Sea-Level Studies." *Marine Micropaleontology* 58 (4): 287–315. https://doi.org/10.1016/j.marmicro.2005.10.006.

Johnson, Beverly J., Karen A. Moore, Charlotte Lehmann, Curtis Bohlen, and Thomas A. Brown. 2007. "Middle to Late Holocene Fluctuations of C3 and C4 Vegetation in a Northern New England Salt Marsh, Sprague Marsh, Phippsburg Maine." *Organic Geochemistry* 38 (3): 394–403. https://doi.org/10.1016/j.orggeochem.2006.06.006.

Kaufman, Leonard, and Peter J. Rousseeuw, eds. 1990. "Partitioning Around Medoids (Program PAM)." In *Wiley Series in Probability and Statistics*, 68–125. Hoboken, NJ, USA: John Wiley & Sons, Inc. https://doi.org/10.1002/9780470316801.ch2.

Kemp, A. C., M. A. Buzas, B. P. Horton, and S. J. Culver. 2011. "Influence of Patchiness on Modern Salt-Marsh Foraminifera Used in Sea-level Studies (North Carolina, USA)." *The Journal of Foraminiferal Research* 41 (2): 114–23. https://doi.org/10.2113/gsjfr.41.2.114.

Kemp, Andrew C, Troy D Hill, Christopher H Vane, Niamh Cahill, Philip M Orton, Stefan A Talke, Andrew C Parnell, Kelsey Sanborn, and Ellen K Hartig. 2017. "Relative Sea-Level Trends in New York City during the Past 1500 Years." *The Holocene* 27 (8): 1169–86. https://doi.org/10.1177/0959683616683263.

Kemp, Andrew C., Benjamin P. Horton, and Stephen J. Culver. 2009. "Distribution of Modern Salt-Marsh Foraminifera in the Albemarle–Pamlico Estuarine System of North Carolina, USA: Implications for Sea-Level Research." *Marine Micropaleontology* 72 (3–4): 222–38. https://doi.org/10.1016/j.marmicro.2009.06.002.

Kemp, Andrew C, Benjamin P Horton, Jeffrey P Donnelly, Michael E Mann, Martin Vermeer, and Stefan Rahmstorf. n.d. "Climate Related Sea-Level Variations over the Past Two Millennia," 6.

Kemp, Andrew C., Benjamin P. Horton, Christopher H. Vane, Christopher E. Bernhardt, D. Reide Corbett, Simon E. Engelhart, Shimon C. Anisfeld, Andrew C. Parnell, and Niamh Cahill. 2013. "Sea-Level Change during the Last 2500 Years in New Jersey, USA." *Quaternary Science Reviews* 81 (December): 90–104. https://doi.org/10.1016/j.quascirev.2013.09.024.

Kemp, Andrew C., Benjamin P. Horton, David R. Vann, Simon E. Engelhart, Candace A. Grand Pre, Christopher H. Vane, Daria Nikitina, and Shimon C. Anisfeld. 2012. "Quantitative Vertical Zonation of Salt-Marsh Foraminifera for Reconstructing

Former Sea Level; an Example from New Jersey, USA." *Quaternary Science Reviews* 54 (October): 26–39. https://doi.org/10.1016/j.quascirev.2011.09.014.

Kemp, Andrew C., and Richard J. Telford. 2015. "Transfer Functions." In *Handbook of Sea-Level Research*, edited by Ian Shennan, Antony J. Long, and Benjamin P. Horton, 470–99. Chichester, UK: John Wiley & Sons, Ltd. https://doi.org/10.1002/9781118452547.ch31.

Kemp, Andrew C., Christopher H. Vane, Benjamin P. Horton, and Stephen J. Culver. 2010. "Stable Carbon Isotopes as Potential Sea-Level Indicators in Salt Marshes, North Carolina, USA." *The Holocene* 20 (4): 623–36. https://doi.org/10.1177/0959683609354302.

Kemp, Andrew C., Christopher H. Vane, Benjamin P. Horton, Simon E. Engelhart, and Daria Nikitina. 2012. "Application of Stable Carbon Isotopes for Reconstructing Salt-Marsh Floral Zones and Relative Sea Level, New Jersey, USA." *Journal of Quaternary Science* 27 (4): 404–14. https://doi.org/10.1002/jqs.1561.

Kemp, Andrew C., Alexander J. Wright, Robert L. Barnett, Andrea D. Hawkes, Dan J. Charman, Colby Sameshima, Alexandra N. King, et al. 2017. "Utility of Salt-Marsh Foraminifera, Testate Amoebae and Bulk-Sediment Δ13C Values as Sea-Level Indicators in Newfoundland, Canada." *Marine Micropaleontology* 130 (January): 43–59. https://doi.org/10.1016/j.marmicro.2016.12.003.

Kemp, Andrew C., Alexander J. Wright, Robin J. Edwards, Robert L. Barnett, Matthew J. Brain, Robert E. Kopp, Niamh Cahill, et al. 2018. "Relative Sea-Level Change in Newfoundland, Canada during the Past ~3000 Years." *Quaternary Science Reviews* 201 (December): 89–110. https://doi.org/10.1016/j.quascirev.2018.10.012.

Kennish, Michael J. 2004. "NERRS Research and Monitoring Initiatives." *Journal of Coastal Research* 10045 (September): 1–8. https://doi.org/10.2112/SI45-001.1.

Khan, Nicole S., Christopher H. Vane, and Benjamin P. Horton. 2015. "Stable Carbon Isotope and C/N Geochemistry of Coastal Wetland Sediments as a Sea-Level Indicator." In *Handbook of Sea-Level Research*, edited by Ian Shennan, Antony J. Long, and Benjamin P. Horton, 295–311. Chichester, UK: John Wiley & Sons, Ltd. https://doi.org/10.1002/9781118452547.ch20.

Lamb, Angela L., Graham P. Wilson, and Melanie J. Leng. 2006. "A Review of Coastal Palaeoclimate and Relative Sea-Level Reconstructions Using Δ13C and C/N Ratios in Organic Material." *Earth-Science Reviews* 75 (1–4): 29–57. https://doi.org/10.1016/j.earscirev.2005.10.003.

Leavitt, Steven W., and Austin Long. 1986. "Stable-Carbon Isotope Variability in Tree Foliage and Wood." *Ecology* 67 (4): 1002–10. https://doi.org/10.2307/1939823.

Lynn, B. 2001. "Carbon Isotopic Compositions of Plants and Sediments of Tide Marshes in the San Francisco Estuary." *Journal of Coastal Research* 17: 13.

Lynts, George W. 1966. "Variation of Foraminiferal Standing Crop Over Short Lateral Distances in Buttonwood Sound, Florida Bay: Foraminiferal Standing Crop in Buttonwood Sound." *Limnology and Oceanography* 11 (4): 562–66. https://doi.org/10.4319/lo.1966.11.4.0562.

Malamud-Roam, Frances, and B. Lynn Ingram. 2004. "Late Holocene Δ13C and Pollen Records of Paleosalinity from Tidal Marshes in the San Francisco Bay Estuary, California☆." *Quaternary Research* 62 (2): 134–45. https://doi.org/10.1016/j.yqres.2004.02.011.

Martin, Ronald E., Scott P. Hippensteel, Daria Nikitina, and James E. Pizzuto. 2002. "Artificial Time-Averaging of Marsh Foraminiferal Assemblages: Linking the Temporal Scales of Ecology and Paleoecology." *Paleobiology* 28 (2): 263–77. https://doi.org/10.1666/0094-8373(2002)028<0263:ATAOMF>2.0.CO;2.

McKee, Karen L., and W. H. Patrick. 1988. "The Relationship of Smooth Cordgrass (Spartina Alterniflora) to Tidal Datums: A Review." *Estuaries* 11 (3): 143–51. https://doi.org/10.2307/1351966.

Middelburg, J.J., J. Nieuwenhuize, R.K. Lubberts, and O. van de Plassche. 1997. "Organic Carbon Isotope Systematics of Coastal Marshes." *Estuarine, Coastal and Shelf Science* 45 (5): 681–87. https://doi.org/10.1006/ecss.1997.0247.

Milker, Y., B. P. Horton, C. H. Vane, S. E. Engelhart, A. R. Nelson, R. C. Witter, N. S. Khan, and W. T. Bridgeland. 2015. "Annual and Seasonal Distribution of Intertidal Foraminifera and Stable Carbon Isotope Geochemistry, Bandon Marsh, Oregon, USA." *The Journal of Foraminiferal Research* 45 (2): 146–55. https://doi.org/10.2113/gsjfr.45.2.146.

Morvan, Julie, Jean-Pierre Debenay, Frans Jorissen, Fabrice Redois, Eric Bénéteau, Malou Delplancke, and Anne-Sophie Amato. 2006. "Patchiness and Life Cycle of Intertidal Foraminifera: Implication for Environmental and Paleoenvironmental Interpretation." *Marine Micropaleontology* 61 (1–3): 131–54. https://doi.org/10.1016/j.marmicro.2006.05.009.

Murray, John W., and Elisabeth Alve. 2000. "Major Aspects of Foraminiferal Variability (Standing Crop and Biomass) on a Monthly Scale in an Intertidal Zone." *Journal of Foraminiferal Research* 30 (3): 177–91. https://doi.org/10.2113/0300177.

Murray, John W, and Samuel S Bowser. 2000. "Mortality, Protoplasm Decay Rate, and Reliability of Staining Techniques to Recognize 'Living' Foraminifera," 17.

Nikitina, Daria L., James E. Pizzuto, Ronald E. Martin, and Scott P. Hippensteel. 2003. "Transgressive Valley-Fill Stratigraphy and Sea-Level History of the Leipsic River, Bombay Hook National Wildlife Refuge, Delaware, U.S.A." http://archives.datapages.com/data/sepm_sp/SP75/Transgressive_Valley-Fill_Stratigraphy.htm.

Patterson, R. Timothy, and Evan Fishbein. 1989. "Re-Examination of the Statistical Methods Used to Determine the Number of Point Counts Needed for Micropaleontological Quantitative Research." *Journal of Paleontology* 63 (02): 245–48. https://doi.org/10.1017/S0022336000019272.

Pilarczyk, Jessica E., Tina Dura, Benjamin P. Horton, Simon E. Engelhart, Andrew C. Kemp, and Yuki Sawai. 2014. "Microfossils from Coastal Environments as Indicators of Paleo-Earthquakes, Tsunamis and Storms." Palaeogeography, Palaeoclimatology, Palaeoecology 413 (November): 144–57. https://doi.org/10.1016/j.palaeo.2014.06.033.

Plassche, Orson van de. 1986. *Sea-Level Research: A Manual for the Collection and Evaluation of Data*. https://doi.org/10.1007/978-94-009-4215-8.

Plater, Andrew J., Jason R. Kirby, John F. Boyle, Timothy Shaw, and Hayley Mills. 2015. "Loss on Ignition and Organic Content." In *Handbook of Sea-Level Research*, edited by Ian Shennan, Antony J. Long, and Benjamin P. Horton, 312–30. Chichester, UK: John Wiley & Sons, Ltd. https://doi.org/10.1002/9781118452547.ch21.

Rijk, S. de, and S.R. Troelstra. 1997. "Salt Marsh Foraminifera from the Great Marshes, Massachusetts: Environmental Controls." *Palaeogeography, Palaeoclimatology, Palaeoecology* 130 (1–4): 81–112. https://doi.org/10.1016/S0031-0182(96)00131-9.

Rijk, Sacha de. 1995. "Salinity Control on the Distribution of Salt Marsh Foraminifera (Great Marshes, Massachusetts)." *Journal of Foraminiferal Research* 25 (2): 156–66. https://doi.org/10.2113/gsjfr.25.2.156.

Robinson, Marci M., and Randolph A. McBride. 2006. "Benthic Foraminifera from a Relict Flood Tidal Delta along the Virginia/North Carolina Outer Banks." *Micropaleontology* 52 (1): 67–80. https://doi.org/10.2113/gsmicropal.52.1.67.

Rousseeuw, Peter J. 1987. "Silhouettes: A Graphical Aid to the Interpretation and Validation of Cluster Analysis." *Journal of Computational and Applied Mathematics* 20 (November): 53–65. https://doi.org/10.1016/0377-0427(87)90125-7.

Schafer, Charles T. 1971. "Sampling and Spatial Distribution of Benthonic Foraminifera1." *Limnology and Oceanography* 16 (6): 944–51. https://doi.org/10.4319/lo.1971.16.6.0944.

Scott, D., and J. O. R. Hermelin. 1993. "A Device for Precision Splitting of Micropaleontological Samples in Liquid Suspension." *Journal of Paleontology* 67 (1): 151–54. https://doi.org/10.1017/S0022336000021302.

Scott, D., and F. S. Medioli. 1978. "Vertical Zonations of Marsh Foraminifera as Accurate Indicators of Former Sea-Levels." *Nature* 272 (5653): 528. https://doi.org/10.1038/272528a0.

Scott, D., and F. S. Medioli. 1980. "Quantitative Studies of Marsh Foraminiferal Distributions in Nova Scotia : Implications for Sea Level Studies." *Special Publication Cushman Foundation for Foraminiferal Research* 17.

Scott, D., Franco S. Medioli, and Charles T. Schafer. 2001. *Monitoring in Coastal Environments Using Foraminifera and Thecamoebian Indicators*. Cambridge University Press.

Shennan, Ian. 1986. "Flandrian Sea-Level Changes in the Fenland. II: Tendencies of Sea-Level Movement, Altitudinal Changes, and Local and Regional Factors." *Journal of Quaternary Science* 1 (2): 155–79. https://doi.org/10.1002/jqs.3390010205.

Spencer, Randall S. 2000. "Foraminiferal Assemblages from a Virginia Salt Marsh, Phillips Creek, Virginia." *Journal of Foraminiferal Research* 30 (2): 143–55. https://doi.org/10.2113/0300143.

Stephenson, R. L., F. C. Tan, and K. H. Mann. 1984. "Stable Carbon Isotope Variability in Marine Macrophytes and Its Implications for Food Web Studies." *Marine Biology* 81 (3): 223–30. https://doi.org/10.1007/BF00393216.

Stouff, V., M. Lesourd, and J.-P. Debenay. 1999. "Laboratory Observations on Asexual Reproduction (Schizogony) and Ontogeny of Ammonia tepida with Comments on the Life Cycle." *Journal of Foraminiferal Research* 29 (1): 75–84. https://doi.org/10.2113/gsjfr.29.1.75.

Stuckey, Irene H. and Lisa Lofland Gould. 2000. *Coastal Plants from Cape Cod to Cape Canaveral*. University of North Carolina Press. http://agris.fao.org/agris-search/search.do?recordID=US201300057076.

Swallow, Jane E. 2000. "Intra-Annual Variability and Patchiness in Living Assemblages of Salt-Marsh Foraminifera from Mill Rythe Creek, Chichester Harbour, England." *Journal of Micropalaeontology* 19 (1): 9–22. https://doi.org/10.1144/jm.19.1.9.

Törnqvist, Torbjörn E., Davin J. Wallace, Joep E. A. Storms, Jakob Wallinga, Remke L. van Dam, Martijn Blaauw, Mayke S. Derksen, Cornelis J. W. Klerks, Camiel Meijneken, and Els M. A. Snijders. 2008. "Mississippi Delta Subsidence Primarily Caused by Compaction of Holocene Strata." *Nature Geoscience* 1 (3): 173–76. https://doi.org/10.1038/ngeo129.

Varekamp, J.C., E. Thomas, and O. Plassche. 1992. "Relative Sea-Level Rise and Climate Change over the Last 1500 Years." *Terra Nova* 4 (3): 293–304. https://doi.org/10.1111/j.1365-3121.1992.tb00818.x.

Walker, David A., Anne E. Linton, and Charles T. Schafer. 1974. "Sudan Black B; a Superior Stain to Rose Bengal for Distinguishing Living from Non-Living Foraminifera." *Journal of Foraminiferal Research* 4 (4): 205–15. https://doi.org/10.2113/gsjfr.4.4.205.

Walton, W. R. 1952. “Techniques for Recognition of Living Foraminifera.” *Cushman Found. Foram. Res. Contr.* 3 (2): 56–60.

Wright, Alexander J., Robin J. Edwards, and Orson van de Plassche. 2011. “Reassessing Transfer-Function Performance in Sea-Level Reconstruction Based on Benthic Salt-Marsh Foraminifera from the Atlantic Coast of NE North America.” *Marine Micropaleontology* 81 (1–2): 43–62. https://doi.org/10.1016/j.marmicro.2011.07.003.

Tables and Figures

Table 1. Monitoring Station site characteristics and environmental variables.

	Station 1	Station 2	Station 3	Station 4
Vegetation	*Spartina alterniflora* (short form)	*Spartina patens*	*Spartina patens, Distichlis spicata*	*Phragmites australis*
Salinity (psu)	39.6 ± 8.8	13.7 ± 4.9	13.1 ± 4.9	2.9 ± 2.0
Elevation (m MTL)	0.68 ± 0.03	0.68 ± 0.03	0.46-0.60	0.61 ± 0.03
Elevation (SWLI)	212-223	211-224	192-228	248-264
Substrate	Sandy silt	Sandy silt	Sandy silt	Fine silt
Organic Content	29.0% ± 7.9%	81.1% ± 3.5%	64.3% ± 3.9%	53% ± 7.6%
Dominant Foraminifera Species	*Trochammina inflata* *Jadammina macrescens* *Tiphotrocha comprimata*	*Jadammina macrescens* *Balticammina pseudomacrescens* *Tiphotrocha comprimata*	*Tiphotrocha comprimata* *Balticammina pseudomacrescens* *Haplophragmoides* spp.	*Jadammina macrescens* *Ammoastuta inepta* *Balticammina pseudomacrescens* *Haplophragmoides* spp.
$\delta^{13}C$	-16.7‰ ± 0.5	-15.7‰ ± 0.5	-17.5‰ ± 1.8	-28.0‰ ± 0.2

Table 2. Elevation estimates and associated uncertainties from the Bayesian transfer function for each monitoring station using the full dataset of dead foraminifera counts, a replicate-aggregate dataset, and a seasonal-aggregate dataset.

	Station 1	**Station 2**	**Station 3**	**Station 4**
Observed SWLI	212-223	211-224	192-228	248-264
Average SWLI Estimates (range in parentheses)				
Full Dataset	212 +/- 4.8 (197-219)	220 +/- 6.4 (195-229)	208 +/- 24.6 (133-240)	249 +/- 21.2 (171-265)
Replicate-Aggregate Dataset	213 +/- 5.2 (204-221)	225 +/- 3.7 (219-229)	201 +/- 28.0 (143-239)	261 +/- 6.1 (246-266)
Seasonal-Aggregate Dataset	213 +/- 4.0 (207-216)	225 +/- 6.0 (217-232)	201 +/- 25.9 (177-230)	265 +/- 2.2 (262-267)
Fall	216	217	215	267
Winter	212	227	230	266
Spring	207	225	181	266
Summer	215	232	177	262
Average SWLI Uncertainty				
Full Dataset				
All Data	26.5	30.5	36.5	33.1
Fall	25.5	30.1	36.2	27.0
Winter	27.3	29.7	34.7	29.1
Spring	27.8	29.9	39.2	44.9
Summer	25.4	32.0	36.0	28.0
Replicate-Aggregate Dataset				
All Data	22.0	25.6	36.9	22.1
Fall	19.4	24.3	34.8	16.7
Winter	22.5	24.4	34.9	14.7
Spring	25.6	25.2	43.0	34.5
Summer	20.7	28.4	35.0	18.2
Seasonal-Aggregate Dataset				
All Data	20.7	25.8	39.2	14.3
Fall	15.6	24.9	38.1	9.3
Winter	22.0	20.9	30.4	12.1
Spring	24.2	29.9	44.9	10.8
Summer	20.9	27.3	43.5	25.0

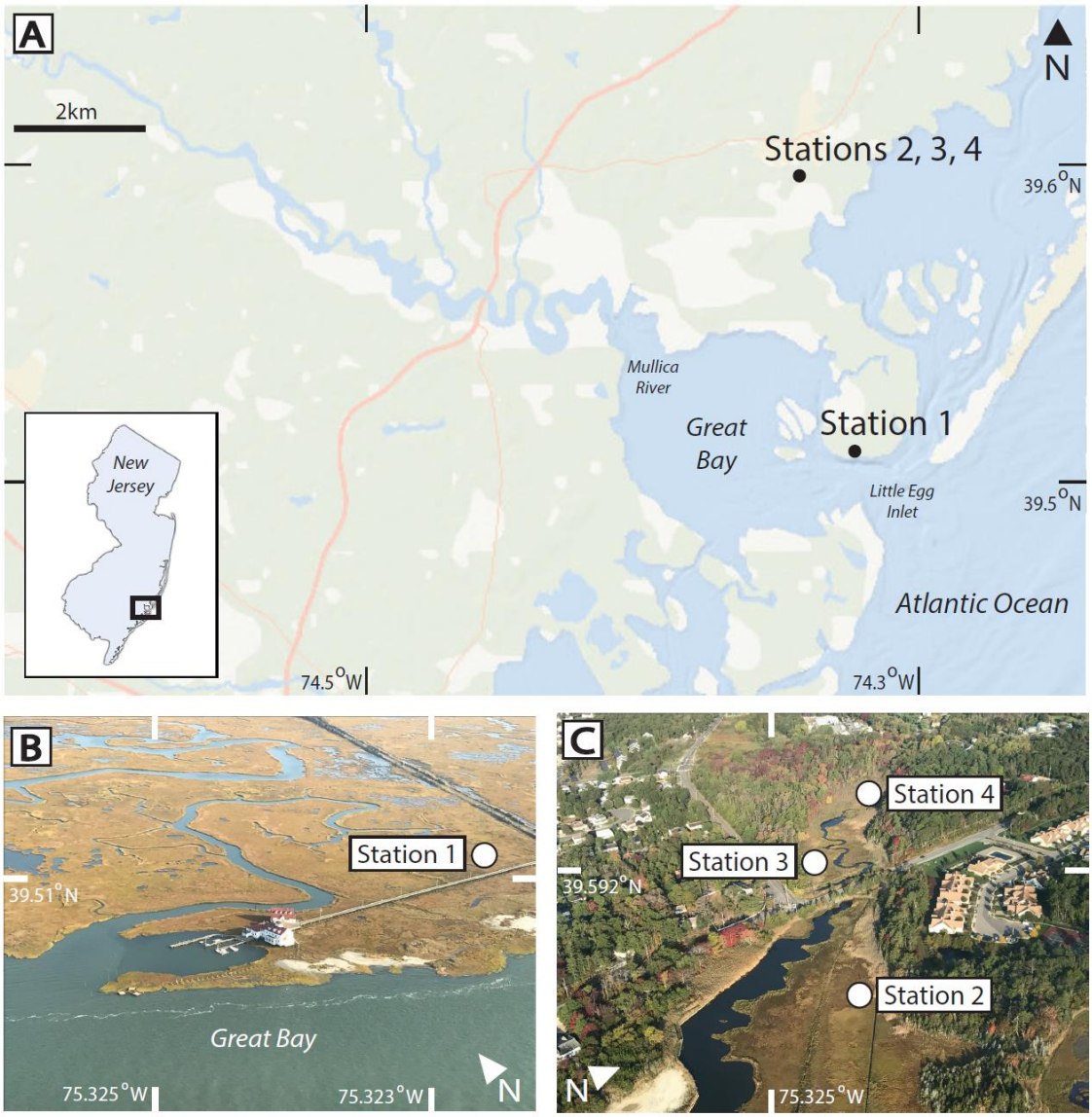

Figure 1. (A) Location of four high marsh monitoring stations in the Mullica River-Great Bay estuary in southern New Jersey. (B) Station 1 is adjacent to the Rutgers University Marine Field Station off of Great Bay. (C) Stations 2, 3, and 4 are located north in Tuckerton, New Jersey.

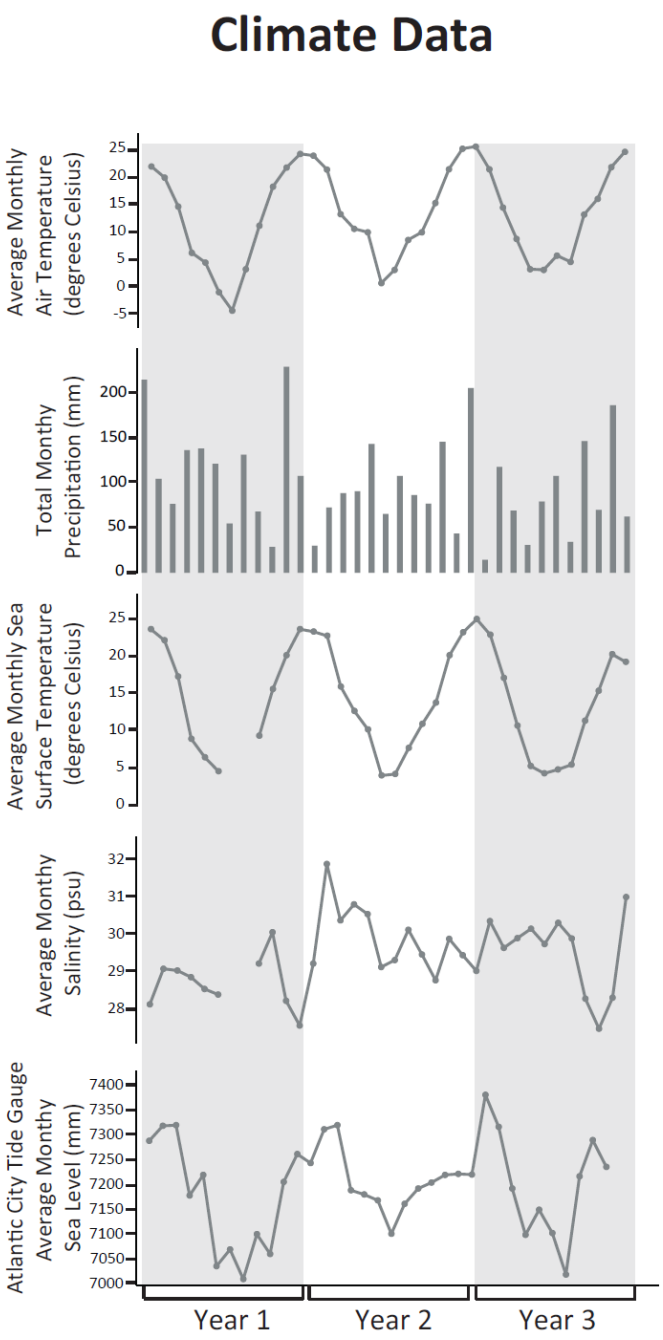

Figure 2. Meteorological data for the region during the three-year sampling timeframe of this study from the Jacques Cousteau National Estuarine Research Reserve meteorological station at Nacote Creek and water quality station in Great Bay showing changes in total monthly precipitation and salinity and cyclical annual patterns in air temperature and sea surface temperature. Tide gauge data was obtained from the Atlantic City tide gauge through the Permanent Service for Mean Sea Level and exhibits a cyclical annual pattern.

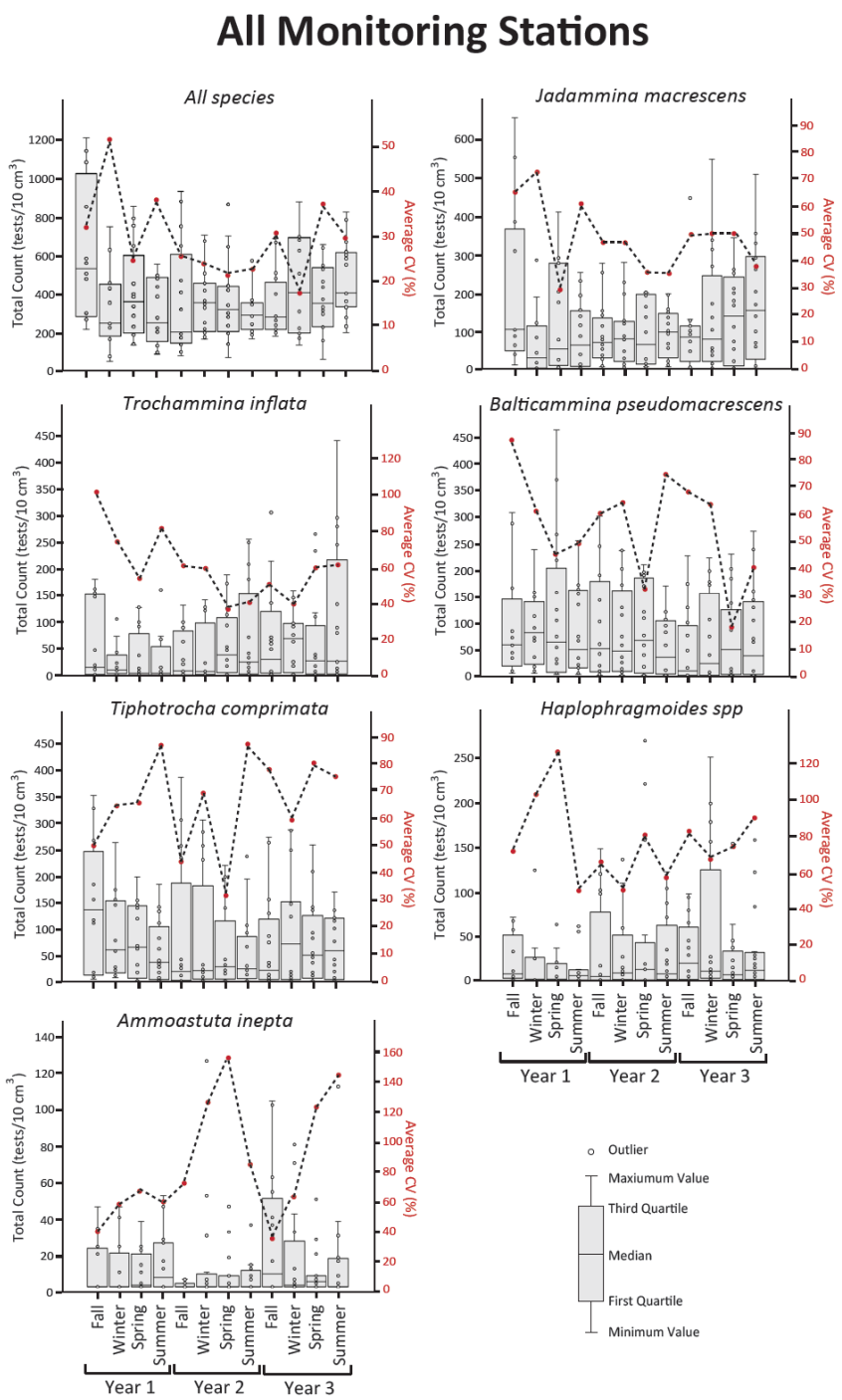

Figure 3. Total counts of all dead species combined and the six dominant species across all four monitoring stations during the three-year sampling timeframe. Distributions in counts for each sampling period represent all samples including replicate samples from all four monitoring stations. Note variable y-axis scales for total count sizes. Coefficient of variation (CV) among replicates is displayed for each sampling period as a secondary y-axis. Note variable y-axis scales for CV.

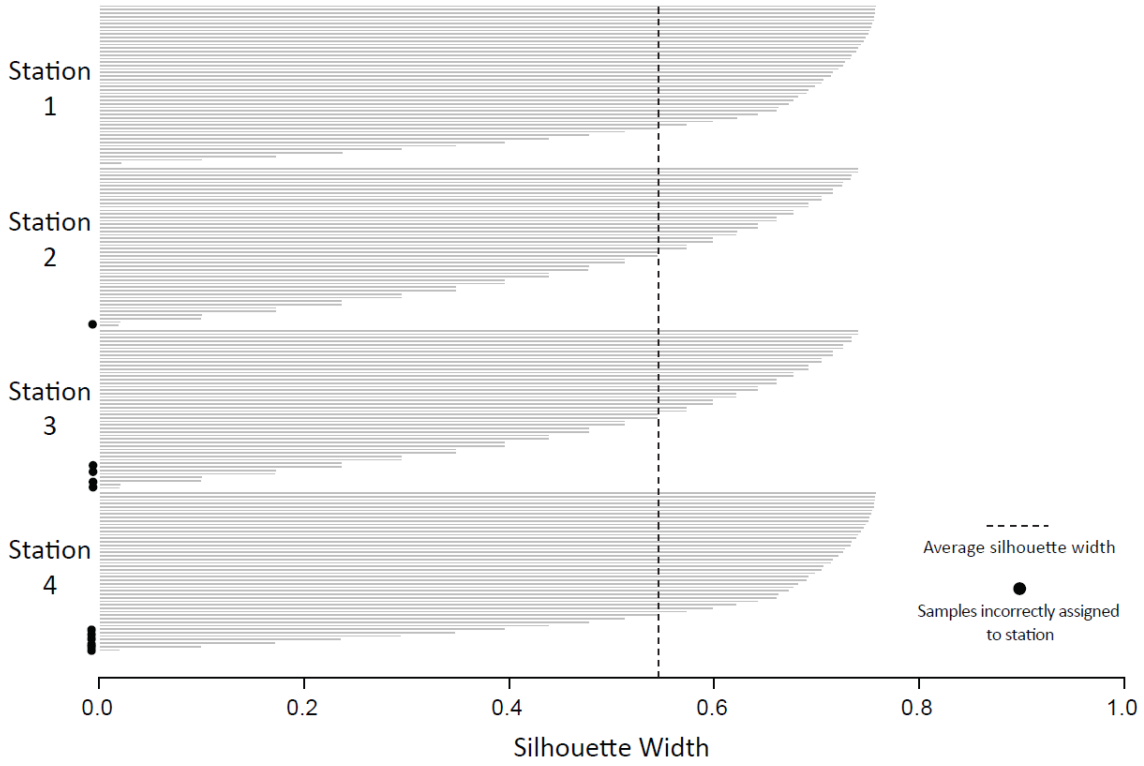

Figure 4. PAM analysis with four groups, showing four site-specific foraminiferal assemblages. All but 11 samples were assigned to a group corresponding to the monitoring station they were sampled from; these 11 samples had the lowest silhouette widths of all samples.

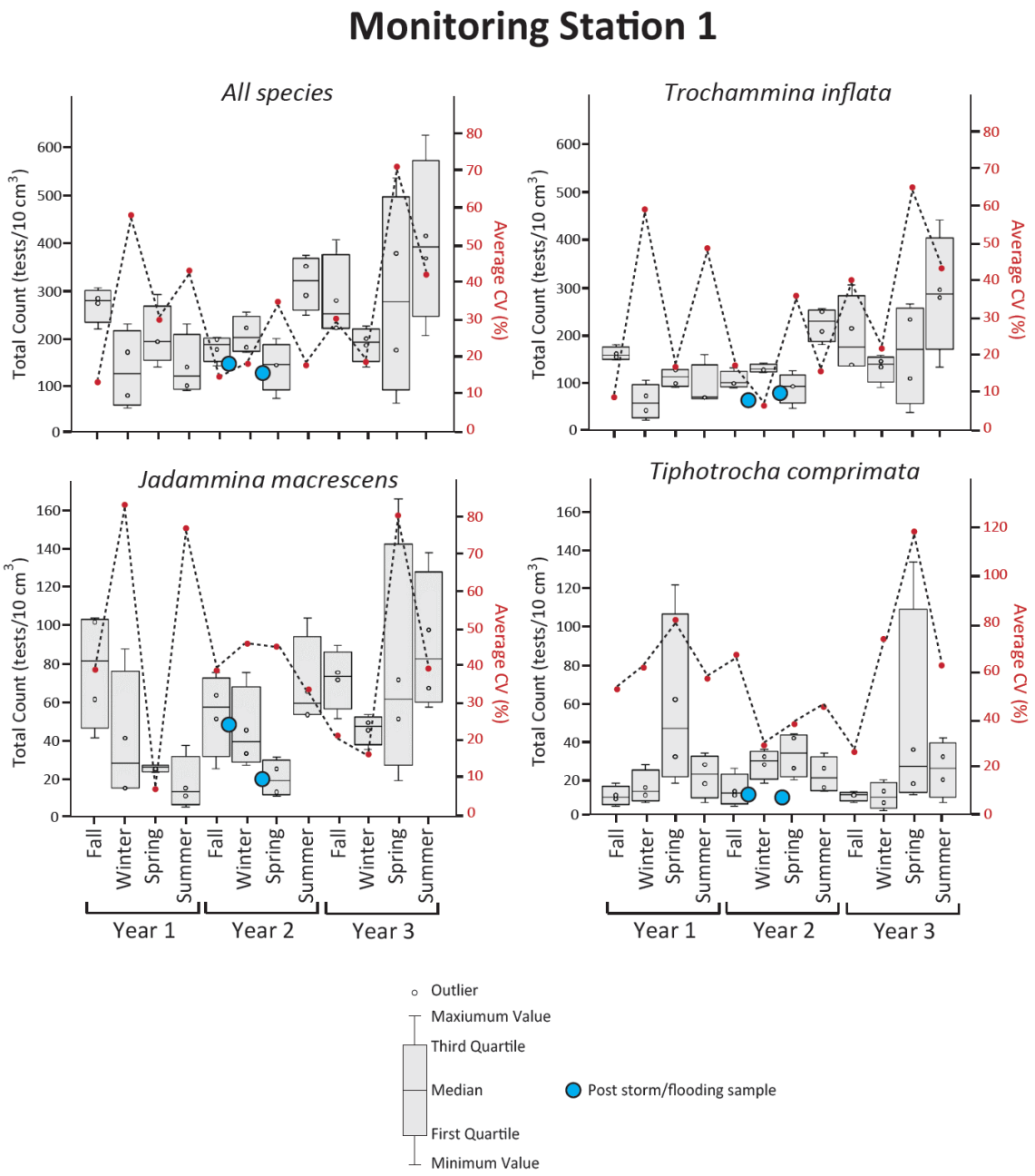

Figure 5. Total counts of all dead species combined and the three dominant species at Monitoring Station 1 during the three-year sampling timeframe. Distributions in counts for each sampling period represent the four replicate samples. Note variable y-axis scales for total count sizes. Coefficient of variation (CV) among replicates is displayed for each sampling period as a secondary y-axis. Note variable y-axis scales for CV. Two post-storm/flooding samples represented by blue circles.

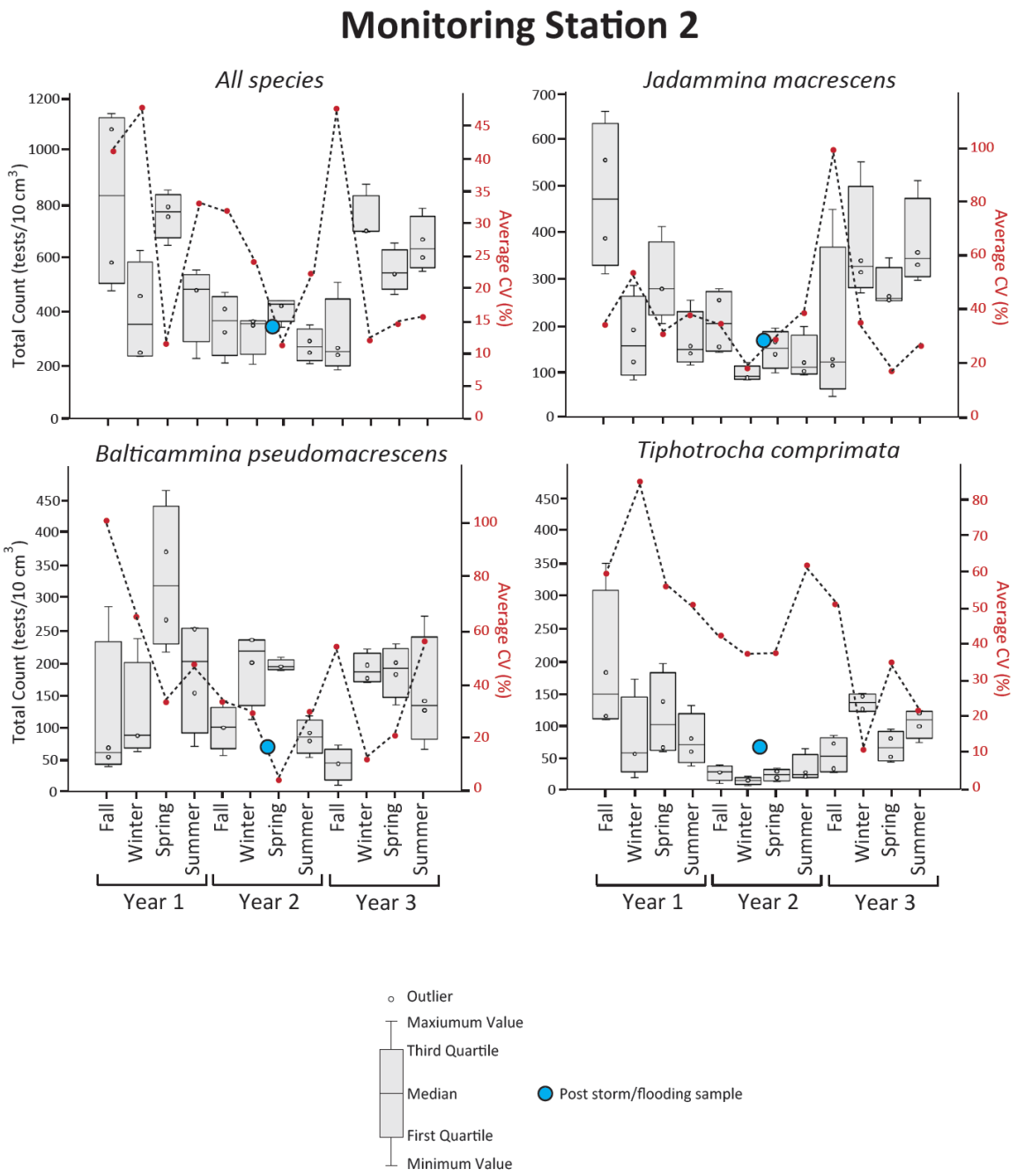

Figure 6. Total counts of all dead species combined and the three dominant species at Monitoring Station 2 during the three-year sampling timeframe. Distributions in counts for each sampling period represent the four replicate samples. Note variable y-axis scales for total count sizes. Coefficient of variation (CV) among replicates is displayed for each sampling period as a secondary y-axis. Note variable y-axis scales for CV. Post-storm/flooding sample represented by blue circles.

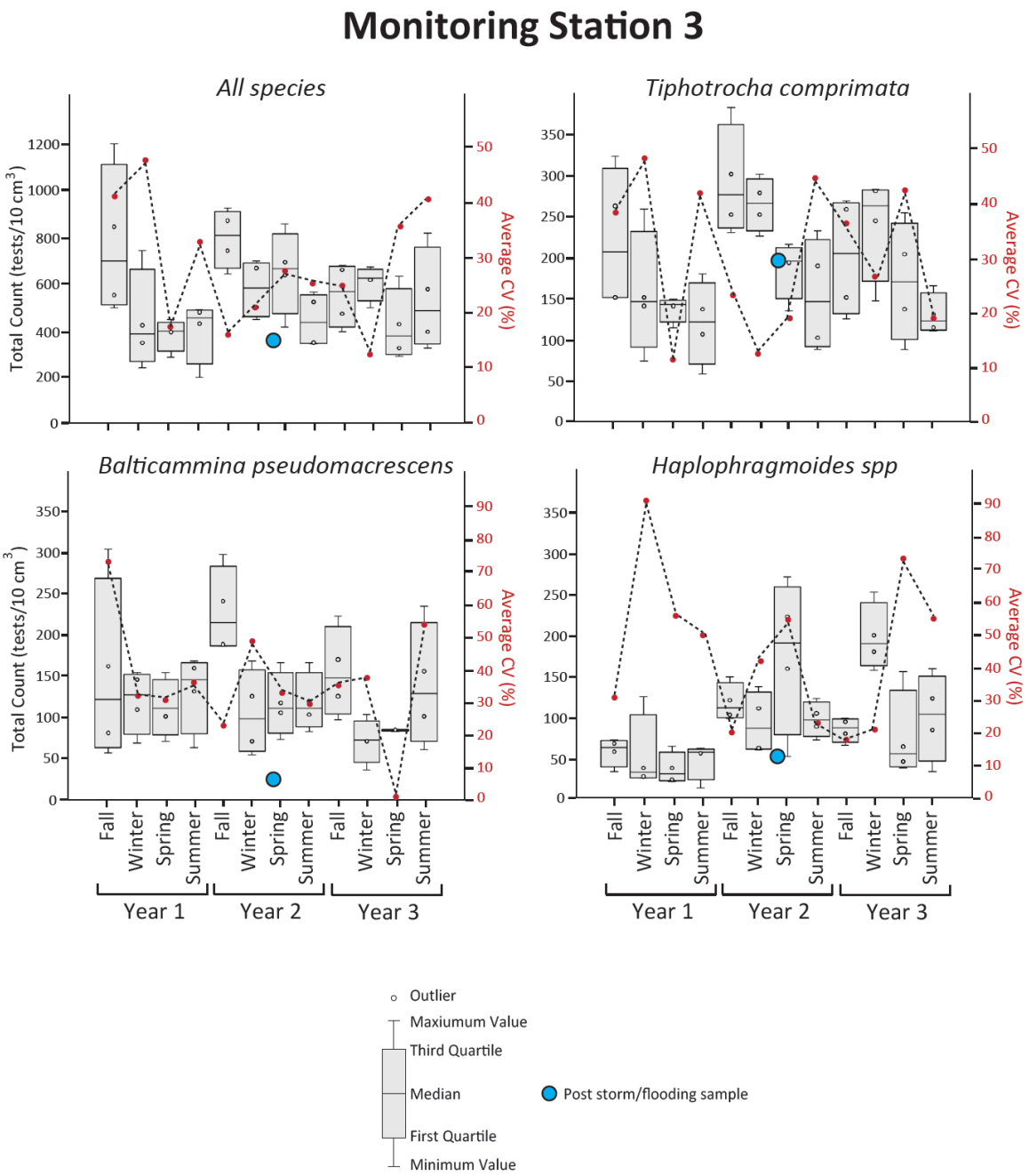

Figure 7. Total counts of all dead species combined and the three dominant species at Monitoring Station 3 during the three-year sampling timeframe. Distributions in counts for each sampling period represent the four replicate samples. Note variable y-axis scales for total count sizes. Coefficient of variation (CV) among replicates is displayed for each sampling period as a secondary y-axis. Note variable y-axis scales for CV. Post-storm/flooding sample represented by blue circles.

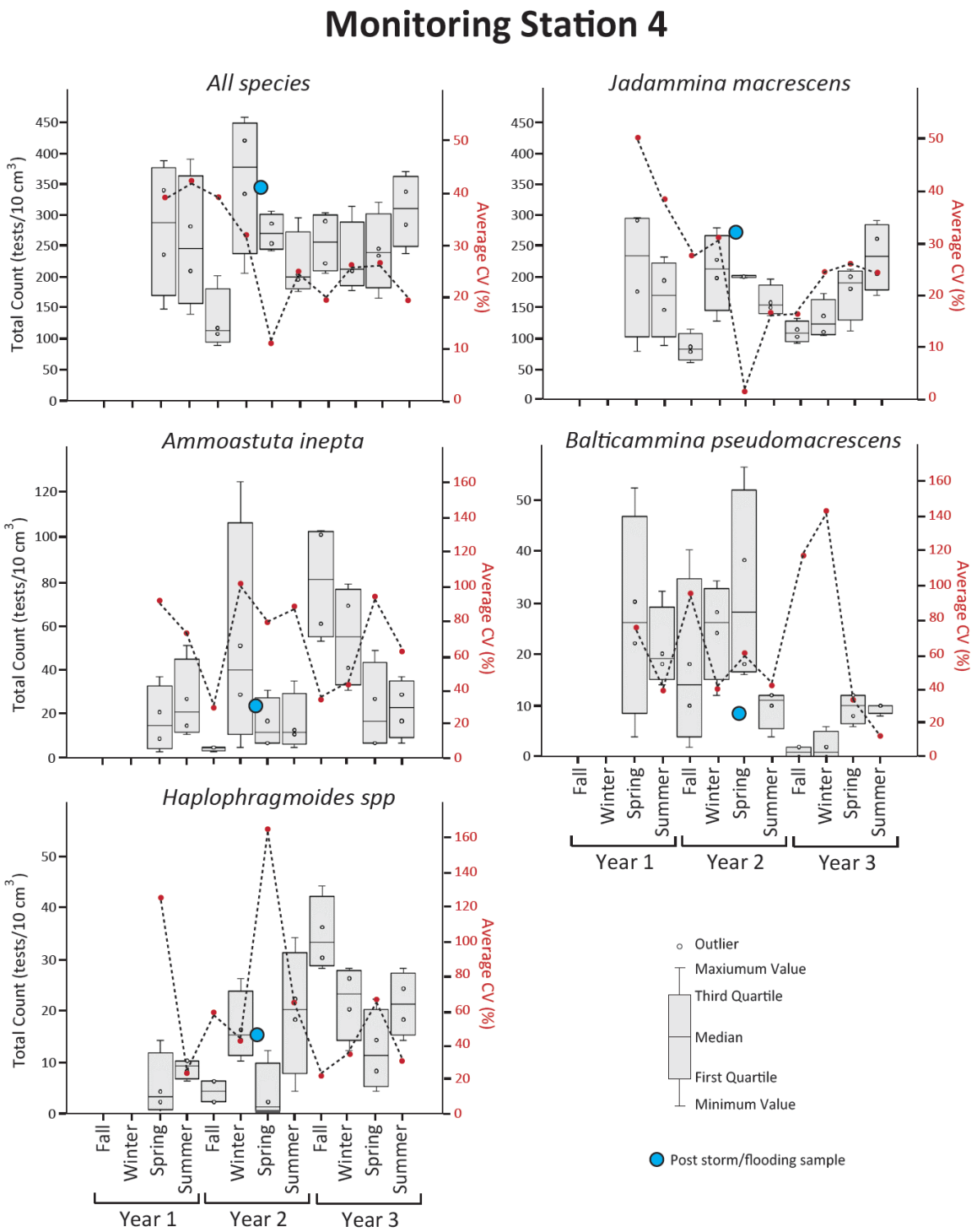

Figure 8. Total counts of all dead species combined and the four dominant species at Monitoring Station 4 during the three-year sampling timeframe. Distributions in counts for each sampling period represent the four replicate samples. Note variable y-axis scales for total count sizes. Coefficient of variation (CV) among replicates is displayed for each sampling period as a secondary y-axis. Note variable y-axis scales for CV. Post-storm/flooding sample represented by blue circles.

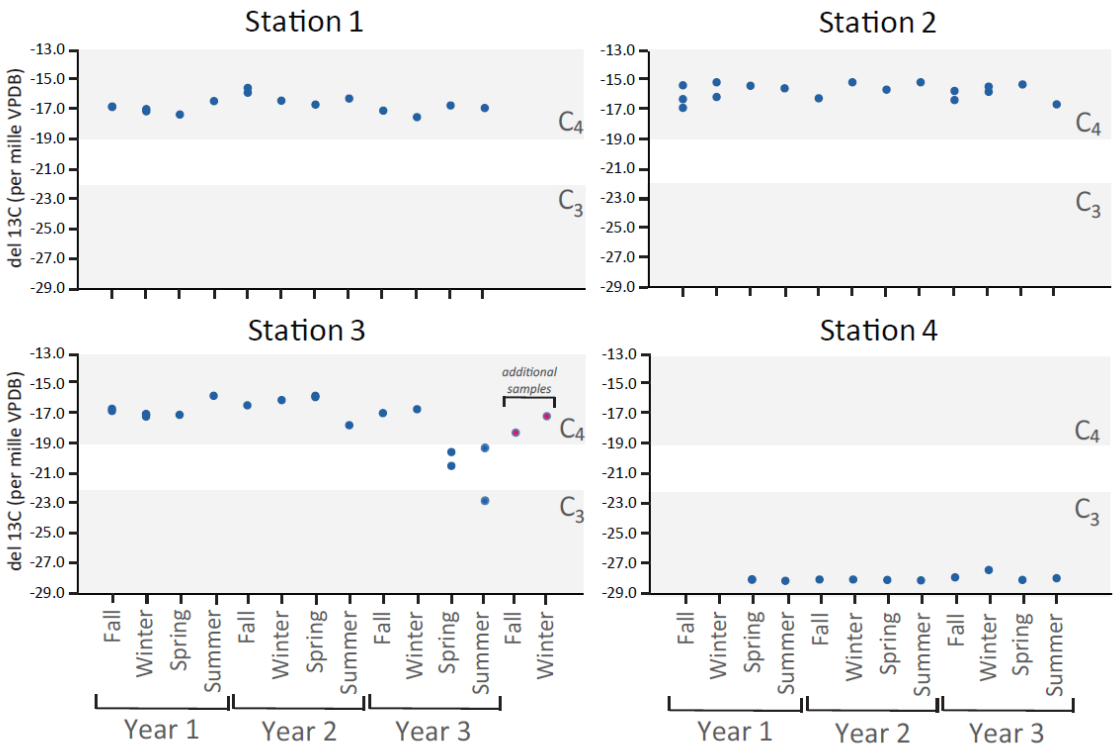

Figure 9. $\delta^{13}C$ values at each monitoring station during the three-year sampling timeframe, with two additional samples at Monitoring Station 3 in the subsequent Fall and Winter. Multiple data points for one sampling period represent replicate samples. Stations 1, 2, and 3 are associated with a C_4 dominated salt-marsh plant community, while Station 4 is associated with a C_3 dominated salt-marsh plant community.

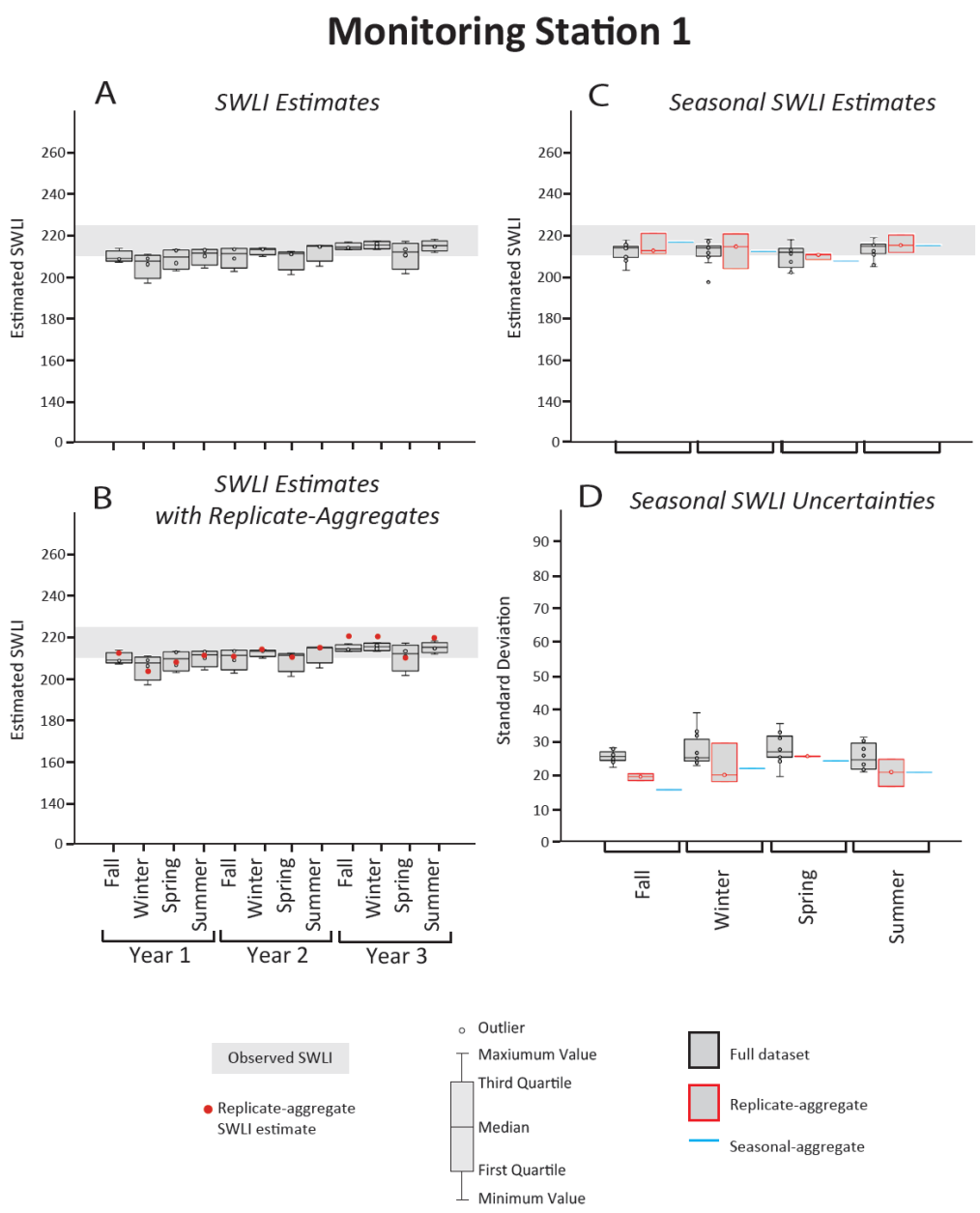

Figure 10. Bayesian transfer function elevation estimates (in SWLI units) from each sampling period for Monitoring Station 1. Observed SWLI for Station 1 is shown by gray bar. (A) SWLI estimates using the full foraminifera dataset of dead counts. Distributions in estimated SWLI for each sampling period represent the four replicate samples. (B) Replicate-aggregate SWLI estimates are shown as red data points on top of the estimated SWLI using the full dataset. (C) Seasonal SWLI estimates are shown for each season (Fall, Winter, Spring, Summer) using the full dataset, the replicate-aggregate dataset, and a seasonal-aggregate dataset. (D) Similarly, seasonal SWLI uncertainties in elevation estimates are shown for each season using the three different datasets. Equivalent analysis for Stations 2, 3, and 4 can be found in Appendix D.

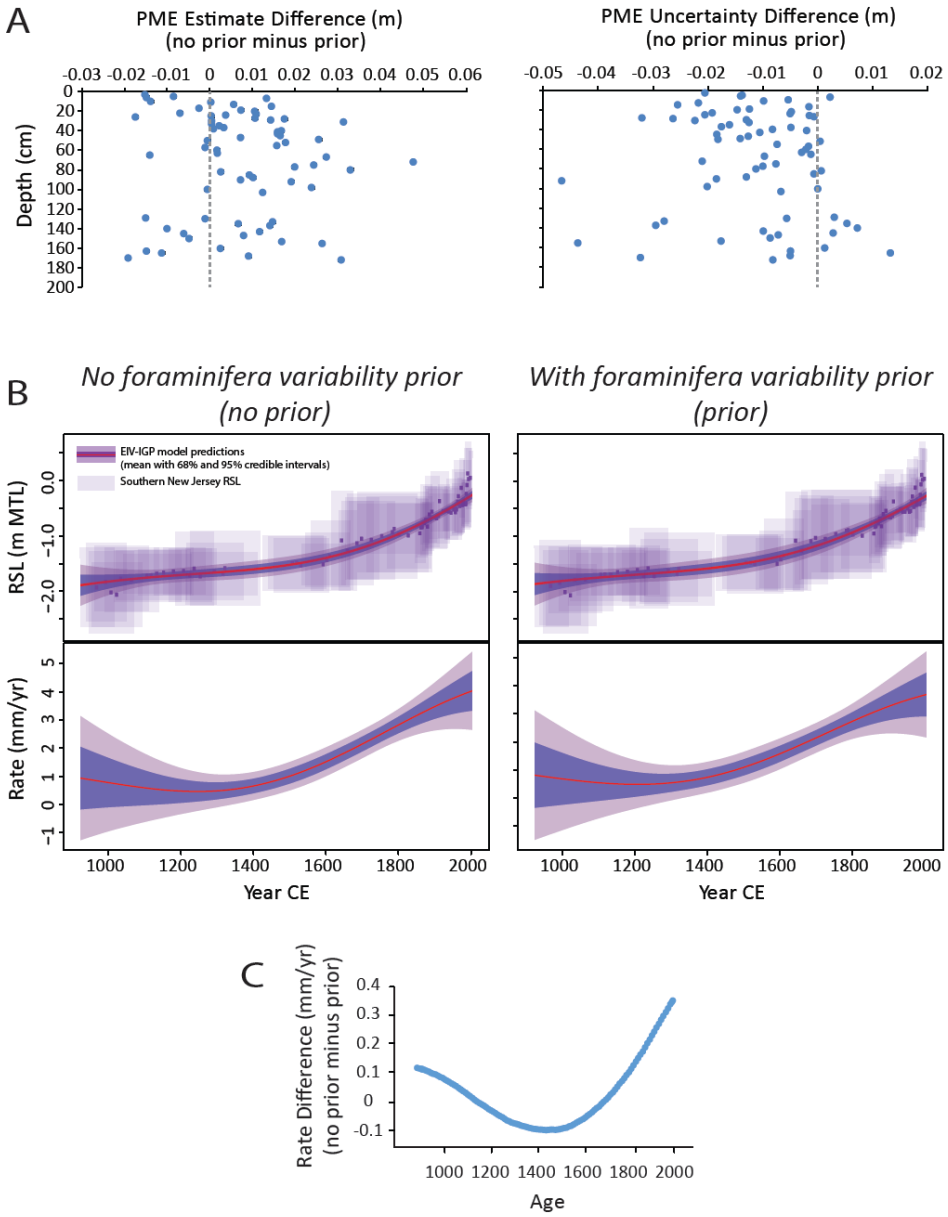

Figure 11. Comparison of southern New Jersey relative sea-level Bayesian transfer function (BTF) reconstruction (Kemp et al., 2013) with and without an informative foraminifera variability prior to account for temporal and spatial uncertainties in modern foraminifera distributions. (A) Paleomarsh elevation (PME) estimates and uncertainties from the BTF are compared by core depth as a difference of estimates/uncertainties with the uninformative foraminifera variability prior minus estimates/uncertainties with the informative prior. (B) An Errors-In-Variables Integrated Gaussian Process model displays the RSL record and rates of change through time with and without using the informative foraminifera variability prior. (C) The difference in predicted rates of change through time is shown as rates with the uninformative foraminifera variability prior minus rates with the informative prior.

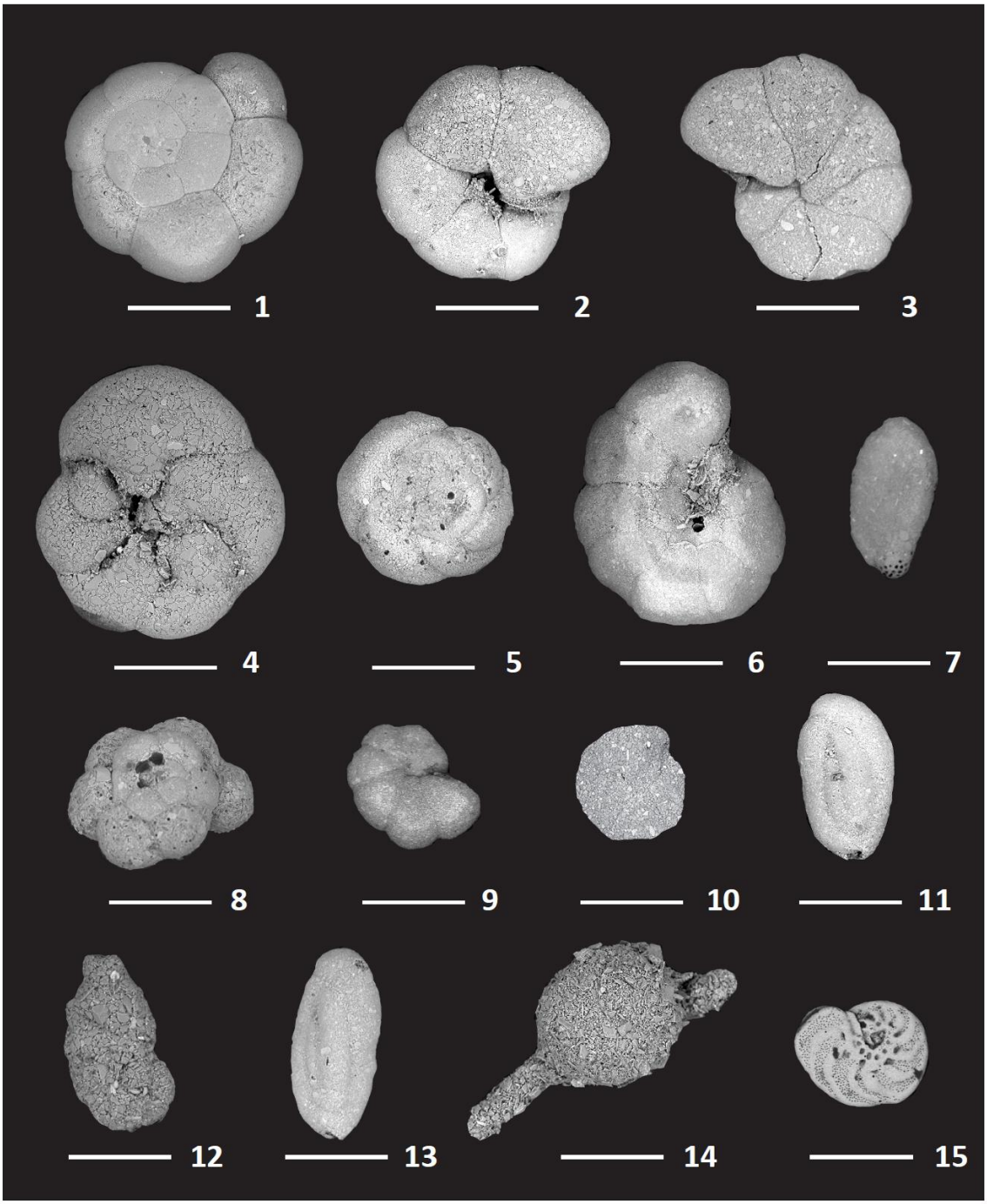

Plate 1. Scanning electron microscope (SEM) images of modern foraminifera. (1,2) *Trochammina inflata*; (3) *Jadammina macrescens*; (4, 5) *Tiphotrocha comprimata*; (6) *Balticammina pseudomacrescens*; (7) *Ammoastuta inepta*; (8) *Siphotrocha lobata*; (9) *Haplophragmoides* spp.; (10) *Arenoparella mexicana*; (11) *Miliammina fusca*; (12) *Ammobaculites* spp.; (13) *Miliammina petila*; (14) *Pseudothurammina limnetis*; (15) *Trochammina ochracea*. White bars represent 200 microns.

Appendix A: Dead foraminifera counts over the three-year study period for all four monitoring stations (continued on next page).

Sampling Date	Sample ID	*T. inflata*	*J. macrescens*	*T. comprimata*	*S. lobata*	*B. pseudomacrescens*	*A. mexicana*	*Haplophragmoides* spp	*M. fusca*	*M. petila*	*A. inepta*	*T. ochracea*	*Textularia* spp	*Ammobaculites* spp	*P. limnetis*
Sep-14	TK1 A	152	42	16	2	8	0	0	0	0	0	0	0	0	0
Sep-14	TK1 B	160	104	8	0	4	6	0	0	0	0	0	0	0	0
Sep-14	TK1 C	146	102	4	0	12	6	2	0	0	0	0	0	0	0
Sep-14	TK1 D	178	62	10	10	32	10	2	0	0	0	0	0	0	0
Sep-14	TK2 A	0	384	108	10	56	12	12	0	0	0	0	0	0	0
Sep-14	TK2 B	2	308	114	10	42	0	2	0	0	0	0	0	0	0
Sep-14	TK2 C	0	552	180	46	282	2	10	0	0	0	0	0	0	0
Sep-14	TK2 D	0	656	346	54	70	0	4	0	0	0	0	0	0	0
Sep-14	TK3 A	46	310	262	168	302	10	32	18	4	44	0	0	0	0
Sep-14	TK3 B	10	86	152	140	58	4	56	16	4	32	0	0	0	0
Sep-14	TK3 C	18	38	322	192	162	12	70	14	0	18	0	0	0	0
Sep-14	TK3 D	4	10	152	134	82	4	66	24	6	22	0	0	0	0
Dec-14	TK1 A	72	88	26	8	34	0	0	2	0	0	0	0	0	0
Dec-14	TK1 B	22	16	14	2	4	0	0	0	0	0	0	0	0	0
Dec-14	TK1 C	42	16	10	4	8	0	0	2	0	0	2	0	0	0
Dec-14	TK1 D	104	42	6	2	16	2	0	0	0	0	0	0	0	0
Dec-14	TK2 A	2	284	60	22	90	0	0	0	0	0	0	0	0	0
Dec-14	TK2 B	0	82	56	32	64	0	0	0	0	0	0	0	0	0
Dec-14	TK2 C	0	120	20	20	88	0	2	0	0	0	0	0	0	0
Dec-14	TK2 D	2	188	170	28	234	0	2	2	0	0	0	0	0	0
Dec-14	TK3 A	8	0	76	24	70	6	36	6	4	22	0	0	0	0
Dec-14	TK3 B	10	4	258	96	154	0	122	20	36	44	0	0	0	0
Dec-14	TK3 C	4	2	152	32	110	4	24	12	8	8	0	0	0	0
Dec-14	TK3 D	14	2	142	40	146	6	26	6	10	38	0	0	0	0
Mar-15	TK1 A	98	24	60	4	6	0	0	0	0	0	0	2	0	0
Mar-15	TK1 B	126	28	120	8	6	0	0	0	0	0	2	0	0	0
Mar-15	TK1 C	90	28	16	2	4	2	0	0	0	0	0	0	0	0
Mar-15	TK1 D	126	26	30	6	2	0	0	2	0	0	2	0	0	0
Mar-15	TK2 A	0	202	60	20	364	0	0	0	0	0	0	0	0	0
Mar-15	TK2 B	0	276	194	18	262	0	0	0	0	0	0	0	0	0
Mar-15	TK2 C	0	276	66	48	456	0	0	0	0	0	2	0	0	0
Mar-15	TK2 D	0	410	136	24	214	0	2	0	0	0	0	0	0	0
Mar-15	TK3 A	8	4	150	68	102	8	20	26	12	12	0	0	0	0
Mar-15	TK3 B	36	4	142	34	122	0	62	20	10	22	0	0	2	0
Mar-15	TK3 C	6	4	116	26	72	0	22	18	12	20	0	0	0	0
Mar-15	TK3 D	12	2	146	10	154	0	36	20	14	8	0	0	0	0
Mar-15	TK4 A	0	76	2	0	22	0	2	2	6	36	0	0	0	0
Mar-15	TK4 B	0	174	2	0	4	0	4	6	24	20	0	0	0	0
Mar-15	TK4 C	0	294	0	0	52	0	14	4	14	8	0	0	0	0
Mar-15	TK4 D	0	290	0	0	30	0	0	6	10	2	0	0	0	0
Jun-15	TK1 A	66	6	16	6	8	0	0	0	0	0	0	2	0	0
Jun-15	TK1 B	158	16	26	14	14	0	0	2	0	0	0	0	0	0
Jun-15	TK1 C	72	12	6	2	2	0	0	0	0	0	0	0	0	0
Jun-15	TK1D	68	38	32	0	4	0	0	0	0	0	0	0	0	0
Jun-15	TK2 A	4	252	60	8	152	0	4	0	0	0	0	0	0	0
Jun-15	TK2 B	0	154	130	18	248	0	4	0	0	0	0	0	0	0
Jun-15	TK2 C	0	114	38	2	72	0	0	2	0	0	0	0	0	0
Jun-15	TK2 D	2	138	80	16	250	0	2	0	0	0	0	0	0	0
Jun-15	TK3 A	14	8	180	40	132	10	56	16	6	24	0	0	0	0
Jun-15	TK3 B	8	2	138	28	168	2	54	10	4	24	0	0	0	0
Jun-15	TK3 C	6	6	108	40	160	10	60	16	8	44	0	0	38	0
Jun-15	TK3 D	2	0	60	14	64	6	12	14	6	14	0	0	20	0
Jun-15	TK4 A	0	86	2	0	20	0	10	0	8	10	0	0	2	0
Jun-15	TK4 B	0	230	0	0	32	0	10	12	20	50	0	0	0	34
Jun-15	TK4 C	0	144	0	0	18	0	6	2	8	14	0	0	0	16
Jun-15	TK4 D	0	192	0	0	14	0	8	6	10	26	0	0	0	24
Sep-15	TK1 A	88	76	24	2	8	2	0	0	0	0	2	0	0	0
Sep-15	TK1 B	100	64	4	4	6	0	0	0	0	0	0	0	0	0
Sep-15	TK1 C	98	26	10	0	2	8	0	0	0	0	0	0	0	0
Sep-15	TK1 D	130	52	12	4	0	0	0	0	0	0	0	0	0	0
Sep-15	TK2 A	8	152	30	16	102	0	16	0	0	0	0	0	0	0
Sep-15	TK2 B	4	276	28	10	140	0	6	6	0	0	0	0	0	0
Sep-15	TK2 C	4	252	40	12	100	0	2	0	0	0	0	0	0	0
Sep-15	TK2 D	0	140	12	2	58	0	0	0	0	0	0	0	0	0
Sep-15	TK3 A	20	8	252	108	240	2	96	6	12	2	0	0	0	0
Sep-15	TK3 B	62	6	300	100	296	2	146	2	2	2	0	0	0	6
Sep-15	TK3 C	28	14	380	134	188	4	118	4	0	0	0	0	0	2
Sep-15	TK3 D	6	36	230	72	186	6	100	6	4	0	0	0	0	0
Sep-15	TK4 A	0	76	0	0	18	0	2	2	2	2	0	0	0	14
Sep-15	TK4 B	0	84	0	0	2	0	2	0	0	4	0	0	0	14
Sep-15	TK4 C	0	112	0	0	40	0	6	6	12	4	0	0	0	20
Sep-15	TK4 D	0	58	0	0	10	0	6	4	0	4	0	0	0	6
Dec-15	TK1 A	130	46	34	4	6	2	0	0	0	0	0	0	0	0
Dec-15	TK1 B	140	76	30	4	2	0	0	0	0	0	0	2	0	0
Dec-15	TK1 C	126	28	26	2	0	0	0	0	0	0	0	0	0	0
Dec-15	TK1 D	120	34	16	2	0	0	0	0	0	0	0	0	0	0
Dec-15	TK2 A	10	86	16	14	232	0	6	0	0	0	0	0	0	0
Dec-15	TK2 B	2	118	22	6	198	0	2	2	0	0	0	0	0	0
Dec-15	TK2 C	2	82	8	2	112	0	2	0	0	0	0	0	0	0
Dec-15	TK2 D	2	92	16	22	232	0	2	2	0	0	0	0	0	0
Dec-15	TK3 A	6	16	300	62	126	20	134	2	0	0	0	0	0	6
Dec-15	TK3 B	26	12	278	54	168	42	108	4	0	0	0	0	0	8
Dec-15	TK3 C	22	0	252	40	56	68	60	2	0	2	0	0	0	4
Dec-15	TK3 D	6	4	226	46	72	24	58	6	2	8	0	0	0	4
Dec-15	TK4 A	0	126	0	0	24	0	10	8	16	4	0	0	0	16
Dec-15	TK4 B	0	278	2	0	34	0	14	10	22	28	0	0	0	30
Dec-15	TK4 C	0	226	0	0	28	0	16	10	24	124	0	0	0	28
Dec-15	TK4 D	0	196	0	0	12	0	26	6	30	50	0	0	0	12
Mar-16	TK1 A	46	14	18	0	0	0	0	0	0	0	0	0	0	0
Mar-16	TK1 B	92	12	42	0	0	0	0	0	0	0	2	0	0	0
Mar-16	TK1 C	124	32	40	2	0	0	0	0	0	0	0	2	0	0
Mar-16	TK1 D	92	26	24	0	0	0	0	2	0	0	2	0	0	0
Mar-16	TK2 A	28	136	34	14	192	0	18	0	0	0	0	0	0	0
Mar-16	TK2 B	18	96	20	8	186	0	12	2	0	2	0	0	0	0
Mar-16	TK2 C	20	162	30	6	206	0	18	0	0	0	0	0	0	0
Mar-16	TK2 D	16	192	14	4	192	0	12	4	0	0	0	0	0	0
Mar-16	TK3 A	170	6	198	4	106	0	156	2	0	0	0	0	0	0
Mar-16	TK3 B	186	6	216	12	166	0	266	6	0	0	0	0	0	0
Mar-16	TK3 C	52	8	136	20	74	0	50	26	0	44	0	0	14	0
Mar-16	TK3 D	112	20	194	22	118	6	218	4	0	2	0	0	0	0
Mar-16	TK4 A	0	200	0	0	56	0	0	2	16	6	0	0	0	4
Mar-16	TK4 B	0	198	0	0	38	0	0	20	18	30	0	0	0	0
Mar-16	TK4 C	0	196	0	0	18	0	12	2	8	16	0	0	0	0
Mar-16	TK4 D	0	200	0	0	16	0	2	6	10	6	0	0	0	0

Jun-16	TK1 A	246	66	32	2	2	0	0	0	0	0	0	0	0	0
Jun-16	TK1 B	178	54	14	2	0	0	0	0	0	0	0	0	0	0
Jun-16	TK1 C	206	54	24	2	0	0	0	2	0	0	0	0	0	0
Jun-16	TK1 D	252	104	12	2	0	0	0	0	0	0	0	0	0	0
Jun-16	TK2 A	14	100	28	6	56	0	4	2	0	0	0	0	0	0
Jun-16	TK2 B	8	118	20	12	80	0	10	2	0	0	0	0	0	0
Jun-16	TK2 C	22	92	64	16	92	0	2	2	2	0	0	0	0	0
Jun-16	TK2 D	6	196	22	8	118	0	2	0	0	0	0	0	0	0
Jun-16	TK3 A	70	6	232	22	104	2	86	0	0	6	0	0	0	0
Jun-16	TK3 B	26	10	104	14	120	2	70	6	0	6	0	0	0	0
Jun-16	TK3 C	32	20	90	18	84	2	102	4	0	0	0	0	0	0
Jun-16	TK3 D	40	10	190	26	166	0	120	6	0	12	0	0	0	0
Jun-16	TK4 A	0	134	0	0	12	0	4	2	8	10	0	0	0	4
Jun-16	TK4 B	0	148	0	0	4	0	22	4	12	4	0	0	0	0
Jun-16	TK4 C	0	194	2	0	10	0	34	0	18	34	0	0	0	2
Jun-16	TK4 D	0	156	0	0	12	0	18	4	0	12	0	0	0	0
Sep-16	TK1 A	212	52	10	2	0	0	2	0	0	0	0	0	0	0
Sep-16	TK1 B	136	72	12	0	0	0	0	0	0	0	0	0	0	0
Sep-16	TK1 C	134	76	10	2	0	0	0	0	0	0	0	0	0	0
Sep-16	TK1 D	302	90	6	4	0	0	0	0	0	0	0	0	0	0
Sep-16	TK2 A	6	112	34	6	74	0	10	0	0	0	0	0	0	0
Sep-16	TK2 B	6	446	28	10	14	0	4	0	0	0	0	0	0	0
Sep-16	TK2 C	6	126	84	4	46	0	0	0	0	0	0	0	0	0
Sep-16	TK2 D	10	46	72	6	48	0	4	0	0	0	0	0	0	0
Sep-16	TK3 A	64	4	126	2	98	10	64	8	0	28	0	0	0	0
Sep-16	TK3 B	48	6	258	4	222	2	78	8	4	34	0	0	0	0
Sep-16	TK3 C	58	10	152	4	126	14	96	4	0	14	0	0	0	2
Sep-16	TK3 D	70	2	268	10	170	10	92	12	10	38	0	0	2	0
Sep-16	TK4 A	0	112	0	0	2	0	36	20	10	102	0	0	0	6
Sep-16	TK4 B	2	90	0	0	2	0	44	4	8	60	0	0	0	10
Sep-16	TK4 C	0	130	2	0	0	0	28	6	26	100	0	0	0	10
Sep-16	TK4 D	2	100	0	0	0	0	30	2	10	52	0	0	0	8
Dec-16	TK1 A	156	54	12	4	0	0	0	0	0	0	0	0	0	0
Dec-16	TK1 B	90	50	2	0	0	0	0	0	0	0	0	0	0	0
Dec-16	TK1 C	144	36	18	0	0	0	2	0	0	0	0	0	0	0
Dec-16	TK1 D	132	46	6	0	0	0	2	0	0	0	0	0	0	0
Dec-16	TK2 A	74	268	120	18	218	0	0	0	0	0	0	0	0	0
Dec-16	TK2 B	26	336	144	12	168	0	8	0	0	0	0	0	0	0
Dec-16	TK2 C	16	548	124	4	174	0	2	0	2	0	0	0	0	0
Dec-16	TK2 D	24	312	148	16	194	0	4	0	0	0	0	0	0	0
Dec-16	TK3 A	94	4	148	12	72	8	154	2	0	10	0	0	0	0
Dec-16	TK3 B	74	14	282	10	38	2	196	2	0	4	0	0	0	0
Dec-16	TK3 C	96	0	244	10	104	4	176	0	0	2	0	0	0	0
Dec-16	TK3 D	62	2	280	4	74	2	248	2	0	2	0	0	0	0
Dec-16	TK4 A	0	134	0	0	2	0	20	6	6	40	0	0	0	0
Dec-16	TK4 B	0	170	0	0	6	0	28	6	18	78	0	0	0	6
Dec-16	TK4 C	0	108	2	0	0	0	26	4	6	30	0	0	0	0
Dec-16	TK4 D	0	102	4	0	0	0	12	4	16	68	0	0	0	6
Mar-17	TK1 A	262	72	34	2	0	0	0	4	0	0	0	0	0	0
Mar-17	TK1 B	230	166	132	0	0	0	0	0	0	0	0	0	0	0
Mar-17	TK1 C	38	20	10	0	0	0	0	0	0	0	0	0	0	0
Mar-17	TK1 D	108	52	16	0	0	0	0	0	0	0	0	0	0	0
Mar-17	TK2 A	6	250	52	2	226	0	2	0	0	0	0	0	0	0
Mar-17	TK2 B	18	260	80	2	180	0	4	0	0	2	0	0	0	0
Mar-17	TK2 C	20	252	44	4	134	0	10	0	0	0	0	0	0	0
Mar-17	TK2 D	16	342	94	2	198	0	2	0	0	0	0	0	0	0
Mar-17	TK3 A	32	4	204	4	84	0	62	16	6	18	0	0	4	2
Mar-17	TK3 B	36	0	90	2	86	2	44	6	4	6	0	0	22	2
Mar-17	TK3 C	116	4	254	14	86	0	152	2	2	4	0	0	0	2
Mar-17	TK3 D	42	2	138	4	86	0	36	10	4	6	0	0	6	0
Mar-17	TK4 A	0	110	0	0	8	0	4	0	12	26	0	0	0	4
Mar-17	TK4 B	0	178	4	0	12	0	8	0	16	6	0	0	0	8
Mar-17	TK4 C	0	198	2	0	12	0	22	10	16	48	0	0	0	10
Mar-17	TK4 D	0	210	0	0	6	0	14	4	2	6	0	0	0	2
Jun-17	TK1 A	132	68	6	0	0	0	0	0	0	0	0	0	0	0
Jun-17	TK1 B	276	58	30	0	0	0	0	0	0	0	0	0	0	0
Jun-17	TK1 C	436	138	40	2	0	0	0	0	0	0	0	0	0	0
Jun-17	TK1 D	292	98	18	0	0	0	2	0	0	0	0	0	0	0
Jun-17	TK2 A	14	294	98	10	126	0	8	0	0	0	0	0	0	0
Jun-17	TK2 B	24	354	122	2	268	0	4	4	0	2	0	0	0	0
Jun-17	TK2 C	6	328	118	2	140	0	6	0	0	0	0	0	0	0
Jun-17	TK2 D	12	508	74	0	68	0	0	0	4	0	0	0	0	0
Jun-17	TK3 A	88	8	116	4	62	2	120	2	0	0	0	0	0	2
Jun-17	TK3 B	26	8	132	0	102	2	32	6	10	14	0	0	0	2
Jun-17	TK3 C	242	2	166	4	234	2	156	6	6	0	0	0	0	0
Jun-17	TK3 D	78	14	112	4	156	4	82	8	12	110	0	0	0	2
Jun-17	TK4 A	0	168	0	0	10	0	24	0	14	16	0	0	0	4
Jun-17	TK4 B	0	202	0	0	10	0	18	8	4	36	0	0	0	4
Jun-17	TK4 C	0	290	0	0	8	0	14	6	12	28	0	0	0	10
Jun-17	TK4 D	0	260	2	0	10	0	28	6	12	6	0	0	0	12

Appendix B: Live foraminifera counts over the three-year study period for all four monitoring stations (continued on next page).

Sampling Date	Sample ID	*T. inflata*	*J. macrescens*	*T. comprimata*	*S. lobata*	*B. pseudomacrescens*	*A. mexicana*	*Haplophragmoides* spp	*M. fusca*	*M. petila*	*A. inepta*	*T. ochracea*	*Textularia* spp	*Ammobaculites* spp	*P. limnetis*
Sep-14	TK1 A	0	0	0	0	0	0	0	0	0	0	0	0	0	0
Sep-14	TK1 B	0	0	0	0	0	0	0	0	0	0	0	0	0	0
Sep-14	TK1 C	0	0	0	0	0	0	0	0	0	0	0	0	0	0
Sep-14	TK1 D	8	6	0	0	0	0	0	0	0	0	0	0	0	0
Sep-14	TK2 A	0	70	6	0	0	2	0	0	0	0	0	0	0	0
Sep-14	TK2 B	0	38	0	2	2	0	0	0	0	0	0	0	0	0
Sep-14	TK2 C	0	12	0	0	0	2	0	0	0	0	0	0	0	0
Sep-14	TK2 D	0	24	0	0	0	0	0	0	0	0	0	0	0	0
Sep-14	TK3 A	0	0	0	0	2	0	0	0	0	0	0	0	0	0
Sep-14	TK3 B	0	0	0	0	0	0	0	0	0	0	0	0	0	0
Sep-14	TK3 C	0	0	0	0	0	0	0	0	0	0	0	0	0	0
Sep-14	TK3 D	0	0	0	0	0	0	0	0	0	0	0	0	0	0
Dec-14	TK1 A	14	24	2	0	18	0	0	0	0	0	0	0	0	0
Dec-14	TK1 B	6	12	2	0	2	0	0	0	0	0	0	0	0	0
Dec-14	TK1 C	16	14	0	0	8	0	0	0	0	0	0	0	0	0
Dec-14	TK1 D	0	2	0	0	0	0	0	0	0	0	0	0	0	0
Dec-14	TK2 A	0	12	0	0	4	0	0	0	0	0	0	0	0	0
Dec-14	TK2 B	0	2	0	2	4	0	0	0	0	0	0	0	0	0
Dec-14	TK2 C	0	4	0	0	4	0	0	0	0	0	0	0	0	0
Dec-14	TK2 D	0	2	0	0	4	0	0	0	0	0	0	0	0	0
Dec-14	TK3 A	0	0	2	2	0	0	0	0	0	0	0	0	0	0
Dec-14	TK3 B	2	0	0	0	2	0	0	0	0	0	0	0	0	0
Dec-14	TK3 C	0	0	0	0	0	0	0	0	0	0	0	0	0	0
Dec-14	TK3 D	0	0	0	0	0	0	0	0	0	0	0	0	0	0
Mar-15	TK1 A	4	0	0	0	2	0	0	0	0	0	0	0	0	0
Mar-15	TK1 B	0	0	0	0	0	0	0	0	0	0	0	0	0	0
Mar-15	TK1 C	0	0	0	0	0	0	0	0	0	0	0	0	0	0
Mar-15	TK1 D	4	0	0	0	0	0	0	0	0	0	0	0	0	0
Mar-15	TK2 A	0	2	0	0	0	0	0	0	0	0	0	0	0	0
Mar-15	TK2 B	0	2	0	0	2	0	0	0	0	0	0	0	0	0
Mar-15	TK2 C	0	2	0	0	0	0	0	0	0	0	0	0	0	0
Mar-15	TK2 D	0	8	0	0	2	0	0	0	0	0	0	0	0	0
Mar-15	TK3 A	0	0	0	0	0	0	0	0	0	0	0	0	0	0
Mar-15	TK3 B	0	0	0	0	0	0	0	0	0	0	0	0	0	0
Mar-15	TK3 C	0	0	0	0	0	0	0	0	0	0	0	0	0	0
Mar-15	TK3 D	0	0	0	0	0	0	0	0	0	0	0	0	0	0
Mar-15	TK4 A	0	0	0	0	0	0	0	0	0	0	0	0	0	0
Mar-15	TK4 B	0	0	0	0	0	0	0	0	0	0	0	0	0	0
Mar-15	TK4 C	0	2	0	0	0	0	0	0	0	0	0	0	0	0
Mar-15	TK4 D	0	2	0	0	0	0	0	0	0	0	0	0	0	0
Jun-15	TK1 A	4	4	0	0	4	0	0	0	0	0	0	0	0	0
Jun-15	TK1 B	2	2	0	0	2	0	0	0	0	0	0	0	0	0
Jun-15	TK1 C	0	0	0	0	2	0	0	0	0	0	0	0	0	0
Jun-15	TK1D	6	4	0	0	4	0	0	0	0	0	0	0	0	0
Jun-15	TK2 A	0	78	0	0	14	0	0	0	0	0	0	0	0	0
Jun-15	TK2 B	0	16	2	0	8	0	0	0	0	0	0	0	0	0
Jun-15	TK2 C	0	52	0	0	12	0	0	2	0	0	0	0	0	0
Jun-15	TK2 D	0	62	4	0	18	0	0	0	0	0	0	0	0	0
Jun-15	TK3 A	0	4	6	0	0	0	0	0	0	6	0	0	0	0
Jun-15	TK3 B	0	0	2	0	14	0	0	0	0	2	0	0	0	0
Jun-15	TK3 C	0	0	16	2	4	0	0	0	0	2	0	0	0	0
Jun-15	TK3 D	0	2	4	0	4	0	0	0	0	0	0	0	2	0
Jun-15	TK4 A	0	58	0	0	2	0	4	0	0	0	0	0	0	0
Jun-15	TK4 B	0	56	0	0	2	0	0	2	0	4	0	0	0	0
Jun-15	TK4 C	0	58	0	0	2	0	0	0	0	0	0	0	0	0
Jun-15	TK4 D	0	86	0	0	10	0	2	0	0	4	0	0	0	0
Sep-15	TK1 A	4	2	0	0	6	0	0	0	0	0	0	0	0	0
Sep-15	TK1 B	4	4	0	0	2	0	0	0	0	0	0	0	0	0
Sep-15	TK1 C	28	8	6	0	0	0	0	0	0	0	0	0	0	0
Sep-15	TK1 D	16	4	0	2	6	0	0	0	0	0	0	0	0	0
Sep-15	TK2 A	0	112	2	2	28	0	0	0	0	0	0	0	0	0
Sep-15	TK2 B	0	158	6	0	32	0	0	0	0	0	0	0	0	0
Sep-15	TK2 C	0	94	4	0	8	0	0	0	0	0	0	0	0	0
Sep-15	TK2 D	0	98	2	0	8	0	0	0	0	0	0	0	0	0
Sep-15	TK3 A	6	4	4	0	18	4	0	0	0	0	0	0	0	0
Sep-15	TK3 B	8	0	2	0	26	0	4	0	0	0	0	0	0	0
Sep-15	TK3 C	8	0	2	10	12	16	16	0	0	0	0	0	0	0
Sep-15	TK3 D	2	0	6	8	4	4	6	0	0	0	0	0	0	0
Sep-15	TK4 A	0	110	0	0	2	0	4	2	0	2	0	0	0	0
Sep-15	TK4 B	0	90	0	0	2	0	2	0	0	2	0	0	0	0
Sep-15	TK4 C	0	76	0	0	2	0	0	0	0	0	0	0	0	0
Sep-15	TK4 D	0	120	2	0	2	0	4	4	0	8	0	0	0	0
Oct-15	TK1 A	48	6	6	0	6	0	0	0	0	0	0	0	0	0
Dec-15	TK1 A	46	16	2	0	10	0	0	0	0	0	0	0	0	0
Dec-15	TK1 B	8	24	2	0	0	0	0	0	0	0	0	0	0	0
Dec-15	TK1 C	40	24	0	0	0	0	0	0	0	0	0	0	0	0
Dec-15	TK1 D	32	14	2	0	2	0	0	0	0	0	0	0	0	0
Dec-15	TK2 A	0	62	2	2	50	0	0	0	0	0	0	0	0	0
Dec-15	TK2 B	0	46	2	4	40	0	0	0	0	0	0	0	0	0
Dec-15	TK2 C	0	94	0	4	56	0	0	2	0	0	0	0	0	0
Dec-15	TK2 D	0	38	0	0	36	0	0	0	0	0	0	0	0	0
Dec-15	TK3 A	0	4	0	0	10	0	0	0	0	0	0	0	0	0
Dec-15	TK3 B	2	0	2	0	10	0	2	0	0	0	0	0	0	0
Dec-15	TK3 C	0	0	6	0	8	2	2	0	0	0	0	0	0	0
Dec-15	TK3 D	0	0	2	0	6	2	0	0	0	4	0	0	0	0
Dec-15	TK4 A	0	110	0	0	8	0	0	2	0	4	0	0	0	0
Dec-15	TK4 B	0	124	0	0	0	0	0	0	0	8	0	0	0	0
Dec-15	TK4 C	0	74	0	0	0	0	0	0	0	30	0	0	0	0
Dec-15	TK4 D	0	124	0	0	0	0	0	2	0	12	0	0	0	0
Feb-16	TK1 A	30	34	0	0	0	0	0	0	0	0	0	0	0	0
Feb-16	TK2 A	0	0	0	0	0	0	0	0	0	0	0	0	0	0
Feb-16	TK3 A	0	0	0	0	0	0	0	0	0	0	0	0	0	0
Feb-16	TK4 A	0	4	0	0	0	0	0	0	0	0	0	0	0	0
Mar-16	TK1 A	2	0	2	0	0	0	0	0	0	0	0	0	0	0
Mar-16	TK1 B	10	2	0	0	0	0	0	0	0	0	0	0	0	0
Mar-16	TK1 C	40	30	0	0	0	0	0	0	0	0	0	0	0	0
Mar-16	TK1 D	0	0	0	0	0	0	0	0	0	0	0	0	0	0
Mar-16	TK2 A	2	0	0	2	0	0	0	0	0	0	0	0	0	0
Mar-16	TK2 B	0	0	0	0	2	0	0	0	0	0	0	0	0	0
Mar-16	TK2 C	0	156	0	0	56	0	0	0	0	0	0	0	0	0
Mar-16	TK2 D	0	60	0	0	10	0	2	0	0	0	0	0	0	0
Mar-16	TK3 A	8	0	0	0	2	0	0	0	0	0	0	0	0	0
Mar-16	TK3 B	0	0	0	0	0	0	0	0	0	0	0	0	0	0
Mar-16	TK3 C	0	0	0	0	6	0	0	0	0	6	0	0	0	0
Mar-16	TK3 D	4	0	0	0	18	0	34	0	0	0	0	0	0	0
Mar-16	TK4 A	2	66	0	0	8	0	2	0	0	6	0	0	0	0
Mar-16	TK4 B	0	128	0	0	4	0	2	0	0	22	0	0	0	0
Mar-16	TK4 C	0	246	0	0	4	0	2	0	0	16	0	0	0	0
Mar-16	TK4 D	0	186	0	0	4	0	0	0	0	42	0	0	0	0

Jun-16	TK1 A	6	0	0	0	0	0	0	0	0	0	0	0	0	0
Jun-16	TK1 B	12	0	0	0	0	0	0	0	0	0	0	0	0	0
Jun-16	TK1 C	20	2	0	0	0	0	0	0	0	0	0	0	0	0
Jun-16	TK1 D	22	0	0	0	0	0	0	0	0	0	0	0	0	0
Jun-16	TK2 A	0	50	16	0	2	0	0	0	0	0	0	0	0	0
Jun-16	TK2 B	0	4	0	0	4	0	0	0	0	0	0	0	0	0
Jun-16	TK2 C	0	0	0	0	0	0	0	0	0	0	0	0	0	0
Jun-16	TK2 D	8	100	10	0	20	0	0	0	0	0	0	0	0	0
Jun-16	TK3 A	6	0	4	0	4	0	2	0	0	2	0	0	0	0
Jun-16	TK3 B	4	2	24	0	4	0	12	0	0	8	0	0	0	0
Jun-16	TK3 C	4	0	22	0	0	2	16	0	0	0	0	0	0	0
Jun-16	TK3 D	0	0	2	0	0	0	0	0	0	4	0	0	0	0
Jun-16	TK4 A	0	46	0	0	8	0	0	0	0	0	0	0	0	0
Jun-16	TK4 B	0	26	0	0	0	0	0	0	0	0	0	0	0	0
Jun-16	TK4 C	0	12	0	0	8	0	0	0	0	6	0	0	0	0
Jun-16	TK4 D	0	64	0	0	8	0	4	0	0	4	0	0	0	0
Sep-16	TK1 A	42	10	0	0	0	0	0	0	0	0	0	0	0	0
Sep-16	TK1 B	28	20	0	0	0	0	0	0	0	0	0	0	0	0
Sep-16	TK1 C	20	6	0	0	0	0	0	0	0	0	0	0	0	0
Sep-16	TK1 D	30	4	0	0	0	0	0	0	0	0	0	0	0	0
Sep-16	TK2 A	4	4	2	0	0	0	0	0	0	0	0	0	0	0
Sep-16	TK2 B	0	56	2	0	0	0	0	0	0	0	0	0	0	0
Sep-16	TK2 C	10	138	18	0	0	0	0	0	0	0	0	0	0	0
Sep-16	TK2 D	4	10	26	0	0	0	0	0	0	0	0	0	0	0
Sep-16	TK3 A	6	0	4	0	0	8	4	0	0	30	0	0	0	0
Sep-16	TK3 B	2	2	2	0	0	0	2	0	0	8	0	0	0	0
Sep-16	TK3 C	10	0	8	0	0	8	4	0	0	16	0	0	0	0
Sep-16	TK3 D	0	0	2	0	0	0	0	0	0	0	0	0	0	0
Sep-16	TK4 A	0	6	0	0	0	0	10	0	0	14	0	0	0	0
Sep-16	TK4 B	0	8	0	0	0	0	6	0	0	12	0	0	0	0
Sep-16	TK4 C	0	6	0	0	0	0	6	0	4	10	0	0	0	0
Sep-16	TK4 D	0	10	0	0	0	0	4	0	0	6	0	0	0	0
Dec-16	TK1 A	34	22	0	0	0	0	0	0	0	0	0	0	0	0
Dec-16	TK1 B	76	26	0	0	0	0	0	0	0	0	0	0	0	0
Dec-16	TK1 C	122	2	0	0	0	0	0	0	0	0	0	0	0	0
Dec-16	TK1 D	20	10	0	0	0	0	0	0	0	0	0	0	0	0
Dec-16	TK2 A	8	26	24	4	10	0	0	0	0	0	0	0	0	0
Dec-16	TK2 B	10	40	34	0	12	0	0	0	0	0	0	0	0	0
Dec-16	TK2 C	6	68	26	2	6	0	0	0	0	0	0	0	0	0
Dec-16	TK2 D	6	44	26	0	6	0	0	0	0	0	0	0	0	0
Dec-16	TK3 A	6	2	2	0	4	0	2	0	0	0	0	0	0	0
Dec-16	TK3 B	2	0	0	0	0	0	2	0	0	0	0	0	0	0
Dec-16	TK3 C	6	0	0	0	2	0	0	0	0	2	0	0	0	0
Dec-16	TK3 D	6	0	6	0	6	0	0	0	0	0	0	0	0	0
Dec-16	TK4 A	0	58	0	0	2	0	0	0	0	22	0	0	0	0
Dec-16	TK4 B	0	46	0	0	0	0	6	0	0	32	0	0	0	0
Dec-16	TK4 C	0	60	0	0	0	0	0	0	0	8	0	0	0	0
Dec-16	TK4 D	0	24	0	0	0	0	2	0	0	24	0	0	0	0
Mar-17	TK1 A	40	34	0	0	0	0	0	0	0	0	0	0	0	0
Mar-17	TK1 B	52	78	4	0	0	0	0	0	0	0	0	0	0	0
Mar-17	TK1 C	20	14	0	0	0	0	0	0	0	0	0	0	0	0
Mar-17	TK1 D	62	42	2	0	0	0	0	0	0	0	0	0	0	0
Mar-17	TK2 A	2	92	2	0	30	0	0	0	0	0	0	0	0	0
Mar-17	TK2 B	4	236	8	0	28	0	2	0	0	4	0	0	0	0
Mar-17	TK2 C	6	184	8	0	10	0	0	0	0	0	0	0	0	0
Mar-17	TK2 D	4	218	12	0	18	0	0	0	0	0	0	0	0	0
Mar-17	TK3 A	0	0	2	0	20	0	6	0	0	4	0	0	0	0
Mar-17	TK3 B	2	0	12	0	8	0	0	0	0	6	0	0	2	0
Mar-17	TK3 C	6	0	4	0	6	2	2	0	0	0	0	0	0	0
Mar-17	TK3 D	8	0	8	0	16	0	4	0	0	6	0	0	4	0
Mar-17	TK4 A	0	54	0	0	0	0	2	0	0	36	0	0	0	0
Mar-17	TK4 B	0	210	0	0	6	0	0	0	2	0	0	0	0	0
Mar-17	TK4 C	0	100	0	0	0	0	4	0	0	26	0	0	0	0
Mar-17	TK4 D	0	190	0	0	2	0	4	0	0	8	0	0	0	0
Jun-17	TK1 A	142	24	6	0	0	0	0	0	0	0	0	0	0	0
Jun-17	TK1 B	18	2	2	0	0	0	0	0	0	0	0	0	0	0
Jun-17	TK1 C	166	46	2	0	0	0	0	0	0	0	0	0	0	0
Jun-17	TK1 D	76	28	2	0	0	0	0	0	0	0	0	0	0	0
Jun-17	TK2 A	0	4	14	0	2	2	0	0	0	0	0	0	0	0
Jun-17	TK2 B	14	16	6	2	2	0	0	0	0	4	0	0	0	0
Jun-17	TK2 C	10	44	20	2	4	0	0	0	0	0	0	0	0	0
Jun-17	TK2 D	0	16	18	0	0	0	0	0	0	0	0	0	0	0
Jun-17	TK3 A	6	0	8	0	0	2	8	0	0	2	0	0	0	0
Jun-17	TK3 B	2	4	20	0	0	2	2	0	0	2	0	0	0	0
Jun-17	TK3 C	48	0	8	0	6	0	2	0	0	10	0	0	0	0
Jun-17	TK3 D	6	0	16	0	2	2	2	0	0	50	0	0	0	0
Jun-17	TK4 A	0	46	0	0	2	0	2	0	0	10	0	0	0	0
Jun-17	TK4 B	0	104	0	0	14	0	0	0	0	6	0	0	0	0
Jun-17	TK4 C	0	64	0	0	2	0	2	0	0	12	0	0	0	0
Jun-17	TK4 D	2	126	0	0	12	0	10	0	4	14	0	0	0	0

Appendix C: Stable carbon isotope geochemical data over the three-year study period for all four monitoring stations.

Sampling Date	Sample ID	del 13C (per mille VPDB)
Sep-14	TK1A	-16.8
Sep-14	TK1B	-16.8
Sep-14	TK2 A1	-16.2
Sep-14	TK2 A2	-16.8
Sep-14	TK2B	-15.3
Sep-14	TK3A	-16.6
Sep-14	TK3B	-16.8
Dec-14	TK1A	-17.1
Dec-14	TK1B	-16.9
Dec-14	TK2A	-16.1
Dec-14	TK2B	-15.1
Dec-14	TK3B	-17.0
Dec-14	TK3 A1	-17.0
Dec-14	TK3 A2	-17.1
Mar-15	TK1A	-17.3
Mar-15	TK2A	-15.3
Mar-15	TK3A	-17.0
Mar-15	TK4A	-28.0
Mar-15	TK4B	-28.0
Jun-15	TK1A	-16.4
Jun-15	TK2A	-15.5
Jun-15	TK3A	-15.8
Jun-15	TK4A	-28.1
Sep-15	TK1A	-15.8
Sep-15	TK1A	-15.5
Sep-15	TK2A	-16.2
Sep-15	TK3A	-16.4
Sep-15	TK4A	-28.0
Dec-15	TK1A	-16.4
Dec-15	TK2A	-15.1
Dec-15	TK3A	-16.0
Dec-15	TK4A	-28.0
Mar-16	TK1A	-16.7
Mar-16	TK2A	-15.6
Mar-16	TK3A	-15.7
Mar-16	TK3A	-15.8
Mar-16	TK4A	-28.0
Jun-16	TK1A	-16.2
Jun-16	TK2A	-15.1
Jun-16	TK3A	-17.7
Jun-16	TK4A	-28.1
Sep-16	TK1A	-17.1
Sep-16	TK2A	-15.7
Sep-16	TK2B	-16.3
Sep-16	TK3A	-16.9
Sep-16	TK4A	-27.9
Dec-16	TK1A	-17.5
Dec-16	TK2A	-15.4
Dec-16	TK2B	-15.7
Dec-16	TK3A	-16.7
Dec-16	TK4A	-27.4
Mar-17	TK1A	-16.7
Mar-17	TK2A	-15.2
Mar-17	TK3A	-20.4
Mar-17	TK3B	-19.5
Mar-17	TK4A	-28.1
Jun-17	TK1A	-16.9
Jun-17	TK2A	-16.6
Jun-17	TK3A	-22.7
Jun-17	TK3B	-19.2
Jun-17	TK4A	-28.0
Oct-17	TK3A	-18.2
Dec-17	TK3A	-17.1

Appendix D: Porewater salinity and loss on ignition data over the three-year study period for all four monitoring stations.

	Salinity (psu)			
Sampling Date	**Station 1**	**Station 2**	**Station 3**	**Station 4**
Sep-14	38.73	10.7	11.24	
Dec-14	34.88	5.25	8.32	
Mar-15	23.47	4.19	3.57	0.58
Jun-15	40.31	10.58	10.96	0.61
Sep-15	56.9	16.86	20.11	5.33
Dec-15	36.37	14.52	14.59	3.14
Mar-16	42.57	17.09	10.09	1.83
Jun-16	36.71	12.13	8.93	0.58
Sep-16	48.78	18.68	18.22	5.23
Dec-16	30.45	18.4	17.18	5.5
Mar-17	41.82	18.45	17.39	3.37
Jun-17	38.7	13.52	11.01	1.22

Sampling Date	Sample ID	LOI %
Sep-14	TK1 B	17.43024
Sep-14	TK2 B	77.67073
Sep-14	TK3 B	61.68789
Dec-14	TK1 B	19.71515
Dec-14	TK2 B	85.28885
Dec-14	TK3 B	61.31553
Mar-15	TK1 B	21.66722
Mar-15	TK2 B	87.9616
Mar-15	TK3 B	61.68533
Mar-15	TK4 B	55.94823
Jun-15	TK1 B	22.04848
Jun-15	TK2 B	80.72311
Jun-15	TK3 B	67.38191
Jun-15	TK4 B	53.524
Sep-15	TK1 B	24.17137
Sep-15	TK2 B	79.7234
Sep-15	TK3 B	60.42876
Sep-15	TK4 B	52.88651
Dec-15	TK1 B	32.20608
Dec-15	TK2 B	81.41069
Dec-15	TK3 B	70.19671
Dec-15	TK4 B	48.26616
Mar-16	TK1 B	31.545
Mar-16	TK2 B	82.35795
Mar-16	TK3 B	61.21884
Mar-16	TK4 B	70.05177
Jun-16	TK1 B	27.62158
Jun-16	TK2 B	83.10361
Jun-16	TK3 B	62.94113
Jun-16	TK4 B	53.90959
Sep-16	TK1 B	37.08803
Sep-16	TK2 B	79.87401
Sep-16	TK3 B	63.493
Sep-16	TK4 B	47.02623
Dec-16	TK1 B	35.70737
Dec-16	TK2 B	80.4101
Dec-16	TK3 B	72.95487
Dec-16	TK4 B	43.29803
Mar-17	TK1 B	38.22437
Mar-17	TK2 B	80.70383
Mar-17	TK3 B	64.64016
Mar-17	TK4 B	60.36558
Jun-17	TK1 B	40.04798
Jun-17	TK2 B	74.33607
Jun-17	TK3 B	63.14568
Jun-17	TK4 B	49.04802

Appendix E: Total counts of all live species combined and the three dominant species for each Monitoring Station during the three-year sampling timeframe. Distributions in counts for each sampling period represent the four replicate samples. Note variable y-axis scales for total count sizes. Coefficient of variation (CV) among replicates is displayed for each sampling period as a secondary y-axis. Note variable y-axis scales for CV.

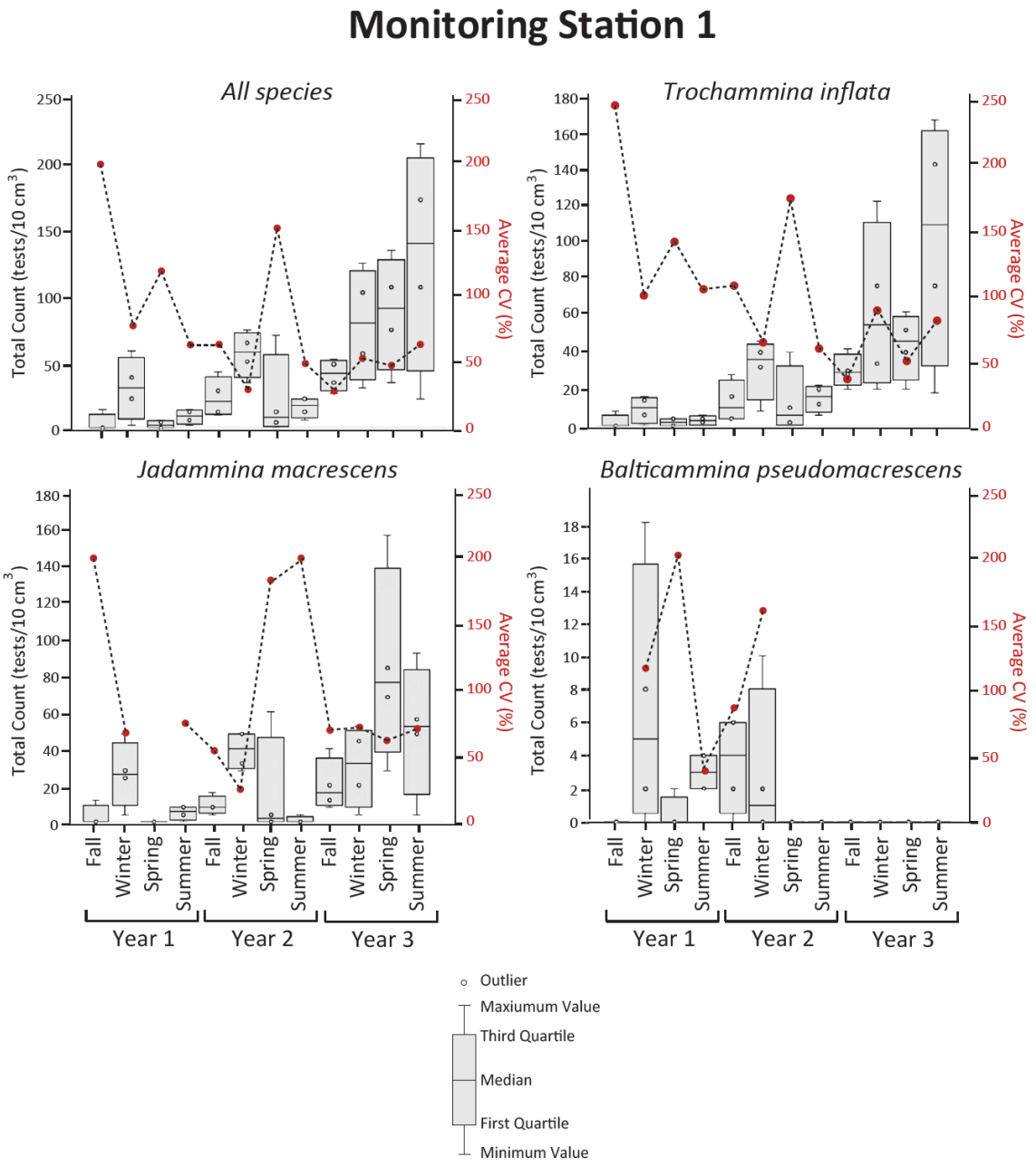

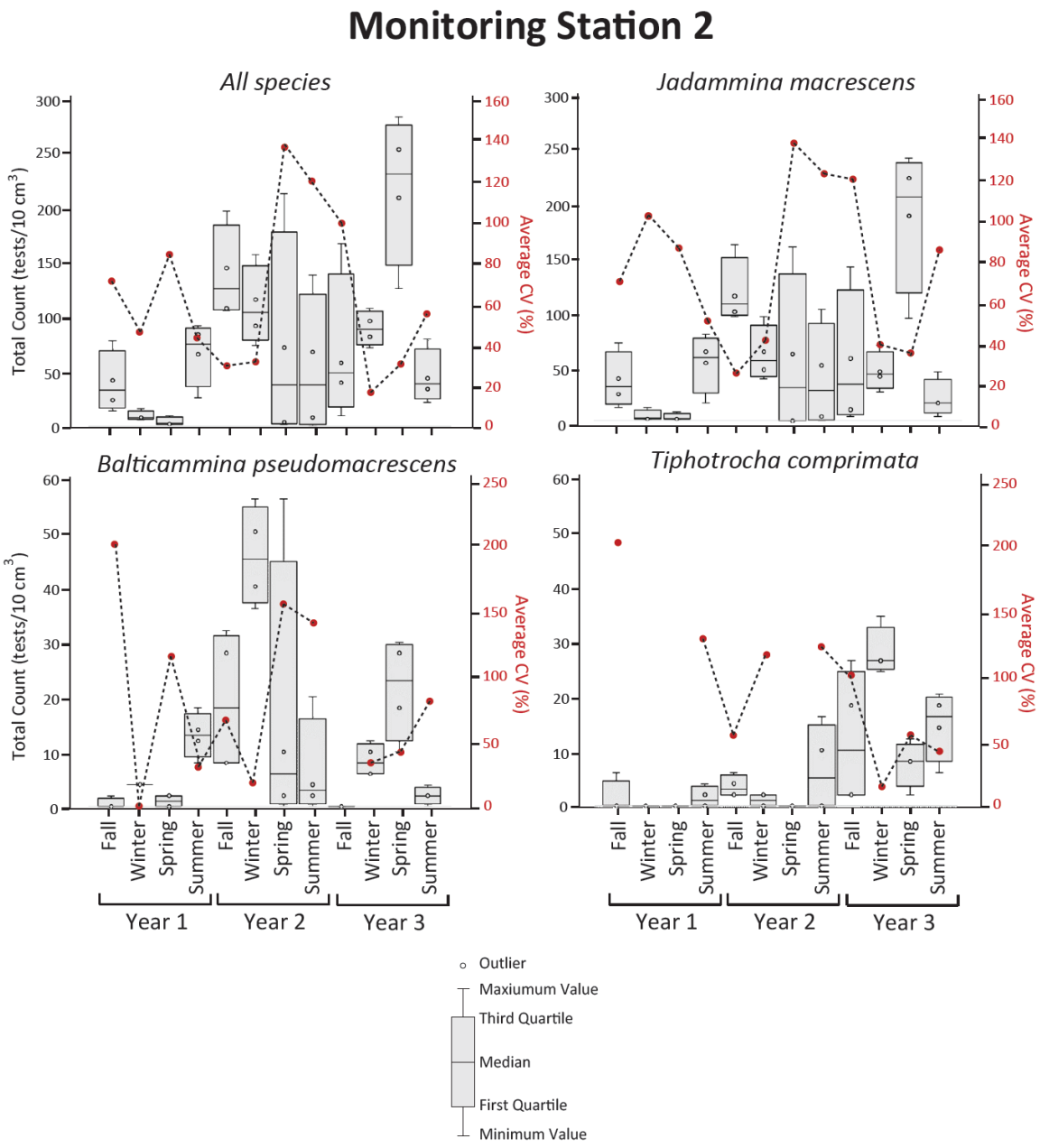
Monitoring Station 2
All species
Jadammina macrescens
Balticammina pseudomacrescens
Tiphotrocha comprimata
Total Count (tests/10 cm3)
Average CV (%)
Fall
Winter
Spring
Summer
Year 1
Year 2
Year 3
Outlier
Maxiumum Value
Third Quartile
Median
First Quartile
Minimum Value

Monitoring Station 3

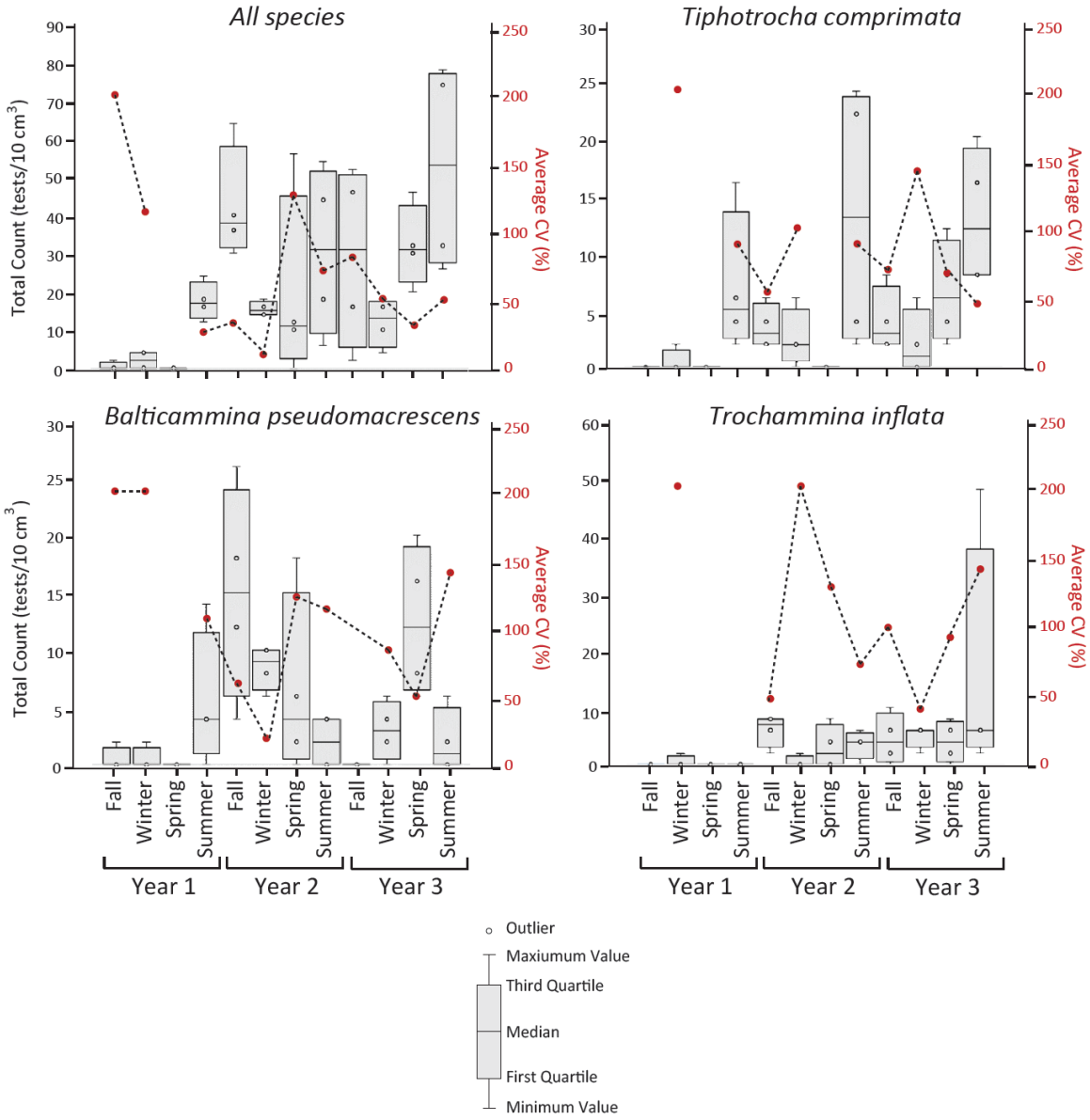

Monitoring Station 4

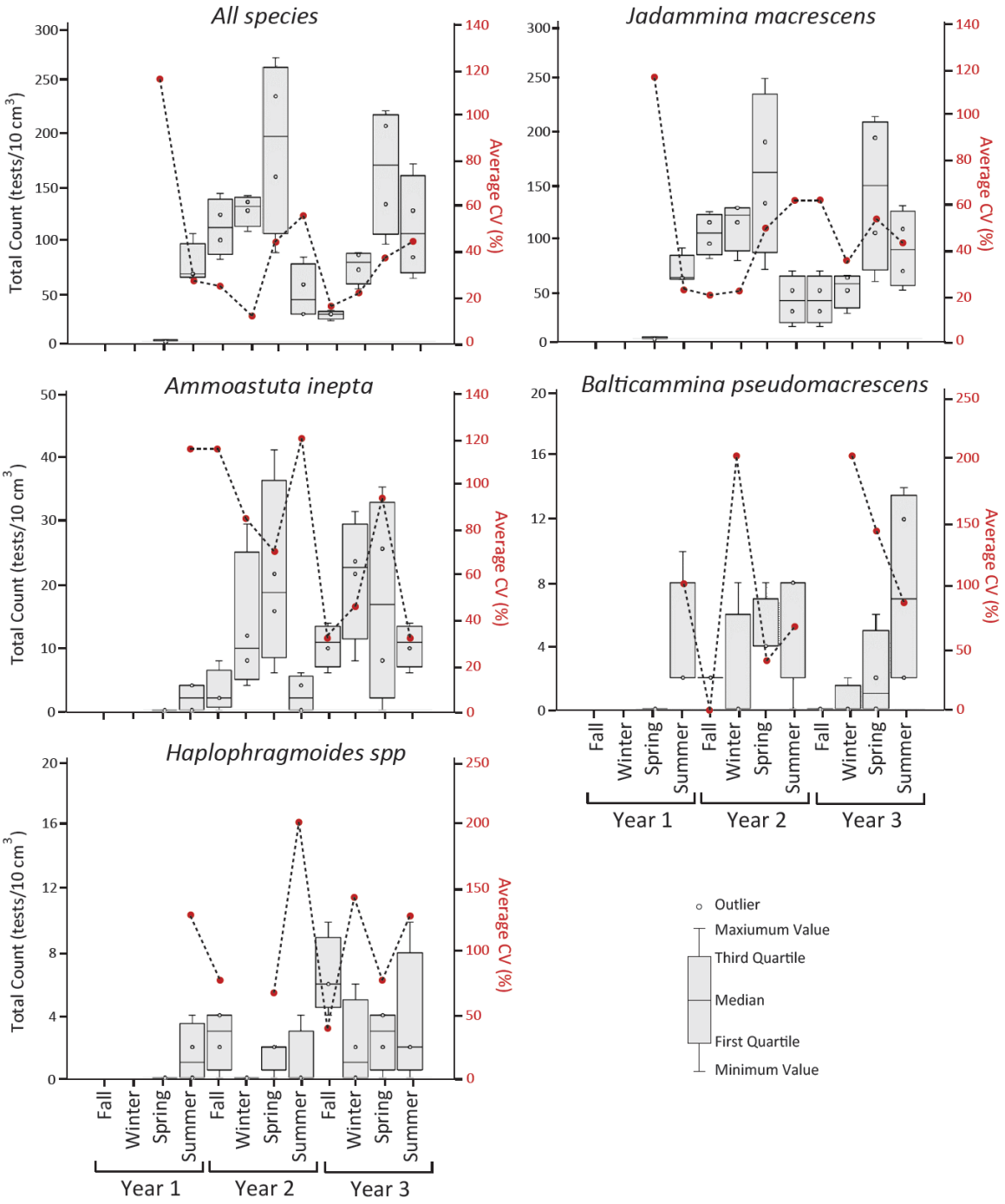

Appendix F: Bayesian transfer function elevation estimates (in SWLI units) from each sampling period for Monitoring Stations 2, 3, and 4. Observed SWLI is shown by gray bar. SWLI estimates uses the full foraminifera dataset of dead counts. Distributions in estimated SWLI for each sampling period represent the four replicate samples. Replicate-aggregate SWLI estimates are shown as red data points on top of the estimated SWLI using the full dataset. Seasonal SWLI estimates are shown for each season (Fall, Winter, Spring, Summer) using the full dataset, the replicate-aggregate dataset, and a seasonal-aggregate dataset. Similarly, seasonal SWLI uncertainties in elevation estimates are shown for each season using the three different datasets.

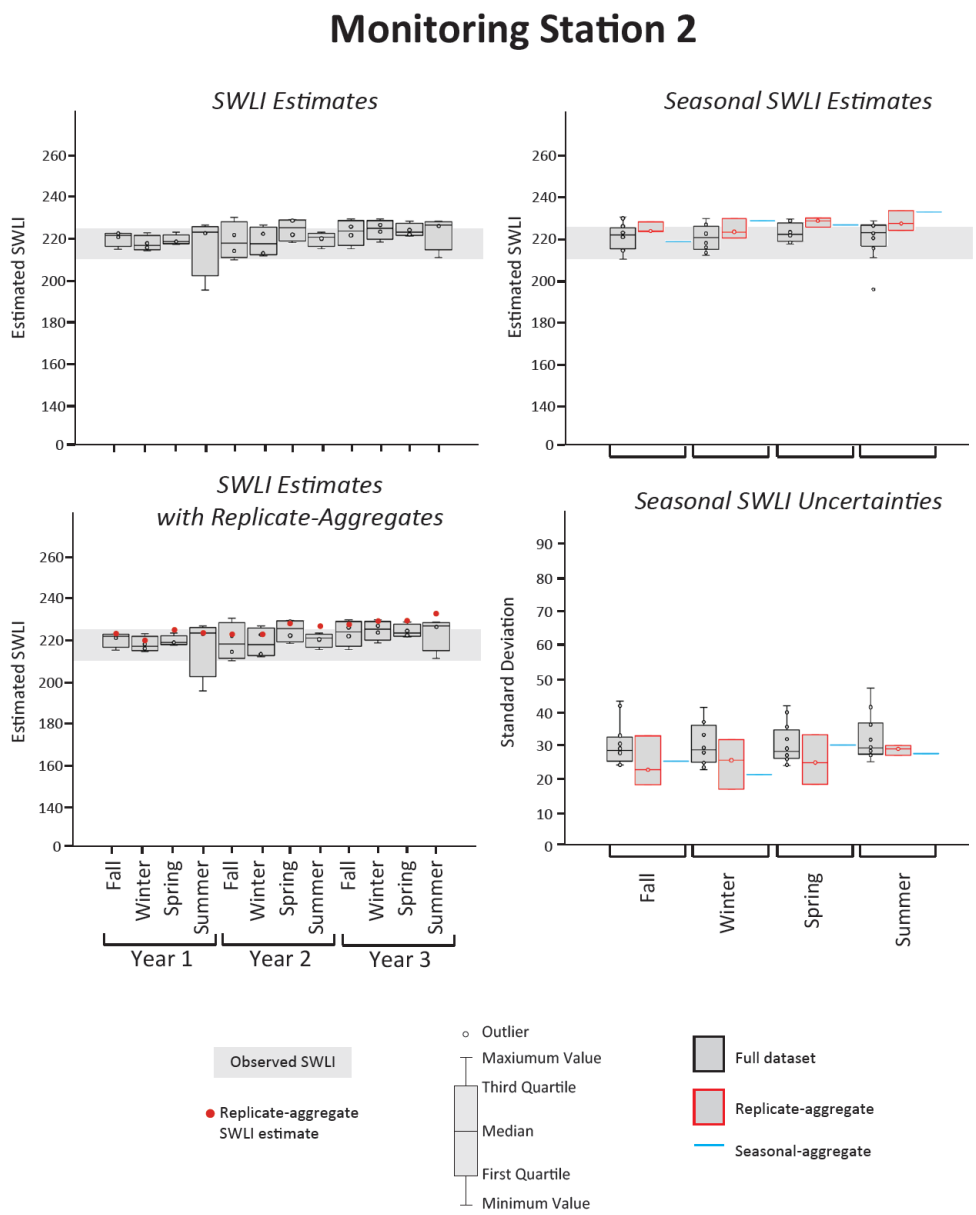

Monitoring Station 3

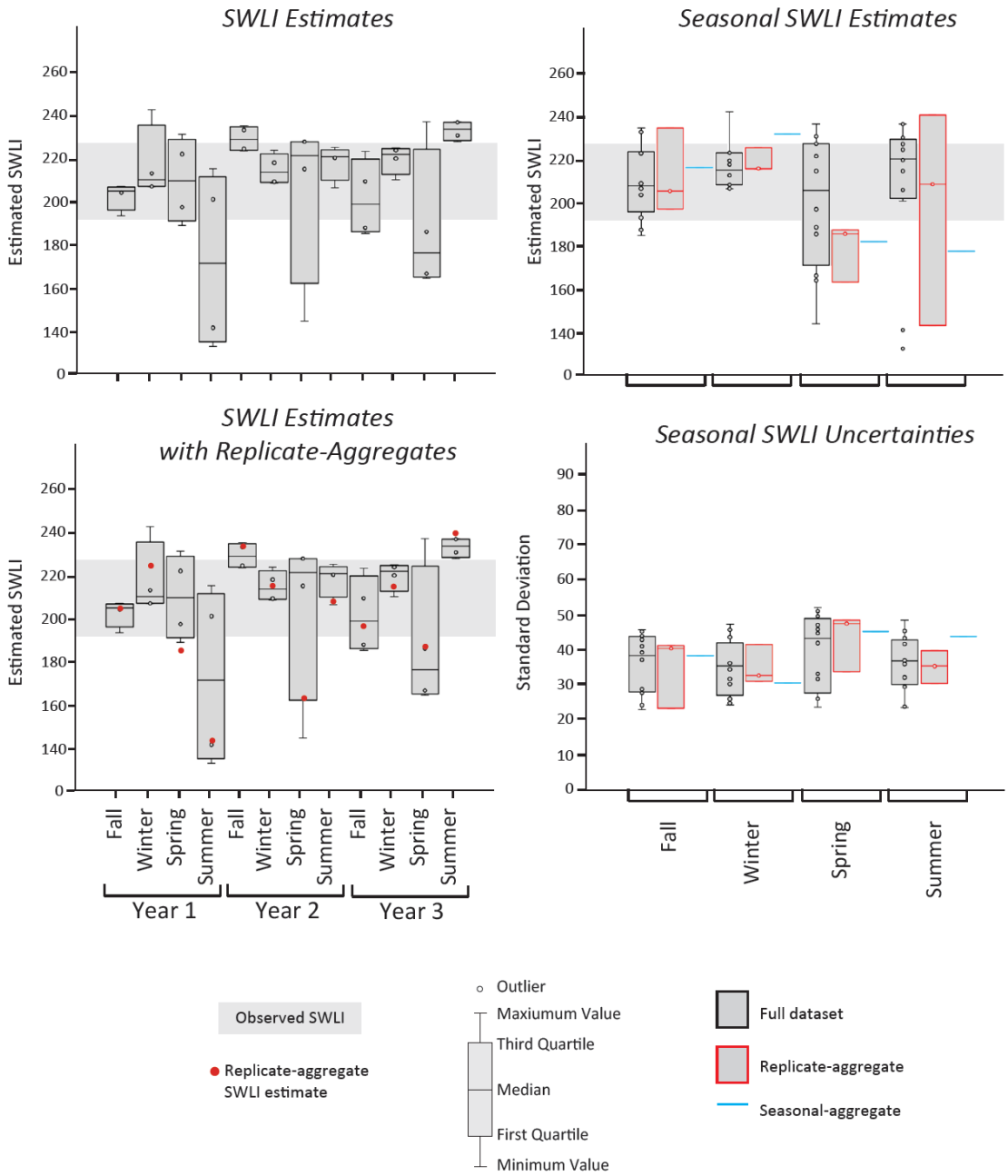

Monitoring Station 4

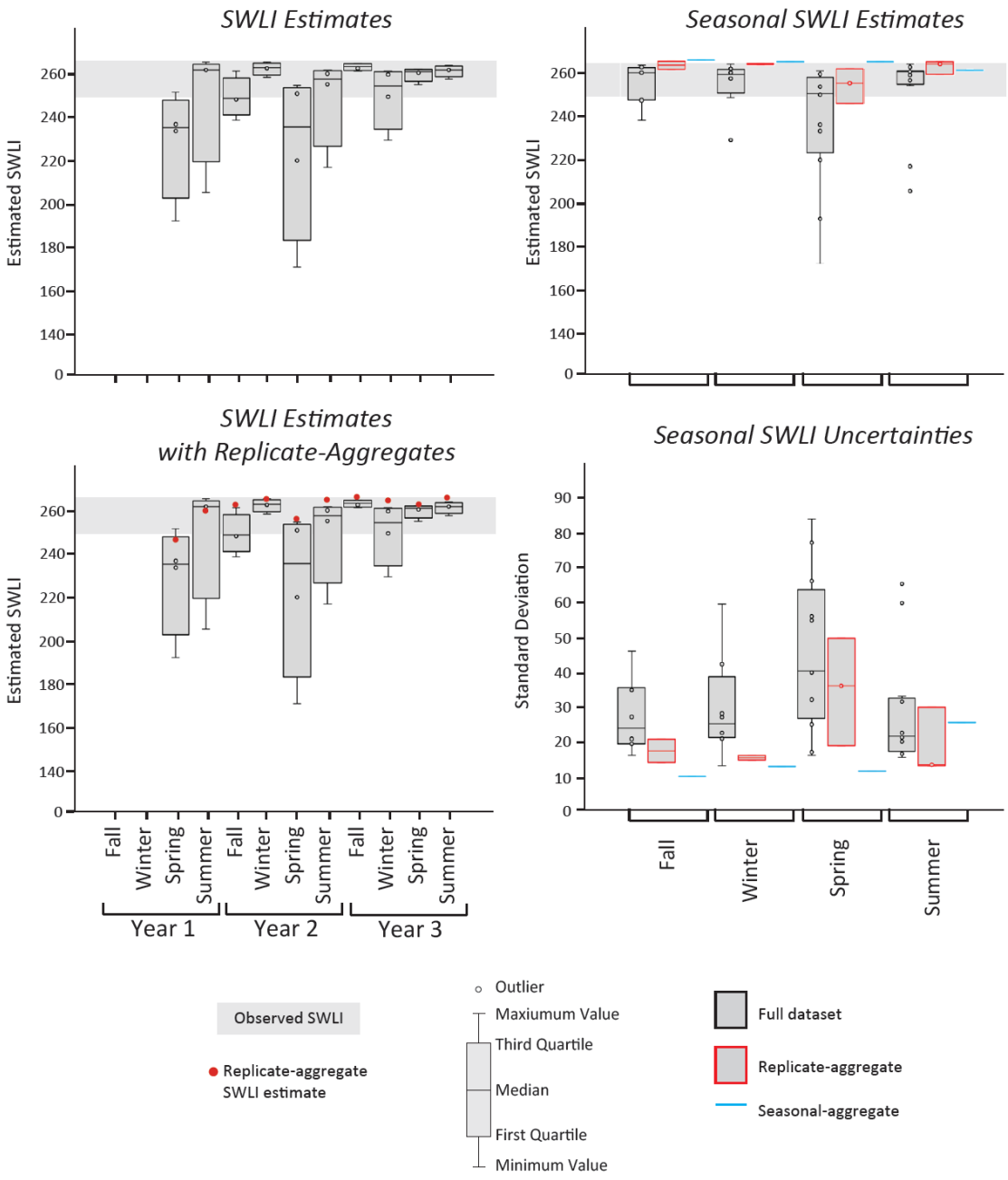

Chapter 2: The inception of modern rates of sea-level rise as revealed by a global database of sea-level records

Abstract

Common Era sea-level reconstructions have improved understanding of magnitudes and rates of sea-level change at centennial to multi-decadal timescales, providing information about sea-level responses to climate change. Although there is agreement that rates of sea-level rise exceed Common Era background rates by the late 18th to early 20th century, the timing of increased modern rates of sea-level rise is uncertain. Here, we produced a new high-resolution (decimeter vertical, decadal temporal) Common Era relative sea-level (RSL) record in northern New Jersey and integrated it into an updated global database of instrumental and proxy sea-level records of the Common Era. We use a spatiotemporal empirical hierarchical model to estimate past RSL and rates of RSL change with associated uncertainty in the context of broader global and regional changes. Globally, it is very likely (probability $P \geq 0.90$) that the 60-year average rate of global mean sea level (GMSL) rise emerged from pre-Industrial Common Era (0-1700 CE) background variability by ~1870 CE, which we propose as the global onset of modern rates of sea-level rise.

We examined the timing of modern elevated rates of RSL rise at nineteen sites in the North Atlantic, which have the highest resolution of all of the proxy locations in the global RSL database. The timing is asynchronous at the North Atlantic sites, but reveals a distinct spatial pattern where the onset of modern rates appears muted and later along the European coast compared to the North American coast. Elevated 60-year average RSL rates appear

earliest in the mid-Atlantic region (e.g. ~1880-1895 CE in New Jersey), followed by the northeastern and southeastern U.S. (e.g. ~1895 CE in Connecticut and ~1895-1925 CE in Florida), and latest in Canada and Europe (e.g. ~1940-1950 CE in Newfoundland and Iceland). The observed spatial pattern in timing appears to follow SST trends from a reduction in Atlantic Meridional Overturning Circulation (AMOC) and northward shift of the Gulf Stream, where the northeast coast of the U.S. warms, with cooling to the south and to the north in the subpolar Atlantic gyre. We suggest that the observed spatial pattern in the timing may be due to a combination of steric and ocean dynamic effects from changes in Atlantic Meridional Overturning Circulation (AMOC) and the Gulf Stream.

1. Introduction

Relative sea level (RSL) reconstructions of the Common Era (last 2000 years) have extended the instrumental record back beyond the 20th century (e.g. Gehrels, 2000; Kemp et al., 2013, 2017). Common Era sea-level reconstructions have improved understanding of magnitudes and rates of sea-level change at centennial to multi-decadal timescales, providing information about sea-level responses to climate change and paleo constraints for model calibration (e.g. Varekamp et al., 1992; Kemp et al., 2011; Horton et al., 2018). Although there is agreement that rates of sea-level rise exceed Common Era background rates by the late 18th to early 20th century (e.g. Shennan and Horton, 2002; Gehrels et al., 2005; Engelhart and Horton, 2012), the timing of increased modern rates of sea-level rise is uncertain. Identifying the accurate timing and examining spatial variability will help decipher underlying mechanisms that have driven the faster rates of modern sea-level rise

and attribute natural and human-caused sea-level drivers (e.g. Kopp et al., 2016), as well as improve calibration of models of sea-level projections (e.g. Grinsted et al., 2009).

The timing of the inception of modern rates of sea-level rise has been estimated by instrumental and/or proxy records (e.g. Church and White 2006, 2011; Jevrejeva et al., 2008; Woodworth et al., 2009; Gehrels and Woodworth, 2012; Kemp et al., 2015). Compilations of global and regional tide gauge data found an acceleration of sea-level rise around 1930 CE (Church and White 2006, 2011; Woodworth et al. 2009) but noted that an initial acceleration began in the 19th century. A global sea level reconstruction using Monte Carlo Singular Spectrum Analysis of tide gauge records suggests an earlier acceleration starting at the end of the 18th century (Jevrejeva et al., 2008); however, only a limited number of tide gauge records extend back through to the 18th and 19th centuries and these records are restricted to north-western Europe (Tamisiea et al., 2014). Common Era sea-level reconstructions provide the necessary high-resolution chronology to establish a quantitative estimate of the beginning of modern rates of rise (e.g. Donnelly et al. 2004, Gehrels et al. 2005, Kemp et al. 2011, 2014). Kopp et al. (2016) estimated global sea-level change through the Common Era by applying a spatiotemporal hierarchical model to a global database of RSL reconstructions. They found that global sea level varied by ~±8 cm over the pre-Industrial Common Era, followed by a significant global sea level acceleration that began in the 19th century. Kemp et al. (2015) used change point analysis to examine timing of increased rates of rise and quantified common timing among western North Atlantic proxy records to 1865-1873 CE, while Gehrels and Woodworth (2012) identified the increase in the rate of rise at ~1925 CE. The range of suggested timings may reflect the

resolution and types of data used or may intriguingly suggest regional variability due to the gravitational, rotational, and deformational fingerprints of mass loss from ice sheet and glacier melt (e.g. Mitrovica et al., 2009), ocean steric effects (e.g. Cazenave and Llovel, 2010), and/or ocean dynamics (e.g. Ezer, 2015). Alternatively, the timing of modern rates may depend on the proxy evidence and the dating methods used and their associated errors (e.g. Gehrels and Woodworth, 2012).

Here, we produced a new high-resolution (decimeter vertical, decadal temporal) Common Era RSL record in northern New Jersey and integrated it into an updated global database of instrumental and proxy sea-level records of the Common Era (Kopp et al., 2016). Following the methods of Kopp et al. (2016), we used a spatiotemporal empirical hierarchical model (Ashe et al., 2019) to analyse the new northern New Jersey record in a broader regional and global context and examine magnitudes and rates of past RSL and global-mean sea level change. Using the reconstructed spatiotemporal sea-level field, we examined the timing of modern elevated rates of sea-level rise in the northern New Jersey record and in other published records along the Northeastern Atlantic coast (Kemp et al. 2013; Kemp et al. 2017), as well as regional variability in magnitudes and rates of past RSL change. We assessed the global timing of the onset of modern rates of sea-level rise and identified spatial variability of elevated rates of sea-level rise among the sites with the highest resolution proxy records.

2. Study Area

New Jersey has an extensive history of Holocene RSL studies (e.g. Psuty, 1986; Miller et al., 2009, 2013; Horton et al., 2013; Kemp et al., 2013; Johnson et al., 2018). Due to New Jersey's close proximity to the former Laurentide Ice Sheet margin, glacial isostatic subsidence has been a significant contributor to RSL rise in the late Holocene (e.g. Engelhart et al., 2009; Roy and Peltier, 2015; Love et al., 2016). Psuty (1986) examined sea-level trends using radiocarbon dates from sediment cores at Cheesequake State Park and elsewhere in northern New Jersey and found rising RSL from at least 7700 years BP to present, with a rapid rate of rise beginning before 7000 years BP, followed by a decrease in rates 2000-2500 years BP. Horton et al. (2013) used a sea-level database for New Jersey, including the data from Psuty (1986); after accounting for compaction and change in tidal range, they found that RSL in New Jersey rose at an average rate of 4 mm/yr from 10-6 ka, 2 mm/yr from 6-2 ka, and 1.3 mm/yr from 2 ka to 1900 CE. Miller et al. (2009) reconstructed RSL in New Jersey over the last 5000 years and found a relatively constant rise of ~1.8 mm/yr from ~5000 to 500 yr BP, while Miller et al. (2013) found a rise of 1.6 ± 0.1 mm/yr from 2.2 to 1.2 ka (800 CE) and 1.4 ± 0.1 mm/yr from 800 to 1800 CE. Kemp et al. (2013) reconstructed RSL over the last 2500 years in southern New Jersey and, after correcting for land-level change (1.4 mm/year), found four multi-centennial sea-level trends: fall at 0.11 mm/year from 500 BCE to 250 CE, rise at 0.62 mm/year from 250 CE to 733 CE, fall at 0.12 mm/year from 733 CE to 1850 CE, and rise at 3.1 mm/year since 1850 CE.

The instrumental RSL record can be examined through tide gauges in the region (Figure 1). The NOAA-operated tide gauge at Sandy Hook, New Jersey (station number 8531680), located ~20 km from Cheesequake State Park, shows a rate of rise of 4.09 mm/yr (95% confidence interval of ± 0.2 mm/yr) from 1932 to 2018. To the north of Cheesequake, at the tide gauge at The Battery, New York (station number 8518750), RSL has risen at a rate of 2.85 mm/yr (95% confidence interval of ± 0.09 mm/yr) from 1856 to 2018. Alternatively, to the south of Cheesequake, the tide gauge at Atlantic City, New Jersey (station number 8534720) shows a rate of rise 4.09 mm/yr (95% confidence interval of ± 0.15 mm/yr) from 1911 to 2018.

We produced a new Common Era RSL record from a salt-marsh field study site at Cheesequake State Park in northern New Jersey off of Raritan Bay, 30 miles from New York City (Figure 2). The state park comprises 1610 acres of salt marshes, freshwater wetlands, cedar swamp, open fields, and upland forest surrounding Cheesequake Creek (New Jersey Department of Environmental Protection, 2015). The estuarine system of Cheesequake State Park drains northward into Raritan Bay and accumulates sediment by combination of fluvial transport, slope wash, and coastwise transport (e.g. Meade, 1969; Renwick and Ashley, 1984; Psuty, 1986; Gaswirth et al, 2002). The drainage channel system is eroded into the sedimentary rock Magothy Formation of the New Jersey coastal plain (e.g. Meade, 1969; Psuty, 1986; Gaswirth et al, 2002). The modern marsh surface intersects steep valley sides of older (Pleistocene) drainage channels due to infilling of the estuary (Meade, 1969; Psuty, 1986; Gaswirth et al, 2002). The modern low marsh is vegetated by *Spartina alterniflora* (long form) and the high marsh is vegetated by *Spartina patens*, *Distichlis spicata*, and *Iva*

fructescens. The border between the salt marsh and freshwater upland is vegetated by *Phragmites australis*. The tidal range is a semidiurnal, micro-tidal (range ~1.6 m) regime.

3. Methods

We used salt-marsh foraminifera as a proxy to reconstruct Common Era sea level, because their modern distributions exhibit vertical zonation (e.g. Scott and Medioli, 1978; Gehrels, 1994; Horton and Edwards, 2006). Foraminiferal-based transfer functions utilize a modern foraminifera training set to quantify species assemblages' relationship with elevation, which is then applied to fossil assemblages to produce continuous records of sea-level at decimeter vertical resolution (e.g., Horton et al., 1999; Gehrels, 2000; Horton and Edwards, 2006). The foraminiferal-based transfer function has been recently enhanced using a Bayesian approach that employs foraminifera and a secondary proxy, geochemistry (Cahill et al., 2016; Kemp et al., 2017). Stable carbon isotope geochemistry ($\delta^{13}C$) in bulk sediment represents the dominant vegetation type and can be used as a proxy for sea level, because the transition between C_3 and C_4 dominated salt-marsh plant communities has been shown to act as the boundary for the mean higher high water (MHHW) tidal datum on the U.S. mid-Atlantic coast (e.g. Middleburg et al., 1997; Johnson et al., 2007; Kemp et al., 2012).

Here, we collected new modern transects of foraminifera and $\delta^{13}C$, and we used a Bayesian transfer function that employs foraminifera and a secondary proxy, $\delta^{13}C$, as an informative prior. We informed the foraminifera variability prior in the transfer function to account for temporal and spatial variability of modern foraminifera distributions (Walker et al., Chapter 1). We reconstructed RSL using the transfer function estimates of paleomarsh

elevations (PME) in combination with a sediment core chronology. We used a geotechnical model (Brain et al., 2011, 2012, 2015) to correct the RSL record for post-depositional lowering through sediment compaction. We used a global Common Era sea-level database updated from Kemp et al. (2018) as input to a spatio-temporal empirical hierarchical model (Kopp et al., 2016; Ashe et al., 2019). Using the model, we examined northern New Jersey RSL and global mean sea level over the Common Era and determined the timing of the onset of modern rates of RSL rise, including spatial variability in timing.

3.1. Modern Sampling and Marsh Stratigraphy

We collected thirty modern samples of two sea-level proxies, foraminifera and $\delta^{13}C$, from surface (0-1 cm) sediment at Cheesequake State Park to produce a modern training set. Modern samples were collected along three transects from low marsh to forested upland to capture changes in elevation and to include a full range of floral environments. Two samples were taken from each modern sampling location: one of a standardized volume of 10 cm^3 (10 cm^2 by 1 cm thick) for foraminiferal analysis to allow comparison with a southern New Jersey modern foraminifera dataset (Kemp et al., 2012); and one of approximately 30 cm^3 (30 cm^2 by 1 cm thick) for $\delta^{13}C$. Foraminifera samples were stored in a buffered ethanol solution. Foraminifera and $\delta^{13}C$ samples were refrigerated until analysis (Scott et al., 2001).

We completed multiple transects of hand cores to describe the underlying stratigraphy of the marsh of Cheesequake State Park. The cores were described in the field using the Troels-Smith (1955) method for organic-rich sediments to record the proportions of

organic matter, silt, clay, and sand, and the presence of wood or shell fragments. A core was chosen with a thick sequence of high marsh peat and collected using a hand-driven Russian-type core to prevent compaction or contamination during sampling. The recovered core was sealed in a pipe section with plastic wrap and refrigerated until analysis to minimize drying and oxidation. We analyzed the collected sediment core for foraminifera and $\delta^{13}C$ in 1-cm slices at 5-cm spaced intervals down core.

We obtained elevations for each modern sample and cores using real time kinematic (RTK) satellite navigation and a total station where elevations were referenced to the North American Vertical Datum (NAVD88). To convert elevations to tidal datums, we deployed three automatic water-level loggers (Solinst Levelogger Edge) in tidal channels adjacent to the core and modern samples. We correlated the water-level logger data with those recorded by the NOAA-operated tide gauge at Sandy Hook, New Jersey (station number 8531680) located ~20 km from the study site.

3.2. Foraminiferal Analysis

We stained the modern foraminifera samples with rose Bengal immediately after collection in order to differentiate live versus dead foraminifera tests (Walton, 1952). Although in some cases rose Bengal may stain dead tests (e.g. Walker et al., 1974; Bernhard, 1988), it remains a reliable method and is unlikely to affect the interpretation of dead assemblages (Murray and Bowser, 2000). Although live specimens were counted, only the dead assemblages are presented here because the dead assemblages most resemble subsurface assemblages and they are thought to minimize temporal variability in modern distributions

(e.g. Horton, 1999; Horton and Edwards, 2003; Morvan et al., 2006). Modern and core foraminifera samples were wet sieved to isolate the 63-500 µm foraminifera-bearing fraction of the sediment and were split into eight equal aliquots using a wet splitter (Scott and Hermelin, 1993). Samples were counted under a binocular microscope while immersed in distilled water (Scott et al., 2001). A minimum of 100 tests were counted, or the entire sample was counted if <100 tests were present to ensure a statistically-sound representation of low-diversity salt-marsh foraminifera assemblages (e.g. Fatela and Taborda, 2002). Identifications of foraminifera were confirmed with type specimens at the National Museum of Natural History, Smithsonian Institute, Washington, D.C. We grouped specimens of the genera *Haplophragmoides* into a single group due to difficulties in identifying them to the species level (Kemp et al., 2009) and in order to combine them with the modern dataset of Kemp et al. (2013) from southern New Jersey.

We combined the modern foraminifera dataset from Cheesequake State Park with the modern dataset of Kemp et al. (2013) from southern New Jersey. We used Principal Component Analysis (PCA) with the program CANOCO 5 (ter Braak and Smilauer, 2012) to compare the modern foraminifera assemblages from Cheesequake State Park with those of Kemp et al. (2013) to ensure that the assemblages were compatible and could be combined into one modern foraminifera training set (New Jersey modern training set). PCA is an ordination technique which projects samples into a multi-dimensional space where similar samples are close together and dissimilar samples are further apart. All modern dead foraminifera data from Cheesequake State Park are presented in Appendix A and all fossil foraminifera data from Cheesequake State Park are presented in Appendix B.

3.3. Stable Carbon Isotope Geochemical Analysis

We analyzed $\delta^{13}C$ in modern and core samples to include $\delta^{13}C$ as a secondary proxy in the BTF as an informative prior used to inform elevation estimates. Modern and core $\delta^{13}C$ values were measured in bulk sediment, since the dominant input to salt-marsh sediment is in situ vegetation. $\delta^{13}C$ was measured at the Departments of Geology and Environmental Studies at Bryn Mawr College using a cavity ring-down laser spectroscopy (CRDS) following the flash combustion technique described by Balslev-Clausen et al (2013). Prior to isotopic analysis, bulk peat samples were freeze-dried in a Virtis™ benchtop freeze dryer to remove moisture and then ground in a Retsch™ ball mill until finely powdered. Approximately two mg (±0.5 mg) of the dried, powdered sample was weighed on a Mettler Toledo™ XP56 microbalance with 4 µg precision. Weighed samples were sealed in pressed-wall tin capsules and flash combusted at 980°C in a Costech™ ECS 4010 element analyzer using N_2 as a carrier gas. The isotopic composition of the CO_2 produced by combustion was analyzed in a Picarro™ G2201-*i* CRDS instrument. Carbon abundance in each sample was calculated from the peak $^{12}CO_2$ concentration measured by the CRDS system, calibrated by analysis of standard reference material (NIST 1547 Peach leaf). Reproducibility of carbon mass concentration is ±0.8% (1 s.d., n=96). Carbon isotopic composition, reported as $\delta^{13}C$, is standardized to Vienna Pee Dee Belemnite (VPDB) by analysis of standard reference material USGS40 (glutamic acid). The reproducibility of δ13C values is <0.2‰ based on repeat analyses of NIST 1547 (0.15‰, 1 s.d., n=96) and USGS40 (0.18‰, 1 s.d., n=27). All $\delta^{13}C$ data are presented in Appendix C.

3.4. Bayesian Transfer Function

We used a foraminiferal-based transfer function using a Bayesian approach that employs foraminifera and a secondary proxy, $\delta^{13}C$, as an informative prior to reduce vertical uncertainty (Cahill et al., 2016; Kemp et al., 2017). The Bayesian transfer function (BTF) was developed using a New Jersey modern training set of salt-marsh foraminifera and $\delta^{13}C$ from Kemp et al. (2013) consisting of 163 samples from 13 sites in southern New Jersey, in addition to the 32 modern samples collected at Cheesequake State Park. Due to differences in tidal range among sampling locations, we converted the tidal elevations of the modern samples into a standardized water level index (SWLI), following the approach of Horton et al. (1999), where a value of 100 corresponds to local mean tide level (MTL) and a value of 200 corresponds to local mean higher high water (MHHW).

The BTF utilizes the modern foraminifera training set to quantify species assemblages' relationship with tidal elevation, which is then applied to fossil assemblages, to estimate a paleomarsh elevation (PME) for each sample with a 1σ sample-specific uncertainty. We formally accounted for temporal and spatial variability of modern foraminifera distributions in the BTF by informing the variability prior for individual foraminifera species using data from a monitoring study of modern foraminifera in southern New Jersey (Walker et al., Chapter 1). The performance of the BTF was evaluated using 10-fold cross validation on the modern training set, where the data is divided into 10 randomly drawn groups of equal size (known as folds). Each fold is removed from the modern dataset in turn and the remaining data is used to create predictions for the removed samples, which is repeated until every sample has an out-of-sample prediction value (Cahill et al., 2016).

We converted the PME estimates from the BTF from SWLI units back into meters relative to MTL specific to Cheesequake State Park. To reconstruct RSL, we used the equation:

$$RSL_i = A_i - PME_i \quad [1]$$

where A_i and PME_i are the altitude and PME of sample i, respectively, and both values are expressed relative to MTL. A_i is established by subtracting the depth of each sample in the core from the measured core-top altitude. PME_i was estimated by the BTF with an associated 1σ uncertainty. RSL is reconstructed under the assumption that the paleotidal range on the coast of New Jersey was relatively constant during the Common Era (Horton et al., 2013). For example, tidal range was estimated to have changed by <5 cm in the last 1000 years in southern New Jersey using a paleotidal model (Walker et al., Chapter 3).

3.5. Compaction

Salt-marsh sediments are prone to sediment compaction, a process that occurs as sediment accumulates, reducing sediment volume and altering the stratigraphic column (Allen, 2000; Horton and Shennan, 2009). We used a geotechnical model (Brain et al., 2011, 2012, 2015) to correct the RSL record for post-depositional lowering through sediment compaction which has been used previously to correct salt-marsh RSL reconstructions for compaction (e.g. Kemp et al., 2017; Kemp et al., 2018).

Modern marsh surface sediments from Cape May Courthouse and Leeds Point in southern New Jersey analogous to those found in the sediment core were used for laboratory geotechnical testing to calibrate the model (Brain et al., 2015). Core samples were tested

under one-dimensional, zero-lateral strain compression using fixed ring, front-loading oedometers (Head, 1988) and the results were used to estimate parameter values of the Brain et al. (2011, 2012) framework to describe changes in volume in response to changes in vertical effective stress. We measured organic content by loss-on-ignition (LOI) and bulk density at 2-cm intervals down core for the entire ~4 meter collected core at Cheesequake State Park. For LOI analysis, we dried the samples in an oven and ignited the samples in a muffle furnace following the methods of Plater et al. (2015). Using relationships between compression properties and measured LOI, we calibrated the decompaction model to predict how the sediment in the core compacted. We compared measured and model-derived estimates of down core dry bulk density to assess the predictive capacity of the model. The model provided depth-specific estimates of post-depositional lowering (PDL) (±1 standard deviation) at 2 cm intervals. Core samples were corrected for compaction using the equation:

$$A_{dep} = PDL + A_{meas} \quad [2]$$

where A_{meas} is the measured sample altitude relative to mean tide level (MTL), established by subtracting the depth of each sample in the core from the measured core-top altitude. A_{dep} is the depositional sample altitude after addition of PDL.

3.6. Chronology

A core chronology between ~0-1700 CE was constructed using Accelerator Mass Spectrometry (AMS) radiocarbon (^{14}C) dating. A plateau in the radiocarbon calibration curve often results in radiocarbon dated material from the past ~300 years to have multiple ages and large uncertainties (Stuiver and Pearson, 1993). Therefore, we developed a

chronology for the more recent top of the sampled core by identifying down-core changes in ^{137}Cs activity, pollen, and pollution concentrations.

Radiocarbon dating was performed on identifiable plant macrofossils (stems and rhizomes) in the sediment core. Plant macrofossils of *Spartina patens* found in growth position were selected from the core, cleaned under a binocular microscope to remove contaminant sediment particles, oven dried, and submitted to the National Ocean Science Accelerator Mass Spectrometry (NOSAMS) facility for radiocarbon dating. Each sample underwent standard acid-base-acid pretreatment at NOSAMS. Reported radiocarbon ages and uncertainties (Table 1) were calibrated using the IntCal13 dataset (Reimer et al., 2013).

The sediment core was analyzed for ^{137}Cs activity at East Carolina University by gamma spectroscopy. The peak in ^{137}Cs in the core is identified as having been deposited around 1963 CE when above-ground nuclear weapons testing was at its maximum (Warneke et al., 2002). Pollen was analyzed from 1 cm^3 samples at 4 cm intervals between 20 and 80 cm from the sediment core following standard procedures after Bernhardt and Willard (2015). A minimum of 500 terrestrial pollen grains were counted per sample to determine pollen percentage abundance to detect the increase in *Ambrosia* associated with land clearance. To examine down-core changes in pollution histories, samples for analysis of 52 elements and isotopes were subsampled from 2 cm intervals in the upper 90 cm of the core, ground to a fine homogenized powder, and sent to SGS Mineral Services Canada laboratory for analysis. At the SGS laboratory, samples were digested using HNO_3 and HCl and were analysed by inductively coupled Mass Spectrometer (ICP-MS) and inductively coupled

plasma Optical Emission Spectrometer (ICP-OES) against known calibration materials to provide quantitative analysis. Instrument calibration and certified reference materials, replicates, duplicates, and blanks were used for method validation and quality control.

Down-core trends in element and isotope concentrations were matched to historic pollution production and consumption, assuming timing and magnitude of atmospheric emissions and deposition approximately coincided (e.g. Gobeil et al., 2013; Kemp et al., 2012; Lima et al., 2005). Here, we use the following pollution markers. A peak in Pb isotopes is associated with early industrial activity and lead pollution from the Upper Mississippi Valley, which was carried to the Northeastern Atlantic Coast by prevailing winds (e.g. Graney et al., 1995; Lima et al., 2005; Gobeil et al., 2013), and was assigned an age of ~1858 CE. The subsequent decline of Upper Mississippi Valley lead pollution output is associated with a decline in Pb isotopes at an age of ~1880 CE (e.g. Graney et al., 1995; Lima et al., 2005; Gobeil et al., 2013). A rise in Cu is associated with the onset of national production of copper in ~1900 CE (USGS Minerals Yearbook). The onset of Pb pollution was assigned an age of ~1875 CE (e.g. Kemp et al., 2012), while a peak in Pb pollution is associated with the introduction of the Clean Air Act and was assigned an age of ~1974 CE (e.g. Kemp et al., 2012). Pb isotope decline was assigned an age of ~1980 CE (e.g. Kemp et al., 2012). A decline in Cd occurred in ~1975 CE and a decline in Ni occurred in ~1997 CE (USGS Minerals Yearbook). The onset of ^{137}Cs activity was assigned an age of 1954 CE before reaching a peak in 1963 CE when above ground nuclear weapons testing was at its maximum (Warneke et al., 2002). The peak abundance of *Ambrosia* pollen was assigned an age of 1850 CE when there were changes in vegetation associated with land

clearance, which occurred when the Europeans settled in New Jersey (e.g. Brugam, 1978; McAndrews, 1988).

Radiocarbon dates, ^{137}Cs activity, pollen, and pollution concentrations were compiled using the Bchron package in R (Haslett and Parnell, 2008; Parnell et al., 2008), which uses a Bayesian framework to produce an age-depth model and estimates ages with associated uncertainties for every 1 cm thick interval in the core. Age estimates in Bchron incorporate the non-parametric likelihood distributions from calibrated radiocarbon ages, while chronohorizons from ^{137}Cs activity, pollen, and pollution concentrations are treated as having normal likelihood distributions. The age estimates and uncertainties from Bchron were applied to all core samples with a reconstructed PME.

3.7. Spatiotemporal Model

We applied a spatiotemporal empirical hierarchical model (Kopp et al., 2016; Ashe et al., 2019) with an expanded global sea-level database to our northern New Jersey RSL record to estimate past RSL and rates of RSL change with associated uncertainty in the context of broader global and regional changes. The expanded sea-level database includes proxy sea-level records with high-resolution chronologies from 35 regions around the world. The 2593 sea-level data points use proxies such as foraminifera, diatoms, testate amoebae, coral microatolls, archaeological evidence, and sediment geochemistry. The database has been updated here from Kemp et al. (2018) to include 709 new RSL data points from 6 new sites in northern New Jersey, USA (this study); Israel (Dean et al., 2019); Croatia (Shaw et al., 2018); Chesapeake Bay, USA (Shaw et al., in prep); and Florida, USA (Khan et al., in

prep). In addition, decadal-average values from instrumental tide gauge records in the Permanent Service for Mean Sea Level (PSMSL; Holgate et al., 2013) were included, provided they were either (1) longer than 150 years, (2) within 5 degrees distance of a proxy site and longer than 70 years, or (3) the nearest tide gauge to a proxy site that is longer than 20 years (Kopp et al., 2016). We also include multicentury records from Amsterdam (1700-1925 CE) (van Veen, 1945), Kronstadt (1773-1993 CE) (Bogdanov and Laitos, 2000), and Stockholm (1774-2000 CE) (Ekman, 1988), as compiled by PSMSL. As in Kopp et al. (2016) and Kemp et al. (2018), the input data also include the global mean sea-level reconstruction of Hay et al. (2015) from tide-gauge records.

The model has (1) a process level that characterizes RSL over space and time; (2) a data level that links RSL observations (reconstructions) to the RSL process; and (3) a hyperparameter level that characterizes prior expectations regarding dominant spatial and temporal scales of RSL variability, set through a maximum-likelihood optimization. The non-linear terms were characterized by three spatial scales (global, regional, and local) and two temporal scales (fast and slow). These different spatial and temporal scales enable RSL to be decomposed into global, regional linear, regional non-linear, and local components.

Here, we used the reconstructed spatiotemporal field to determine the timing at which the rates in the last three centuries of the records emerge above the spread of previous variability over the Common Era in northern New Jersey and globally. To minimize the effects of interdecadal fluctuations (Douglas, 1991; Jevrejeva et al., 2008) and limited reconstruction resolutions, we focused on 60-year average rates. Background variability is

defined by the distribution of 60-year average rates during the pre-Industrial Common Era from 0 to 1700 CE at 20-year increments (e.g. 0-60, 20-80, CE, etc.). Rates over 60-year intervals beginning in 1700 CE were compared to this background distribution. For each 60-year interval from 1700-1760 CE to 1940-2000 CE, we estimated the probability using a Monte Carlo approach that the rates during that 60-year interval and all subsequent intervals are greater than a random 60-year interval during the pre-Industrial Common Era (0-1700 CE). We defined the inception of modern rates of RSL rise when it is very likely (probability $P \geq 0.90$) that the average rate of RSL rise from a 60-year interval and from all subsequent 60-year time periods were greater than a random 60-year interval in the past (0-1700 CE). In addition, representing each 60-year interval by its central year, we interpolated the probability curve to identify the year in which the probability reaches 0.90.

We also used the global RSL database with the spatiotemporal hierarchical model to examine the inception of modern elevated rates of RSL at other individual sites using the same methodology described above. However, the proxy records utilize different types of environmental evidence and dating methods and cover a range of time periods, so there is variability in the resolution of the available proxy data (Gehrels and Woodworth, 2012). To increase the likelihood that any variability in the timing of modern rates we observed is due to process and not the proxy data resolution, we examined all of the proxy data in the RSL database to only include records that fit the following criteria: 1) the proxy record is at least ~1000 years in length to provide sufficient background information; 2) the proxy record has data from 1700-2000 CE; 3) the 2σ errors of the model-predicted rates from 1700-1800 CE, 1800-1900 CE, and 1900-2000 CE are less than 0.70 (2σ values for all sites

ranged from 0.4-0.9). In addition, we established a null hypothesis by predicting RSL at a site (indicatively taken as Seoul, South Korea) far from proxy data; thus, the prediction constitutes estimated global sea level plus additional uncertainty. We compared the RSL rate predictions and probabilities with global mean sea level and individual records, where probabilities that differ from Seoul reflect the influence of meaningful local information at individual sites.

4. Results

4.1. Modern Foraminifera and $\delta^{13}C$ Training Set

We identified 14 species of dead foraminifera in the 32 modern surface samples across three transects at Cheesequake State Park. Sample count sizes ranged from 78 to 420 tests/10 cm^3 with an average of 207 tests/10 cm^3. The assemblages across the three transects were dominated by *Tiphotrocha comprimata* and *Trochammina inflata*, representing ~20-80% of each sample (Figure 3). The assemblages display a vertical zonation. Along Transect A, the lowest elevations (<210 SWLI) where *Spartina alterniflora* was the dominant vegetation, had greater abundances of *Miliammina fusca* and *Arenoparella mexicana* (up to 65% of sample assemblages). The middle of the transect, where *Spartina patens* and *Distichlis spicata* were the dominant vegetation, there was a more mixed foraminifera assemblage dominated by *Tiphotrocha comprimata* and *Trochammina inflata*. The highest elevations of Transect A (>220 SWLI), where *Phragmites australis* was the dominant vegetation, had greater abundances of *Jadammina macrescens*, *Miliammina petila*, and *Haplophragmoides* spp. (up to 55% of samples assemblages). Transect B was similar to Transect A, where the lowest elevations (<210

SWLI) had greater abundances of *M. fusca* and *A. mexicana* (up to 25% of sample assemblages), the middle of the transect had a more mixed assemblage dominated by *T. comprimata* and *T. inflata*, and the highest elevations (>225 SWLI) had greater abundances of *M. petila* and *Haplophragmoides* spp. (up to 19% of samples assemblages). Transect C had a greater abundance of *Balticammina pseudomacrescens* across the entire transect, up to 26% of sample assemblages. Similar to Transects A and B, the lowest elevations of Transect C (<230 SWLI) had greater abundances of *M. fusca* and *A. mexicana* (up to 36% of sample assemblages), while the remainder of the transect had a more uniform elevation with a mixed assemblage dominated by *T. comprimata* and *T. inflata*. Foraminifera were absent above elevations > ~250 SWLI units along all three transects in the uppermost zones of *Phragmites australis* and into the freshwater upland environment.

PCA illustrates that the modern foraminifera assemblages from Cheesequake State Park are comparable with those of Kemp et al. (2013) from southern New Jersey because the samples fall close to one another along both first and second principal component axes (Figure 4). For example, Kemp et al. (2013) also found greater abundances of *M. fusca* and *A. mexicana* at lower elevations and greater abundances of *Jadammina macrescens*, *Miliammina petila*, and *Haplophragmoides* spp. at higher elevations at several sampling locations.

We calibrated the BTF using the combined New Jersey modern training set and evaluated its performance using cross validation. The measured elevation falls within the 95% uncertainty intervals for 96% of the modern samples, indicating that the BTF has good

predictive power (Figure 5). Trends between residual values and measured elevations of modern samples revealed no visible structure; therefore, the BTF did not systematically overestimate or underestimate PME across tidal elevations (Figure 5).

All three modern transects at Cheesequake State Park had similar trends in $\delta^{13}C$ values by elevation, with less depleted values at lower elevations with a shift towards more depleted values at higher elevations (Figure 3). Samples taken from environments dominated by C_3 vegetation (*Spartina alterniflora*, *Spartina patens*, *Distichlis spicata*) found at lower elevations all had $\delta^{13}C$ values less depleted than -22‰, while samples from environments dominated by C_4 vegetation (*Phragmites australis*, and freshwater upland trees) found at higher elevations all had $\delta^{13}C$ values more depleted than -22‰. In addition, a sample from the middle of one of the modern transects from an area including C_4 vegetation, *Iva fructescens*, had $\delta^{13}C$ values more depleted than -22‰. The modern transects of $\delta^{13}C$ at Cheesequake State Park differed slightly from Kemp et al. (2012) in relation to tidal elevation boundaries. Samples with $\delta^{13}C$ values more depleted than -19.2‰ were consistently found above MHHW (SWLI > 200), while values less depleted than -19.2‰ were found from MTL to above MHHW (SWLI 100-280). Additionally, samples with $\delta^{13}C$ values less depleted than -16.9‰ were consistently found below a SWLI of 250. In contrast, in southern New Jersey, Kemp et al. (2012) found that $\delta^{13}C$ values of salt-marsh bulk sediment more depleted than -22.0‰ were found above MHHW (SWLI > 200), while values less depleted than -18.9‰ were found between mean tide level (MTL) and MHHW (SWLI 100-200). Therefore, to use the $\delta^{13}C$ data as a prior, the PME was reconstructed in

one of three ways to incorporate the $\delta^{13}C$ findings from Kemp et al. (2012) in addition to the new modern $\delta^{13}C$ data from this study:

(1) For samples with a $\delta^{13}C$ value more depleted than -22.0‰, the transfer function estimate was given a lower limit for a reconstructed PME of a SWLI > 200 (above MHHW);

(2) For samples with a $\delta^{13}C$ value less depleted than -16.9‰, the transfer function estimate was given an upper limit for a reconstructed PME of a SWLI < 250;

(3) For samples with intermediate $\delta^{13}C$ values (-22.0‰ to -16.9‰), the transfer function estimate was not given an upper or lower limit for a reconstructed PME.

4.2. Estimating Paleomarsh Elevation

We described the stratigraphy at Cheesequake State Park through 17 cores, 3.5 to 11 meters deep, through three transects (A-A'; B-B'; and C-C'; Figure 2). The stratigraphy among the three transects had basal units varying from a ~0.5 to 1 m amorphous peat layer with charcoal and woody fragments to a shelly or sandy clay unit. Overlying the basal unit was ~0.5 to 4 m of shelly clay or clay with organics, above which was up to several meters of high marsh peat to the surface, some with interspersed clay layers. Psuty (1986) also noted a highly variable sequence of stratigraphic units at Cheesequake State Park due to the presence of small drainage channel basins that could have undergone variable infilling rates. We selected transect A-A' for more detailed analyses (Figure 2c). Across transect A-A' was a basal unit of gray incompressible sandy clay which was reached at depths varying from 3.4 m in the highest marsh to 10.3 m in the lowest marsh close to a tidal creek. Cores

located closest to the creek were overlain by a ~3 to 5 m layer of gray shelly clay. Above was a ~0.3 to 4 m layer of brown minerogenic salt marsh sediment that was thickest closest to the creek. The upper ~2 to 3 m of the transect was a dark brown organic high marsh peat that was thickest in the highest areas of the marsh.

The core sampled for analysis (CQ/15/C1) from transect A-A' had a gray incompressible basal sandy clay unit from 4.1 to 3.4 m that became increasingly sandy with depth. From 3.4 to 3.1 m was a brown minerogenic salt marsh sediment of peaty mud. The upper 3.1 m of the core was a dark brown organic high marsh peat (Figure 2c). The core was analyzed for foraminifera and $\delta^{13}C$ in the upper 1.2 m (Figure 6). From 1.2 to 0.65 m, the core was dominated by *J. macrescens* and *M. petila*, comprising 70-98% of each sample. There was a decrease in total foraminiferal counts with depth below 0.9 m (<100 tests/sample). In contrast, between 0.9 and 0.65 m, count sizes ranged from ~100 to 1400 tests/sample. From 0.65 to 0.35 m, the foraminiferal assemblages were dominated by *J. macrescens*, *M. petila*, and *T. comprimata* with count sizes ranging from ~100-300 tests/sample. The upper 0.35 m of the core had a more diverse foraminifera assemblage including up to 9 species, but dominated by *T. comprimata* and *T. inflata* with count sizes ranging from ~70-350 tests/sample.

From 1.2 to 0.85 m, $\delta^{13}C$ values were all more depleted than -22‰, ranging from -22.8‰ to -26.6‰, which is associated with C_3 vegetation and elevations consistently above MHHW. All but two samples (-23.0‰ and -23.3‰) in the upper 0.85 m had $\delta^{13}C$ values

less depleted than -22‰, ranging from -16.9‰ to -20.9‰, which is associated with C_4 vegetation or intermediate values between C_3 and C_4 vegetation.

The BTF was applied to the core foraminifera and $\delta^{13}C$ data to provide PME estimates for each core sample. PME estimates ranged from 0.89 to 1.26 m MTL with sample-specific uncertainties (1σ) ranging from 0.16 to 0.33 m (Figure 6). From a depth of 1.2 to 0.65 m, PME estimates were the highest, ranging from 1.17 m MTL to 1.26 m MTL, which corresponds to a portion of the core with $\delta^{13}C$ values mostly more depleted than -22‰ which is associated with C_3 vegetation and foraminifera assemblages dominated by *J. macrescens* and *M. petila*, which are associated with high marsh elevations. From 0.65 to 0.35 m, PME estimates were slightly lower than the bottom portion of the core, ranging from to 1.08 to 1.20 m, corresponding to a portion of the core with foraminiferal assemblages dominated by *J. macrescens*, *M. petila*, and *T. comprimata* and intermediate $\delta^{13}C$ values associated with C_3 or C_4 vegetation. The upper 0.35 m of the core had the lowest PME estimates compared to the rest of the core, ranging from 0.89 m MTL to 1.04 m MTL, which correlates with the more diverse foraminifera assemblages associated with middle to high marsh environments and greater range in $\delta^{13}C$ values observed in this portion of the core.

4.3. Compaction

Measured LOI for the ~4 m collected core varied from 75% to 4% at the base of the core in the basal sandy clay unit. The average LOI in the lower 0.5 m of the core was 9%, and then increased to an average of 56% in the upper 3.5 m. For the analyzed part of the core

(surface to 1.2 m), LOI ranged from 23-76% with an average of 56%. Measured dry bulk density varied from 0.11 g/cm^3 to 1.32 g/cm^3 at the base of the core. Similar to LOI, the average dry bulk density in the lower 0.5 m of the core was 0.82 g/cm^3, and then markedly decreased to an average 0.17 g/cm^3 in the upper 3.5 m of the core. For the analyzed part of the core, bulk density varied from 0.12-0.31 g/cm^3 with an average of 0.17 g/cm^3.

Maximum post-depositional lowering (PDL) predicted by the geotechnical model was ~0.02 m in the middle of the core around 2 m depth. For the analyzed part of the core (surface to 1.2 m), PDL ranged from 0 to 0.017 m at 1.2 m depth (Figure 7), which is accounted for by adjusting the PME estimates to include the effects of sediment compaction.

4.4. Chronology

Radiocarbon dating was performed on the upper 120 cm of the collected core to capture the last ~1000 years in order to examine background rates of RSL and the subsequent modern elevated rates of RSL rise in the latter half of the millennium. Eight radiocarbon dates (Table 1) reveal a core chronology extending back to ~1000 CE with an average radiocarbon error (^{14}C years) of ~18 years.

Changes in *Ambrosia* pollen abundances, regional-scale pollution markers (recognized in changes in down-core concentrations of lead, copper, cadmium, and nickel), the ratio of lead isotopes (^{206}Pb:^{207}Pb), and ^{137}Cs activity were used to provide a chronology for the upper 50 cm of the core representing the last several hundred years based on trends in

national and regional industrial production (Figure 8). We use the following pollution markers to build a core chronology: a peak in Pb isotopes (~1858 CE, 0.43 ± 0.05 m), a decline in Pb isotopes (~1880 CE, 0.34 ± 0.05 m), a rise in Cu (~1900 CE, 0.33 ± 0.02 m), the onset of Pb pollution (~1875 CE, 0.40 ± 0.05 m), a peak in Pb pollution (~1974 CE, 0.12 ± 0.05 m), a Pb isotope decline (~1980 CE, 0.11 ± 0.02 m), a decline in Cd (~1975 CE, 0.09 ± 0.02 m), and a decline in Ni (~1997 CE, 0.04 ± 0.02 m). In addition, we use the onset (1954 CE, 0.19 ± 0.02 m) and peak (1963 CE, 0.13 ± 0.02 m) of ^{137}Cs activity and the peak abundance of *Ambrosia* pollen (1850 CE, 0.48 ± 0.08 m).

All radiocarbon dates and pollen and pollution chronohorizons were used to develop an age-depth model from ~1000 CE to present (Figure 9). The average chronological uncertainty of the RSL data points was 38 years (2σ).

4.5. Relative Sea Level: magnitude, rates, and timing of change

We produced 23 RSL data points from Cheesequake State Park from 1017 ± 67 to 2006 ± 10 CE (2σ), which we incorporated into the global proxy database and analysed using the spatio-temporal empirical hierarchical model (Kopp et al., 2016) to examine magnitudes and rates of RSL change. We found that RSL in northern New Jersey continuously rose over the last 1000 years by 1.5 ± 0.1 m (1σ) (Figure 10). RSL rose at a rate of 1.2 ± 0.2 mm/yr (2σ) from 1000 to 1700 CE before accelerating to a rate of rise of 2.1 ± 0.3 mm/yr from 1700 CE to present. Rates successively increased from 1.3 ± 0.7 mm/yr from 1700-1800 CE to 1.8 ± 0.6 mm/yr from 1800-1900 CE to 3.0 ± 0.6 mm/yr from 1900-2000 CE. The NOAA-operated tide gauge at Sandy Hook, New Jersey (station number 8531680),

located ~20 km from Cheesequake State Park, shows a ~0.3 m RSL rise since 1940 CE at a rate of 4.1 ± 0.1 mm/yr using the spatiotemporal model compared to the proxy-based reconstruction record of 3.2 ± 0.4 mm/yr from 1940-2000 CE.

Sixty-year average rates from 1700-2000 CE increase concurrently with the probability that each 60-year interval and all subsequent 60-year intervals were greater than a random 60-year interval during the pre-Industrial Common Era (Figure 11). From the period 1700-1760 CE, the average rate of RSL was 1.3 ± 0.5 mm/yr (1σ), which increased to 3.2 ± 0.4 mm/yr from 1940-2000 CE. In northern New Jersey at Cheesequake State Park, it is very likely (probability $P \geq 0.90$) that the average rates of RSL rise during 1880-1940 CE (2.7 ± 0.4 mm/yr) and during all subsequent 60-year time periods were greater than a random 60-year interval during the pre-Industrial Common Era (0-1700 CE). Interpolation from the probability curve suggests this probability reaches 0.90 by ~1895 CE, which is the timing when rates emerged above pre-Industrial Common Era (0-1700 CE) background variability (Figure 11).

5. Discussion

5.1. Regional Relative Sea-Level Change

We can examine the magnitudes and rates of RSL change in northern New Jersey in the Common Era using the spatiotemporal model, as well as compare to other nearby proxy-based reconstructions from southern New Jersey (Kemp et al., 2013) and New York City (Kemp et al., 2017). The spatiotemporal model estimates RSL in northern New Jersey rose 2.9 ± 0.2 m (1σ) over the last ~2000 years with a 0.3 ± 0.04 m rise in the last century. Kemp

et al. (2013) reconstructed RSL in southern New Jersey and the spatiotemporal model reveals a slightly larger magnitude of RSL rise over the last ~2000 years at 3.3 ± 0.1 m, with a similar 0.4 ± 0.02 m rise in the last century (Figure 10). Alternatively, to the north of Cheesequake State Park, Kemp et al. (2017) completed a high resolution RSL record near New York City in The Bronx where RSL rose continuously over the last ~2000 years to present by 2.6 ± 0.07 m, with a 0.3 ± 0.02 m rise in the last century (Figure 10). RSL in northern New Jersey at Cheesequake State Park rose at a rate of 1.3 ± 0.2 mm/yr (2σ) from 0-1700 CE before accelerating to a rate of rise of 2.1 ± 0.3 mm/yr from 1700 CE to present. The southern New Jersey RSL record reveals comparable trends to northern New Jersey: a rate of rise of 1.5 ± 0.1 mm/yr from 0-1700 CE accelerating to 2.5 ± 0.3 mm/yr from 1700 CE to present. Using a sea-level database for New Jersey and accounting for compaction and tidal range change, Horton et al. (2013) found similar background rates of RSL rise over the last 2000 years of an average of 1.3 mm/yr. Similarly, Miller et al. (2013) found a rise of 1.6 ± 0.1 mm/yr from 2.2 to 1.2 ka (800 CE) and 1.4 ± 0.1 mm/yr from 800 to 1800 CE in New Jersey. In New York City, the spatiotemporal model reveals slightly slower rates of rise of 1.2 ± 0.1 mm/yr from 0-1700 CE, followed by a rise of 2.0 ± 0.2 mm/yr from 1700 CE to present. Engelhart and Horton (2012) used a U.S. Atlantic coast RSL database and found that RSL rose at a rate of ~1.3 mm/yr from 4 ka BP to 1900 CE in New York.

We use the spatiotemporal hierarchical model to decompose the northern New Jersey, southern New Jersey, and New York City records into linear, regional non-linear, and local components (Figure 10c). Most of the RSL rise during the past ~2000 years is attributed to

regional-scale linear processes that we interpret primarily as GIA (e.g. Love et al, 2016; Peltier, 2004). A significant contributor to RSL rise in the mid-Atlantic region during the Common Era has been glacial isostatic adjustment (GIA) due to the mid-Atlantic's proximity to the margin of the former Laurentide Ice Sheet (e.g. Engelhart and Horton, 2012; Roy and Peltier, 2015; Love et al., 2016). The linear component exhibits a north to south gradient, contributing ~3.1 m of RSL rise in southern New Jersey, ~2.7 m in northern New Jersey, and ~2.4 m in New York City. The collapsing peripheral forebulge at the former ice margin caused maximum rates of RSL in New Jersey and Delaware, with a slightly lower rise in New York (e.g. Dyke et al., 2003; Engelhart and Horton, 2012). Additionally, vertical motions from GPS observations reconcile with geologic rates in the mid-Atlantic (e.g. Karegar et al., 2016). Coastal plain locations (New Jersey) have also experienced higher rates of RSL rise than bedrock locations (New York City) due to the natural compaction of unconsolidated coastal plain Holocene sediments with an average 20th century compaction rate of 0.16 mm/yr (90% Confidence Interval, 0.06-0.32 mm/yr) (e.g. Miller et al., 2013; Johnson et al., 2018). Due to coastal plain subsidence from natural compaction and groundwater withdrawal, these locations have rates of RSL rise 0.3-1.3 mm/yr higher than at bedrock locations (e.g. Miller et al., 2013).

The regional-scale non-linear contribution from all three sites have a magnitude <10 cm and are nearly identical because they fall within the same regional scale determined by the spatiotemporal model. New York City and northern and southern New Jersey experienced a regional non-linear several centimeter decline from 0-500 CE to a minimum of approximately -5 cm followed by a stable contribution from 500-1000 CE. A second

negative contribution began at ~1000 CE before reaching a minimum of approximately -8 cm at 1600 CE, which then increased until present. The regional non-linear trends are likely explained by a combination of physical processes. The evolving mass of the Greenland Ice Sheet could contribute to regional-scale non-linear RSL trends in the mid-Atlantic over the Common Era; however, the behaviour of the ice sheet is not well constrained over this time period (e.g. Alley et al., 2010). The Greenland Ice Sheet likely advanced and reached a peak in mass by the end of the Little Ice Age and subsequently began melting and losing mass to the global ocean (e.g. Weidick et al., 2004; Long et al., 2012; Marcott et al., 2013). However, the changes in mass of the Greenland Ice Sheet may be too small and/or overprinted by other processes to be detected in the regional-scale non-linear trends (Kemp et al., 2018). The falling sea-level change from 0-500 CE could be explained by long-term cooling from early to mid-Holocene maxima (e.g. Marcott et al., 2013; Kemp et al., 2018; Marsicek et al., 2018) since steric effects can produce regional sea-level trends (Roemmich and Gilson, 2009; Willis et al., 2004). The varied regional non-linear contribution from 500 CE to present could be due to ocean mass changes from atmospheric circulation and prevailing winds and ocean currents which are causing regional sea-level changes (Kemp et al., 2018). For example, meridional ocean circulation can cause sea-level changes along the Atlantic coast (e.g. Levermann et al., 2005; Ezer, 2016) Additionally, proxy reconstructions of the North Atlantic Oscillation provide evidence for changing atmospheric circulation over the Common Era, which could manifest changes in regional sea level (e.g. Trouet et al., 2009; Ortega et al., 2015).

The local-scale contribution is less than 10 cm in New York City and northern and southern New Jersey. Northern and southern New Jersey have similar local contributions with a near-zero contribution from 0-1000 CE, followed by a negative contribution, reaching a minimum of approximately -8 cm in southern New Jersey, and -2 cm in northern New Jersey at 1700 CE and then an increase to present. In contrast, New York City had a local contribution rise to ~500 CE, followed by a decline to a minimum of approximately -6 cm at 1200 CE, and then an increase to present. Post-depositional lowering through sediment compaction could contribute to the local-scale component; however, we corrected the RSL record for compaction in northern New Jersey, and sediment compaction has been shown to have a minimal contribution to RSL reconstructions from continuous sequences of high salt-marsh peat (e.g. Brain et al., 2015, 2017; Kemp et al., 2018). Anthropogenic groundwater withdrawal in the last several hundred years can cause local-scale RSL differences across geographically proximal locations (e.g. Miller et al., 2013; Johnson et al., 2018). Coastal New Jersey has been shown to experience up to ~0.7 mm/yr of subsidence due to groundwater withdrawal in the 20th century (Johnson et al., 2018), which could explain some of the increasing local contribution in the last century. Additionally, tidal range changes through time could cause local differences in RSL through changing bathymetric depths from the effects of sedimentation or through anthropogenic changes such as a loss of wetlands (e.g. Kemp et al., 2017), which could have contributed to the increasing local contribution in both New York City and New Jersey over the last several hundred years after European settlement.

5.2 Global Mean Sea-Level Change

We use the spatiotemporal empirical hierarchical model (Kopp et al., 2016) with the expanded global Common Era sea-level database to examine global mean sea level (GMSL) over the Common Era and to define the global timing of the onset of modern rates of sea-level rise and identify any spatial variability of elevated rates of sea-level rise.

The global component of reconstructed RSL has similar trends to the results from Kopp et al. (2016), and is consistent with a more recent compilation from Kemp et al. (2018) (Figure 12). Global sea-level (GSL) gradually rose from 0 CE to 500 CE at a rate of 0.2 ± 0.1 mm/yr, but then gradually fell from 500 CE to 1300 to CE at a rate of -0.1 ± 0.1 mm/yr. GSL then rose from 1300 CE to 1600 CE and fell from 1600 CE to 1800 CE. GSL has continued to rise since 1800 CE. There is a 99.9% probability that the rate of RSL from the most recent 60-year interval, 1940-2000 CE (1.4 ± 0.1 mm/yr), was faster than all previous 60-year intervals in at least the last 3000 years. Kopp et al. (2016) and Kemp et al. (2018) found that the 20th century rise was extremely likely, ($P \geq 0.95$) and ($P > 0.999$), respectively, faster than during any preceding century since at least -800 CE.

5.3 Global Onset of Modern Sea-level Rise

We examined the timing of modern rates of RSL using the global database and the spatiotemporal model (Figure 13). It is very likely (probability $P \geq 0.90$) that the average rate of GMSL rise from 1860-1920 CE (0.7 ± 0.2 mm/yr, 1σ) and from all subsequent 60-year time periods were greater than a random 60-year interval during the pre-Industrial Common Era (0-1700 CE). Interpolation from the probability curve suggests this

probability reaches 0.90 by ~1870 CE, which we propose as the global onset of modern rates of sea-level rise. Church and White (2006, 2011) used a global tide-gauge compilation extending back to 1870 CE and noted that acceleration began in the 19th century. Jevrejeva et al. (2008) produced a global reconstruction of GSL since 1700 CE using tide gauge records and found a sea level acceleration beginning at the end of the 18th century; however, they used only three tide gauge records (Amsterdam, Liverpool, and Stockholm) extending prior to 1850 CE and these records may not be representative of global change. Kemp et al. (2015) applied change point analysis to the global tide gauge compilation of Jevrejeva et al. (2008), which revealed a primary rate increase at 1827-1860 CE and a secondary increase at 1924-1943 CE (Kemp et al. 2015).

The onset of global modern elevated rates of sea-level rise is in response to increased ocean mass and volume from glacier/ice sheet melt and thermal expansion (Church et al., 2013). We can compare our timing of the onset of modern sea-level rise (~1870 CE) to the onset of warming from air and sea surface temperature reconstructions that drove ocean mass/volume changes (Figure 13). Abram et al. (2016) found that greenhouse forcing of industrial-era warming commenced during the mid-19th century. Sea surface temperatures (SST) suggested an onset of warming ranging from 1827-1834 CE among the Western Atlantic, Western Pacific and Indian oceans. The onset of warming of surface air temperatures (SAT) occurred slightly later, ranging from 1831-1904 CE across the globe. Therefore, the onset of SST warming precedes our timing of modern sea-level rise, while the global average of the onset of SAT warming (1868 CE) is synchronous with the timing of our modern sea-level rise (~1870 CE). The increased rates of RSL rise are likely caused

primarily by thermal expansion and melting of mountain glaciers (Church et al., 2013) in response to the warming SST and SAT. For example, global glacier volume began to decline in the middle of the 19th century and significantly contributed to global sea-level rise (LeClercq et al., 2011; Marzeion et al., 2012). The behaviour of the Greenland and Antarctic Ice Sheets is not well constrained over this time period, but it is unlikely they had large positive contributions to global sea-level rise until the 20th century (e.g. Gregory et al., 2006; Alley et al., 2010; Davies et al., 2012; Box and Colgan, 2013).

5.4 Spatial Variability of Modern Elevated Rates in the North Atlantic

We used the spatiotemporal model to examine the timing of modern rates of RSL rise at the proxy locations with the highest resolution. All of the sites that fit the resolution criteria were in the North Atlantic – four sites in Europe and fifteen sites along the eastern coast of North America (Table 2). The nineteen sites also had comparable average RSL (< 0.36 m) and age (< 113 yr) errors from their reconstructions. The null hypothesis of RSL for Seoul, South Korea, a location where there is no available RSL data, follows global sea level in changes in mean rate, but with a larger standard deviation. Therefore, individual sites with RSL predictions and probability estimates that differ from Seoul reflect the influence of meaningful local information at that site.

We examined the probability when the average rate of RSL rise from a 60-year interval and from all subsequent 60-year intervals were greater than a random 60-year interval in the past (0-1700 CE). Average background RSL rates from 0-1700 CE ranged from -0.24 ± 0.20 mm/yr in Scotland to 1.72 ± 0.12 mm/yr in Nova Scotia. Average RSL rates from

1700-2000 CE ranged from 0.13 ± 0.35 mm/yr in Scotland to 2.48 ± 0.25 mm/yr in southern New Jersey. Rates of RSL rise in the last three centuries are fastest in the mid-Atlantic region of the U.S., followed by the northeast and southeast U.S., and slowest in Canada and Europe (e.g. Engelhart et al., 2011; Barlow et al., 2014).

Global sea level has the earliest onset of modern rates of RSL rise (~1870 CE) before individual locations because it is less noisy than an individual record, as it combines all of the records around the globe. In the North Atlantic, we observe spatial variability in the timing of the onset of modern elevated rates of RSL (Figure 14). The onset occurs the earliest in the mid-Atlantic region (New York, New Jersey, Maryland, North Carolina), where it is very likely (probability $P \geq 0.90$) that the average rate of RSL rise from 1860-1920 CE or 1880-1940 CE and from all subsequent 60-year time periods were greater than a random 60-year interval in the past. In the mid-Atlantic, Kemp et al. (2017) reconstructed RSL in New York City and using change point analysis, found that the rate of RSL rise markedly increased at 1812-1913 CE (95% credible interval). Here, interpolation from the probability curve using the spatiotemporal model for New York City suggests a similar timing, when the 0.90 probability is reached by ~1875 CE. Similarly, Kemp et al. (2013) and Kemp et al. (2017) applied change point analysis to the southern New Jersey and North Carolina RSL records, respectively, and found a rate increase between 1830 and 1873 CE in New Jersey and between 1865 and 1892 CE in North Carolina. Here, we suggest modern rates occur later in southern New Jersey (~1880 CE), but at a similar time in North Carolina (~1875 and 1890 CE from two sites).

The northeastern (Connecticut, Massachusetts) and southeastern (Florida) U.S. revealed a slightly later onset of modern rates of RSL rise. It is very likely (probability $P \geq 0.90$) that the average rate of RSL rise from 1880-1940 CE or 1900-1960 CE and from all subsequent 60-year time periods were greater than a random 60-year interval in the past. Change point analysis on a RSL record in Connecticut showed a rate increase between 1850 and 1886 CE (Kemp et al., 2015) compared to ~1895 using the spatiotemporal model. Similar analyses in Little Manatee River, Florida and Nassau, Florida revealed a change point at 1830-1940 CE and 1830-1920, respectively (Kemp et al., 2015; Gerlach et al., 2017). Here, we interpolate similar elevated rate timings at ~1895 CE in Little Manatee River and ~1920 in Nassau. Although change point analysis is a different process level model that does not allow for acceleration over time, the change point analyses performed on RSL records along the U.S. east coast are largely consistent with our results using the spatiotemporal model.

Canada (Nova Scotia, Newfoundland) and Europe (Iceland, Denmark, Scotland) have the latest onset of modern elevated rates of RSL rise. It is very likely (probability $P \geq 0.90$) that the average rate of RSL rise from 1920-1980 CE or 1940-2000 CE and from all subsequent 60-year time periods were greater than a random 60-year interval in the past. Gehrels et al. (2005) noted an acceleration in rates in Nova Scotia between 1900 and 1920 CE, while we suggest elevated rates occur in ~1930 CE. In Iceland, a 0.90 probability is reached in ~1950 CE. Gehrels et al. (2006) found that recent rise began much earlier in Iceland in 1820 ± 20 CE as dated by paleomagnetism and Pb produced by European coal burning; however, a new record from Iceland does not find this early acceleration, but

instead notes three periods of rapid RSL rise from 1620-1650 CE, 1780-1850 CE, and 1950-2000 CE (Saher et al., 2015). Scotland had the latest onset of modern elevated rates, reaching a 0.90 probability in ~1960-1965 CE. The onset of elevated rates appears muted and later along the eastern North Atlantic margin (European coast) compared to the western North Atlantic margin (North American coast) (Barlow et al., 2014; Long et al., 2014).

The spatial asynchronies that we observe in the timing of the onset of modern rates of RSL may suggest regional variability in the underlying mechanisms driving faster rates of sea-level rise. Whereas a synchronous timing of the onset may suggest forcing by ice sheet and/or glacier melt into the global ocean, an asynchronous timing might signal the role of ocean dynamics or ocean steric changes (Gehrels and Woodworth, 2012). The spatial pattern we observe in the timing (U.S. mid-Atlantic earliest, followed by northeastern and southeastern U.S, and Canada and Europe the latest) does not suggest fingerprinting of the Greenland Ice Sheet where we would expect to see a north to south pattern of increasing RSL rise (e.g. Mitrovica et al., 2001). Instead, our observed spatial pattern may be due to a combination of steric and ocean dynamic effects from changes in Atlantic Meriodional Overturning Circulation (AMOC) and the Gulf Stream. The strength and/or position of the Gulf Stream can affect regional sea level on the U.S. Atlantic coast (e.g. Levermann et al., 2005; Yin et al., 2009; Ezer et al., 2013; Yin and Goddard, 2013). For example, proxy evidence revealed a ~3 Sv reduction in Gulf Stream strength during the Little Ice Age (at ~1350-1750 CE; Lund et al., 2006), which models suggest would cause a 1.5-6 cm rise north of Cape Hatteras (Kienert and Rahmstorf, 2012). The strength of the Gulf Stream changes with variability in AMOC (e.g. Bryden et al., 2005; Srokosz et al., 2012), as well

as in response to changing patterns of atmospheric winds and pressure, such as those connected with the North Atlantic Oscillation (NAO) (e.g. Lozier, 2012). Caesar et al. (2018) used a SST-based AMOC index and show a fingerprint of SST in the North Atlantic due to a northward shift of the Gulf Stream, which is associated with a reduction in AMOC. Observed SST trends from 1870 to 2016 reveal a distinct pattern in the North Atlantic (Caesar et al., 2018) similar to the spatial trend in timing of the onset of modern rates of RSL (Figure 15). The Gulf Stream shifts northwards and closer to the coast as AMOC slows down, causing extreme warming along the northeast coast of the U.S. with cooling to the south and to the north in the subpolar Atlantic gyre due to reduced heat transport (Caesar et al., 2018). If the AMOC reduction and subsequent Gulf Stream shift did begin in the mid-nineteenth century, it is a potential explanation for the earliest onset of modern elevated rates of RSL in the mid-Atlantic and the latest onset in northwest Europe, supporting the differences in RSL histories between the North American and European coastlines over the last several centuries (Barlow et al., 2014; Long et al., 2014).

6. Conclusion

We produced a new high-resolution Common Era RSL record from northern New Jersey and included it in an updated global database of instrumental and proxy sea-level records. Using a spatiotemporal model, we examine magnitudes and rates of past RSL in northern New Jersey in the context of broader global and regional changes. Using the reconstructed spatiotemporal sea-level field, we determine the inception of modern rates of sea-level rise as the 60-year interval in the last three centuries when rates emerge above the spread of previous variability over the pre-Industrial Common Era from 0 to 1700 CE. Globally, it

is very likely (probability $P \geq 0.90$) that the average rate of RSL rise from 1860-1920 CE (0.7 ± 0.2 mm/yr, 1σ) and from all subsequent 60-year time periods were greater than a random 60-year interval during the pre-Industrial Common Era (0-1700 CE). We interpolate when the probability reaches 0.90 and suggest that ~1870 CE is the global onset of modern rates of sea-level rise, which is likely in response to increased ocean mass and volume from glacier melt and thermal expansion.

We used the spatiotemporal model to examine the timing of modern elevated rates of RSL rise at individual proxy locations with the highest resolution: four sites in Europe and fifteen sites along the eastern coast of North America. The timing is asynchronous at the North Atlantic sites, but reveals a distinct spatial pattern where the onset of modern rates appears muted and later along the European coast compared to the North American coast. Elevated rates in RSL appear earliest in the mid-Atlantic region (New York, New Jersey, Maryland, North Carolina) from 1860-1920 CE or 1880-1940 CE. The northeastern (Connecticut, Massachusetts) and southeastern U.S. (Florida) revealed a slightly later onset of modern elevated rates of RSL rise from 1880-1940 CE or 1900-1960 CE. Canada (Nova Scotia, Newfoundland) and Europe (Iceland, Denmark, Scotland) have the latest onset of modern elevated rates of RSL rise from 1920-1980 CE or 1940-2000 CE. The observed spatial pattern in timing appears to follow SST trends from a reduction in Atlantic Meridional Overturning Circulation (AMOC) and northward shift of the Gulf Stream, where the northeast coast of the U.S. warms, with cooling to the south and to the north in the subpolar Atlantic gyre. Therefore, we suggest that a combination of steric and ocean

dynamic effects could be a potential explanation for the earliest onset of elevated rates of RSL in the mid-Atlantic and the latest onset in northwest Europe.

Acknowledgements

Author Jennifer Walker thanks Kristen Joyse, Ane Garcia-Artola, and Margaret Christie for their assistance in the field. JW was funded by the David and Arleen McGlade Foundation and a Cushman Foundation for Foraminiferal Research Student Research Award. NSF award 1804999 also supported this work.

References

Abram, Nerilie J., Helen V. McGregor, Jessica E. Tierney, Michael N. Evans, Nicholas P. McKay, Darrell S. Kaufman, the PAGES 2k Consortium, et al. 2016. "Early Onset of Industrial-Era Warming across the Oceans and Continents." Nature 536 (7617): 411–18. https://doi.org/10.1038/nature19082.

Allen, J. R. L. 2000. "Morphodynamics of Holocene Salt Marshes: A Review Sketch from the Atlantic and Southern North Sea Coasts of Europe." *Quaternary Science Reviews* 19 (12): 1155–1231. https://doi.org/10.1016/S0277-3791(99)00034-7.

Alley, Richard B., J.T. Andrews, J. Brigham-Grette, G.K.C. Clarke, K.M. Cuffey, J.J. Fitzpatrick, S. Funder, et al. 2010. "History of the Greenland Ice Sheet: Paleoclimatic Insights." *Quaternary Science Reviews* 29 (15–16): 1728–56. https://doi.org/10.1016/j.quascirev.2010.02.007.

Ashe, Erica L., Niamh Cahill, Carling Hay, Nicole S. Khan, Andrew Kemp, Simon E. Engelhart, Benjamin P. Horton, Andrew C. Parnell, and Robert E. Kopp. 2019. "Statistical Modeling of Rates and Trends in Holocene Relative Sea Level." *Quaternary Science Reviews* 204 (January): 58–77. https://doi.org/10.1016/j.quascirev.2018.10.032.

Balslev-Clausen, David, Tais W. Dahl, Nabil Saad, and Minik T. Rosing. 2013. "Precise and Accurate Δ13C Analysis of Rock Samples Using Flash Combustion–Cavity Ring Down Laser Spectroscopy." *Journal of Analytical Atomic Spectrometry* 28 (4): 516. https://doi.org/10.1039/c2ja30240c.

Bernhard, J. M. 1988. "Postmortem Vital Staining in Benthic Foraminifera; Duration and Importance in Population and Distributional Studies." *Journal of Foraminiferal Research* 18 (2): 143–46. https://doi.org/10.2113/gsjfr.18.2.143.

Bernhardt, Christopher E., and Debra A Willard. 2015. "Pollen and Spores of Terrestrial Plants." In *Handbook of Sea-Level Research*. John Wiley & Sons.

Bogdanov, VI, and G Laitos. 2000. *Mean Monthly Series of Sea Level Observations (1777-1993) at the Kronstadt Gauge* (Finnish Geodetic Inst, Kirkkonummi, Finland).

Box, Jason E., and William Colgan. 2013. "Greenland Ice Sheet Mass Balance Reconstruction. Part III: Marine Ice Loss and Total Mass Balance (1840–2010)." *Journal of Climate* 26 (18): 6990–7002. https://doi.org/10.1175/JCLI-D-12-00546.1.

Braak, C. J. F. ter, and P. Smilauer. 2012. "Canoco Reference Manual and User's Guide: Software for Ordination, Version 5.0." https://research.wur.nl/en/publications/canoco-reference-manual-and-users-guide-software-for-ordination-v.

Brain, Matthew J., Andrew C. Kemp, Benjamin P. Horton, Stephen J. Culver, Andrew C. Parnell, and Niamh Cahill. 2015. "Quantifying the Contribution of Sediment Compaction to Late Holocene Salt-Marsh Sea-Level Reconstructions, North Carolina, USA." *Quaternary Research* 83 (1): 41–51. https://doi.org/10.1016/j.yqres.2014.08.003.

Brain, Matthew J., Antony J. Long, David N. Petley, Benjamin P. Horton, and Robert J. Allison. 2011. "Compression Behaviour of Minerogenic Low Energy Intertidal Sediments." *Sedimentary Geology* 233 (1): 28–41. https://doi.org/10.1016/j.sedgeo.2010.10.005.

Brain, Matthew J., Antony J. Long, Sarah A. Woodroffe, David N. Petley, David G. Milledge, and Andrew C. Parnell. 2012. "Modelling the Effects of Sediment Compaction on Salt Marsh Reconstructions of Recent Sea-Level Rise." *Earth and Planetary Science Letters* 345–348 (September): 180–93. https://doi.org/10.1016/j.epsl.2012.06.045.

Brugam, Richard B. 1978. "Pollen Indicators of Land-Use Change in Southern Connecticut." *Quaternary Research* 9 (3): 349–62. https://doi.org/10.1016/0033-5894(78)90038-8.

Bryden, Harry L., Hannah R. Longworth, and Stuart A. Cunningham. 2005. "Slowing of the Atlantic Meridional Overturning Circulation at 25° N." *Nature* 438 (7068): 655. https://doi.org/10.1038/nature04385.

Caesar, L., S. Rahmstorf, A. Robinson, G. Feulner, and V. Saba. 2018. "Observed Fingerprint of a Weakening Atlantic Ocean Overturning Circulation." *Nature* 556 (7700): 191–96. https://doi.org/10.1038/s41586-018-0006-5.

Cahill, Niamh, Andrew C. Kemp, Benjamin P. Horton, and Andrew C. Parnell. 2016. "A Bayesian Hierarchical Model for Reconstructing Relative Sea Level: From Raw Data to Rates of Change." *Climate of the Past* 12 (2): 525–42. https://doi.org/10.5194/cp-12-525-2016.

Cazenave, Anny, and William Llovel. 2010. "Contemporary Sea Level Rise." *Annual Review of Marine Science* 2 (1): 145–73. https://doi.org/10.1146/annurev-marine-120308-081105.

Church, J. A., P. U. Clark, A. Cazenave, J. M. Gregory, S. Jevrejeva, A. Levermann, M. A. Merrifield, et al. 2013. "Sea Level Change." Technical Report. P.M.Cambridge University Press. http://drs.nio.org/drs/handle/2264/4605.

Church, John A., and Neil J. White. 2006. "A 20th Century Acceleration in Global Sea-Level Rise: An Acceleration in Global Sea-Level Rise." *Geophysical Research Letters* 33 (1): n/a-n/a. https://doi.org/10.1029/2005GL024826.

———. 2011. "Sea-Level Rise from the Late 19th to the Early 21st Century." *Surveys in Geophysics* 32 (4–5): 585–602. https://doi.org/10.1007/s10712-011-9119-1.

Davies, Bethan J., Michael J. Hambrey, John L. Smellie, Jonathan L. Carrivick, and Neil F. Glasser. 2012. "Antarctic Peninsula Ice Sheet Evolution during the Cenozoic Era." *Quaternary Science Reviews* 31 (January): 30–66. https://doi.org/10.1016/j.quascirev.2011.10.012.

Dean, S., Benjamin P. Horton, Niki Evelpidou, Niamh Cahill, Giorgio Spada, and Dorit Sivan. 2019. "Can We Detect Centennial Sea-Level Variations over the Last Three Thousand Years in Israeli Archaeological Records?" *Quaternary Science Reviews* 210 (April): 125–35. https://doi.org/10.1016/j.quascirev.2019.02.021.

Donnelly, Jeffrey P., Peter Cleary, Paige Newby, and Robert Ettinger. 2004. "Coupling Instrumental and Geological Records of Sea-Level Change: Evidence from Southern New England of an Increase in the Rate of Sea-Level Rise in the Late 19th Century: INCREASE IN THE RATE OF SEA-LEVEL RISE." *Geophysical Research Letters* 31 (5): n/a-n/a. https://doi.org/10.1029/2003GL018933.

Douglas, Bruce C. 1991. "Global Sea Level Rise." *Journal of Geophysical Research* 96 (C4): 6981. https://doi.org/10.1029/91JC00064.

Dyke, A.S., A Moore, and L Robinson. 2003. "Deglaciation of North America." Geological Survey of Canada. Open File 1574.

Ekman, Martin. 1988. "The World's Longest Continued Series of Sea Level Observations." Pure and Applied Geophysics 127 (1): 73–77. https://doi.org/10.1007/BF00878691.

Engelhart, Simon E., and Benjamin P. Horton. 2012. "Holocene Sea Level Database for the Atlantic Coast of the United States." *Quaternary Science Reviews* 54 (October): 12–25. https://doi.org/10.1016/j.quascirev.2011.09.013.

Engelhart, Simon E, Benjamin P Horton, Bruce C Douglas, W Richard Peltier, and Torbjörn E Törnqvist. 2009. "Spatial Variability of Late Holocene and 20th Century Sea-Level Rise along the Atlantic Coast of the United States," 5.

Engelhart, Simon, Benjamin Horton, and Andrew Kemp. 2011. "Holocene Sea-Level Changes Along the United States' Atlantic Coast." *Oceanography* 24 (2): 70–79. https://doi.org/10.5670/oceanog.2011.28.

Ezer, Tal. 2015. "Detecting Changes in the Transport of the Gulf Stream and the Atlantic Overturning Circulation from Coastal Sea Level Data: The Extreme Decline in 2009–2010 and Estimated Variations for 1935–2012." *Global and Planetary Change* 129 (June): 23–36. https://doi.org/10.1016/j.gloplacha.2015.03.002.

———. 2016. "Can the Gulf Stream Induce Coherent Short-Term Fluctuations in Sea Level along the US East Coast? A Modeling Study." *Ocean Dynamics* 66 (2): 207–20. https://doi.org/10.1007/s10236-016-0928-0.

Ezer, Tal, Larry P. Atkinson, William B. Corlett, and Jose L. Blanco. 2013. "Gulf Stream's Induced Sea Level Rise and Variability along the U.S. Mid-Atlantic Coast." *Journal of Geophysical Research: Oceans* 118 (2): 685–97. https://doi.org/10.1002/jgrc.20091.

Fatela, F, and R Taborda. 2002. "Con¢dence Limits of Species Proportions in Microfossil Assemblages." *Marine Micropaleontology*, 6.

Gaswirth, Stephanie B., Gail M. Ashley, and Robert E. Sheridan. 2002. "Use of Seismic Stratigraphy to Identify Conduits for Saltwater Intrusion in the Vicinity of Raritan Bay, New Jersey." *Environmental and Engineering Geoscience* 8 (3): 209–18. https://doi.org/10.2113/8.3.209.

Gehrels, W. R. 1994. "Determining Relative Sea-Level Change from Salt-Marsh Foraminifera and Plant Zones on the Coast of Maine, U.S.A." *Journal of Coastal Research* 10 (4): 21.

Gehrels, W. Roland. 2000. "Using Foraminiferal Transfer Functions to Produce High-Resolution Sea-Level Records from Salt-Marsh Deposits, Maine, USA." *The Holocene* 10 (3): 367–76. https://doi.org/10.1191/095968300670746884.

Gehrels, W. Roland, Jason R. Kirby, Andreas Prokoph, Rewi M. Newnham, Eric P. Achterberg, Hywel Evans, Stuart Black, and David B. Scott. 2005. "Onset of Recent Rapid Sea-Level Rise in the Western Atlantic Ocean." *Quaternary Science Reviews* 24 (18–19): 2083–2100. https://doi.org/10.1016/j.quascirev.2004.11.016.

Gehrels, W. Roland, William A. Marshall, Maria J. Gehrels, Gudrún Larsen, Jason R. Kirby, Jón Eiríksson, Jan Heinemeier, and Tracy Shimmield. 2006. "Rapid Sea-Level Rise in the North Atlantic Ocean since the First Half of the Nineteenth Century." *The Holocene* 16 (7): 949–65. https://doi.org/10.1177/0959683606hl986rp.

Gehrels, W. Roland, and Philip L. Woodworth. 2013. "When Did Modern Rates of Sea-Level Rise Start?" *Global and Planetary Change* 100 (January): 263–77. https://doi.org/10.1016/j.gloplacha.2012.10.020.

Gerlach, Matthew J., Simon E. Engelhart, Andrew C. Kemp, Ryan P. Moyer, Joseph M. Smoak, Christopher E. Bernhardt, and Niamh Cahill. 2017. "Reconstructing Common Era Relative Sea-Level Change on the Gulf Coast of Florida." *Marine Geology* 390 (August): 254–69. https://doi.org/10.1016/j.margeo.2017.07.001.

Gobeil, Charles, André Tessier, and Raoul-Marie Couture. 2013. "Upper Mississippi Pb as a Mid-1800s Chronostratigraphic Marker in Sediments from Seasonally Anoxic Lakes in Eastern Canada." *Geochimica et Cosmochimica Acta* 113 (July): 125–35. https://doi.org/10.1016/j.gca.2013.02.023.

Graney, J. R., A. N. Halliday, G. J. Keeler, J. O. Nriagu, J. A. Robbins, and S. A. Norton. 1995. "Isotopic Record of Lead Pollution in Lake Sediments from the Northeastern

United States." *Geochimica et Cosmochimica Acta* 59 (9): 1715–28. https://doi.org/10.1016/0016-7037(95)00077-D.

Gregory, J. M., J. A. Lowe, and S. F. B. Tett. 2006. "Simulated Global-Mean Sea Level Changes over the Last Half-Millennium." *Journal of Climate* 19 (18): 4576–91. https://doi.org/10.1175/JCLI3881.1.

Grinsted, Aslak, J. C. Moore, and S. Jevrejeva. 2010. "Reconstructing Sea Level from Paleo and Projected Temperatures 200 to 2100 Ad." *Climate Dynamics* 34 (4): 461–72. https://doi.org/10.1007/s00382-008-0507-2.

Haslett, John, and Andrew Parnell. 2008. "A Simple Monotone Process with Application to Radiocarbon-Dated Depth Chronologies." *Journal of the Royal Statistical Society: Series C (Applied Statistics)* 57 (4): 399–418. https://doi.org/10.1111/j.1467-9876.2008.00623.x.

Hay, Carling C., Eric Morrow, Robert E. Kopp, and Jerry X. Mitrovica. 2015. "Probabilistic Reanalysis of Twentieth-Century Sea-Level Rise." Nature 517 (7535): 481–84. https://doi.org/10.1038/nature14093.

Head, K.H. 1988. *Manual of Soil Laboratory Testing: Permeability, Shear Strength and Compressibility Tests*. London/Plymouth: Pentech Press.

Holgate, Simon J., Andrew Matthews, Philip L. Woodworth, Lesley J. Rickards, Mark E. Tamisiea, Elizabeth Bradshaw, Peter R. Foden, Kathleen M. Gordon, Svetlana Jevrejeva, and Jeff Pugh. 2013. "New Data Systems and Products at the Permanent Service for Mean Sea Level." Journal of Coastal Research, 493–504. https://doi.org/10.2112/JCOASTRES-D-12-00175.1.

Horton, B. P., R. J. Edwards, and J. M. Lloyd. 1999. "A Foraminiferal-Based Transfer Function: Implications for Sea-Level Studies." *Journal of Foraminiferal Research* 29 (2): 117–29. https://doi.org/10.2113/gsjfr.29.2.117.

Horton, B. P., and I. Shennan. 2009. "Compaction of Holocene Strata and the Implications for Relative Sealevel Change on the East Coast of England." *Geology* 37 (12): 1083–86. https://doi.org/10.1130/G30042A.1.

Horton, Benjamin P, and Robin J Edwards. n.d. "Quantifying Holocene Sea Level Change Using Intertidal Foraminifera: Lessons from the British Isles," 100.

Horton, Benjamin P., Simon E. Engelhart, David F. Hill, Andrew C. Kemp, Daria Nikitina, Kenneth G. Miller, and W. Richard Peltier. 2013. "Influence of Tidal-Range Change and Sediment Compaction on Holocene Relative Sea-Level Change in New Jersey, USA: Influence of Tidal-Range Change and Sediment Compaction." *Journal of Quaternary Science* 28 (4): 403–11. https://doi.org/10.1002/jqs.2634.

Horton, Benjamin P, Robert E Kopp, Andra J Garner, Carling C Hay, Nicole S Khan, Keven Roy, and Timothy A Shaw. 2018. "Mapping Sea-Level Change in Time, Space, and Probability," 44.

Horton, B.P. 1999. "The Distribution of Contemporary Intertidal Foraminifera at Cowpen Marsh, Tees Estuary, UK: Implications for Studies of Holocene Sea-Level Changes." *Palaeogeography, Palaeoclimatology, Palaeoecology* 149 (1–4): 127–49. https://doi.org/10.1016/S0031-0182(98)00197-7.

Jevrejeva, S., J. C. Moore, A. Grinsted, and P. L. Woodworth. 2008. "Recent Global Sea Level Acceleration Started over 200 Years Ago?" *Geophysical Research Letters* 35 (8). https://doi.org/10.1029/2008GL033611.

Johnson, Beverly J., Karen A. Moore, Charlotte Lehmann, Curtis Bohlen, and Thomas A. Brown. 2007. "Middle to Late Holocene Fluctuations of C3 and C4 Vegetation in a Northern New England Salt Marsh, Sprague Marsh, Phippsburg Maine." *Organic Geochemistry* 38 (3): 394–403. https://doi.org/10.1016/j.orggeochem.2006.06.006.

Johnson, Christopher S., Kenneth G. Miller, James V. Browning, Robert E. Kopp, Nicole S. Khan, Ying Fan, Scott D. Stanford, and Benjamin P. Horton. 2018. "The Role of Sediment Compaction and Groundwater Withdrawal in Local Sea-Level Rise, Sandy Hook, New Jersey, USA." *Quaternary Science Reviews* 181 (February): 30–42. https://doi.org/10.1016/j.quascirev.2017.11.031.

Karegar, Makan A., Timothy H. Dixon, and Simon E. Engelhart. 2016. "Subsidence along the Atlantic Coast of North America: Insights from GPS and Late Holocene Relative Sea Level Data." *Geophysical Research Letters* 43 (7): 3126–33. https://doi.org/10.1002/2016GL068015.

Kemp, Andrew C., Christopher E. Bernhardt, Benjamin P. Horton, Robert E. Kopp, Christopher H. Vane, W. Richard Peltier, Andrea D. Hawkes, Jeffrey P. Donnelly, Andrew C. Parnell, and Niamh Cahill. 2014. "Late Holocene Sea- and Land-Level Change on the U.S. Southeastern Atlantic Coast." *Marine Geology* 357 (November): 90–100. https://doi.org/10.1016/j.margeo.2014.07.010.

Kemp, Andrew C., Andrea D. Hawkes, Jeffrey P. Donnelly, Christopher H. Vane, Benjamin P. Horton, Troy D. Hill, Shimon C. Anisfeld, Andrew C. Parnell, and Niamh Cahill. 2015. "Relative Sea-Level Change in Connecticut (USA) during the Last 2200 Yrs." *Earth and Planetary Science Letters* 428 (October): 217–29. https://doi.org/10.1016/j.epsl.2015.07.034.

Kemp, Andrew C, Troy D Hill, Christopher H Vane, Niamh Cahill, Philip M Orton, Stefan A Talke, Andrew C Parnell, Kelsey Sanborn, and Ellen K Hartig. 2017. "Relative Sea-Level Trends in New York City during the Past 1500 Years." *The Holocene* 27 (8): 1169–86. https://doi.org/10.1177/0959683616683263.

Kemp, Andrew C., Benjamin P. Horton, and Stephen J. Culver. 2009. "Distribution of Modern Salt-Marsh Foraminifera in the Albemarle–Pamlico Estuarine System of North Carolina, USA: Implications for Sea-Level Research." *Marine Micropaleontology* 72 (3–4): 222–38. https://doi.org/10.1016/j.marmicro.2009.06.002.

Kemp, Andrew C, Benjamin P Horton, Jeffrey P Donnelly, Michael E Mann, Martin Vermeer, and Stefan Rahmstorf. n.d. "Climate Related Sea-Level Variations over the Past Two Millennia," 6.

Kemp, Andrew C., Benjamin P. Horton, Christopher H. Vane, Christopher E. Bernhardt, D. Reide Corbett, Simon E. Engelhart, Shimon C. Anisfeld, Andrew C. Parnell, and Niamh Cahill. 2013. "Sea-Level Change during the Last 2500 Years in New Jersey, USA." *Quaternary Science Reviews* 81 (December): 90–104. https://doi.org/10.1016/j.quascirev.2013.09.024.

Kemp, Andrew C., Benjamin P. Horton, David R. Vann, Simon E. Engelhart, Candace A. Grand Pre, Christopher H. Vane, Daria Nikitina, and Shimon C. Anisfeld. 2012. "Quantitative Vertical Zonation of Salt-Marsh Foraminifera for Reconstructing Former Sea Level; an Example from New Jersey, USA." *Quaternary Science Reviews* 54 (October): 26–39. https://doi.org/10.1016/j.quascirev.2011.09.014.

Kemp, Andrew C., Jessica J. Kegel, Stephen J. Culver, Donald C. Barber, David J. Mallinson, Eduardo Leorri, Christopher E. Bernhardt, et al. 2017. "Extended Late Holocene Relative Sea-Level Histories for North Carolina, USA." *Quaternary Science Reviews* 160 (March): 13–30. https://doi.org/10.1016/j.quascirev.2017.01.012.

Kemp, Andrew C., Christopher H. Vane, Benjamin P. Horton, Simon E. Engelhart, and Daria Nikitina. 2012. "Application of Stable Carbon Isotopes for Reconstructing Salt-Marsh Floral Zones and Relative Sea Level, New Jersey, USA." *Journal of Quaternary Science* 27 (4): 404–14. https://doi.org/10.1002/jqs.1561.

Kemp, Andrew C., Alexander J. Wright, Robin J. Edwards, Robert L. Barnett, Matthew J. Brain, Robert E. Kopp, Niamh Cahill, et al. 2018. "Relative Sea-Level Change in Newfoundland, Canada during the Past ∼3000 Years." *Quaternary Science Reviews* 201 (December): 89–110. https://doi.org/10.1016/j.quascirev.2018.10.012.

Kienert, H., and S. Rahmstorf. 2012. "On the Relation between Meridional Overturning Circulation and Sea-Level Gradients in the Atlantic." *Earth System Dynamics* 3 (2): 109–20. https://doi.org/10.5194/esd-3-109-2012.

Kopp, Robert E., Andrew C. Kemp, Klaus Bittermann, Benjamin P. Horton, Jeffrey P. Donnelly, W. Roland Gehrels, Carling C. Hay, Jerry X. Mitrovica, Eric D. Morrow, and Stefan Rahmstorf. 2016. "Temperature-Driven Global Sea-Level Variability in the Common Era." *Proceedings of the National Academy of Sciences* 113 (11): E1434–41. https://doi.org/10.1073/pnas.1517056113.

Leclercq, P. W., J. Oerlemans, and J. G. Cogley. 2011. "Estimating the Glacier Contribution to Sea-Level Rise for the Period 1800–2005." *Surveys in Geophysics* 32 (4): 519. https://doi.org/10.1007/s10712-011-9121-7.

Levermann, Anders, Alexa Griesel, Matthias Hofmann, Marisa Montoya, and Stefan Rahmstorf. 2005. "Dynamic Sea Level Changes Following Changes in the Thermohaline Circulation." *Climate Dynamics* 24 (4): 347–54. https://doi.org/10.1007/s00382-004-0505-y.

Lima, Ana Lúcia, Bridget A. Bergquist, Edward A. Boyle, Matthew K. Reuer, Francis O. Dudas, Christopher M. Reddy, and Timothy I. Eglinton. 2005. "High-Resolution Historical Records from Pettaquamscutt River Basin Sediments: 2. Pb Isotopes Reveal a Potential New Stratigraphic Marker." *Geochimica et Cosmochimica Acta* 69 (7): 1813–24. https://doi.org/10.1016/j.gca.2004.10.008.

Long, A. J., N. L. M. Barlow, W. R. Gehrels, M. H. Saher, P. L. Woodworth, R. G. Scaife, M. J. Brain, and N. Cahill. 2014. "Contrasting Records of Sea-Level Change in the Eastern and Western North Atlantic during the Last 300 Years." *Earth and Planetary Science Letters* 388 (February): 110–22. https://doi.org/10.1016/j.epsl.2013.11.012.

Long, Antony J., Sarah A. Woodroffe, Glenn A. Milne, Charlotte L. Bryant, Matthew J. R. Simpson, and Leanne M. Wake. 2012. "Relative Sea-Level Change in Greenland during the Last 700yrs and Ice Sheet Response to the Little Ice Age." *Earth and Planetary Science Letters*, Sea Level and Ice Sheet Evolution: A PALSEA Special Edition, 315–316 (January): 76–85. https://doi.org/10.1016/j.epsl.2011.06.027.

Love, Ryan, Glenn A. Milne, Lev Tarasov, Simon E. Engelhart, Marc P. Hijma, Konstantin Latychev, Benjamin P. Horton, and Torbjörn E. Törnqvist. 2016. "The Contribution of Glacial Isostatic Adjustment to Projections of Sea-Level Change along the Atlantic and Gulf Coasts of North America: GIA AND FUTURE SEA-LEVEL CHANGE." *Earth's Future* 4 (10): 440–64. https://doi.org/10.1002/2016EF000363.

Lozier, M. Susan. 2012. "Overturning in the North Atlantic." *Annual Review of Marine Science* 4 (1): 291–315. https://doi.org/10.1146/annurev-marine-120710-100740.

Lund, David C., Jean Lynch-Stieglitz, and William B. Curry. 2006. "Gulf Stream Density Structure and Transport during the Past Millennium." *Nature* 444 (7119): 601. https://doi.org/10.1038/nature05277.

Marcott, Shaun A., Jeremy D. Shakun, Peter U. Clark, and Alan C. Mix. 2013. "A Reconstruction of Regional and Global Temperature for the Past 11,300 Years." *Science* 339 (6124): 1198–1201. https://doi.org/10.1126/science.1228026.

Marsicek, Jeremiah, Bryan N. Shuman, Patrick J. Bartlein, Sarah L. Shafer, and Simon Brewer. 2018. "Reconciling Divergent Trends and Millennial Variations in

Holocene Temperatures." *Nature* 554 (7690): 92–96. https://doi.org/10.1038/nature25464.

Marzeion, B., A. H. Jarosch, and M. Hofer. 2012. "Past and Future Sea-Level Change from the Surface Mass Balance of Glaciers." *The Cryosphere* 6 (6): 1295–1322. https://doi.org/10.5194/tc-6-1295-2012.

Mcandrews, John H. 1988. "Human Disturbance of North American Forests and Grasslands: The Fossil Pollen Record." In *Vegetation History*, edited by B. Huntley and T. Webb, 673–97. Handbook of Vegetation Science. Dordrecht: Springer Netherlands. https://doi.org/10.1007/978-94-009-3081-0_18.

Meade, Robert H. 1969. "Landward Transport of Bottom Sediments in Estuaries of the Atlantic Coastal Plain." *Journal of Sedimentary Research* 39 (1): 222–34. https://doi.org/10.1306/74D71C1C-2B21-11D7-8648000102C1865D.

Middelburg, J.J., J. Nieuwenhuize, R.K. Lubberts, and O. van de Plassche. 1997. "Organic Carbon Isotope Systematics of Coastal Marshes." *Estuarine, Coastal and Shelf Science* 45 (5): 681–87. https://doi.org/10.1006/ecss.1997.0247.

Miller, Kenneth G., Robert E. Kopp, Benjamin P. Horton, James V. Browning, and Andrew C. Kemp. 2013. "A Geological Perspective on Sea-Level Rise and Its Impacts along the U.S. Mid-Atlantic Coast." *Earth's Future* 1 (1): 3–18. https://doi.org/10.1002/2013EF000135.

Miller, Kenneth G., Peter J. Sugarman, James V. Browning, Benjamin P. Horton, Alissa Stanley, Alicia Kahn, Jane Uptegrove, and Michael Aucott. 2009. "Sea-Level Rise in New Jersey over the Past 5000 Years: Implications to Anthropogenic Changes." *Global and Planetary Change* 66 (1–2): 10–18. https://doi.org/10.1016/j.gloplacha.2008.03.008.

Mitrovica, Jerry X., Natalya Gomez, and Peter U. Clark. 2009. "The Sea-Level Fingerprint of West Antarctic Collapse." *Science* 323 (5915): 753–753. https://doi.org/10.1126/science.1166510.

Mitrovica, Jerry X., Mark E. Tamisiea, James L. Davis, and Glenn A. Milne. 2001. "Recent Mass Balance of Polar Ice Sheets Inferred from Patterns of Global Sea-Level Change." *Nature* 409 (6823): 1026. https://doi.org/10.1038/35059054.

Morvan, Julie, Jean-Pierre Debenay, Frans Jorissen, Fabrice Redois, Eric Bénéteau, Malou Delplancke, and Anne-Sophie Amato. 2006. "Patchiness and Life Cycle of Intertidal Foraminifera: Implication for Environmental and Paleoenvironmental Interpretation." *Marine Micropaleontology* 61 (1–3): 131–54. https://doi.org/10.1016/j.marmicro.2006.05.009.

Murray, John W, and Samuel S Bowser. n.d. "Mortality, Protoplasm Decay Rate, and Reliability of Staining Techniques to Recognize 'Living' Foraminifera," 17.

Olson, Hilary Clement, and R. Mark Leckie, eds. 2003. *Micropaleontologic Proxies for Sea-Level Change and Stratigraphic Discontinuities*. SEPM (Society for Sedimentary Geology). https://doi.org/10.2110/pec.03.75.

Ortega, Pablo, Flavio Lehner, Didier Swingedouw, Valerie Masson-Delmotte, Christoph C. Raible, Mathieu Casado, and Pascal Yiou. 2015. "A Model-Tested North Atlantic Oscillation Reconstruction for the Past Millennium." *Nature* 523 (7558): 71–74. https://doi.org/10.1038/nature14518.

Parnell, A. C., J. Haslett, J. R. M. Allen, C. E. Buck, and B. Huntley. 2008. "A Flexible Approach to Assessing Synchroneity of Past Events Using Bayesian Reconstructions of Sedimentation History." *Quaternary Science Reviews* 27 (19): 1872–85. https://doi.org/10.1016/j.quascirev.2008.07.009.

Peltier, W.R. 2004. "Global Glacial Isostasy and the Surface of the Ice-Age Earth: The ICE-5G (VM2) Model and GRACE." *Annual Review of Earth and Planetary Sciences* 32 (1): 111–49. https://doi.org/10.1146/annurev.earth.32.082503.144359.

Plater, Andrew J., Jason R. Kirby, John F. Boyle, Timothy Shaw, and Hayley Mills. 2015. "Loss on Ignition and Organic Content." In *Handbook of Sea-Level Research*. John Wiley & Sons.

Psuty, Norbert P. 1986. "Holocene Sea Level in New Jersey." *Physical Geography* 7 (2): 156–67. https://doi.org/10.1080/02723646.1986.10642288.

Reimer, PJ, E Bard, and A Bayliss. 2013. "IntCal13 and Marine13 Radiocarbon Age Calibration Curves 0-50,000 Years Cal BP." *Radiocarbon* 55: 1869–87.

Renwick, William H., and Gail M. Ashley. 1984. "Sources, Storages, and Sinks of Fine-Grained Sediments in a Fluvial-Estuarine System." *Geological Society of America Bulletin* 95 (11): 1343. https://doi.org/10.1130/0016-7606(1984)95<1343:SSASOF>2.0.CO;2.

Roemmich, Dean, and John Gilson. 2009. "The 2004–2008 Mean and Annual Cycle of Temperature, Salinity, and Steric Height in the Global Ocean from the Argo Program." *Progress in Oceanography* 82 (2): 81–100. https://doi.org/10.1016/j.pocean.2009.03.004.

Roy, Keven, and W.R. Peltier. 2015. "Glacial Isostatic Adjustment, Relative Sea Level History and Mantle Viscosity: Reconciling Relative Sea Level Model Predictions for the U.S. East Coast with Geological Constraints." *Geophysical Journal International* 201 (2): 1156–81. https://doi.org/10.1093/gji/ggv066.

Saher, Margot H., W. Roland Gehrels, Natasha L. M. Barlow, Antony J. Long, Ivan D. Haigh, and Maarten Blaauw. 2015. "Sea-Level Changes in Iceland and the Influence of the North Atlantic Oscillation during the Last Half Millennium." *Quaternary Science Reviews* 108 (January): 23–36. https://doi.org/10.1016/j.quascirev.2014.11.005.

Scott, D. B., and J. O. R. Hermelin. 1993. "A Device for Precision Splitting of Micropaleontological Samples in Liquid Suspension." *Journal of Paleontology* 67 (1): 151–54. https://doi.org/10.1017/S0022336000021302.

Scott, D. S., and F. S. Medioli. 1978. "Vertical Zonations of Marsh Foraminifera as Accurate Indicators of Former Sea-Levels." *Nature* 272 (5653): 528. https://doi.org/10.1038/272528a0.

Scott, David B., Franco S. Medioli, and Charles T. Schafer. 2001. *Monitoring in Coastal Environments Using Foraminifera and Thecamoebian Indicators*. Cambridge University Press.

Shaw, Timothy A., Andrew J. Plater, Jason R. Kirby, Keven Roy, Simon Holgate, Pero Tutman, Niamh Cahill, and Benjamin P. Horton. 2018. "Tectonic Influences on Late Holocene Relative Sea Levels from the Central-Eastern Adriatic Coast of Croatia." *Quaternary Science Reviews* 200 (November): 262–75. https://doi.org/10.1016/j.quascirev.2018.09.015.

Shennan, Ian, and Ben Horton. 2002. "Holocene Land- and Sea-Level Changes in Great Britain." *Journal of Quaternary Science* 17 (5–6): 511–26. https://doi.org/10.1002/jqs.710.

Srokosz, M., M. Baringer, H. Bryden, S. Cunningham, T. Delworth, S. Lozier, J. Marotzke, and R. Sutton. 2012. "Past, Present, and Future Changes in the Atlantic Meridional Overturning Circulation." *Bulletin of the American Meteorological Society* 93 (11): 1663–76. https://doi.org/10.1175/BAMS-D-11-00151.1.

Stuiver, Minze, and Gordon W. Pearson. 1993. "High-Precision Bidecadal Calibration of the Radiocarbon Time Scale, AD 1950–500 BC and 2500–6000 BC." *Radiocarbon* 35 (1): 1–23. https://doi.org/10.1017/S0033822200013783.

Tamisiea Mark E., Hughes Chris W., Williams Simon D. P., and Bingley Richard M. 2014. "Sea Level: Measuring the Bounding Surfaces of the Ocean." *Philosophical Transactions of the Royal Society A: Mathematical, Physical and Engineering Sciences* 372 (2025): 20130336. https://doi.org/10.1098/rsta.2013.0336.

the PAGES 2k Consortium, Nerilie J. Abram, Helen V. McGregor, Jessica E. Tierney, Michael N. Evans, Nicholas P. McKay, and Darrell S. Kaufman. 2016. "Early Onset of Industrial-Era Warming across the Oceans and Continents." *Nature* 536 (7617): 411–18. https://doi.org/10.1038/nature19082.

Troels-Smith, J. 19550000. "Characterization of unconsolidated sediments." https://www.bcin.ca/bcin/detail.app?id=22215&wbdisable=true.

Trouet, Valérie, Jan Esper, Nicholas E. Graham, Andy Baker, James D. Scourse, and David C. Frank. 2009. "Persistent Positive North Atlantic Oscillation Mode Dominated the Medieval Climate Anomaly." *Science* 324 (5923): 78–80. https://doi.org/10.1126/science.1166349.

Van Veen, J. 1945. “Bestaat Er Een Geologische Bodemdaling Te Amsterdam Sedert 1700.” Tijdschr K Ned Aardr Gen 62: 2–36.

Varekamp, J.C., E. Thomas, and O. Plassche. 1992. “Relative Sea-Level Rise and Climate Change over the Last 1500 Years.” *Terra Nova* 4 (3): 293–304. https://doi.org/10.1111/j.1365-3121.1992.tb00818.x.

Walker, David A., Anne E. Linton, and Charles T. Schafer. 1974. “Sudan Black B; a Superior Stain to Rose Bengal for Distinguishing Living from Non-Living Foraminifera.” *Journal of Foraminiferal Research* 4 (4): 205–15. https://doi.org/10.2113/gsjfr.4.4.205.

Walton, W. R. 1952. “Techniques for Recognition of Living Foraminifera.” *Cushman Found. Foram. Res. Contr.* 3 (2): 56–60.

Warneke, Thorsten, Ian W. Croudace, Phillip E. Warwick, and Rex N. Taylor. 2002. “A New Ground-Level Fallout Record of Uranium and Plutonium Isotopes for Northern Temperate Latitudes.” *Earth and Planetary Science Letters* 203 (3): 1047–57. https://doi.org/10.1016/S0012-821X(02)00930-5.

Weidick, Anker, Michael Kelly, and Ole Bennike. 2004. “Late Quaternary Development of the Southern Sector of the Greenland Ice Sheet, with Particular Reference to the Qassimiut Lobe.” *Boreas* 33 (4): 284–99. https://doi.org/10.1111/j.1502-3885.2004.tb01242.x.

Willis, Josh K., Dean Roemmich, and Bruce Cornuelle. 2004. “Interannual Variability in Upper Ocean Heat Content, Temperature, and Thermosteric Expansion on Global Scales.” *Journal of Geophysical Research: Oceans* 109 (C12). https://doi.org/10.1029/2003JC002260.

Woodworth, P. L., N. J. White, S. Jevrejeva, S. J. Holgate, J. A. Church, and W. R. Gehrels. 2009. “Evidence for the Accelerations of Sea Level on Multi-Decade and Century Timescales.” *International Journal of Climatology* 29 (6): 777–89. https://doi.org/10.1002/joc.1771.

Yin, Jianjun, and Paul B. Goddard. 2013. “Oceanic Control of Sea Level Rise Patterns along the East Coast of the United States: U.S. East Coast Sea Level Rise.” *Geophysical Research Letters* 40 (20): 5514–20. https://doi.org/10.1002/2013GL057992.

Yin, Jianjun, Michael E. Schlesinger, and Ronald J. Stouffer. 2009. “Model Projections of Rapid Sea-Level Rise on the Northeast Coast of the United States.” *Nature Geoscience* 2 (4): 262–66. https://doi.org/10.1038/ngeo462.

Tables and Figures

Table 1. Reported radiocarbon ages and uncertainties from the Cheesequake State Park core with calibrated ages using the IntCal13 dataset.

Depth (cm)	NOSAMS Sample ID	Radiocarbon Age (14C years)	Radiocarbon Error (14C years)	Calibrated Age (cal yrs. BP; 2 sigma range)
62	OS-123395	155	15	4-281
73	OS-141226	320	15	308-454
81	OS-130641	380	15	333-501
93	OS-130642	605	20	547-651
104	OS-141227	855	15	732-788
116	OS-141228	945	20	796-922
128	OS-142280	1180	20	1014-1177
136	OS-142281	1160	15	1001-1174

Table 2. Nineteen sites that fit the data resolution criteria to examine the timing of the onset of modern rates of RSL rise.

Site	Reference	*From Proxy Data*					*From Spatiotemporal Model*					
		# Data Points (0-1700 CE)	# Data Points (1700-2000 CE)	Average RSL Error (1s, 1700-2000 CE)	Average Age Error (2s, 1700-2000 CE)	Oldest Data Point (CE)	Background 0-1700 CE Rate (mm/yr)	Background 0-1700 CE Rate Error (2s)	1700-2000 CE Rate (mm/yr)	1700-2000 CE Rate Error (2s)	60 Year Interval when 0.90 Probability is Reached	Approximate Year when 0.90 Probability is Reached
Global Sea Level	This Study			NA			0	0.02	0.52	0.11	1860-1920	1870
Seoul (null hypothesis)	This Study						-0.44	2.2	0.08	2.23	1920-1980	1940
Ho Bugt, Denmark	Gehrels et al., 2006; Sekornik et al., 2008	19	1	0.22	112.50	-808	0.49	0.11	0.88	0.33	1940-2000	1960
Kyle of Tongue, Scotland	Barlow et al., 2014	21	17	0.35	31.78	583	-0.24	0.20	0.13	0.35	1940-2000	1965
Loch Laxford, Scotland	Barlow et al., 2014	30	30	0.35	12.33	235	0.06	0.14	0.41	0.33	1940-2000	1960
Vioarholmi, Iceland	Gehrels et al., 2006	50	35	0.18	11.46	-141	0.64	0.07	1.13	0.30	1920-1980	1950
Placentia, Newfoundland	Kemp et al., 2018	35	16	0.12	30.16	-634	0.48	0.06	0.97	0.27	1920-1940	1950
Big River Marsh, Newfoundland	Kemp et al., 2018	86	24	0.09	25.05	-814	0.98	0.05	1.54	0.24	1920-1980	1940
Chezzetcook, Nova Scotia	Gehrels et al., 2005	27	49	0.06	17.08	-1021	1.72	0.12	2.20	0.24	1920-1980	1930
Wood Island, Massachusetts	Kemp et al., 2011	14	4	0.06	21.50	463	0.57	0.09	1.27	0.26	1880-1940	1905
East River Marsh, Connecticut	Kemp et al., 2015	73	28	0.16	19.63	-233	0.96	0.06	1.70	0.28	1880-1940	1895
Pelham Bay, New York	Kemp et al., 2017	45	30	0.06	18.28	574	1.17	0.09	1.99	0.23	1860-1920	1875
Northern New Jersey (Cheesequake)	This Study	12	10	0.10	19.04	1017	1.60	0.18	2.44	0.32	1880-1940	1895
Southern New Jersey (Cape May Courthouse)	Kemp et al., 2013	27	41	0.12	12.89	977	1.49	0.13	2.48	0.25	1860-1920	1880
Chesapeake Bay, Maryland	Shaw et al., in prep	64	47	0.07	17.91	-1902	1.65	0.05	2.46	0.23	1880-1940	1890
Roanoke Island, North Carolina	Kemp et al., 2011; Kemp et al., 2017	72	34	0.08	25.87	-1138	1.08	0.05	1.89	0.23	1880-1940	1890
Cedar Island, North Carolina	Kemp et al., 2011; Kemp et al., 2017	66	26	0.06	19.48	-1003	0.84	0.09	1.77	0.22	1860-1920	1875
Nassau, Florida	Kemp et al., 2014	39	10	0.07	16.63	-499	0.40	0.05	0.99	0.26	1900-1960	1920
Little Manatee River, Florida	Gerlach et al., 2017	37	15	0.072	31.93	-343	0.36	0.05	1.30	0.24	1880-1940	1895
Biscayne, Florida	Khan et al., in prep	65	33	0.06	32.57	-3192	0.75	0.05	1.22	0.22	1900-1960	1920
Snipe, Lower Keys	Khan et al., in prep	50	14	0.115	35.69	-3006	0.58	0.06	1.07	0.29	1900-1960	1925

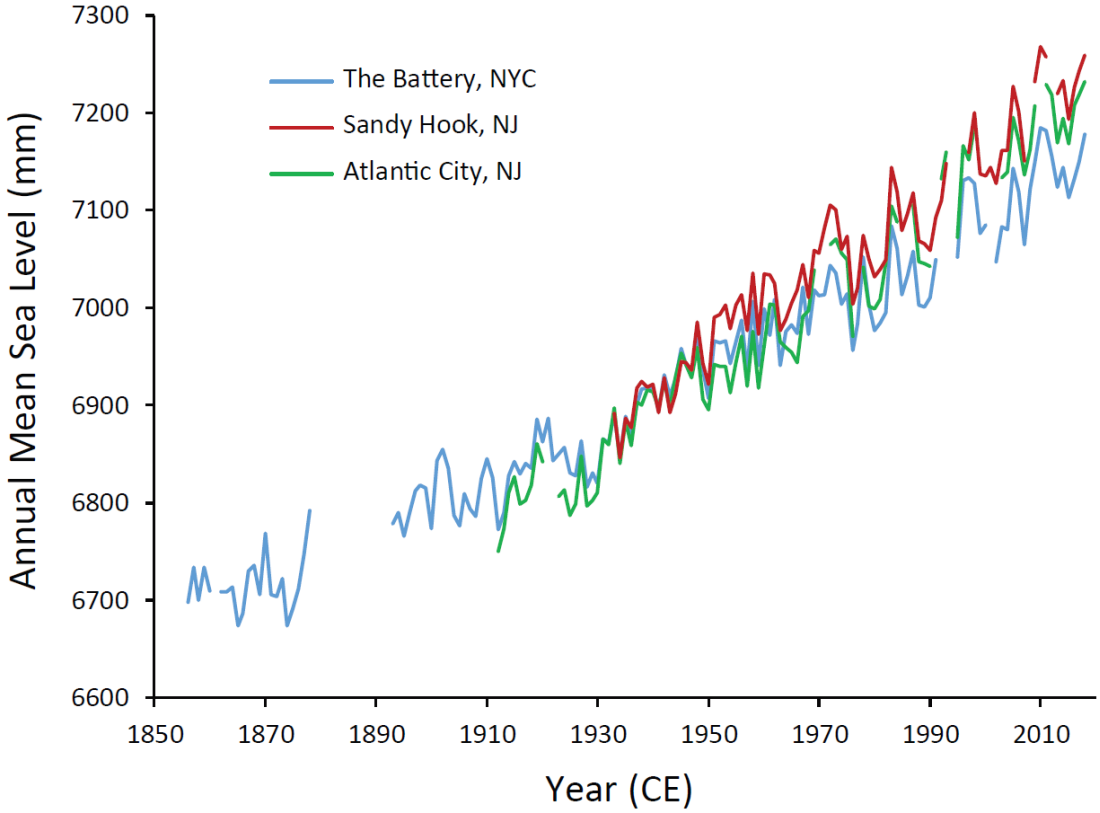

Figure 1. Annual mean sea level from tide gauges at The Battery, New York; Sandy Hook, New Jersey; and Atlantic City, New Jersey; obtained through the Permanent Service for Mean Sea Level.

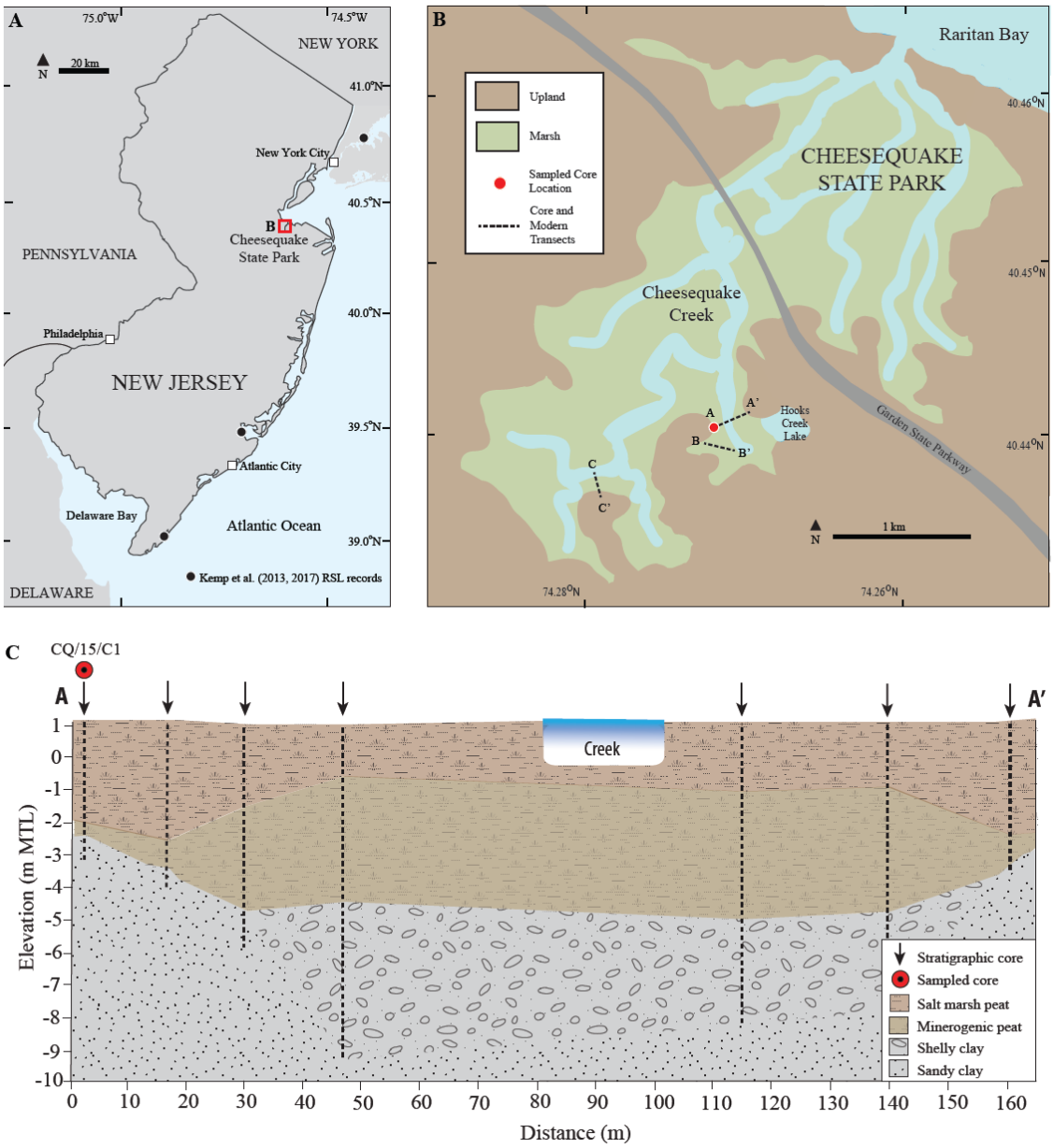

Figure 2. (A) Location of Cheesequake State Park in northern New Jersey off of Raritan Bay on the Northeastern Atlantic coast where a new Common Era RSL record was produced. (B) Salt-marsh study site showing core and modern transect locations, including location of the sampled core for detailed analysis. (C) Stratigraphy at Cheesequake State Park salt-marsh study site with location of sediment core used to reconstruct RSL.

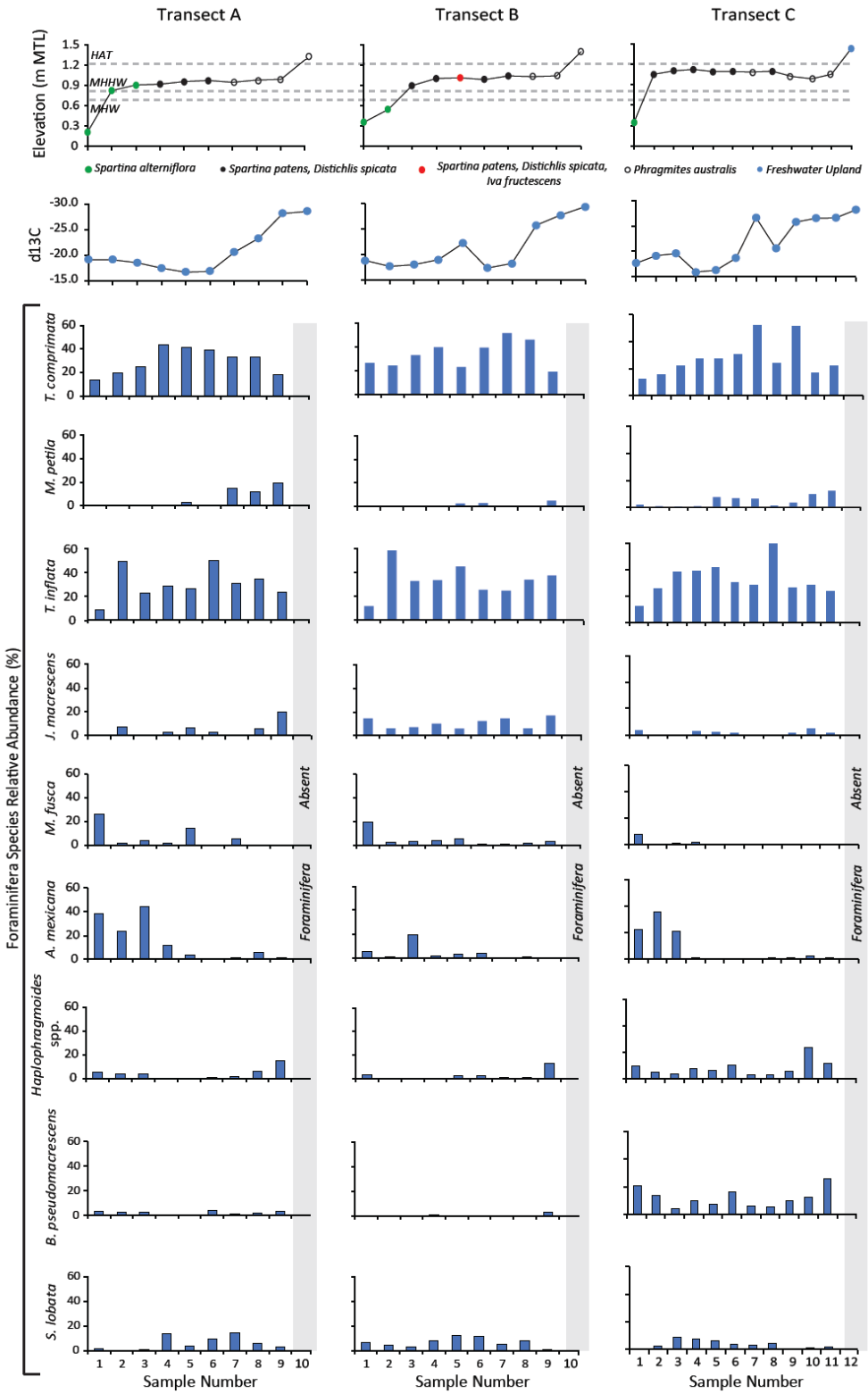

Figure 3. Three modern transects at Cheesequake State Park with elevation, stable carbon isotope geochemistry, and foraminifera distributions that were used in the Bayesian transfer function.

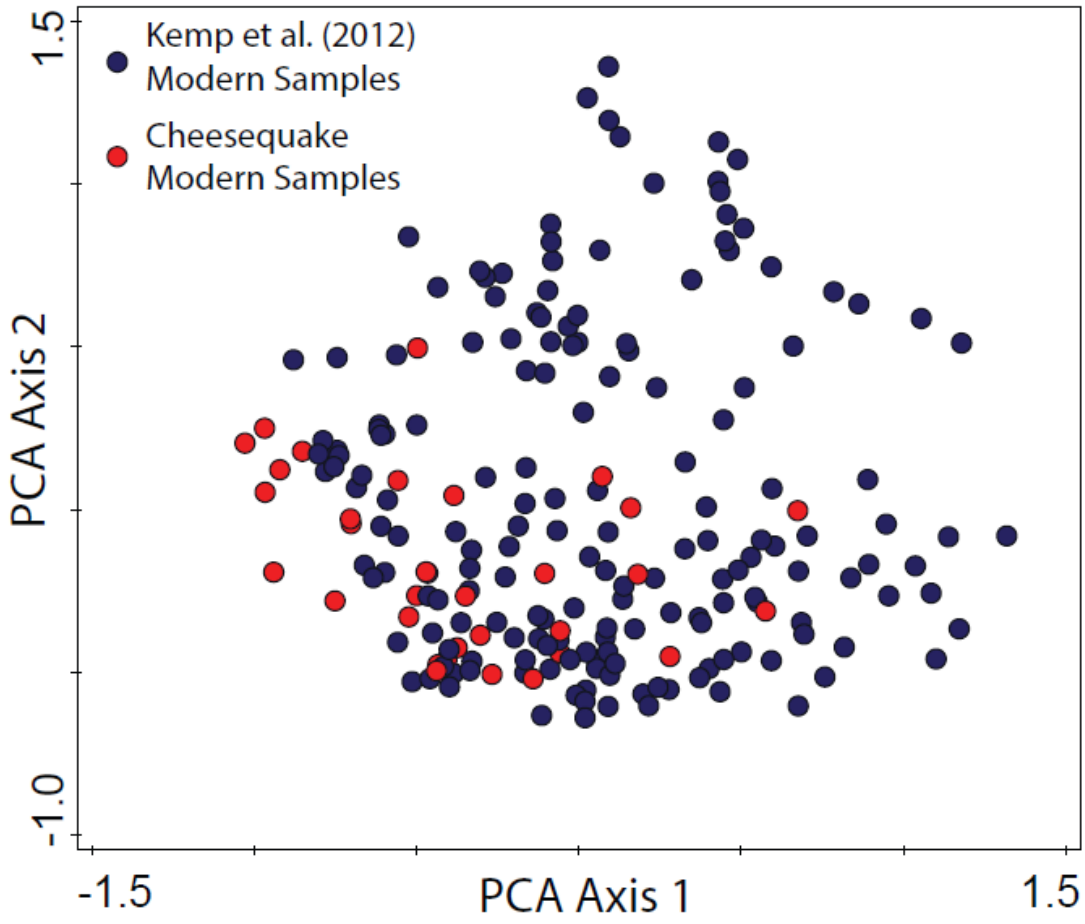

Figure 4. PCA analysis of modern foraminifera assemblages from southern New Jersey from Kemp et al. (2012) and from Cheesequake State Park, which shows the compatibility of the two datasets.

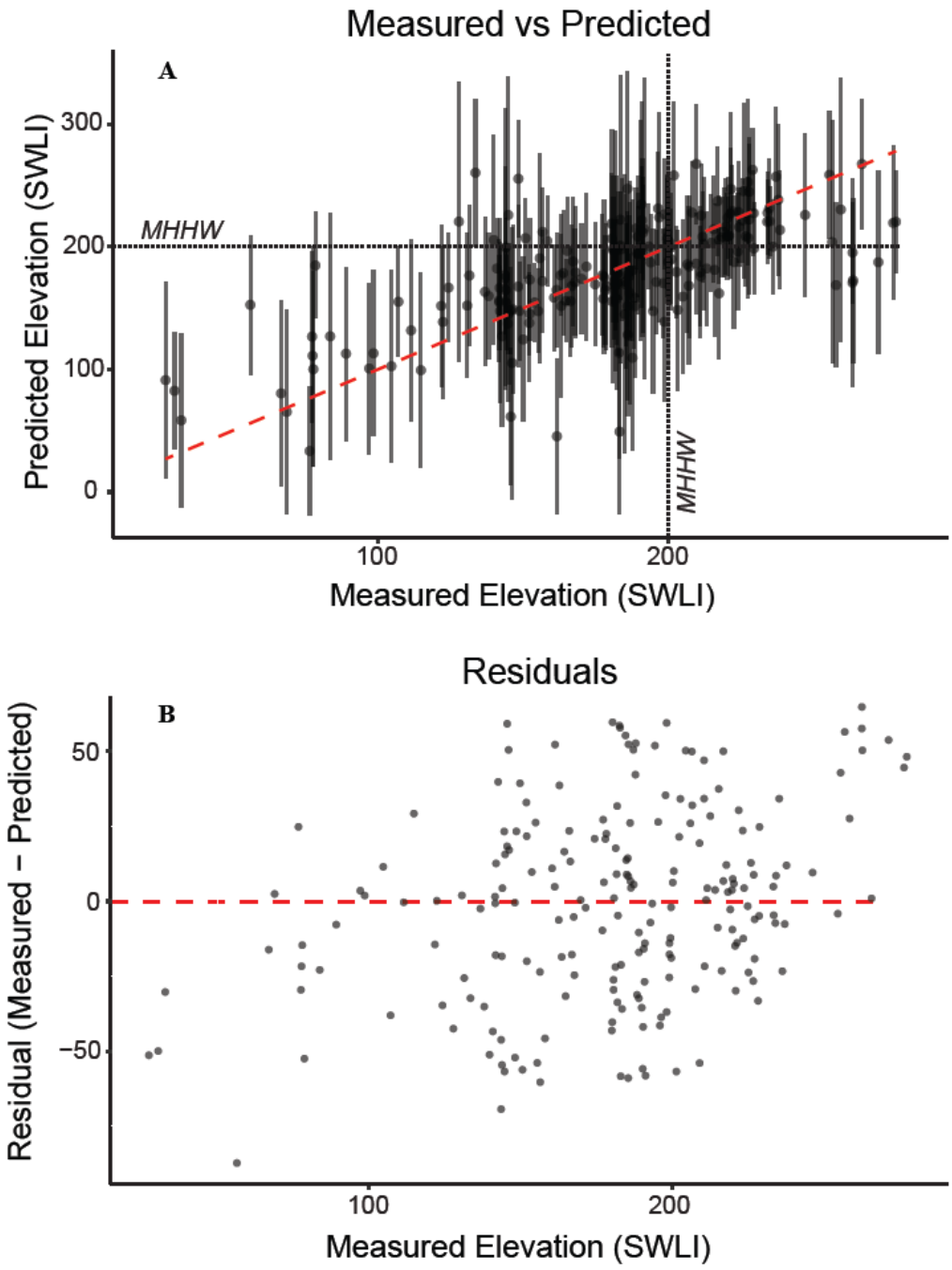

Figure 5. (A) Predicted versus measured elevations using the BTF, which we calibrated using the combined New Jersey modern training set and evaluated its performance using 10-fold cross validation. (B) Trends between residual values and measured elevations of modern samples revealed no visible structure; therefore, the BTF did not systematically overestimate or underestimate PME across tidal elevations.

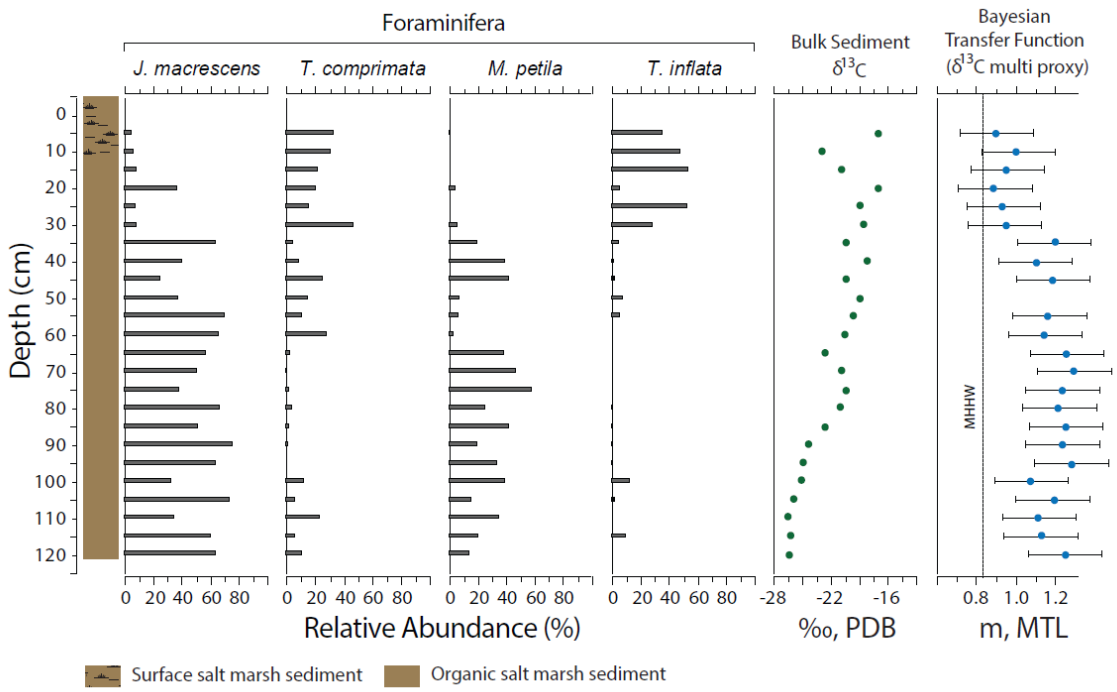

Figure 6. Core foraminifera and δ13C in the upper 1.2 m of the sampled sediment core (CQ/15/C1) from Cheesequake State Park. Only the four most abundant foraminifera species are shown here. The BTF was applied to the core foraminifera and δ13C data to provide PME estimates for each core sample.

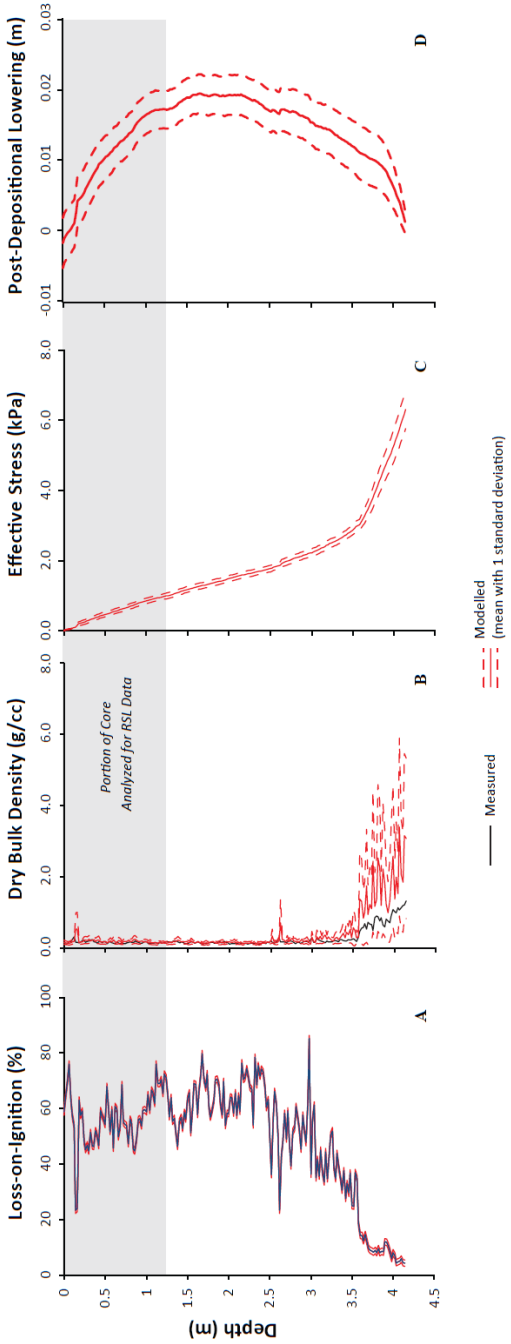

Figure 7. Estimation of post-depositional lowering caused by sediment compaction in the sampled sediment core (CQ/15/C1) from Cheesequake State Park. (A) Measured and modeled (using a geotechnical model) loss-on-ignition of the sediment core. (B) Measured and modeled dry bulk density of the sediment core. (C) Modeled effective stress through the sediment core. (C) Modeled post-depositional lowering predicted by the geotechnical model with a maximum of ~0.02 m in the middle of the core around 2 m depth.

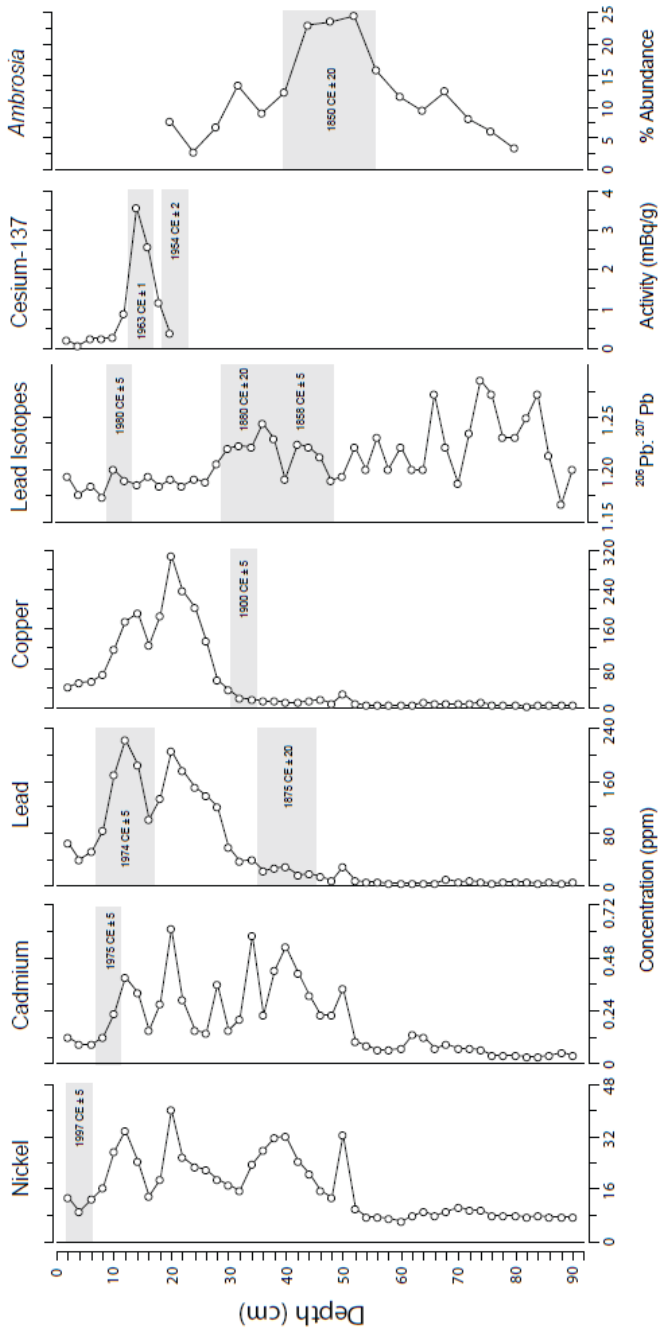

Figure 8. Changes in *Ambrosia* pollen abundances and regional-scale pollution markers, recognized in changes in down-core concentrations of lead, copper, cadmium, and nickel; the ratio of lead isotopes (^{206}Pb:^{207}Pb); and ^{137}Cs activity, which were used to provide a chronology for the upper 50 cm of the core representing the last several hundred years.

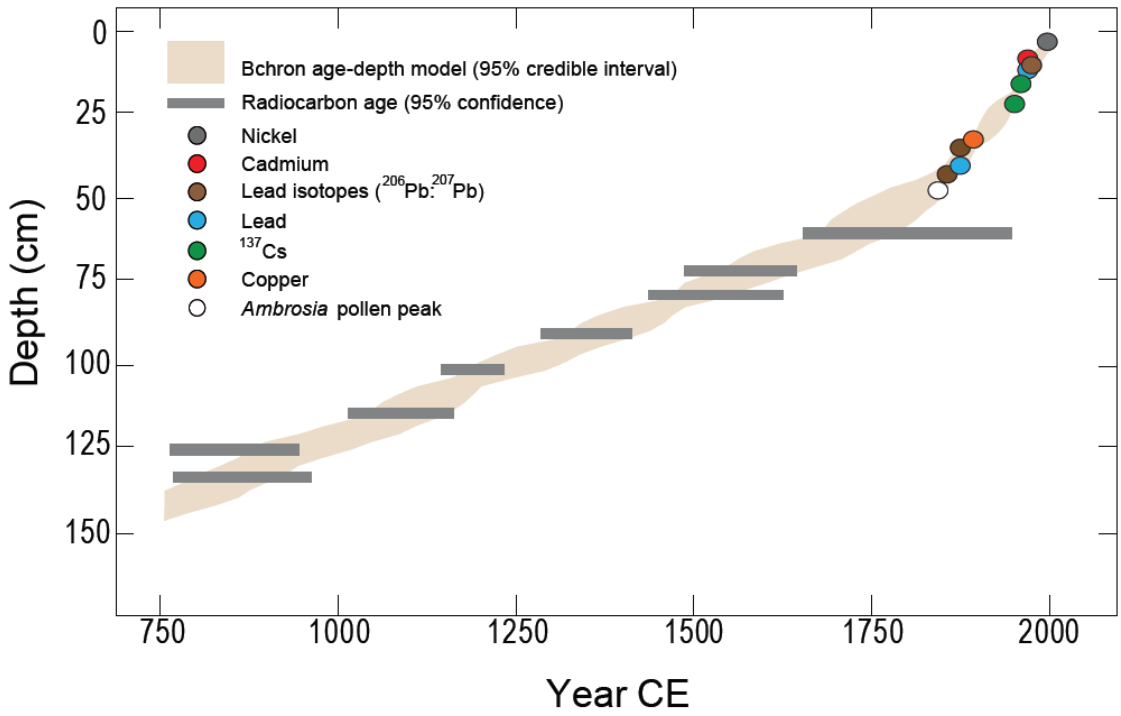

Figure 9. Age-depth model from ~1000 CE to present developed from all radiocarbon dates and pollen and pollution chronohorizons. The average chronological uncertainty of the RSL data points was 38 years (2σ).

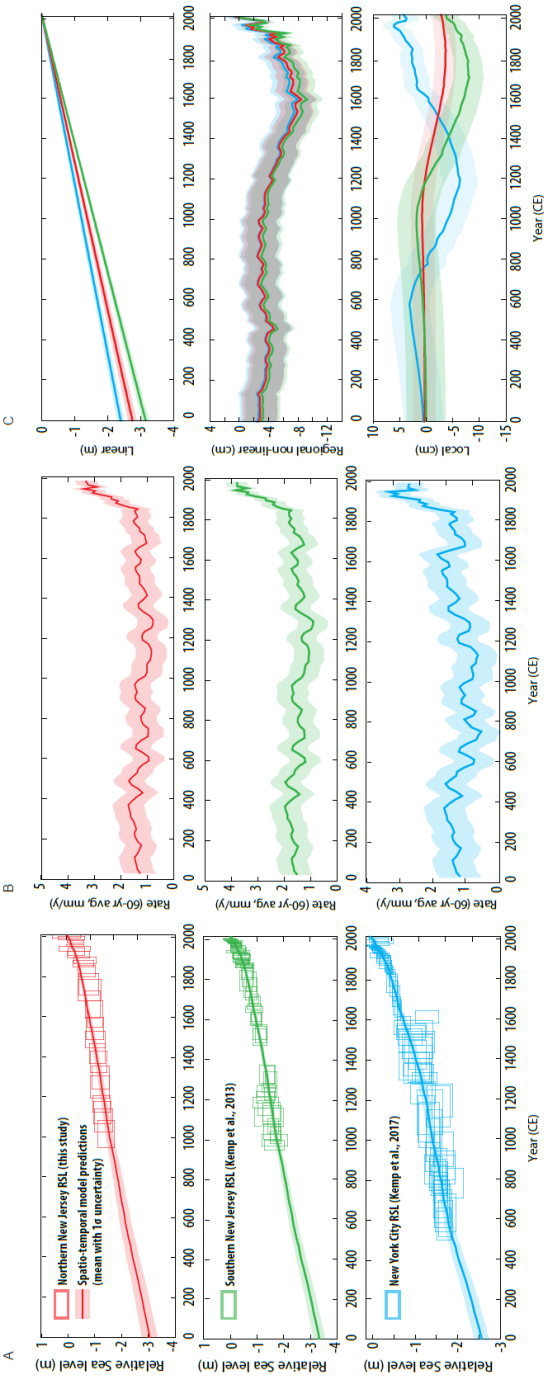

Figure 10. (A) RSL data and spatiotemporal model predictions from 0 to 2000 CE for northern New Jersey, southern New Jersey (Kemp et al., 2013), and New York City (Kemp et al., 2017). Boxes represent the vertical and chronological uncertainty for each data point. (B) Spatiotemporal model predictions for rates of RSL from 0 to 2000 CE for northern New Jersey, southern New Jersey (Kemp et al., 2013), and New York City (Kemp et al., 2017). (C) Spatiotemporal model decomposition of the northern New Jersey, southern New Jersey, and New York City records into linear, regional non-linear, and local components.

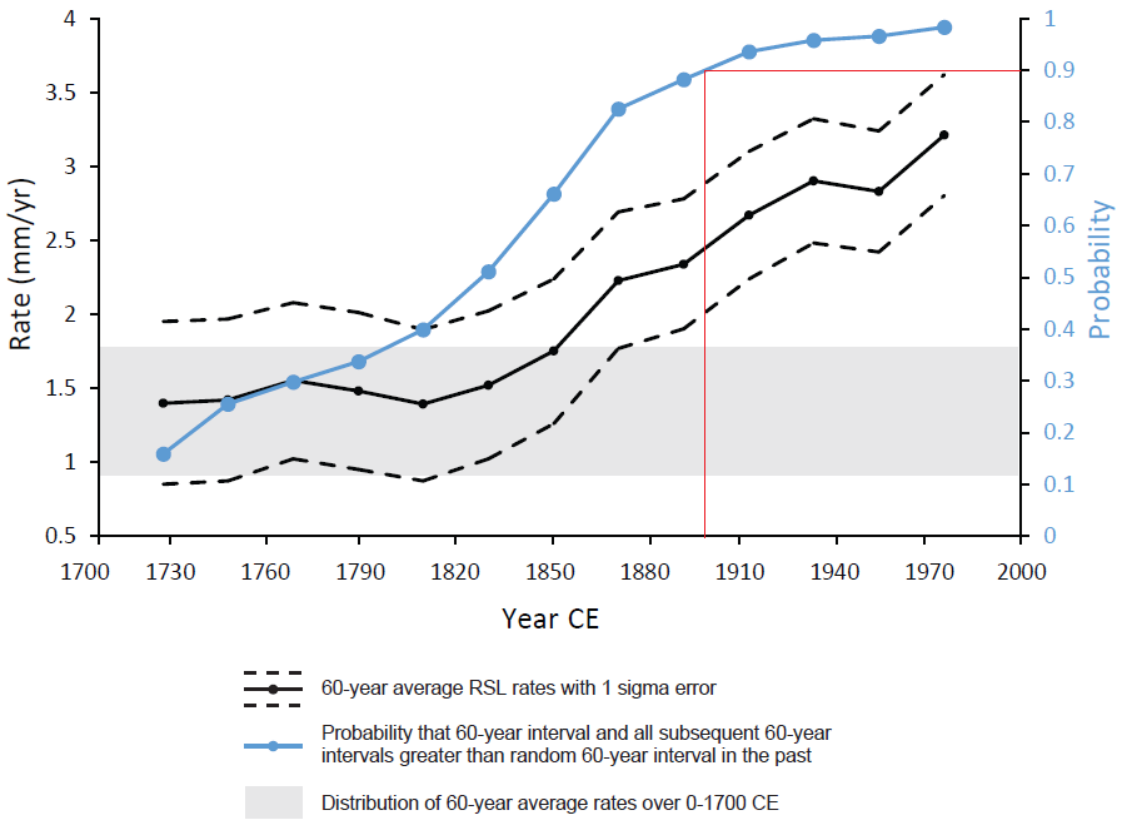

Figure 11. Sixty-year average rates from 1700-2000 CE for northern New Jersey, which increase concurrently with the probability that each 60-year interval and all subsequent 60-year intervals were greater than a random 60-year interval during the pre-Industrial Common Era (0-1700 CE). Interpolation from the probability curve suggests this probability reaches 0.90 by ~1895 CE.

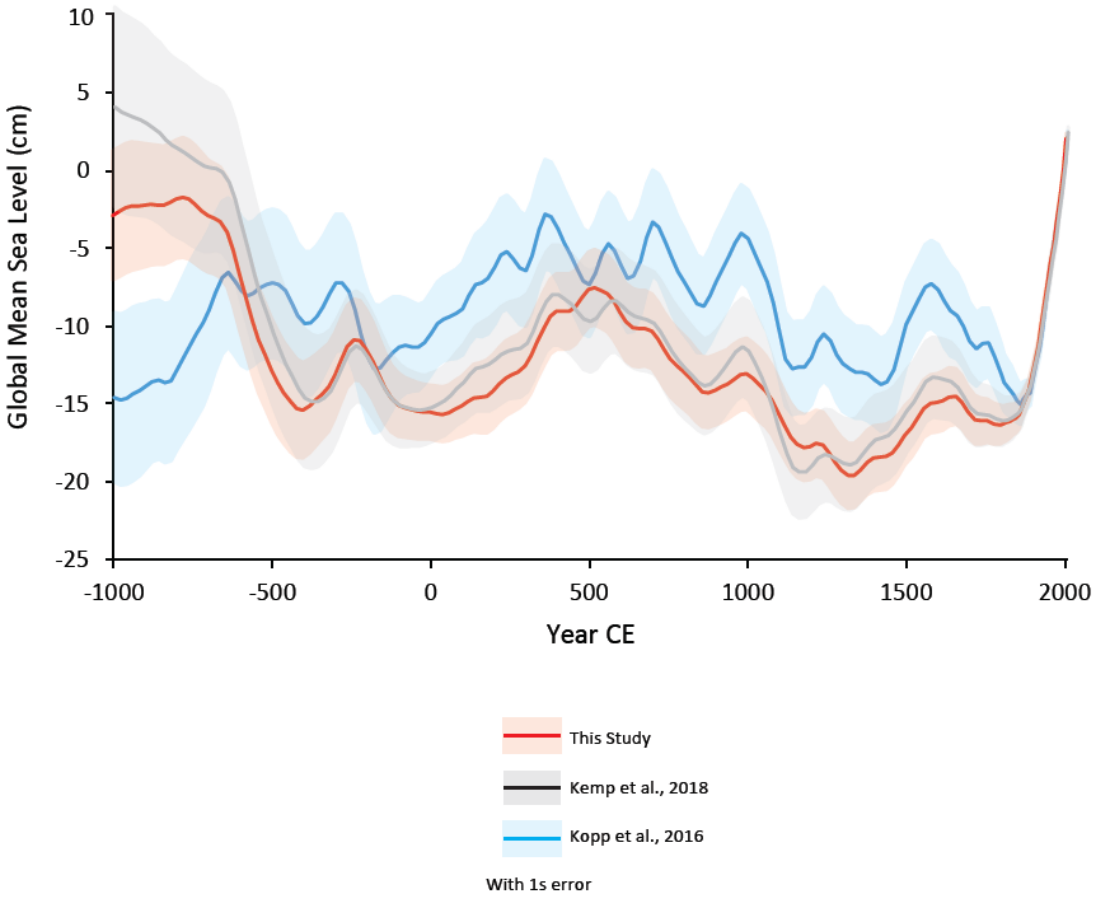

Figure 12. Reconstructed global mean sea level using the spatiotemporal model from this study compared to the results from Kopp et al. (2016) and Kemp et al. (2018).

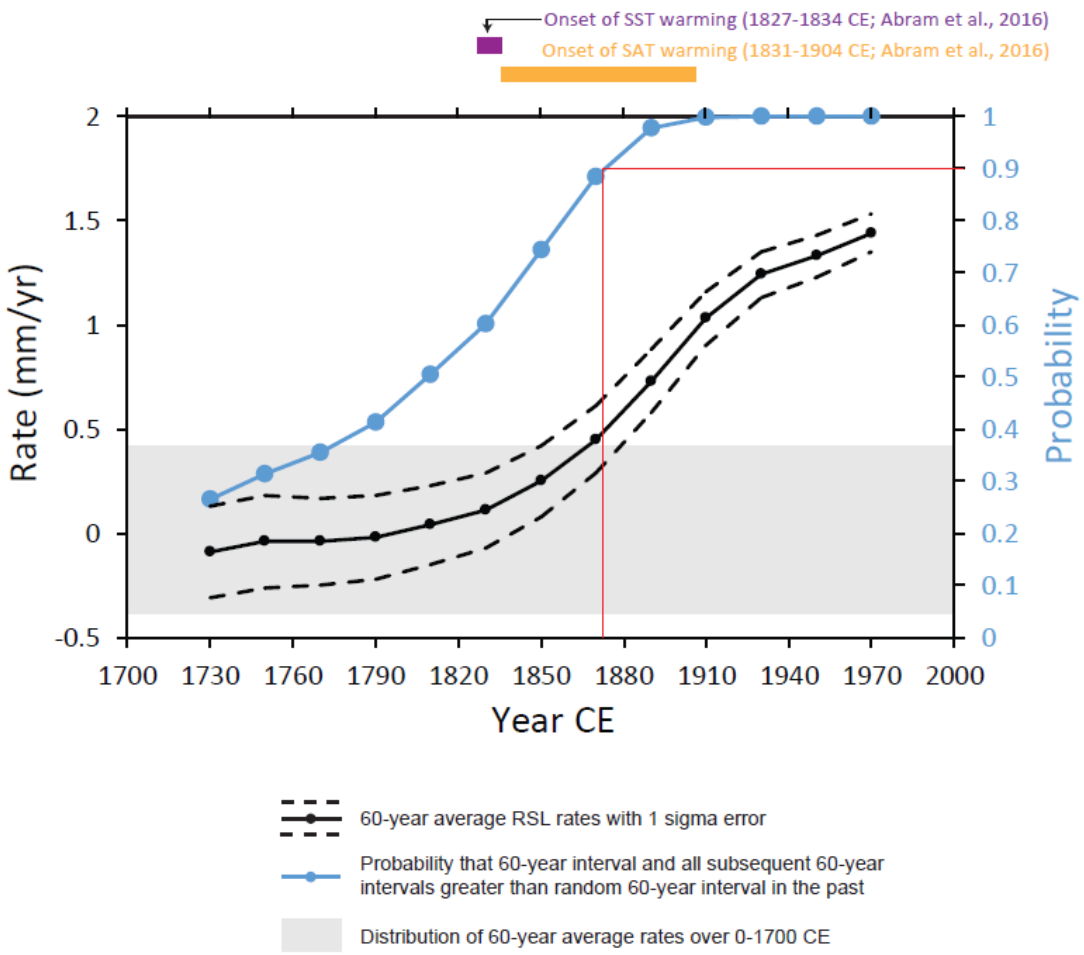

Figure 13. Sixty-year average rates from 1700-2000 CE for global sea level, which increase concurrently with the probability that each 60-year interval and all subsequent 60-year intervals were greater than a random 60-year interval during the pre-Industrial Common Era (0-1700 CE). Interpolation from the probability curve suggests this probability reaches 0.90 by ~1870 CE. We compare our timing of elevated rates of sea-level rise to the onset of warming from air and sea surface temperature reconstructions that drove ocean mass/volume changes (Abram et al., 2016).

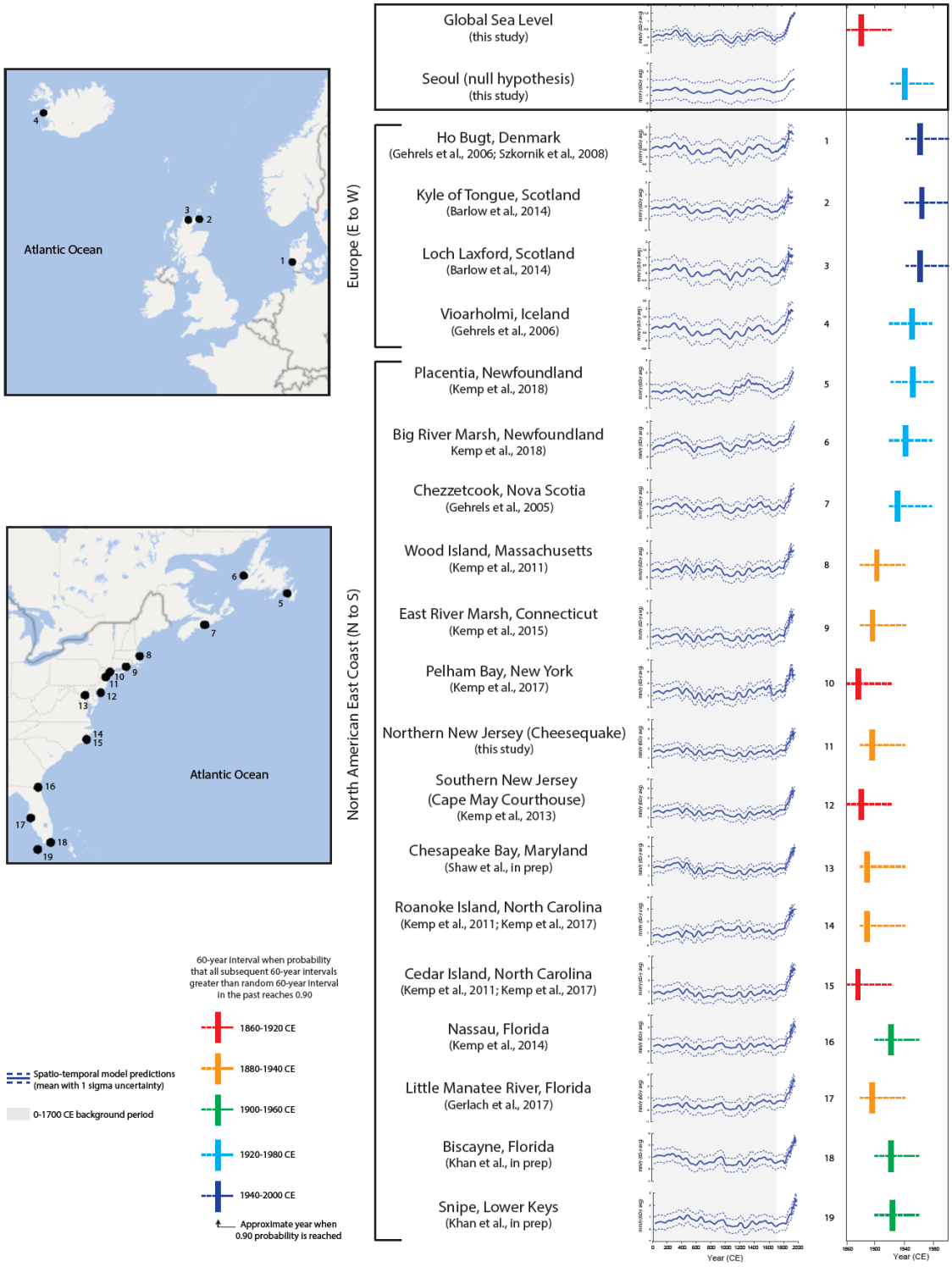

Figure 14. Nineteen sites that fit the data resolution criteria to examine the timing of the onset of modern rates of RSL rise. Spatiotemporal model predictions of rates of RSL are shown with 60-year intervals when the probability that all subsequent 60-year intervals are greater than a random 60-year interval in the past reaches 0.90, including the approximate year when the 0.90 probability is reached.

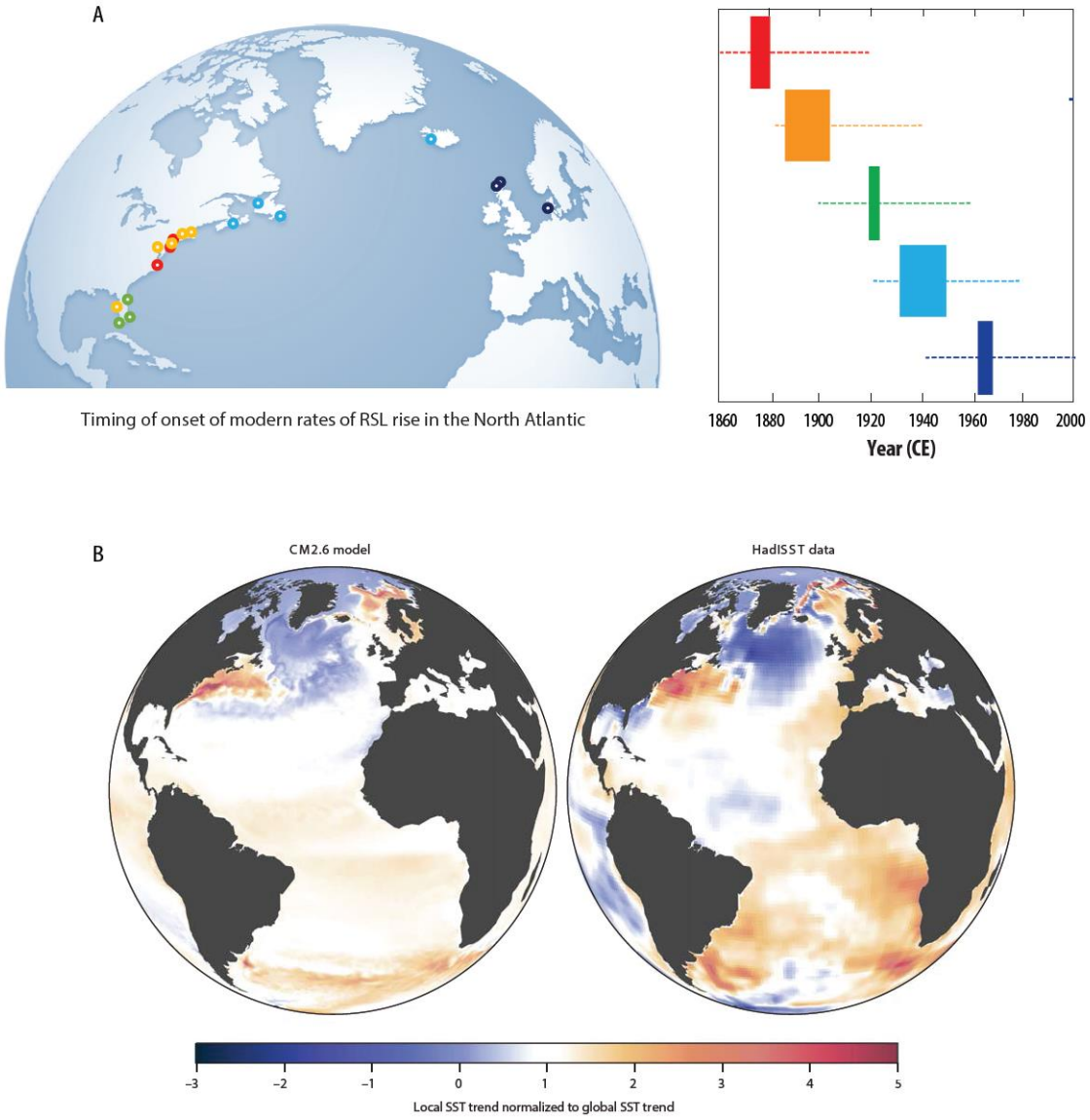

Figure 15. (A) Observed spatial variability in the timing of the onset of modern elevated rates of RSL in the North Atlantic where elevated rates in RSL appear earliest in the mid-Atlantic region followed by the northeastern and southeastern U.S., and latest in Canada and Europe. (B) From Caesar et al., 2018 where observed SST trends from 1870 to 2016 reveal a distinct pattern in the North Atlantic similar to the spatial trend in timing of the onset of modern rates of RSL rise.

Appendix A: All modern dead foraminifera counts from Cheesequake State Park.

Sample ID	*T. comprimata*	*T. inflata*	*S. lobata*	*J. macrescens*	*B. pseudomacrescens*	*Haplophragmoides* spp.	*M. fusca*	*M. petila*	*A. mexicana*	*Ammonia* spp	*Ammobaculites* spp.	*A. inepta*	*P. limnetis*	Elevation (m MTL)	Elevation (SWLI)
CQ/1/2	15	8	2	1	4	6	29	1	42	0	0	2	0	0.21	124
CQ/1/3	24	49	0	9	3	5	2	0	28	0	0	0	0	0.83	201
CQ/1/4	25	19	1	0	3	4	4	0	45	0	0	0	0	0.90	211
CQ/1/5	72	39	23	5	1	1	3	0	20	1	0	0	0	0.92	213
CQ/1/6	32	17	3	5	0	0	11	2	3	4	1	0	0	0.96	217
CQ/1/7	93	99	23	6	10	2	1	2	1	0	0	0	1	0.97	220
CQ/1/8	41	32	18	1	1	2	7	18	2	0	2	0	1	0.94	216
CQ/1/9	94	80	16	16	6	17	0	34	16	0	0	0	3	0.98	220
CQ/1/10	32	34	5	35	6	27	0	34	3	0	0	0	0	0.99	222
CQ/1/11	0	0	0	0	0	0	0	0	2	0	0	0	0	1.28	257
CQ/2/1	39	17	9	21	0	5	28	1	8	4	3	2	0	0.35	142
CQ/2/3	35	83	6	9	0	0	4	0	1	3	0	0	1	0.54	165
CQ/2/4	114	112	11	24	0	2	10	0	67	0	0	0	2	0.89	209
CQ/2/5	39	33	8	10	1	0	4	1	2	0	0	0	0	1.00	222
CQ/2/6	43	83	23	11	0	5	10	5	5	0	0	0	0	1.01	224
CQ/2/7	51	33	15	16	0	4	1	4	5	0	0	0	0	0.98	221
CQ/2/8	93	44	10	26	1	2	2	1	0	0	0	0	0	1.04	227
CQ/2/9	106	78	19	14	0	3	4	2	2	0	0	0	2	1.03	226
CQ/2/10	23	44	1	20	4	16	4	6	0	0	0	0	0	1.04	228
CQ/2/11	0	1	0	0	0	0	0	0	0	0	0	0	0	1.39	272
CQ/3/1	31	32	0	9	53	26	21	5	57	0	0	21	2	0.35	141
CQ/3/2	36	59	6	1	32	12	2	2	82	0	0	0	0	1.05	229
CQ/3/3	91	158	35	1	18	17	4	3	86	0	0	0	0	1.10	236
CQ/3/4	54	76	15	5	19	15	4	2	2	0	0	0	4	1.12	238
CQ/3/5	103	158	24	9	28	24	1	29	0	0	0	0	5	1.09	234
CQ/3/6	104	102	14	6	54	35	3	23	0	0	0	0	1	1.09	235
CQ/3/7	144	79	8	0	16	8	1	18	2	0	0	0	1	1.09	234
CQ/3/8	102	251	18	1	23	13	0	6	5	0	0	0	1	1.09	235
CQ/3/9	101	52	1	3	19	12	0	7	2	0	0	0	0	1.02	225
CQ/3/10	19	31	1	5	14	26	0	11	3	0	0	1	0	0.99	221
CQ/3/11	76	80	7	4	89	40	0	42	4	0	0	0	0	1.05	229
CQ/3/12	1	3	0	1	0	19	0	0	0	0	0	0	0	1.43	277

Appendix B: All fossil core foraminifera counts from Cheesequake State Park.

Depth (cm)	*J. macrescens*	*T. comprimata*	*B. pseudomacrescens*	*M. fusca*	*M. petila*	*S. lobata*	*Haplophragmoides* spp.	*T. inflata*	*A. mexicana*
0	7	101	12	19	2	28	21	12	8
5	13	86	7	16	4	22	14	94	0
10	24	113	31	3	0	5	8	173	0
15	14	35	0	0	0	12	9	84	2
20	50	29	3	13	7	5	18	9	2
25	24	54	8	0	0	22	20	168	22
30	6	31	4	0	4	0	0	19	2
35	180	14	6	2	56	4	4	14	0
40	86	21	0	0	84	5	5	3	8
45	64	66	0	0	106	0	6	6	0
50	5	2	0	0	1	1	0	1	3
55	70	11	1	0	7	1	3	6	0
60	67	29	0	0	4	0	1	0	0
65	268	16	0	0	184	0	0	0	0
70	111	2	0	0	103	0	1	0	0
75	542	42	0	0	812	0	0	0	0
80	111	7	0	0	42	0	4	1	1
85	280	12	0	0	228	4	8	4	0
90	74	2	0	0	20	0	0	1	0
95	56	0	0	0	30	0	0	1	0
100	5	2	0	0	6	0	0	2	0
105	32	3	0	0	7	0	0	1	0
110	6	4	0	0	6	1	0	0	0
115	17	2	0	0	6	0	0	3	0
120	22	4	2	0	5	0	1	0	0

Appendix C: All modern and core stable carbon isotope geochemical ($\delta^{13}C$) data from Cheesequake State Park.

Sample ID	d13C (per mille VPDB)	Elevation (m MTL)	Elevation (SWLI)
CQ/1/2	-19.1	0.21	124
CQ/1/3	-19.1	0.83	201
CQ/1/4	-18.5	0.90	211
CQ/1/5	-17.5	0.92	213
CQ/1/6	-16.7	0.96	217
CQ/1/7	-16.8	0.97	220
CQ/1/8	-20.5	0.94	216
CQ/1/9	-23.2	0.98	220
CQ/1/10	-28.1	0.99	222
CQ/1/11	-28.5	1.28	257
CQ/2/1	-18.8	0.35	142
CQ/2/3	-17.6	0.54	165
CQ/2/4	-18.0	0.89	209
CQ/2/5	-18.9	1.00	222
CQ/2/6	-22.2	1.01	224
CQ/2/7	-17.3	0.98	221
CQ/2/8	-18.2	1.04	227
CQ/2/9	-25.7	1.03	226
CQ/2/10	-27.7	1.04	228
CQ/2/11	-29.4	1.39	272
CQ/3/1	-17.7	0.35	141
CQ/3/2	-19.2	1.05	229
CQ/3/3	-19.6	1.10	236
CQ/3/4	-15.9	1.12	238
CQ/3/5	-16.3	1.09	234
CQ/3/6	-18.7	1.09	235
CQ/3/7	-26.7	1.09	234
CQ/3/8	-20.6	1.09	235
CQ/3/9	-25.8	1.02	225
CQ/3/10	-26.5	0.99	221
CQ/3/11	-26.6	1.05	229
CQ/3/12	-28.2	1.43	277

Depth (cm)	d13C (per mille VPDB)
0	-15.6
5	-16.9
10	-23.3
15	-20.7
20	-16.9
25	-19.0
30	-19.0
35	-20.2
40	-18.9
45	-20.1
50	-19.2
55	-19.4
60	-19.9
65	-23.0
70	-20.7
75	-20.2
80	-20.9
85	-22.8
90	-24.3
95	-24.6
100	-24.8
105	-25.6
110	-26.4
115	-26.4
120	-26.6

Chapter 3: Relative sea-level changes in New Jersey during the last 5000 years

Abstract

Glacial isostatic adjustment (GIA) is the dominant cause of late Holocene relative sea-level (RSL) rise in New Jersey. Geological reconstructions of past RSL record the temporal and geographical evolution of coastlines and can be used to constrain models of GIA. We produced a new late Holocene RSL record in southern New Jersey from salt marsh sediment cores. Our sea-level data are from basal peat units overlying an incompressible substrate, which minimizes the influence of sediment compaction. We used a geotechnical model to account for compaction, and we used a paleotidal model to include an error for tidal range change through time. We used a transfer function that employs salt-marsh foraminifera assemblages and bulk sediment stable carbon isotope geochemistry to estimate the paleomarsh elevation at which each sample was formed. Ages were determined from high precision Accelerator Mass Spectrometry radiocarbon dating on plant macrofossils. We found that RSL rose continuously through the late Holocene, increasing by ~6.4 m from 4.6 ka BP to 1.2 ka BP at an average rate of 1.9 ± 0.3 mm/yr. We compared our observed RSL changes from the basal peat record with site-specific GIA models that combine the ICE-6G_C glaciation-deglaciation with ten viscosity models. We used one 1D (VM5a) and nine 3D mantle viscosity models to examine GIA predictions at 1000 year intervals over the last 5000 years. We found a misfit between model predictions and RSL observations, although the 3D models are an improvement over the 1D model. The remaining misfits suggest the importance of utilizing a wide array of ice model and

viscosity model parameters to find a better fit between site-specific GIA predictions and RSL observations.

1. Introduction

Glacial isostatic adjustment (GIA) is the dominant driver of late Holocene relative sea-level (RSL) rise in the U.S. mid-Atlantic region, including New Jersey, due to its proximity to the margin of the former Laurentide Ice Sheet (e.g. Engelhart and Horton, 2012; Roy and Peltier, 2015; Love et al., 2016). As the ice sheet retreated, the peripheral forebulge began to collapse, causing land subsidence and late Holocene RSL rise along the U.S. mid-Atlantic (e.g. Clark et al., 1978; Davis and Mitrovica, 1996; Engelhart and Horton, 2012; Roy and Peltier, 2015). An accurate estimate of the contribution of GIA to late Holocene RSL is important for coastal adaptation, because in many regions subsidence is a principal reason for differences between regional and global-mean sea-level projections (e.g. Kopp et al., 2014; Love et al., 2016).

GIA is the dynamic response of the solid Earth to surface ice and water redistribution during the cycles of an ice age (e.g. Clark et al., 1978). Models of the GIA process use an array of geophysical data (e.g. geological and instrumental RSL reconstructions, space-geodetic measurements of crustal motion, time-dependent gravity measurements) to constrain the geophysical properties of the Earth's interior, most notably the effective viscosity (Peltier, 1998; Lambeck and Johnston, 1998; Mitrovica and Forte, 1997). GIA models also take as input reconstructions of past ice sheet cover (extent and thickness) and

simulate the evolution of RSL through time as the solid Earth responds to ice sheet changes (e.g. Peltier, 2004; Lambeck et al., 2014). One-dimensional Earth models assume the lithosphere and mantle are laterally homogeneous, but Earth material properties vary radially and laterally (Ekstrom and Dziewonski, 1988; Bunge and Grand, 2000) creating uncertainties regarding ice history, mantle viscosity, and lithospheric thickness (e.g. Davis and Mitrovica, 1996).

Among the geophysical data sources that are used to constrain GIA models, geological reconstructions of past RSL are of particular importance, since they record the temporal and geographical evolution of coastlines (e.g. Wu et al., 2013; Li et al., 2018). Early GIA models (Clark et al., 1978) did not fit the observed RSL data from the U.S. Atlantic coast. GIA models have improved with changes in global ice sheet reconstructions (e.g. ICE-6G-C; Peltier et al., 2015), regional ice models (e.g. Kaufmann et al., 2005; Wu, 2005; Steffen et al., 2006), and mantle viscosity models (VM5a, b and VM6) where viscosity is not independent of depth (Peltier and Drummond, 2008; Engelhart et al., 2011; Roy and Peltier, 2015; Hawkes et al., 2016). However, Engelhart et al. (2011) and Roy and Peltier (2015) still found misfits between RSL observations and GIA predictions when comparing a Holocene sea-level database with ice sheet and mantle viscosity GIA models on the U.S. Atlantic coast. Love et al. (2016) used 363 Earth viscosity models with 35 North American ice histories to accommodate 3D Earth structure and estimate GIA contributions to fit RSL data on the U.S. Atlantic coast. Li et al. (2018) demonstrated the need for 3D laterally heterogeneous mantle viscosity models to examine the misfit between GIA predictions and

RSL observational data and finds that the introduction of lateral viscosity variations can help resolve some misfits in global RSL data.

Accurate RSL reconstructions at a high resolution are needed to validate GIA models on the U.S. mid-Atlantic coast. Such RSL reconstructions are provided by salt marsh sediments, but they are limited by the depth and specific stratigraphy of sediment sequences available (Engelhart and Horton, 2012) as well as local processes involving sediment compaction (e.g. Long et al., 2006; Horton and Shennan, 2009) and tidal range change (e.g. Gehrels et al., 1995; Shennan et al., 2003; Hill et al., 2011). Salt-marsh sediments are prone to sediment compaction, a process that occurs as sediment accumulates, reducing sediment volume and altering the stratigraphic column (Allen, 2000; Horton and Shennan, 2009), resulting in an underestimation of past sea-level (e.g. Allen, 2000; Edwards, 2006; Long et al., 2006). Changes in tidal range through time from factors such as changing bathymetry, coastlines, and shelf width can also affect RSL reconstructions, creating scatter among sea-level index points (e.g. Gehrels et al., 1995; Hill et al., 2011; Horton et al. 2013).

Here, we produced a high resolution late Holocene RSL reconstruction from a salt marsh in southern New Jersey, a region that experienced high rates of RSL rise due to the collapsing peripheral forebulge at the former ice margin (e.g. Dyke et al., 2003; Engelhart and Horton, 2012). We use basal peat units, which experience minimal sediment compaction (e.g. Shennan and Horton, 2002; Tornqvist et al., 2008). Each data point includes an error for tidal range change and an error for the minimal compaction from a

basal peat layer overlying an incompressible substrate. Ages were produced through high precision Accelerator Mass Spectrometry (AMS) radiocarbon dating on salt-marsh plant macrofossils. Our resulting high resolution RSL record was compared to an ensemble of site-specific 1D and 3D mantle viscosity models from Li et al. (2018).

2. Study Area

The southern New Jersey coast is characterized by a barrier island and lagoon system adjacent to the Atlantic Ocean. The barrier island coastline is characteristic of trailing edges of passive continental margins and transgressive barriers (Inman and Nordstrom, 1971), which shelters the lagoon system in front of the geologically older Pleistocene mainland (e.g. Psuty, 1986). This region is a tectonically stable, passive continental margin with a coastal plain consisting of Cretaceous to Holocene unconsolidated sands, silts, clays and gravels (e.g. Field and Duane, 1976). These coastal plain sediments have slowly subsided (<1 mm/yr) since the Cretaceous due to thermal subsidence, sediment loading offshore, and compaction (e.g. Kominz et al., 1998).

The salt-marsh field study site is at Leeds Point in Edwin B. Forsythe National Wildlife Refuge on the west side of Great Bay in southern New Jersey (Figure 1). The Refuge comprises and protects over 47,000 acres of a network of land and waters of the southern New Jersey coast, including over 35,000 acres of salt marshes (U.S. Fish and Wildlife Service, 2019). The coast forms extensive gently sloping platforms of modern salt marshes with tidal channels (Ferland, 1990). The salt marshes of Edwin B. Forsythe National

Wildlife Refuge were investigated by Kemp et al. (2013). They reconstructed RSL over the last 2500 years in southern New Jersey using a foraminiferal-based transfer function. After correcting for land-level change (1.4 mm/year), they found four multi-centennial sea-level trends using change point analysis: fall at 0.11 mm/year from -500 to 250 CE, rise at 0.62 mm/year from 250 to 733 CE, fall at 0.12 mm/year from 733 to 1850 CE, and rise at 3.1 mm/year since 1850 CE, which exceeds the global average estimate for the 20th century.

The southern New Jersey coast has a semidiurnal, microtidal (range <2 m) regime, but varies between the ocean and lagoon side of the barriers. The tidal range at our field site is 1.1 m. Water exchange primarily occurs between the Atlantic Ocean and Little Egg Inlet leading into Great Bay (Chant et al., 1996).

3. Methods

3.1. Sampling Design

We completed multiple transects of hand cores to better understand the underlying stratigraphy of the marsh and to track the basal peat unit. The cores were described in the field using the Troels-Smith (1955) method for organic-rich sediments to record the proportions of organic matter, silt, clay, and sand, and the presence of wood or shell fragments. A transect of 14 core locations was selected to retrieve basal peat sediments. The lower ~1 m of each of the 14 cores was collected so that the entire basal peat section was obtained, including the transitions into overlying sediment sequences and the top of

the underlying incompressible substrate. Basal samples were collected so that each core overlaps in depth with the sampled section from the next core in the transect. Each core was collected using a hand-driven Russian-type core to minimize compaction or contamination during sampling. The recovered basal core sections were sealed in pipe sections with plastic wrap and refrigerated until analysis to minimize drying and oxidation.

We obtained elevations for each core location using a temporary benchmark with real time kinematic (RTK) satellite navigation and a total station where elevations were referenced to the North American Vertical Datum (NAVD88). We used VDatum (Yang et al., 2008) to convert from orthometric to tidal datums.

3.2. Estimating Paleomarsh Elevation

We chose one sample at the base of the basal peat stratigraphic unit from each core to reconstruct RSL. We used salt-marsh foraminifera as a proxy to reconstruct sea level, because their modern distributions exhibit vertical zonation (e.g. Scott and Medioli, 1978; Gehrels, 1994; Horton and Edwards, 2006). Foraminiferal-based transfer functions utilize a modern foraminifera training set to quantify species assemblages' relationship with elevation, which is then applied to fossil assemblages to estimate a paleomarsh elevation (PME) for each sample with a 1σ sample-specific uncertainty (e.g., Horton et al., 1999; Gehrels, 2000; Horton and Edwards, 2006). We used a Bayesian transfer function that employs foraminifera and a secondary proxy, $\delta^{13}C$, as an informative prior to reduce vertical uncertainty (Cahill et al., 2016; Kemp et al., 2017). Stable carbon isotope

geochemistry (δ13C) in bulk sediment represents the dominant vegetation type and can be used as a proxy for sea level, because the transition between C_3 and C_4 dominated salt-marsh plant communities has been shown to act as the boundary for the mean higher high water (MHHW) tidal datum on the U.S. mid-Atlantic coast (e.g. Middleburg et al., 1997; Johnson et al., 2007; Kemp et al., 2012). The Bayesian transfer function (BTF) was developed using a New Jersey modern training set of salt-marsh foraminifera and $\delta^{13}C$ from Kemp et al. (2013) consisting of 163 samples from 13 sites in southern New Jersey, in addition to 32 modern samples from northern New Jersey (Walker et al., Chapter 2). Due to differences in tidal range among sampling locations, we converted the tidal elevations of the modern samples into a standardized water level index (SWLI), following the approach of Horton et al. (1999), where a value of 100 corresponds to local mean tide level (MTL) and a value of 200 corresponds to local mean higher high water (MHHW).

We formally accounted for temporal and spatial variability of modern foraminifera distributions in the BTF by informing the variability prior for individual foraminifera species using data from a monitoring study of modern foraminifera in southern New Jersey (Walker et al., Chapter 1). The performance of the BTF was evaluated using 10-fold cross validation on the modern training set, where the data is divided into 10 randomly drawn groups of equal size (known as folds). Each fold is removed from the modern dataset in turn and the remaining data is used to create predictions for the removed samples, which is repeated until every sample has an out-of-sample prediction value (Cahill et al., 2016).

We also used a series of terrestrial limiting points from the basal cores to further constrain RSL. Samples that indicate deposition in terrestrial or marine environments are classified as limiting dates (e.g. Engelhart and Horton, 2012). These terrestrial limiting points did not contain any foraminifera and were assigned an indicative range (the elevational range over which a sample would occur at present) above MHHW, because MHHW is the lowest elevation at which foraminifera became absent in modern foraminifera transects in New Jersey (Kemp et al., 2013). Therefore, reconstructed RSL must fall above marine limiting dates and below freshwater limiting dates.

3.3. Foraminifera and Geochemistry

We analyzed the collected basal cores for foraminifera and $\delta^{13}C$ in 1-cm slices at 5-cm spaced intervals down core. Core samples for foraminifera were wet sieved to isolate the 63-500 µm foraminiferal-bearing fraction of the sediment and were split into eight equal aliquots using a wet splitter (Scott and Hermelin, 1993). Samples were counted under a binocular microscope while immersed in distilled water (Scott et al., 2001). A minimum of 100 tests were counted, or the entire sample was counted if <100 tests were present to ensure a statistically-sound representation of low-diversity salt-marsh foraminifera assemblages (e.g. Fatela and Taborda, 2002). Identifications of foraminifera were confirmed with type specimens at the National Museum of Natural History, Smithsonian Institute, Washington, D.C. We grouped specimens of the genus *Haplophragmoides* into a single group due to difficulties in identification to the species level (Kemp et al., 2009).

$\delta^{13}C$ values were measured in bulk sediment, since the dominant input to salt-marsh sediment is in situ vegetation. $\delta^{13}C$ was measured at the Departments of Geology and Environmental Studies at Bryn Mawr College using a cavity ring-down laser spectroscopy (CRDS) following the flash combustion technique described by Balslev-Clausen et al (2013). Prior to isotopic analysis, bulk peat samples were freeze-dried in a Virtis™ benchtop freeze dryer to remove moisture and then ground in a Retsch™ ball mill until finely powdered. Approximately two mg (±0.5 mg) of the dried, powdered sample was weighed on a Mettler Toledo™ XP56 microbalance with 4 µg precision. Weighed samples were sealed in pressed-wall tin capsules and flash combusted at 980°C in a Costech™ ECS 4010 element analyzer using N2 as a carrier gas. The isotopic composition of the CO_2 produced by combustion was analyzed in a Picarro™ G2201-i CRDS instrument. Carbon abundance in each sample was calculated from the peak $^{12}CO_2$ concentration measured by the CRDS system, calibrated by analysis of standard reference material (NIST 1547 Peach leaf). Reproducibility of carbon mass concentration is ±0.8% (1 s.d., n=96). Carbon isotopic composition, reported as $\delta^{13}C$, is standardized to Vienna Pee Dee Belemnite (VPDB) by analysis of standard reference material USGS40 (glutamic acid). The reproducibility of $\delta^{13}C$ values is <0.2‰ based on repeat analyses of NIST 1547 (0.15‰, 1 s.d., n=96) and USGS40 (0.18‰, 1 s.d., n=27).

3.4. Chronology

All sample ages were measured using Accelerator Mass Spectrometry (AMS) radiocarbon dating. 4-6 plant macrofossils (stems and rhizomes) found in growth position were selected from the basal peat sequence in each core, cleaned under a microscope to remove

contaminant sediment particles, oven dried, and submitted for AMS ^{14}C dating to the National Ocean Science Accelerator Mass Spectrometry (NOSAMS) facility and Beta Analytic. Reported radiocarbon ages and uncertainties (Table 1) were calibrated using the IntCal13 dataset (Reimer et al., 2013).

The radiocarbon dates for each basal core were compiled using the Bchron package in R (Haslett and Parnell, 2008; Parnell et al., 2008), which uses a Bayesian framework to produce an age-depth model and estimates ages with associated uncertainties for every 1 cm thick interval in the core. Age estimates in Bchron incorporate the non-parametric likelihood distributions from calibrated radiocarbon ages. The age estimates and uncertainties from Bchron were applied to each basal core sample with a reconstructed PME.

3.5. Compaction

Basal peats are more resistant to sediment compaction since they overly an incompressible substrate (e.g. Shennan and Horton, 2002); however, only base of basal index points in direct contact with the incompressible substrate are completely unaffected by compaction (Törnqvist et al., 2008). We used a geotechnical model (Brain et al., 2011, 2012, 2015) to estimate post-depositional lowering through sediment compaction on the shortest and longest sediment cores to evaluate the benefit of using basal peats for RSL reconstructions when dealing with deep sediment sequences (e.g. Tornqvist et al., 2008; Horton and Shennan, 2009) and to include an error for each sea-level index point to account for the

minimal sediment compaction within the basal peat units. The geotechnical model has been used previously to correct salt-marsh RSL reconstructions for compaction (e.g. Kemp et al., 2017; Kemp et al., 2018), and here we applied the model to the shortest and longest sediment cores to estimate the maximum potential influence of compaction for each sampled basal peat section.

Modern marsh surface sediments from Cape May Courthouse and Leeds Point in southern New Jersey similar to those found in the sediment core were used for laboratory geotechnical testing to calibrate the model (Brain et al., 2015). Core samples were tested under one-dimensional, zero-lateral strain compression using fixed ring, front-loading oedometers (Head, 1988) and the results were used to estimate parameter values of the Brain et al. (2011, 2012) framework describing changes in volume in response to changes in vertical effective stress. We measured organic content by loss-on-ignition (LOI) and bulk density at 2-cm intervals down core for the entire length of the shortest (247 cm) and longest (863 cm) cores from the Leeds Point transect. For LOI analysis, we dried the samples in an oven and ignited the samples in a muffle furnace following the methods of Plater et al. (2015). Using relationships between compression properties and measured LOI, we calibrated the decompaction model to predict how the sediment in the core compacted. We compared measured and model-derived estimates of down core dry bulk density to assess the predictive capacity of the model.

The model provided depth-specific estimates of post-depositional lowering (PDL) (±1 standard deviation) at 2 cm intervals. For samples from the shortest and longest cores, the samples were corrected for compaction by adding the PDL estimate at the depth of the sample to the measured sample altitude relative to MTL. Due to the comparable stratigraphy along the basal core transect, for the remaining 12 cores, an error was added to each sea-level index point using the PDL estimates from the longest core to represent the maximum potential PDL that each basal index point could have undergone.

3.6. Tidal Range Change

Tidal amplitudes can change through time due to astronomical forcing, ocean depth, density stratification, and coastal configuration (e.g. Griffiths and Hill, 2015). As tidal amplitudes are used in sea-level reconstructions, tidal changes must be accounted for through time. For example, if tidal range was greater in the past, the PME would be greater and, consequently RSL would be lower, resulting in an underestimation of past sea-level change. We used a numerical paleotidal model following the methods of Horton et al. (2013) that predicts paleotidal data for New Jersey using a nested modeling approach (Hill et al., 2011; Hall et al., 2013), to include an error in the RSL data to account for changes in tidal amplitudes through time. First, a global tidal model (Griffiths and Peltier, 2008, 2009) was used to compute tidal amplitudes and phases on an 800 x 800 regular grid. A regional model (ADCIRC; Luettich and Westerink, 1991) allows for variable spatial resolution with nearshore resolution of 1–2 km to retain coastal embayment and estuary features. Hill et al. (2011) validated the model with approximately 250 NOAA tide-gauges on the U.S. Atlantic and Gulf coasts and showed very good agreement between

observations and model predictions. Depth changes from the ICE-5G GIA model of Peltier (2004) were used for paleobathymetries. Tidal amplitudes and phases from analysis of the regional model results were converted to tidal data using the harmonic constant datum method of Mofjeld et al. (2004).

An error was included in each data point to account for changes in tidal range from the time of sample deposition using the data from the paleotidal model. The model was run at 1 ka intervals, and data were extrapolated for our study site based on nearby model grid points. Following Hill et al. (2011), the percentage change in tidal range between present and the model runs was used to provide absolute values.

3.7. Reconstructing Relative Sea Level

We converted the PME estimates from the Bayesian transfer function from SWLI units back into meters relative to MTL specific to our study site. The reconstructed RSL of sample i, denoted RSL_i, is given by:

$$RSL_i = A_i - PME_i \qquad [1]$$

where A_i and PME_i are the altitude and paleomarsh elevation of sample i, respectively, and both values are expressed relative to MTL. A_i was established by subtracting the depth of each sample in the core from the measured core-top altitude. PME_i was estimated by the BTF with an associated 1σ uncertainty. Each sample also has additional errors specific to sea-level research (e.g. Shennan, 1986; Engelhart and Horton, 2012), with total error for each sample given by (Shennan and Horton, 2002):

$$E_i = (e_1^2 + e_2^2 + e_n^2)^{1/2} \quad [2]$$

These errors include a ±0.05 m high precision surveying error (e.g. Shennan, 1986; Gehrels, 1999), a sample thickness error of ±half of sample thickness (e.g. Shennan, 1986), an angle of borehole error of ±1% overburden (e.g. Tornqvist e al., 2008), and a ±0.01 error for compaction from the Russian hand corer (e.g. Shennan, 1986). In addition, we included the sediment compaction error estimated by the geotechnical model and the tidal range change error estimated by the paleotidal model.

We used an Errors-In-Variables Integrated Gaussian Process (EIV-IGP) model (Cahill et al., 2015), which accounts for the vertical and chronological uncertainties of the RSL data, to probabilistically assess past RSL changes and rates of change. Each data point includes the sample-specific uncertainties with associated probability distributions. The model also has edge effects, where uncertainty at the beginning and end of the record gets larger.

3.8. GIA Models

We compared the observed RSL changes over the last ~5000 years from our basal peat record with GIA models. The models include two components: the ice glaciation-deglaciation history from the global ICE-6G_C model (Argus et al., 2014; Peltier et al., 2015) and the viscosity models (e.g. VM5a and 3D viscosity models from Li et al., 2018). We used one 1D (VM5a) and nine 3D mantle viscosity models to examine GIA predictions at 1000-year intervals over the last 5000 years. The viscosity models are labeled, for example, as VM_0.2_0_0.6_L140, VM_0.3_0.25_0.6_L140, and VM_0.3_0.5_0.6_L140

(Li et al., 2018) where the first digit indicates the background viscosity in the upper mantle (e.g. $0.3x10^{21}$ Pas), the second digit represents the lateral heterogeneity scaling factor in the upper mantle ranging from 0 to 1 depending on the percentage of lateral viscosity variations that are induced by thermal effects, and the third digit represents the lateral heterogeneity scaling factor in the lower mantle. The final digit indicates that the model includes the laterally heterogeneous lithosphere thickness, where here, 'L140' means the maximum lithospheric thickness beneath stable cratonic area is 140 km (Li and Wu, 2018).

4. Results

4.1. Stratigraphy

Stratigraphy at the salt-marsh field study site was completed through a transect of 14 sediment cores collected over a distance of ~500 meters ranging from ~2 meters deep at the inland end of the transect to ~9 meters deep at the coastal edge of the marsh (Figure 1c). The stratigraphy across the transect had a 0.5 to 1-meter basal unit of dark brown amorphous organic peat overlying a gray incompressible sand and gravel. There is a very uniform gradient in the basal sand contact from a depth of ~2 m in the shortest core which deepens towards the coast to a depth of ~9 m. The basal peat unit thins away from the coast until it is no longer detectable above ~2 m depth. Above the basal peat is ~1-3 meters of dark brown organic-rich sediment that varies in thickness along the transect. The stratigraphy of the upper portion of the marsh is a brown minerogenic sediment which increases in thickness towards the coast from ~1 m in the shortest core to ~6 m in the longest core.

4.2. Paleomarsh Elevation

We chose one basal sample in each of the 14 basal cores, as well as limiting points in several cores (Figure 2). The basal samples were located at a depth where foraminifera counts were declining, before disappearing altogether as the basal incompressible sand was reached. The deepest assemblages of foraminifera in each core were dominated by *Jadammina macrescens*, *Milliammina petila*, *Haplophragmoides* spp., and *Tiphotrocha comprimata*. For example, in the shortest core (EF20), the upper portion of the basal peat unit was dominated by *T. comprimata* and *Arenoparella mexicana* (~85% of the assemblage together), but transitioned to an assemblage dominated by *J. macrescens* and *M. petila* (up to 100% of the assemblage together) with depth until the foraminifera became absent altogether below 190 cm. Our basal sample is at a depth of 190 cm where *J. macrescens* and *M. petila* are the dominant species. Similar foraminifera assemblage trends were found in the other basal cores, where the upper portion includes include greater abundances of species such as *A. mexicana* or *T. inflata*, but are less prevalent with depth. The most consistent trend among the basal cores was that *J. macrescens* and/or *M. petila* were dominant species at the lowest depths where foraminifera were present and were also two of the most dominant species in our samples. The $\delta^{13}C$ values in each basal core became more depleted with depth. The $\delta^{13}C$ values at the depth of each sea-level index point or the nearest depth where $\delta^{13}C$ was measured ranged from -16.2‰ to -26.6‰, which are consistent with measurements in high salt marsh environments in New Jersey (Walker et al., Chapters 1 and 2).

The dominant foraminifera species in our samples are indicative of a high salt marsh environment. Maximum abundances of *J. macrescens* have commonly been found in high marsh-upland transition environments (e.g. Scott and Medioli, 1978, 1980; Spencer, 2000; Nikitina et al., 2003; Robinson and McBride, 2006; Horton and Culver, 2008; Kemp et al., 2009). In New Jersey, high marsh assemblages have been dominated by *J. macrescens* and *T. comprimata*, and *Haplophragmoides* spp. has been found to be a dominant species in high marsh and transitional high marsh-upland environments, often above MHHW (Kemp et al., 2012, 2013). Kemp et al. (2013) also found high abundances of *M. petila* in the lower portion of a core from Edwin B. Forsythe National Wildlife Refuge. The high marsh species of foraminifera, combined with $\delta^{13}C$ values more depleted than -16‰, indicate that each sample formed at a high salt marsh environment, which is consistent with the reconstructed PME estimates from the Bayesian transfer function. PME estimates for the basal samples ranged from 0.58 m MTL to 0.95 m MTL with sample-specific uncertainties (1σ) ranging from 0.12 to 0.34 m.

In addition, we also chose nine limiting points from the basal cores. These samples were located at depths where foraminifera were absent. For example, in the shortest core (EF20), foraminifera are present until a depth of 190 cm and we chose a limiting point at 195 cm. The $\delta^{13}C$ values at the depth of each limiting point or the nearest depth where $\delta^{13}C$ was measured ranged from -18.0‰ to -29.1‰, which are consistent with measurements in high salt marsh to upland environments in New Jersey (Walker et al., Chapters 1 and 2). The absence of foraminifera and the $\delta^{13}C$ values more depleted than -18‰ at the depths of our limiting points allow us to assign each of these points an indicative range above MHHW.

4.3. Chronology

Each basal core had a set of radiocarbon dates that was used to develop an age-depth model for that core (Table 1). Using the individual age-depth models, each of the 23 basal samples and limiting points had an associated age estimate, extending back ~4.6 ka BP. The average chronological uncertainty of the RSL data points was 81 years (2σ). The youngest point was at a depth of 190 cm in the shortest core (EF20) and had an age of 1262 ± 45 cal yr BP. The oldest point was at a depth of 830 cm in the longest core (EF5) and had an age of 4680 ± 146 cal yr BP.

4.4. Compaction

We used measured LOI and dry bulk density with a geotechnical model to analyze effective stress and post-depositional lowering of the shortest (~2.5 m) and longest (~8.5 m) sediment cores (Figure 3). Measured LOI for the shortest core (EF20) varied from ~50% at the top of the core to ~2% at the base of the core in the basal sand unit. The average LOI in the lower ~0.5 m of the core was ~4%, and then increased to an average of 27% in the upper 2 m. The longest core (EF5) had a much smaller LOI % at the top of the core of ~15%, but a slightly higher LOI % at the base of 7% compared to the shortest core. LOI was variable in the upper ~8.3 m, ranging from 7% to 49%, before continually decreasing to the base. Measured dry bulk density for the shortest core varied from ~0.2 g/cm^3 at the top of the core to ~2.0 g/cm^3 at the base of the core. Similar to LOI, the average dry bulk density in the lower ~0.5 m of the core was ~1.6 g/cm^3, and then markedly decreased to an average 0.3 g/cm^3 in the upper 2 m of the core. Measured dry bulk density for the longest

core varied from ~0.4 g/cm^3 at the top of the core to ~1.4 g/cm^3 at the base of the core. Similar to LOI, the dry bulk density varied in the upper ~8.3 m from 0.2 g/cm^3 to 1.0 g/cm^3, and then rapidly increased to the base.

The effective stress predicted by the geotechnical model in the shortest core increased with depth to 3.3 kPa at 2 m depth before increasing rapidly in the lower 0.5 m of the core to 6.5 kPa at the base. The longest core had a continually increasing effective stress, reaching a maximum of ~23 kPa at the base of the core. Post-depositional lowering estimated by the model for the shortest core was 0 m at the surface, increased to a maximum PDL of ~0.01 m in the middle of the core around 1.3 m depth, and then decreased back to 0 at the base of the core. The PDL estimates for the longest core was also 0 m at the surface, but then increased to a much larger maximum PDL of ~0.65 m in the middle of the core around 5.5 m depth, before decreasing back to 0 at the base of the core. The significant PDL in the longest core clearly exhibits the influence of sediment compaction within deep sequences of salt-marsh sediment, which could influence RSL reconstructed from continuous sequences of sediment.

The estimated PDL for samples at 1.95 m and 1.85 m depth in the shortest core were 0.009 m and 0.01 m, respectively, which were used to correct these two samples for sediment compaction. Alternatively, the samples in the longest core at a depth of 8.30 m and 8.11 m had a PDL estimate of 0.10 m and 0.15 m, which were used to correct these two samples for compaction. To account for sediment compaction of the index points in the other 12

cores in which we did not estimate PDL with the geotechnical model, we included the PDL estimate from the longest core (0.15 m) as an error to each PME estimate, as this value is the largest magnitude PDL we would expect in any shorter core.

4.5. Tidal Range Change

The Great Diurnal Range (GT) is the difference between mean higher high water and mean lower low water (NOAA, 2000) and in New Jersey, the GT is microtidal (<2 m). Paleotidal modeling indicates that the GT was 24% greater in the past, reaching ~0.24 m higher at 5 ka compared to present. The maximum increase in tidal range for our samples is ~0.22 m at ~4.6 ka. An error was included for each sample to account for differences in tidal range at the time of sample deposition.

4.6 Reconstructing Relative Sea Level

We produced 14 basal sea-level index points and 9 limiting points from southern New Jersey from 1262 ± 45 cal yr BP to 4680 ± 146 cal yr BP (Figure 5). The calculation of RSL and age, including errors, was as follows (using an example with the sample at a depth of 190 cm in the shortest core, EF20):

$$RSL = (-1.31\ m_{altitude} + 0.01\ m_{post\text{-}depositional\ lowering}) - 0.776\ m_{paleomarsh\ elevation}$$

Where paleomarsh elevation was estimated from the Bayesian transfer function

= -2.08 m

$$Error = \Sigma(0.21\ m^2_{PME\ error} + 0.005\ m^2_{thickness} + 0.05\ m^2_{leveling} + 0.01\ m^2_{sampling}$$

$+ 0.02\ m^2_{borehole} + 0.05\ m^2_{tidal\ range})^{1/2}$

$= \pm 0.30$ m

Age = 1262 ± 45cal yr BP (2σ range)

We applied our index points to the EIV-IGP model to examine past RSL and rates of change (Figure 6). RSL rose continuously by an approximate magnitude of 6.4 m, from -8.5 m (95% confidence interval of -9.4 m to -7.6 m) at 4.6 ka BP to -2.1 m (95% confidence interval of -2.8 m to -1.4 m) at 1.2 ka BP. The average rate of rise over this period was 1.9 ± 0.3 mm/yr (1σ).

5. Discussion

5.1. Relative Sea Level

RSL has risen along the entire U.S. Atlantic coast during the late Holocene at differing rates due to spatially variable GIA-induced subsidence and other processes (e.g. oceanographic effects). Late Holocene RSL rise in New Jersey has been dominated by GIA due to New Jersey's close proximity to the former Laurentide Ice Sheet margin (e.g. Engelhart et al., 2009; Roy and Peltier, 2015; Love et al., 2016). Our southern New Jersey record shows continuously rising sea level through the late Holocene. Previous studies from New Jersey also show continuous RSL rise of similar magnitude (~8 m) during the last 4 ka (e.g. Daddario, 1961; Bloom, 1967; Psuty, 1986; Miller et al., 2009; Engelhart and Horton, 2012). For example, Psuty (1986) examined sea-level trends using radiocarbon dates from sediment cores around Great Bay and elsewhere in New Jersey and found rising

RSL from at least 7700 years BP to present, with a rapid rate of rise beginning before 7000 years BP, followed by a decrease in rates 2000-2500 years BP. We found an average rate of rise of 1.9 ± 0.3 mm/yr at our study site over the last ~4.6 ka, which is also comparable to previous findings over the late Holocene. Miller et al. (2009) reconstructed RSL in New Jersey over the last 5000 years and found a similar relatively constant rise of 1.8 mm/yr from -5000 to 500 yr BP, while Miller et al. (2013) found a rise of 1.6 ± 0.1 mm/yr from 2.2 to 1.2 ka. Horton et al. (2013) used a sea-level database for New Jersey and, after accounting for compaction and change in tidal range, found that RSL in New Jersey rose at an average rate of 4 mm/year from 10-6 ka, 2 mm/year from 6-2 ka, and 1.3 mm/year from 2 ka to 1900 CE. Kemp et al. (2013) reconstructed RSL over the last 2500 years at Edwin B. Forsythe National Wildlife Refuge and, after correcting for land-level change (1.4 mm/year), found falling sea level of 0.11 mm/year from -500 to 250 CE and rising sea level of 0.62 mm/year from 250 CE to 733 CE.

Although GIA is the dominant cause of RSL rise in New Jersey during the late Holocene, there are also eustatic, regional, and local contributions to consider that could contribute to the RSL changes we observe. For example, the late Holocene ice melt history has not been resolved (e.g. Gehrels, 2009; Alley et al., 2010). The Greenland Ice Sheet (Sparrenbom et al., 2006; Mikkelsen et al., 2008; Long et al., 2012; Marcott et al., 2013) and small glaciers (Jansen et al., 2007) were growing in the late Holocene, so any late Holocene ice melt must be due to Antarctica. Peltier (2002) argued that there was no ice melt after 4 ka, while Lambeck and Bard (2000) found a small (<0.5 m) component of ice-equivalent sea-level rise during the last 4 ka, and Lambeck (1988) argued that the Antarctic Ice Sheet was

contributing to sea-level rise as late as 2 ka ago. These model-based estimates are difficult to constrain as they rely on a small subset of global geological sea-level observations, and there are regional misfits between model output and observations (Gehrels, 2009). More recently, Lambeck et al. (2014) used ∼1,000 observations from locations far from former ice margins and found a decline in the rate of sea-level rise from 6.7 ka with a rise of ≤1 m from 4.2 ka to time of recent sea-level rise ~100-150 years ago. Additionally, in this time period, there was no evidence for oscillations in global mean sea level >15-20 cm on time scales of ~200 years.

Regionally, tectonics do not contribute measurably to RSL on Kyr timescales because New Jersey has been a tectonically stable, passive continental margin through the Holocene (e.g. Field and Duane, 1976; Sykes et al., 2008). Here, we accounted for sediment compaction and included an error, which was minimal since we utilized basal peat samples. Additionally, we accounted for tidal range change, which is also small (~0.24 m) compared to the >20 m of RSL rise observed during the Holocene in New Jersey (e.g. Horton et al., 2013). Coastal plain locations like New Jersey have experienced higher rates of RSL rise than bedrock locations due to the natural compaction of unconsolidated coastal plain Holocene sediments (e.g. Miller et al., 2013; Johnson et al., 2018). Due to coastal plain subsidence, these locations have rates of RSL rise 0.3-1.3 mm/yr higher than at bedrock locations (e.g. Miller et al., 2013). Ocean mass changes from atmospheric circulation and prevailing winds and ocean currents can also cause regional sea-level changes (Kemp et al., 2018). For example, meridional ocean circulation can cause sea-level changes along the Atlantic coast (e.g. Levermann et al., 2005; Ezer, 2016).

5.2. Comparison with GIA Models

We compare our basal RSL record with a suite of GIA models (Figure 7). The ice model ICE-6G_C is used with one 1D and nine 3D viscosity models. ICE-6G_C was first released with the VM5a viscosity model, which is the 1D viscosity model used here. Although more recent viscosity models have been developed (VM6, VM7; Roy and Peltier, 2017), VM6 has been shown to have a significant misfit to the totality of the available space-geodetic observations (Roy and Peltier, 2017), and the ICE-7G_NA (VM7) model cannot be adopted with ice model ICE-6G_C directly.

None of the GIA models fit the complete observed RSL trend in the late Holocene. Most of the GIA models appear to overestimate the magnitude of sea-level rise over the last 5 ka. While the EIV-IGP model predicts a rise of ~8 m over this time period, the GIA models predict up to ~15 m of rise. Two models match the overall magnitude of sea-level change the best: VM_0.2_0.25_0.6_L140 and VM_0.2_0.5_0.6_L140 with magnitudes of ~8.5 and ~8.9 m, respectively. These two models have a lower background viscosity in the upper mantle (e.g. 0.2×10^{21} Pas), as well as a lower lateral heterogeneity scaling factor in the upper mantle.

We can examine individual time steps to compare the EIV-IGP model results with the GIA model predictions. At 4 ka, the EIV-IGP model predicts RSL at -6.9 m. Models VM_0.2_0_0.6_L140 and VM_0.2_0.75_0.6_L140 have predictions of -6.5 m and -7.4,

respectively. At 3 ka, the EIV-IGP model predicts RSL at -5 m and models VM_0.3_0.05_0.6_L140 and VM_0.3_0.25_0.6_L140 predict -5.1 m and -4.9 m. Finally, at 2 ka, EIV-IGP predicts -3.5 m and VM_0.2_1_0.6_L140 predicts -3.5 m and VM5a/VM_0.5_0_0 predicts -3.7 m. Therefore, earlier in the RSL record around 4 ka, the viscosity models with a lower background viscosity in the upper mantle (e.g. $0.2x10^{21}$ Pas) have a better fit to the data, while in the middle of the record around 3 ka, the models with a higher background viscosity in the upper mantle (e.g. $0.3x10^{21}$ Pas) have a better fit to the data. However, later in the record around 2 ka, a model with a lower background viscosity in the upper mantle (e.g. $0.2x10^{21}$ Pas) has the best fit. Engelhart et al. (2011) found that an upper mantle viscosity of $0.25x10^{21}$ Pas (VM5b) removed discrepancies between RSL observations and GIA predictions along the U.S. mid-Atlantic.

The 3D viscosity models appear to have an overall improved fit compared to the 1D model. The 1D model largely overestimated the magnitude of RSL change in the late Holocene and plots below almost of the RSL index points. Only one 3D model has a similar lack of fit to the data: VM_0.3_0.75_0.6_L140, which has the largest viscosity parameters (highest background viscosity in the upper mantle and largest lateral heterogeneity scaling factor in the upper mantle) of all the 3D models used here. Therefore, 3D viscosity models improve the fit with RSL data; however, the viscosity parameters are important to further refine the model. Further, Love et al. (2016) used 35 North American ice complex model reconstructions (here we only used 1 ice model) and 363 different viscosity models to more precisely fit the GIA models to site-specific RSL data on the North American coastline,

suggesting the importance of using a wide array of ice and viscosity models to appropriately fit observed RSL data at a particular location.

6. Conclusion

Glacial isostatic adjustment (GIA) is a significant contributor to late Holocene relative sea-level (RSL) change in the U.S. mid-Atlantic region, including New Jersey, due to its proximity to the margin of the former Laurentide Ice Sheet. Accurate high resolution RSL reconstructions are needed to validate GIA models on the U.S. mid-Atlantic coast. Here, we produced a new high resolution late Holocene RSL reconstruction from a salt marsh in southern New Jersey, a region that experienced maximum rates of RSL rise due to the collapsing peripheral forebulge at the former ice margin. We accounted for sediment compaction by using samples from basal peat units, and used a geotechnical model to incorporate an error for the minimal compaction from a basal peat layer overlying an incompressible substrate. We also accounted for tidal range change by using a paleotidal model and included an error in each data point for past changes in tidal datums. A Bayesian transfer function using salt-marsh foraminifera assemblages and bulk sediment stable carbon isotope geochemistry was used to estimate the paleomarsh elevation at which each sample was formed. Each sample was provided an age through high precision Accelerator Mass Spectrometry (AMS) radiocarbon dating and an age-depth model. We found that RSL rose continuously through the late Holocene by an approximate magnitude of 6.4 m from 4.6 ka BP to 1.2 ka BP at an average rate of 1.9 ± 0.3 mm/yr.

GIA models have improved with the combination of global ice sheet reconstructions, regional ice models, and mantle viscosity models. The misfit between GIA predictions and RSL observations has demonstrated the need for models such as 3D laterally heterogeneous mantle viscosity models to introduce lateral viscosity variations. We compared our new RSL record from southern New Jersey to an ensemble of site-specific 1D and 3D mantle viscosity models. The models use the ice glaciation-deglaciation history from the global ICE-6G_C model. We examined GIA predictions at 1000 year intervals over the last 5000 years and found a misfit between model predictions and RSL observations. The 3D models are an improvement over the 1D model, but the remaining misfits suggest the importance of utilizing a wide array of ice model and viscosity model parameters to find a better fit between site-specific GIA predictions and RSL observations.

Acknowledgements

Author Jennifer Walker thanks Isabel Hong, Kristen Joyse, and Andra Garner for their assistance in the field and thanks the Rutgers University Marine Field Station, Roland Hagan, and Ryan Larum for boat use in the field. JW was funded by the David and Arleen McGlade Foundation and a Cushman Foundation for Foraminiferal Research Student Research Award.

References

Allen, J. R. L. 2000. "Morphodynamics of Holocene Salt Marshes: A Review Sketch from the Atlantic and Southern North Sea Coasts of Europe." Quaternary Science Reviews 19 (12): 1155–1231. https://doi.org/10.1016/S0277-3791(99)00034-7.

Andrews, J. E, A. M Greenaway, and P. F Dennis. 1998. "Combined Carbon Isotope and C/N Ratios as Indicators of Source and Fate of Organic Matter in a Poorly Flushed, Tropical Estuary: Hunts Bay, Kingston Harbour, Jamaica." Estuarine, Coastal and Shelf Science 46 (5): 743–56. https://doi.org/10.1006/ecss.1997.0305.

Argus, Donald F., W. R. Peltier, R. Drummond, and Angelyn W. Moore. 2014. "The Antarctica Component of Postglacial Rebound Model ICE-6G_C (VM5a) Based on GPS Positioning, Exposure Age Dating of Ice Thicknesses, and Relative Sea Level Histories." Geophysical Journal International 198 (1): 537–63. https://doi.org/10.1093/gji/ggu140.

Balslev-Clausen, David, Tais W. Dahl, Nabil Saad, and Minik T. Rosing. 2013. "Precise and Accurate Δ13C Analysis of Rock Samples Using Flash Combustion–Cavity Ring Down Laser Spectroscopy." Journal of Analytical Atomic Spectrometry 28 (4): 516. https://doi.org/10.1039/c2ja30240c.

Barlow, Natasha L.M., Ian Shennan, Antony J. Long, W. Roland Gehrels, Margot H. Saher, Sarah A. Woodroffe, and Caroline Hillier. 2013. "Salt Marshes as Late Holocene Tide Gauges." Global and Planetary Change 106 (July): 90–110. https://doi.org/10.1016/j.gloplacha.2013.03.003.

Barnett, Robert L., Michelle Garneau, and Pascal Bernatchez. 2016. "Salt-Marsh Sea-Level Indicators and Transfer Function Development for the Magdalen Islands in the Gulf of St. Lawrence, Canada." Marine Micropaleontology 122 (January): 13–26. https://doi.org/10.1016/j.marmicro.2015.11.003.

Bloom, Arthur L. 1963. "Late-Pleistocene Fluctuations of Sealevel and Postglacial Crustal Rebound in Coastal Maine." American Journal of Science 261 (9): 862–79. https://doi.org/10.2475/ajs.261.9.862.

———. 1967. "Pleistocene Shorelines: A New Test of Isostasy." GSA Bulletin 78 (12): 1477–94. https://doi.org/10.1130/0016-7606(1967)78[1477:PSANTO]2.0.CO;2.

Brain, Matthew J., Andrew C. Kemp, Benjamin P. Horton, Stephen J. Culver, Andrew C. Parnell, and Niamh Cahill. 2015. "Quantifying the Contribution of Sediment Compaction to Late Holocene Salt-Marsh Sea-Level Reconstructions, North Carolina, USA." Quaternary Research 83 (1): 41–51. https://doi.org/10.1016/j.yqres.2014.08.003.

Brain, Matthew J., Antony J. Long, David N. Petley, Benjamin P. Horton, and Robert J. Allison. 2011. "Compression Behaviour of Minerogenic Low Energy Intertidal

Sediments." Sedimentary Geology 233 (1): 28–41. https://doi.org/10.1016/j.sedgeo.2010.10.005.

Brain, Matthew J., Antony J. Long, Sarah A. Woodroffe, David N. Petley, David G. Milledge, and Andrew C. Parnell. 2012. "Modelling the Effects of Sediment Compaction on Salt Marsh Reconstructions of Recent Sea-Level Rise." Earth and Planetary Science Letters 345–348 (September): 180–93. https://doi.org/10.1016/j.epsl.2012.06.045.

Bratton, John F., Steven M. Colman, E. Robert Thieler, and Robert R. Seal. 2002. "Birth of the Modern Chesapeake Bay Estuary between 7.4 and 8.2 Ka and Implications for Global Sea-Level Rise." Geo-Marine Letters 22 (4): 188–97. https://doi.org/10.1007/s00367-002-0112-z.

Bunge, Hans-Peter, and Stephen P. Grand. 2000. "Mesozoic Plate-Motion History below the Northeast Pacific Ocean from Seismic Images of the Subducted Farallon Slab." Nature 405 (6784): 337. https://doi.org/10.1038/35012586.

Cahill, Niamh, Andrew C. Kemp, Benjamin P. Horton, and Andrew C. Parnell. 2015. "Modeling Sea-Level Change Using Errors-in-Variables Integrated Gaussian Processes." The Annals of Applied Statistics 9 (2): 547–71. https://doi.org/10.1214/15-AOAS824.

———. 2016. "A Bayesian Hierarchical Model for Reconstructing Relative Sea Level: From Raw Data to Rates of Change." Climate of the Past 12 (2): 525–42. https://doi.org/10.5194/cp-12-525-2016.

Chant, R. J., M. C. Curran, K. W. Able, and S. M. Glenn. 2000. "Delivery of Winter Flounder (Pseudopleuronectes Americanus) Larvae to Settlement Habitats in Coves Near Tidal Inlets." Estuarine, Coastal and Shelf Science 51 (5): 529–41. https://doi.org/10.1006/ecss.2000.0694.

Clark, James A., William E. Farrell, and W.Richard Peltier. 1978. "Global Changes in Postglacial Sea Level: A Numerical Calculation." Quaternary Research 9 (3): 265–87. https://doi.org/10.1016/0033-5894(78)90033-9.

Daddario, J.J. 1961. A Lagoon Deposit Profile near Atlantic City, New Jersey. Vol. 6.

Davis, James L., and Jerry X. Mitrovica. 1996. "Glacial Isostatic Adjustment and the Anomalous Tide Gauge Record of Eastern North America." Nature 379 (6563): 331. https://doi.org/10.1038/379331a0.

Dyke, Arthur S, and David J A Evans. 2003. "Ice-Marginal Terrestrial Landsystems: Northern Laurentide and Innuitian Ice Sheet Margins." Glacial Landsystems, 24.

Edwards, R.J., A.J. Wright, and O. van de Plassche. 2004. "Surface Distributions of Salt-Marsh Foraminifera from Connecticut, USA: Modern Analogues for High-

Resolution Sea Level Studies." Marine Micropaleontology 51 (1–2): 1–21. https://doi.org/10.1016/j.marmicro.2003.08.002.

Edwards, Robin J. 2006. "Mid-to Late-Holocene Relative Sea-Level Change in Southwest Britain and the Influence of Sediment Compaction." The Holocene 16 (4): 575–87. https://doi.org/10.1191/0959683606hl941rp.

Ekström, Göran, and Adam M. Dziewonski. 1988. "Evidence of Bias in Estimations of Earthquake Size." Nature 332 (6162): 319. https://doi.org/10.1038/332319a0.

Engelhart, S E, W R Peltier, and B P Horton. 2011. "Holocene Relative Sea-Level Changes and Glacial Isostatic Adjustment of the U.S. Atlantic Coast." Geology, 4.

Engelhart, Simon E., and Benjamin P. Horton. 2012. "Holocene Sea Level Database for the Atlantic Coast of the United States." Quaternary Science Reviews 54 (October): 12–25. https://doi.org/10.1016/j.quascirev.2011.09.013.

Engelhart, Simon E, Benjamin P Horton, Bruce C Douglas, W Richard Peltier, and Torbjörn E Törnqvist. 2009. "Spatial Variability of Late Holocene and 20th Century Sea-Level Rise along the Atlantic Coast of the United States." Geology, 5.

Ezer, Tal. 2016. "Can the Gulf Stream Induce Coherent Short-Term Fluctuations in Sea Level along the US East Coast? A Modeling Study." Ocean Dynamics 66 (2): 207–20. https://doi.org/10.1007/s10236-016-0928-0.

Fatela, F, and R Taborda. 2002. "Confidence Limits of Species Proportions in Microfossil Assemblages." Marine Micropaleontology, 6.

Ferland, Mariel A. 1990. "Holocene Depositional History of the Southern New Jersey Barrier and Backbarrier Regions." CERC-TR-90-2. COASTAL ENGINEERING RESEARCH CENTER VICKSBURG MS. https://apps.dtic.mil/docs/citations/ADA220085.

Field, Michael E., and David B. Duane. 1976. "Post-Pleistocene History of the United States Inner Continental Shelf: Significance to Origin of Barrier Islands." GSA Bulletin 87 (5): 691–702. https://doi.org/10.1130/0016-7606(1976)87<691:PHOTUS>2.0.CO;2.

Gehrels, Roland. 2010. "Sea-Level Changes since the Last Glacial Maximum: An Appraisal of the IPCC Fourth Assessment Report." Journal of Quaternary Science 25 (1): 26–38. https://doi.org/10.1002/jqs.1273.

Gehrels, W. R. 1994. "Determining Relative Sea-Level Change from Salt-Marsh Foraminifera and Plant Zones on the Coast of Maine, U.S.A." Journal of Coastal Research 10 (4): 21.

Gehrels, W. Roland. 2000. "Using Foraminiferal Transfer Functions to Produce High-Resolution Sea-Level Records from Salt-Marsh Deposits, Maine, USA." The Holocene 10 (3): 367–76. https://doi.org/10.1191/095968300670746884.

Gehrels, W.Roland. 1999. “Middle and Late Holocene Sea-Level Changes in Eastern Maine Reconstructed from Foraminiferal Saltmarsh Stratigraphy and AMS 14 C Dates on Basal Peat.” Quaternary Research 52 (3): 350–59. https://doi.org/10.1006/qres.1999.2076.

Gehrels, W.Roland, Daniel F. Belknap, Bryan R. Pearce, and Bin Gong. 1995. “Modeling the Contribution of M2 Tidal Amplification to the Holocene Rise of Mean High Water in the Gulf of Maine and the Bay of Fundy.” Marine Geology 124 (1–4): 71–85. https://doi.org/10.1016/0025-3227(95)00033-U.

González, Juan L., and Torbjörn E. Törnqvist. 2009. “A New Late Holocene Sea-Level Record from the Mississippi Delta: Evidence for a Climate/Sea Level Connection?” Quaternary Science Reviews, Quaternary Ice Sheet-Ocean Interactions and Landscape Responses, 28 (17): 1737–49. https://doi.org/10.1016/j.quascirev.2009.04.003.

Griffiths, Stephen D., and W. R. Peltier. 2008. “Megatides in the Arctic Ocean under Glacial Conditions.” Geophysical Research Letters 35 (8). https://doi.org/10.1029/2008GL033263.

Griffiths, Stephen D., and W. Richard Peltier. 2009. “Modeling of Polar Ocean Tides at the Last Glacial Maximum: Amplification, Sensitivity, and Climatological Implications.” Journal of Climate 22 (11): 2905–24. https://doi.org/10.1175/2008JCLI2540.1.

Hawkes, Andrea D., Andrew C. Kemp, Jeffrey P. Donnelly, Benjamin P. Horton, W. Richard Peltier, Niamh Cahill, David F. Hill, Erica Ashe, and Clark R. Alexander. 2016. “Relative Sea-Level Change in Northeastern Florida (USA) during the Last ~8.0 Ka.” Quaternary Science Reviews 142 (June): 90–101. https://doi.org/10.1016/j.quascirev.2016.04.016.

Head, K.H. 1988. Manual of Soil Laboratory Testing: Permeability, Shear Strength and Compressibility Tests. London/Plymouth: Pentech Press.

Hill, D. F., S. D. Griffiths, W. R. Peltier, B. P. Horton, and T. E. Törnqvist. 2011. “High-Resolution Numerical Modeling of Tides in the Western Atlantic, Gulf of Mexico, and Caribbean Sea during the Holocene.” Journal of Geophysical Research 116 (C10). https://doi.org/10.1029/2010JC006896.

Horton, B. P., R. J. Edwards, and J. M. Lloyd. 1999. “A Foraminiferal-Based Transfer Function: Implications for Sea-Level Studies.” Journal of Foraminiferal Research 29 (2): 117–29. https://doi.org/10.2113/gsjfr.29.2.117.

Horton, B. P., and I. Shennan. 2009. “Compaction of Holocene Strata and the Implications for Relative Sealevel Change on the East Coast of England.” Geology 37 (12): 1083–86. https://doi.org/10.1130/G30042A.1.

Horton, Benjamin P., and Stephen J. Culver. 2008. "Modern Intertidal Foraminifera of the Outer Banks, North Carolina, U.S.A., and Their Applicability for Sea-Level Studies." Journal of Coastal Research 245 (September): 1110–25. https://doi.org/10.2112/08A-0004.1.

Horton, Benjamin P, and Robin J Edwards. 2006. "Quantifying Holocene Sea Level Change Using Intertidal Foraminifera: Lessons from the British Isles." Cushman Foundation for Foraminiferal Research Special Publication 40: 100.

Horton, Benjamin P., Simon E. Engelhart, David F. Hill, Andrew C. Kemp, Daria Nikitina, Kenneth G. Miller, and W. Richard Peltier. 2013. "Influence of Tidal-Range Change and Sediment Compaction on Holocene Relative Sea-Level Change in New Jersey, USA: Influence of Tidal-Range Change and Sediment Compaction." Journal of Quaternary Science 28 (4): 403–11. https://doi.org/10.1002/jqs.2634.

Horton, B.P., W.R. Peltier, S.J. Culver, R. Drummond, S.E. Engelhart, A.C. Kemp, D. Mallinson, et al. 2009. "Holocene Sea-Level Changes along the North Carolina Coastline and Their Implications for Glacial Isostatic Adjustment Models." Quaternary Science Reviews 28 (17–18): 1725–36. https://doi.org/10.1016/j.quascirev.2009.02.002.

Inman, D. L., and C. E. Nordstrom. 1971. "On the Tectonic and Morphologic Classification of Coasts." The Journal of Geology 79 (1): 1–21. https://doi.org/10.1086/627583.

Jackson, Ian. 2000. The Earth's Mantle: Composition, Structure, and Evolution. Cambridge University Press.

Jansen, E, J Overpeck, KR Briffa, JC Duplessy, F Joos, Valerie Masson-Delmotte, D Olago, et al. 2007. "Palaeoclimate." In Climate Change 2007: The Physical Science Basis. Contribution of Working Group I to the Fourth Assessment Report of the Intergovernmental Panel on Climate Change, 433–97. Cambridge, UK: Cambridge University Press.

Johnson, Beverly J., Karen A. Moore, Charlotte Lehmann, Curtis Bohlen, and Thomas A. Brown. 2007. "Middle to Late Holocene Fluctuations of C3 and C4 Vegetation in a Northern New England Salt Marsh, Sprague Marsh, Phippsburg Maine." Organic Geochemistry 38 (3): 394–403. https://doi.org/10.1016/j.orggeochem.2006.06.006.

Johnson, Christopher S., Kenneth G. Miller, James V. Browning, Robert E. Kopp, Nicole S. Khan, Ying Fan, Scott D. Stanford, and Benjamin P. Horton. 2018. "The Role of Sediment Compaction and Groundwater Withdrawal in Local Sea-Level Rise, Sandy Hook, New Jersey, USA." Quaternary Science Reviews 181 (February): 30–42. https://doi.org/10.1016/j.quascirev.2017.11.031.

Juggins, Steve, and H. John B. Birks. 2012. "Quantitative Environmental Reconstructions from Biological Data." In Tracking Environmental Change Using Lake Sediments:

Data Handling and Numerical Techniques, edited by H. John B. Birks, André F. Lotter, Steve Juggins, and John P. Smol, 431–94. Developments in Paleoenvironmental Research. Dordrecht: Springer Netherlands. https://doi.org/10.1007/978-94-007-2745-8_14.

Kaufmann, Georg, Patrick Wu, and Erik R. Ivins. 2005. "Lateral Viscosity Variations beneath Antarctica and Their Implications on Regional Rebound Motions and Seismotectonics." Journal of Geodynamics 39 (2): 165–81. https://doi.org/10.1016/j.jog.2004.08.009.

Kemp, Andrew C., Christopher E. Bernhardt, Benjamin P. Horton, Robert E. Kopp, Christopher H. Vane, W. Richard Peltier, Andrea D. Hawkes, Jeffrey P. Donnelly, Andrew C. Parnell, and Niamh Cahill. 2014. "Late Holocene Sea- and Land-Level Change on the U.S. Southeastern Atlantic Coast." Marine Geology 357 (November): 90–100. https://doi.org/10.1016/j.margeo.2014.07.010.

Kemp, Andrew C, Troy D Hill, Christopher H Vane, Niamh Cahill, Philip M Orton, Stefan A Talke, Andrew C Parnell, Kelsey Sanborn, and Ellen K Hartig. 2017. "Relative Sea-Level Trends in New York City during the Past 1500 Years." The Holocene 27 (8): 1169–86. https://doi.org/10.1177/0959683616683263.

Kemp, Andrew C., Benjamin P. Horton, and Stephen J. Culver. 2009. "Distribution of Modern Salt-Marsh Foraminifera in the Albemarle–Pamlico Estuarine System of North Carolina, USA: Implications for Sea-Level Research." Marine Micropaleontology 72 (3–4): 222–38. https://doi.org/10.1016/j.marmicro.2009.06.002.

Kemp, Andrew C., Benjamin P. Horton, Christopher H. Vane, Christopher E. Bernhardt, D. Reide Corbett, Simon E. Engelhart, Shimon C. Anisfeld, Andrew C. Parnell, and Niamh Cahill. 2013. "Sea-Level Change during the Last 2500 Years in New Jersey, USA." Quaternary Science Reviews 81 (December): 90–104. https://doi.org/10.1016/j.quascirev.2013.09.024.

Kemp, Andrew C., Jessica J. Kegel, Stephen J. Culver, Donald C. Barber, David J. Mallinson, Eduardo Leorri, Christopher E. Bernhardt, et al. 2017. "Extended Late Holocene Relative Sea-Level Histories for North Carolina, USA." Quaternary Science Reviews 160 (March): 13–30. https://doi.org/10.1016/j.quascirev.2017.01.012.

Kemp, Andrew C., and Richard J. Telford. 2015. "Transfer Functions." In Handbook of Sea-Level Research, edited by Ian Shennan, Antony J. Long, and Benjamin P. Horton, 470–99. Chichester, UK: John Wiley & Sons, Ltd. https://doi.org/10.1002/9781118452547.ch31.

Kemp, Andrew C., Christopher H. Vane, Benjamin P. Horton, Simon E. Engelhart, and Daria Nikitina. 2012. "Application of Stable Carbon Isotopes for Reconstructing

Salt-Marsh Floral Zones and Relative Sea Level, New Jersey, USA." Journal of Quaternary Science 27 (4): 404–14. https://doi.org/10.1002/jqs.1561.

Kemp, Andrew C., Alexander J. Wright, Robin J. Edwards, Robert L. Barnett, Matthew J. Brain, Robert E. Kopp, Niamh Cahill, et al. 2018. "Relative Sea-Level Change in Newfoundland, Canada during the Past ∼3000 Years." Quaternary Science Reviews 201 (December): 89–110. https://doi.org/10.1016/j.quascirev.2018.10.012.

Kominz, Michelle A., Kenneth G. Miller, and James V. Browning. 1998. "Long-Term and Short-Term Global Cenozoic Sea-Level Estimates." Geology 26 (4): 311–14. https://doi.org/10.1130/0091-7613(1998)026<0311:LTASTG>2.3.CO;2.

Kopp, Robert E., Radley M. Horton, Christopher M. Little, Jerry X. Mitrovica, Michael Oppenheimer, D. J. Rasmussen, Benjamin H. Strauss, and Claudia Tebaldi. 2014. "Probabilistic 21st and 22nd Century Sea-Level Projections at a Global Network of Tide-Gauge Sites: KOPP ET AL." Earth's Future 2 (8): 383–406. https://doi.org/10.1002/2014EF000239.

Lamb, Angela L., Graham P. Wilson, and Melanie J. Leng. 2006. "A Review of Coastal Palaeoclimate and Relative Sea-Level Reconstructions Using Δ13C and C/N Ratios in Organic Material." Earth-Science Reviews 75 (1–4): 29–57. https://doi.org/10.1016/j.earscirev.2005.10.003.

Lambeck, K., H. Rouby, A. Purcell, Y. Sun, and M. Sambridge. 2014. "Sea Level and Global Ice Volumes from the Last Glacial Maximum to the Holocene." Proceedings of the National Academy of Sciences 111 (43): 15296–303. https://doi.org/10.1073/pnas.1411762111.

Lambeck, Kurt, and Edouard Bard. 2000. "Sea-Level Change along the French Mediterranean Coast for the Past 30 000 Years." Earth and Planetary Science Letters 175 (3): 203–22. https://doi.org/10.1016/S0012-821X(99)00289-7.

Lambeck, Kurt, Hélène Rouby, Anthony Purcell, Yiying Sun, and Malcolm Sambridge. 2014. "Sea Level and Global Ice Volumes from the Last Glacial Maximum to the Holocene." Proceedings of the National Academy of Sciences 111 (43): 15296–303. https://doi.org/10.1073/pnas.1411762111.

Levermann, Anders, Alexa Griesel, Matthias Hofmann, Marisa Montoya, and Stefan Rahmstorf. 2005. "Dynamic Sea Level Changes Following Changes in the Thermohaline Circulation." Climate Dynamics 24 (4): 347–54. https://doi.org/10.1007/s00382-004-0505-y.

Li, Tanghua, and Patrick Wu. 2019. "Laterally Heterogeneous Lithosphere, Asthenosphere and Sub-Lithospheric Properties under Laurentia and Fennoscandia from Glacial Isostatic Adjustment." Geophysical Journal International 216 (3): 1633–47. https://doi.org/10.1093/gji/ggy475.

Li, Tanghua, Patrick Wu, Holger Steffen, and Hansheng Wang. 2018. “In Search of Laterally Heterogeneous Viscosity Models of Glacial Isostatic Adjustment with the ICE-6G_C Global Ice History Model.” Geophysical Journal International 214 (2): 1191–1205. https://doi.org/10.1093/gji/ggy181.

Lloyd, Jeremy. 2000. “Combined Foraminiferal and Thecamoebian Environmental Reconstruction from an Isolation Basin in NW Scotland: Implications for Sea-Level Studies.” Journal of Foraminiferal Research 30 (4): 294–305. https://doi.org/10.2113/0300294.

Long, A.J., M.P. Waller, and P. Stupples. 2006. “Driving Mechanisms of Coastal Change: Peat Compaction and the Destruction of Late Holocene Coastal Wetlands.” Marine Geology 225 (1–4): 63–84. https://doi.org/10.1016/j.margeo.2005.09.004.

Long, Antony J., David H. Roberts, and Morten Rasch. 2003. “New Observations on the Relative Sea Level and Deglacial History of Greenland from Innaarsuit, Disko Bugt.” Quaternary Research 60 (2): 162–71. https://doi.org/10.1016/S0033-5894(03)00085-1.

Love, Ryan, Glenn A. Milne, Lev Tarasov, Simon E. Engelhart, Marc P. Hijma, Konstantin Latychev, Benjamin P. Horton, and Torbjörn E. Törnqvist. 2016. “The Contribution of Glacial Isostatic Adjustment to Projections of Sea-Level Change along the Atlantic and Gulf Coasts of North America: GIA AND FUTURE SEA-LEVEL CHANGE.” Earth’s Future 4 (10): 440–64. https://doi.org/10.1002/2016EF000363.

Luettich, Richard A., and Joannes J. Westerink. 1991. “A Solution for the Vertical Variation of Stress, Rather than Velocity, in a Three-Dimensional Circulation Model.” International Journal for Numerical Methods in Fluids 12 (10): 911–28. https://doi.org/10.1002/fld.1650121002.

McKee, Karen L., and W. H. Patrick. 1988. “The Relationship of Smooth Cordgrass (Spartina Alterniflora) to Tidal Datums: A Review.” Estuaries 11 (3): 143–51. https://doi.org/10.2307/1351966.

Middelburg, J.J., J. Nieuwenhuize, R.K. Lubberts, and O. van de Plassche. 1997. “Organic Carbon Isotope Systematics of Coastal Marshes.” Estuarine, Coastal and Shelf Science 45 (5): 681–87. https://doi.org/10.1006/ecss.1997.0247.

Mikkelsen, Naja, Antoon Kuijpers, and Jette Arneborg. 2008. “The Norse in Greenland and Late Holocene Sea-Level Change.” Polar Record 44 (1): 45–50. https://doi.org/10.1017/S0032247407006948.

Miller, Kenneth G., Robert E. Kopp, Benjamin P. Horton, James V. Browning, and Andrew C. Kemp. 2013. “A Geological Perspective on Sea-Level Rise and Its Impacts along the U.S. Mid-Atlantic Coast.” Earth’s Future 1 (1): 3–18. https://doi.org/10.1002/2013EF000135.

Miller, Kenneth G., Peter J. Sugarman, James V. Browning, Benjamin P. Horton, Alissa Stanley, Alicia Kahn, Jane Uptegrove, and Michael Aucott. 2009. "Sea-Level Rise in New Jersey over the Past 5000 Years: Implications to Anthropogenic Changes." Global and Planetary Change 66 (1–2): 10–18. https://doi.org/10.1016/j.gloplacha.2008.03.008.

Mitrovica, Jerry X., and Alessandro M. Forte. 1997. "Radial Profile of Mantle Viscosity: Results from the Joint Inversion of Convection and Postglacial Rebound Observables." Journal of Geophysical Research: Solid Earth 102 (B2): 2751–69. https://doi.org/10.1029/96JB03175.

Mofjeld, Harold O., Angie J. Venturato, Frank I. González, Vasily V. Titov, and Jean C. Newman. 2004. "The Harmonic Constant Datum Method: Options for Overcoming Datum Discontinuities at Mixed–Diurnal Tidal Transitions." Journal of Atmospheric and Oceanic Technology 21 (1): 95–104. https://doi.org/10.1175/1520-0426(2004)021<0095:THCDMO>2.0.CO;2.

Nakada, M., and K. Lambeck. 1988. "The Melting History of the Late Pleistocene Antarctic Ice Sheet." Nature 333 (6168): 36. https://doi.org/10.1038/333036a0.

Nikitina, Daria L., James E. Pizzuto, Ronald E. Martin, and Scott P. Hippensteel. 2003. "Transgressive Valley-Fill Stratigraphy and Sea-Level History of the Leipsic River, Bombay Hook National Wildlife Refuge, Delaware, U.S.A." Special Publications of SEPM. http://archives.datapages.com/data/sepm_sp/SP75/Transgressive_Valley-Fill_Stratigraphy.htm.

Peltier, W. R. 1998. "The Inverse Problem for Mantle Viscosity." Inverse Problems 14 (3): 441–478. https://doi.org/10.1088/0266-5611/14/3/006.

———. 2002. "On Eustatic Sea Level History: Last Glacial Maximum to Holocene." Quaternary Science Reviews, EPILOG, 21 (1): 377–96. https://doi.org/10.1016/S0277-3791(01)00084-1.

Peltier, W. R., D. F. Argus, and R. Drummond. 2015. "Space Geodesy Constrains Ice Age Terminal Deglaciation: The Global ICE-6G_C (VM5a) Model." Journal of Geophysical Research: Solid Earth 120 (1): 450–87. https://doi.org/10.1002/2014JB011176.

Peltier, W. R., and Rosemarie Drummond. 2008. "Rheological Stratification of the Lithosphere: A Direct Inference Based upon the Geodetically Observed Pattern of the Glacial Isostatic Adjustment of the North American Continent." Geophysical Research Letters 35 (16). https://doi.org/10.1029/2008GL034586.

Peltier, W.R. 2004. "Global Glacial Isostasy and the Surface of the Ice-Age Earth: The ICE-5G (VM2) Model and GRACE." Annual Review of Earth and Planetary Sciences 32 (1): 111–49. https://doi.org/10.1146/annurev.earth.32.082503.144359.

Plassche, O. van de, ed. 1986. Sea-Level Research: A Manual for the Collection and Evaluation of Data: A Manual for the Collection and Evaluation of Data. Springer Netherlands. https://www.springer.com/gp/book/9789401083706.

———. 1991. “Late Holocene Sea-Level Fluctuations on the Shore of Connecticut Inferred from Transgressive and Regressive Overlap Boundaries in Salt-Marsh Deposits.” Journal of Coastal Research, 159–79.

Plater, Andrew J., Jason R. Kirby, John F. Boyle, Timothy Shaw, and Hayley Mills. 2015. “Loss on Ignition and Organic Content.” In Handbook of Sea-Level Research. John Wiley & Sons.

Psuty, Norbert P. 1986. “Holocene Sea Level in New Jersey.” Physical Geography 7 (2): 156–67. https://doi.org/10.1080/02723646.1986.10642288.

Reimer, PJ, E Bard, and A Bayliss. 2013. “IntCal13 and Marine13 Radiocarbon Age Calibration Curves 0-50,000 Years Cal BP.” Radiocarbon 55: 1869–87.

Robinson, Marci M., and Randolph A. McBride. 2006. “Benthic Foraminifera from a Relict Flood Tidal Delta along the Virginia/North Carolina Outer Banks.” Micropaleontology 52 (1): 67–80. https://doi.org/10.2113/gsmicropal.52.1.67.

Roe, Helen M., Dan J. Charman, and W. Roland Gehrels. 2002. “Fossil Testate Amoebae in Coastal Deposits in the UK: Implications for Studies of Sea-Level Change.” Journal of Quaternary Science 17 (5–6): 411–29. https://doi.org/10.1002/jqs.704.

Roy, Keven, and W. R. Peltier. 2017. “Space-Geodetic and Water Level Gauge Constraints on Continental Uplift and Tilting over North America: Regional Convergence of the ICE-6G_C (VM5a/VM6) Models.” Geophysical Journal International 210 (2): 1115–42. https://doi.org/10.1093/gji/ggx156.

Roy, Keven, and W.R. Peltier. 2015. “Glacial Isostatic Adjustment, Relative Sea Level History and Mantle Viscosity: Reconciling Relative Sea Level Model Predictions for the U.S. East Coast with Geological Constraints.” Geophysical Journal International 201 (2): 1156–81. https://doi.org/10.1093/gji/ggv066.

Scott, D. B., and J. O. R. Hermelin. 1993. “A Device for Precision Splitting of Micropaleontological Samples in Liquid Suspension.” Journal of Paleontology 67 (1): 151–54. https://doi.org/10.1017/S0022336000021302.

Scott, D. S., and F. S. Medioli. 1978. “Vertical Zonations of Marsh Foraminifera as Accurate Indicators of Former Sea-Levels.” Nature 272 (5653): 528. https://doi.org/10.1038/272528a0.

———. 1980. “Quantitative Studies of Marsh Foraminiferal Distributions in Nova Scotia : Implications for Sea Level Studies.” Special Publication Cushman Foundation for Foraminiferal Research 17.

Scott, David B., Franco S. Medioli, and Charles T. Schafer. 2001. Monitoring in Coastal Environments Using Foraminifera and Thecamoebian Indicators. Cambridge University Press.

Shennan, I, T Coulthard, R Flather, B Horton, M Macklin, J Rees, and M Wright. 2003. "Integration of Shelf Evolution and River Basin Models to Simulate Holocene Sediment Dynamics of the Humber Estuary during Periods of Sea-Level Change and Variations in Catchment Sediment Supply." The Science of The Total Environment 314–316 (October): 737–54. https://doi.org/10.1016/S0048-9697(03)00081-0.

Shennan, Ian. 1986. "Flandrian Sea-Level Changes in the Fenland. II: Tendencies of Sea-Level Movement, Altitudinal Changes, and Local and Regional Factors." Journal of Quaternary Science 1 (2): 155–79. https://doi.org/10.1002/jqs.3390010205.

———. 1989. "Holocene Crustal Movements and Sea-Level Changes in Great Britain." Journal of Quaternary Science 4 (1): 77–89. https://doi.org/10.1002/jqs.3390040109.

Shennan, Ian, and Ben Horton. 2002. "Holocene Land- and Sea-Level Changes in Great Britain." Journal of Quaternary Science 17 (5–6): 511–26. https://doi.org/10.1002/jqs.710.

Sparrenbom, Charlotte J., Ole Bennike, Svante Björck, and Kurt Lambeck. 2006. "Holocene Relative Sea-Level Changes in the Qaqortoq Area, Southern Greenland." Boreas 35 (2): 171–87. https://doi.org/10.1111/j.1502-3885.2006.tb01148.x.

Spencer, Randall S. 2000. "Foraminiferal Assemblages from a Virginia Salt Marsh, Phillips Creek, Virginia." Journal of Foraminiferal Research 30 (2): 143–55. https://doi.org/10.2113/0300143.

Steffen, Holger, Georg Kaufmann, and Patrick Wu. 2006. "Three-Dimensional Finite-Element Modeling of the Glacial Isostatic Adjustment in Fennoscandia." Earth and Planetary Science Letters 250 (1): 358–75. https://doi.org/10.1016/j.epsl.2006.08.003.

Stuckey, Irene H. (Irene Hawkins), and Lisa L Gould. 2000. Coastal Plants from Cape Cod to Cape Canaveral. University of North Carolina Press. http://agris.fao.org/agris-search/search.do?recordID=US201300057076.

Sykes, Lynn R., John G. Armbruster, Won-Young Kim, and Leonardo Seeber. 2008. "Observations and Tectonic Setting of Historic and Instrumentally Located Earthquakes in the Greater New York City–Philadelphia AreaObservations and Tectonic Setting of Historic and Instrumentally Located Earthquakes." Bulletin of the Seismological Society of America 98 (4): 1696–1719. https://doi.org/10.1785/0120070167.

Törnqvist, Torbjörn E., Davin J. Wallace, Joep E. A. Storms, Jakob Wallinga, Remke L. van Dam, Martijn Blaauw, Mayke S. Derksen, Cornelis J. W. Klerks, Camiel Meijneken, and Els M. A. Snijders. 2008. "Mississippi Delta Subsidence Primarily

Caused by Compaction of Holocene Strata." Nature Geoscience 1 (3): 173–76. https://doi.org/10.1038/ngeo129.

Troels-Smith, J. 19550000. "Characterization of unconsolidated sediments." https://www.bcin.ca/bcin/detail.app?id=22215&wbdisable=true.

Wright, Alexander J., Robin J. Edwards, and Orson van de Plassche. 2011. "Reassessing Transfer-Function Performance in Sea-Level Reconstruction Based on Benthic Salt-Marsh Foraminifera from the Atlantic Coast of NE North America." Marine Micropaleontology 81 (1–2): 43–62. https://doi.org/10.1016/j.marmicro.2011.07.003.

Wu, Patrick. 2005. "Effects of Lateral Variations in Lithospheric Thickness and Mantle Viscosity on Glacially Induced Surface Motion in Laurentia." Earth and Planetary Science Letters 235 (3): 549–63. https://doi.org/10.1016/j.epsl.2005.04.038.

Wu, Patrick, Hansheng Wang, and Holger Steffen. 2013. "The Role of Thermal Effect on Mantle Seismic Anomalies under Laurentia and Fennoscandia from Observations of Glacial Isostatic Adjustment." Geophysical Journal International 192 (1): 7–17. https://doi.org/10.1093/gji/ggs009.

Yang, Z., E.P. Myers, A. Wong, and S. White. 2008. "Vdatum for Chesapeake Bay, Delaware Bay, and Adjacent Coastal Water Areas: Tidal Datums and Sea Surface Topography." NOAA Technical Memorandum NOS CS 15. U.S. Department of Commerce, National Oceanic and Atmospheric Administration.

Tables and Figures

Table 1. Reported radiocarbon ages and uncertainties from Edwin B. Forsythe National Wildlife Refuge cores with calibrated ages using the IntCal13 dataset. OS samples analyzed by NOSAMS; Beta samples analyzed by Beta Analytic.

Core	Depth (cm)	Lab Sample ID	Radiocarbon Age (14C years)	Radiocarbon Error (14C years)	Calibrated Age (cal yrs. BP; 2 sigma range)
EF20	170	OS-135969	1050	15	930-972
EF20	175	OS-135970	1060	20	929-1048
EF20	177	Beta-516335	980	30	796-956
EF20	185	OS-135371	1310	15	1186-1288
EF20	195	OS-135971	1400	20	1289-1338
EF18	216	Beta-516340	1540	30	1365-1524
EF18	220	OS-138254	1610	20	1415-1554
EF18	226	OS-138258	1600	20	1414-1544
EF18	235	OS-138362	1640	25	1418-1610
EF17	227	OS-138057	1070	45	915-1168
EF17	238	Beta-516336	1610	30	1415-1554
EF17	251	OS-138252	1700	20	1552-1692
EF17	260	Beta-516337	1660	30	1422-1689
EF17	269	OS-138253	1770	20	1612-1736
EF16	281	OS-138361	1720	20	1563-1697
EF16	298	OS-138251	1880	20	1737-1878
EF16	307	Beta-516334	1790	30	1620-1817
EF16	314	OS-135372	2930	25	2993-3165
EF16	322	OS-138079	1840	15	1721-1821
EF15	349	OS-137895	1970	20	1876-1986
EF15	364	OS-137938	2240	20	2158-2332
EF15	368	Beta-516341	2310	30	2185-2359
EF15	374	OS-137939	2240	20	2158-2332
EF15	384	OS-137940	2190	30	2128-2310
EF13	384	OS-137945	2330	20	2330-2357
EF13	396	OS-138148	2240	25	2156-2336
EF13	411	OS-138074	2360	20	2340-2433
EF13	428	OS-138075	2530	20	2501-2742
EF13	446	OS-138076	2600	15	2735-2756
EF12	432	OS-137898	2460	20	2379-2705
EF12	454	OS-137896	2520	25	2494-2741
EF12	463	Beta-516324	2680	30	2751-2845
EF12	466	OS-137897	2850	20	2879-3055
EF12	492	OS-137899	2910	25	2963-3155
EF7	478	OS-137784	3350	25	3485-3684
EF7	486	Beta-516338	2850	30	2876-3059
EF7	500	OS-137785	3060	20	3212-3348
EF7	504	Beta-516339	2910	30	2961-3157
EF7	514	OS-137786	2990	20	3077-3228
EF7	545	OS-137787	3020	20	3158-3330
EF10	523	Beta-516333	2900	30	2953-3156
EF10	531	OS-137788	2950	20	3007-3174
EF10	544	OS-137789	2960	25	3008-3210
EF10	555	OS-137791	3050	15	3185-3341
EF10	570	OS-137790	3090	20	3241-3364
EF11	582	OS-138359	3040	30	3165-3345
EF11	609	OS-138077	3250	20	3403-3558
EF11	625	OS-138360	3550	30	3721-3956
EF11	633	Beta-516330	3490	30	3649-3842
EF11	645	OS-138078	3540	25	3722-3896
EF9	609	Beta-516331	3060	30	3181-3359
EF9	649	OS-135374	3320	25	3476-3630
EF9	657	Beta-516332	3640	30	3869-4081
EF9	666	OS-138168	3720	25	3984-4147
EF9	679	OS-138169	3580	20	3834-3961
EF14	688	Beta-516329	3700	30	3930-4147
EF14	695	OS-138162	3630	20	3877-4062
EF14	712	OS-138163	3810	20	4098-4282
EF14	732	OS-138164	3860	25	4160-4409
EF14	746	OS-138165	3870	25	4183-4412
EF14	765	OS-138166	3910	25	4254-4420
EF8	746	Beta-516325	3790	30	4084-4285
EF8	763	OS-137941	3850	20	4157-4405
EF8	775	OS-137942	3950	25	4296-4515
EF8	794	OS-137943	4060	25	4439-4784
EF8	805	OS-137944	4150	25	4582-4823
EF5	800	OS-137900	3820	25	4097-4348
EF5	811	Beta-516328	3800	30	4088-4287
EF5	824	OS-135375	4100	25	4523-4808
EF5	830	OS-137901	4070	35	4438-4805

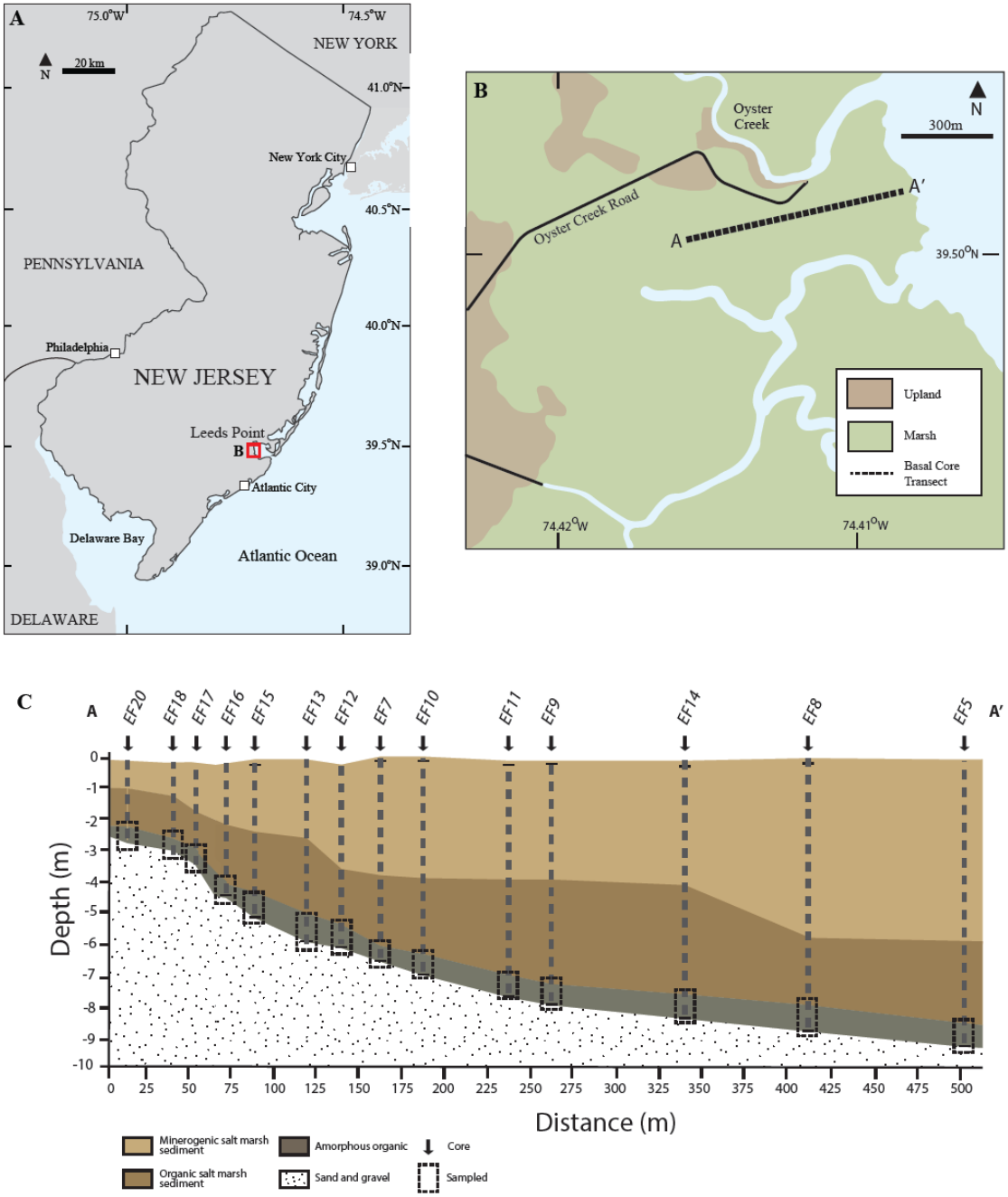

Figure 1. (A) Location of Leeds Point at Edwin B. Forsythe National Wildlife Refuge in southern New Jersey off of Great Bay. (B) Salt-marsh study site showing basal core transect location. (C) Stratigraphy at salt-marsh study site with location of sediment cores and sampled basal unit of each core.

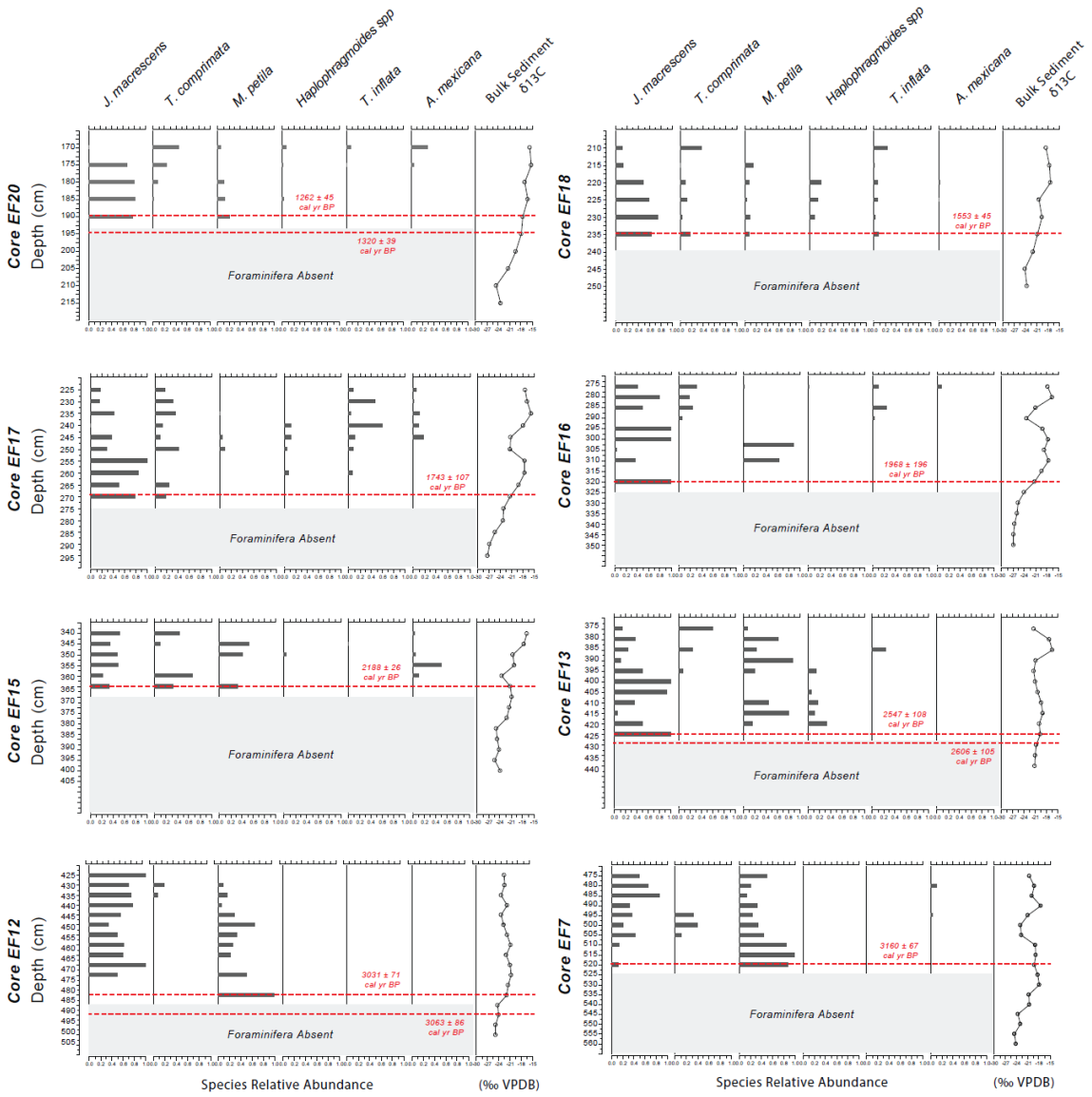

(caption on following page)

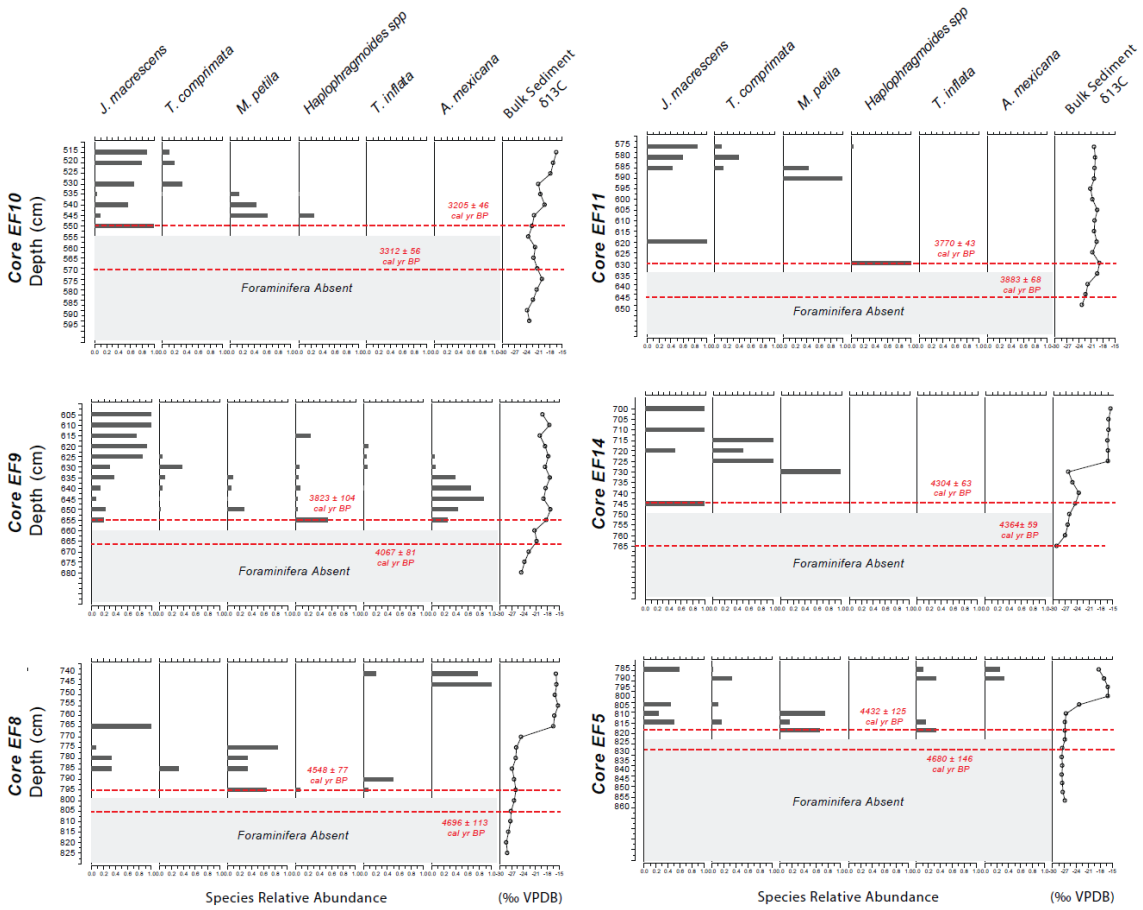

Figure 2. Foraminifera and $\delta^{13}C$ in the 14 basal sediment cores from Edwin B. Forsythe National Wildlife Refuge. Only the six most abundant foraminifera species are shown here. Red dashed lines indicate depth and calibrated radiocarbon ages of sea-level index points and limiting points.

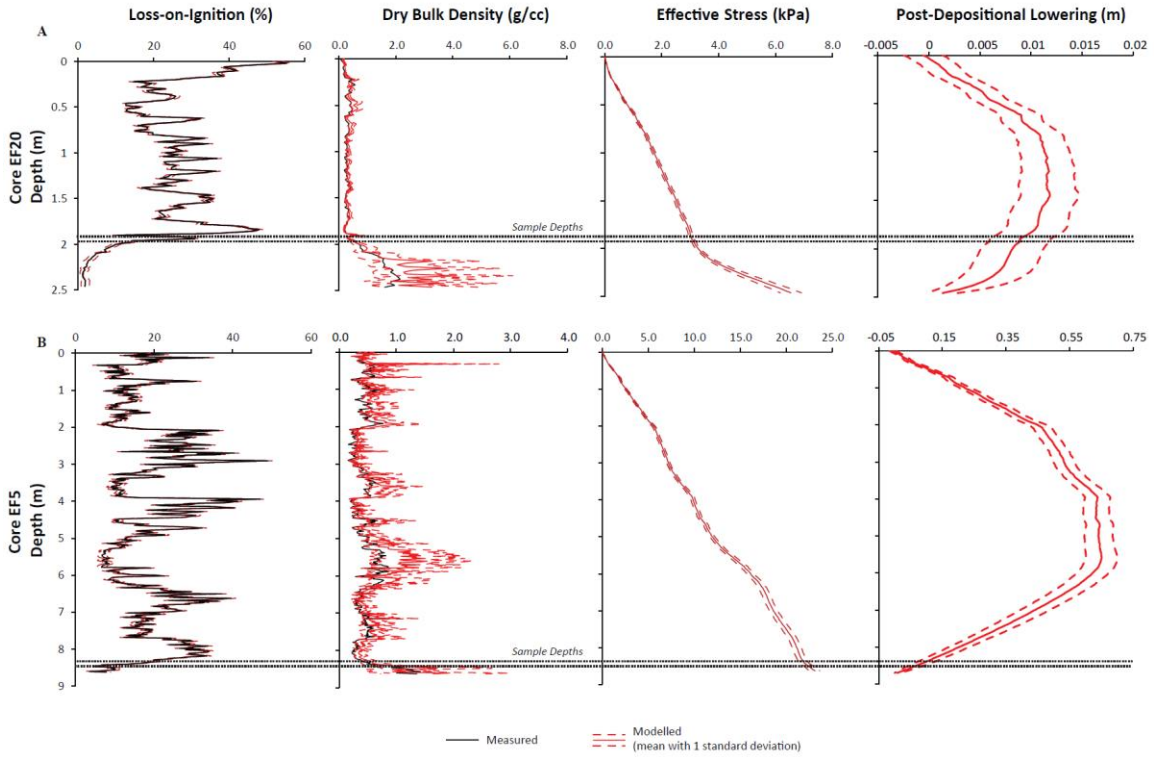

Figure 3. Estimation of post-depositional lowering caused by sediment compaction. (A) Measured and modeled loss-on-ignition and dry bulk density and modeled effective stress and post-depositional lowering predicted by the geotechnical model for the shortest sediment core (EF20). Black dashed lines indicate depth of samples. (B) Measured and modeled loss-on-ignition and dry bulk density and modeled effective stress and post-depositional lowering predicted by the geotechnical model for the longest sediment core (EF5). Black dashed lines indicate depth of samples.

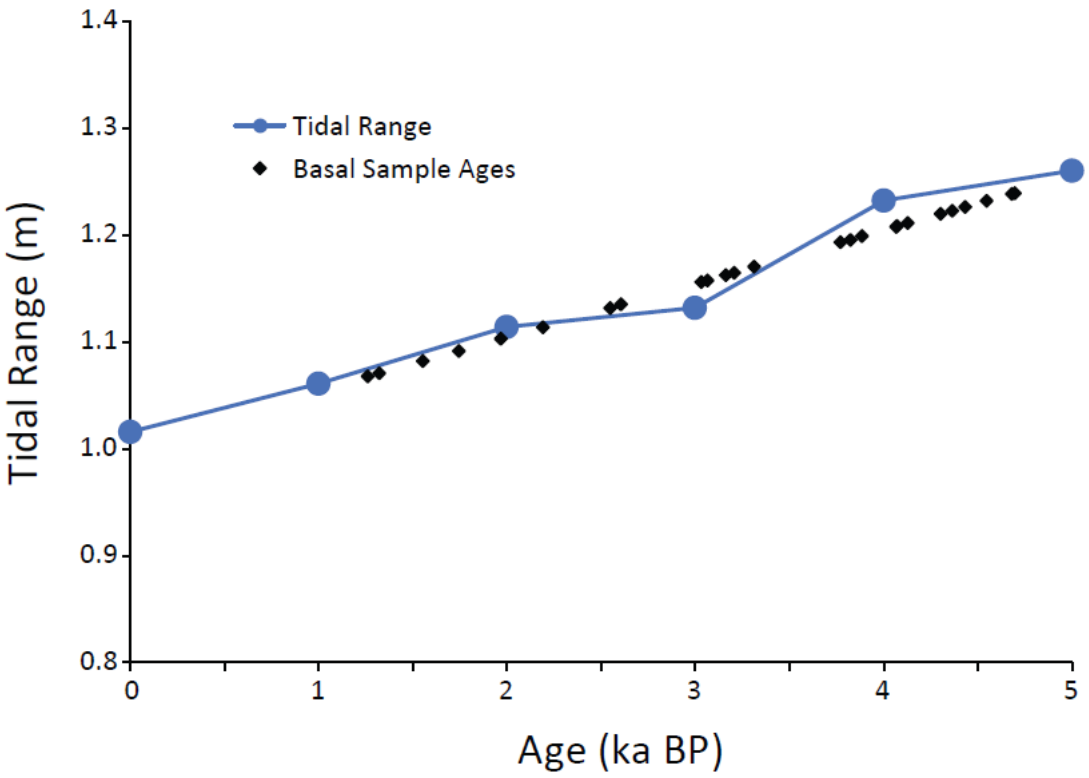

Figure 4. Tidal range change during the late Holocene from the paleotidal model with samples used in this study.

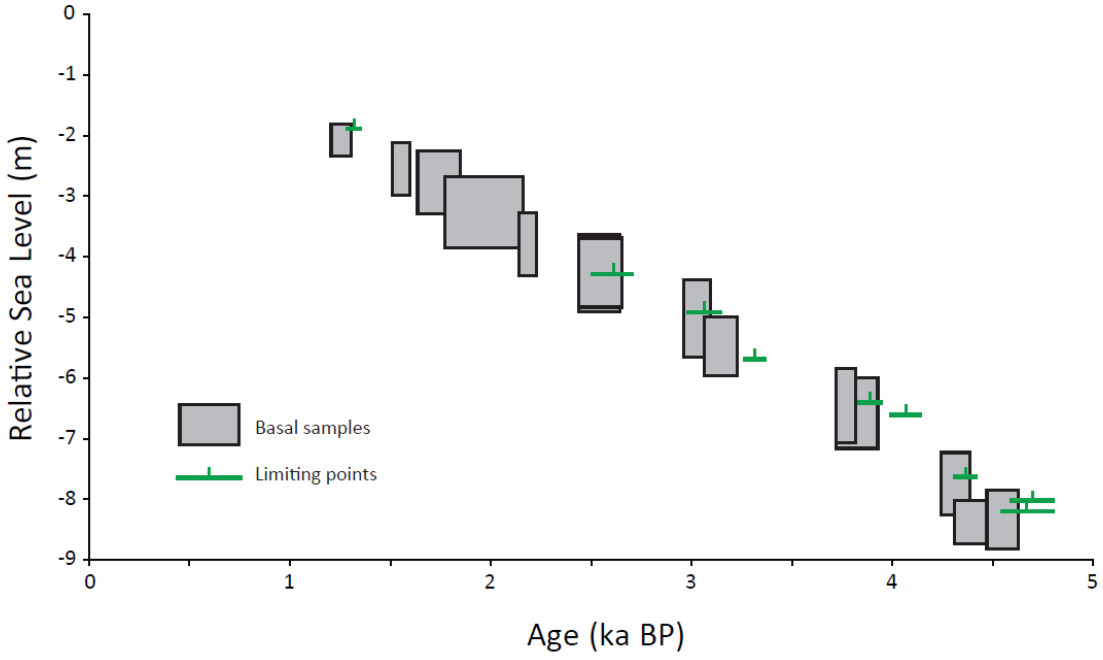

Figure 5. Late Holocene sea level index points and limiting points for southern New Jersey. Index points are plotted as boxes with 2σ vertical and calibrated age errors.

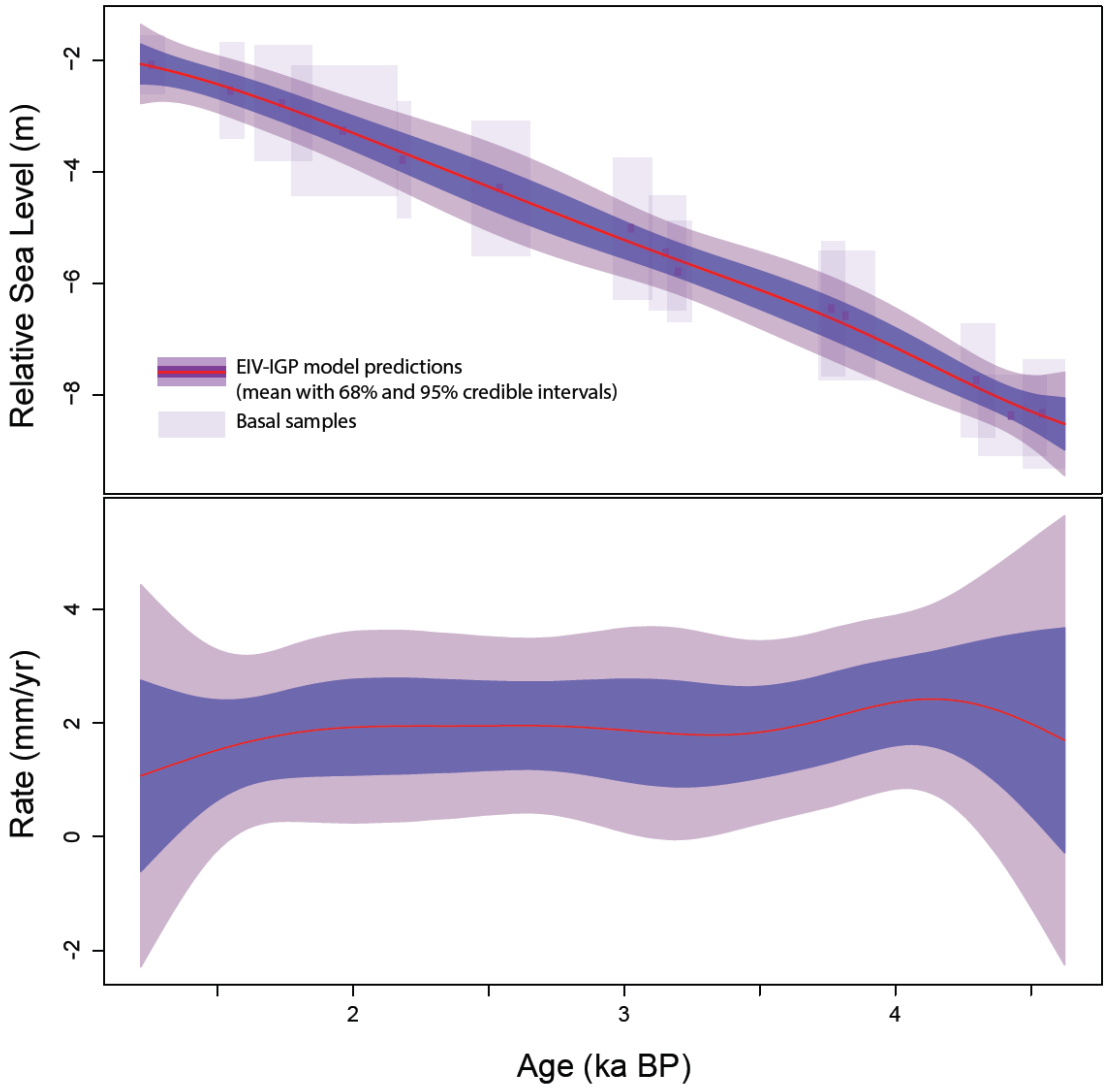

Figure 6. Basal index points applied to the Errors-In-Variables Integrated Gaussian Process model to examine the RSL change and rates of change through the late Holocene.

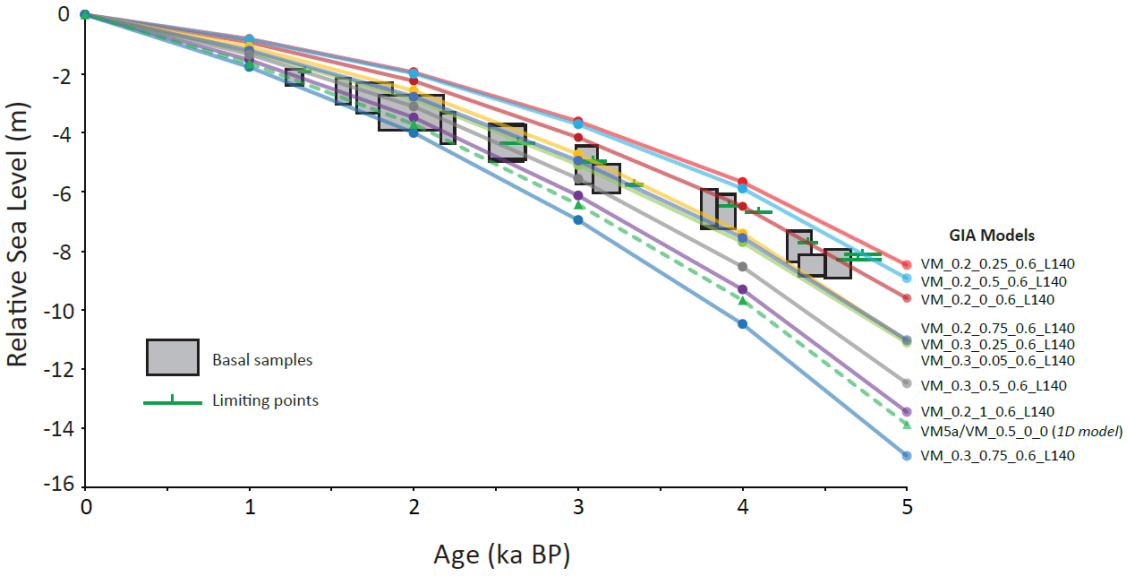

Figure 7. Basal index points and limiting points with 10 GIA model predictions (one 1D model and 9 3D models) over the last 5 ka BP.

Conclusions

In this dissertation, I examined sea-level proxies, timing of rates of change of sea-level rise, and mechanisms contributing to sea-level change in New Jersey during the late Holocene.

In Chapter 1, I examined temporal and spatial variability of salt-marsh foraminifera and showed that even when incorporating variability of modern foraminiferal distributions into a Bayesian transfer function, foraminifera-based RSL reconstructions from high marsh environments remain robust and reproducible. Variability of foraminifera distributions can be included in the transfer function for future RSL reconstructions where modern foraminifera assemblages are comparable.

In Chapter 2, I produced a new RSL record in northern New Jersey and estimated the timing of the onset of modern elevated rates of sea-level rise. The global onset of modern rates of sea-level rise occurs in ~1870 CE. The timing of modern elevated rates of RSL rise at nineteen sites in the North Atlantic reveals asynchronous timing with a distinct spatial pattern where the onset appears muted and later along the European coast compared to the North American coast.

In Chapter 3, I produced a new late Holocene RSL record in southern New Jersey, accounting for sediment compaction and tidal range change. I found that RSL rose continuously through the late Holocene by an approximate magnitude of 6.1 m from 4.5 ka BP to 1.3 ka BP at an average rate of 1.9 ± 0.6 mm/yr, but there is a misfit between these observations and predictions from site-specific 1D and 3D GIA models, although the 3D models are an improvement over the 1D model. Further testing is needed with a larger

selection of ice models and 3D viscosity model parameters to provide a better fit between GIA model predictions and RSL observations.

Here, I also describe several aspects of my thesis that did not work to highlight the fact that research does not always go as planned. For example, in Chapter 2, at Cheesequake State Park, I originally tried to do a basal peat study as deep sequences of basal peat had been identified in the marshes previously. However, after extensive coring there, I found only isolated sections of basal peats located beneath thick sections of clays, which made the site unsuitable for a basal peat study. Additionally, the RSL record I did produce from Cheesequake State Park was expected to be a complete 2000-year long Common Era record. I radiocarbon dated the core and obtained dates extending back 2000 years, but found a plateau in the radiocarbon dates around 1000 years BP. Therefore, I was only able to produce a 1000-year long RSL record.

In Chapter 3, the original objective was to use a new method of RSL reconstruction involving three sea-level proxies (foraminifera, testate amoebae, and stable carbon isotope geochemistry) in the basal peat units. While the foraminifera and geochemistry proxies worked as expected, the testate amoebae were nearly completely absent from the basal cores, perhaps due to preservation issues. Therefore, I was not able to use testate amoebae as an additional indicator of environmental deposition as expected. In addition, I planned to produce short RSL reconstructions (using the Bayesian transfer function with foraminifera and geochemistry) for each basal core and stack them into one continuous record to obtain a higher resolution late Holocene record. However, there is not a suitable existing method for stacking individual age depth models from basal cores along a ~500

km transect, which led me to using only one individual sample from each basal core for the reconstruction.

The results of my thesis lead to potential areas of future work. Specifically, for Chapter 2, further investigation of ocean dynamic processes such as AMOC changes and Gulf Stream shifts could improve understanding of the mechanisms driving the asynchronous timing of the onset of elevated rates of sea-level rise. Alternative potential mechanisms should also be explored, such as local factors contributing to earlier elevated rates at specific sites. The variability in timing could be compared to observational data or models of oceanographic processes to examine similar spatial patterns. Additionally, for Chapter 3, each basal core has a chronology and foraminifera and geochemistry data, allowing for the potential of producing short RSL reconstructions for each core and stacking them. A suitable method would need to be developed to stack age depth models from separate cores along a transect, which could lead to an even higher resolution late Holocene RSL reconstruction to examine magnitudes and rates of change.